Synthesis, Surface Immobilization and Characterization of Metal Complexes for Olefin Metathesis

TECHNISCHE UNIVERSITÄT DARMSTADT

Vom Fachbereich Chemie
der Technischen Universität Darmstadt

zur Erlangung des akademischen Grades eines

Doctor rerum naturalium (Dr. rer. nat.)

genehmigte Dissertation

vorgelegt von

Jetmire Mersini, "M.Sc."

aus Gostivar, Mazedonien

Referent:	Prof. Dr. H. Plenio
Korreferent:	Prof. Dr. G. Buntkowsky
Tag der Einreichung:	28 Oktober 2014
Tag der mündlichen Prüfung:	12 Januar 2015

Darmstadt 2015

D17

Acknowledgement

Foremost, I would like to express my sincere gratitude to my advisor Prof. Dr. Herbet Plenio for the support of my Ph.D study and research, for his patience, motivation, enthusiasm, and immense knowledge.

My sincere thanks also go to Ms Eleonore Pfeifer, who was always ready to help me in all spheres of my life. I wish to thank my dear lab-mates: M. Sc. Meike Egert, M. Sc. Pavlo Kos, Dr. Roman Savka, M. Sc. Roman Vasiuta, Dipl.-Ing. Natalie Peschek, Dipl.-Chem. Andreas Hegelein, Dr.-Ing. Marc Schilz, Dipl.-Ing. Heike Jansohn, Dr.rer.nat. Vasco Thiel and Jonas Bang, in particular Götz Hoffmann and M. Sc. Oliver Halter with whom I enjoyed so much discussing about workout routines and nutrition plans.

My special thanks are extended to Dr. Markus Gallei for the nice cooperation regarding the first project of my work (Modulation of surface bound ruthenium catalyst by redox responsive ferrocene containing polymers). Furthermore I would like to give huge thanks to the following research groups (listed in alphabetical order), who made my work possible: research group of: Prof. Dr. Markus Biesalski: Dr. Alexander Böhm (polymer modified paper synthesis and characterization), Dr. Kai Zhang (CNC synthesis and characterization), Center of smart interfaces (AFM measurements) and Dipl.-Ing.Heike Herbert (GPC measurements), Prof. Dr. Anette Andrieu-Brunsen: Dipl.Chem. Fabio Krohm (mesoporous SiO_2 and SP-norbornene monomer synthesis and characterization), Prof. Dr. Gerd Buntkowsky: Dr. Hergen Breitzke (^{29}Si-NMR measurements), Prof. Dr. Matthias Rehahn: M.Sc. Johannes Elbert (PvFc-TEOS and SiO_2 particle synthesis), Dr. Nicole Vilbrandt (CV measurements), Dr. Matthias Witterman (SEC measurements), Prof. Dr. Bernd Stühn: Dipl.-Phys. Christina Lederle and Dr. Martin Kraska (DLS measurements), Prof. Dr. Rainer Winter (interpretation of CV's), R. Pleixats and A. Monge-Marcet for adcive with synthesis of Grubbs Hoveyda 2nd generation type catalyst. I would also like to thank "Landesoffensive zur Entwicklung wissenschaftlich-ökonomischer Exzellenz" (LOEWE Soft Control) for the financial support. In addition, I would like to thank Dr. Klaus J. Wannowius who was always willing to help and support me during my studies.

Special thanks should be given to Prof. Dr. Ahmet Önal who gave me the very first opportunity to conduct research in his research group where my love for synthesis grew up.

Last but not least, I wish to thank my parents, my beloved friends Jovana Jakovleska, Todorka Banova and Naciye Keklik for their full support throughout my life.

"Work hard, believe in your dreams, and follow those dreams with no excuses"

Oksana Grishina

Die vorliegende Arbeit wurde am Eduard-Zintl-Institut für Anorganische und Physikalische Chemie der Technischen Universität Darmstadt unter der Leitung von Prof. Dr. H. Plenio in der Zeit von März 2011 bis Juni 2014 angefertigt.

Teile dieser Arbeit sind bereits veröffentlicht oder zur Veröffentlichung eingereicht:

Elbert, J.; Mersini, J.; Vilbrandt, N.; Lederle, C.; Kraska, M.; Gallei, M.; Stu, B.; Plenio, H.; Rehahn, M. *Macromolecules*, **2013**, *46*, *4255-4267*.

Outline

Abbreviations

ATR-IR	attentuated total reflectance infrared spectroscopy
BP	benzophenone
Cy	cyclohexyl
CNC	crystalline nanocellulose
CV	cyclic voltammetry
DCM	dichloromethane
DLS	dynamic light scattering
EDS	energy-dispersive X-ray spectroscopy
Et	ethyl
Fc	ferrocene
GPC	gel permeation chromatography
ITO	indium tin oxide
SEM	scanning electron microscopy
MABP	4-methaclyloyloxybenzophenone
MAC_2AE	N-methaclyloyl-ß-alanine succinimide ester
MCC	microcrystalline cellulose
NHC	*N*-heterocyclic carbene
NHS	*N*-Hydroxysuccinimide
NMR	nuclear magnetic resonance
PDI	polydirspersity index
PvFc	polyvinyl ferrocene
RCM	ring closing metathesis
ROMP	ring opening metathesis polymerization
r.t.	room temperature
SI-ROMP	surface initiated ring opening metathesis polymerization
TEM	transmission electron microscopy
TEOS	tetraethyl orthosilicate
THF	tetrahydrofuran
UV/Vis	ultraviolet–visible spectroscopy

1. Motivation

1.1. Aims of the work

Aim 1: Activity modulation of surface bound ruthenium catalysts using redox responsive polymers

Objective of the work: Synthesis and surface immobilization of ruthenium complexes and their application in ring opening metathesis polymerization (ROMP).

The first plan of this work of this work was to synthesize –Si(OEt)$_3$ or –Si(OiPr)$_3$ bearing *N*-heterocyclic carbenes, in cooperation with Dr. Markus Gallei.

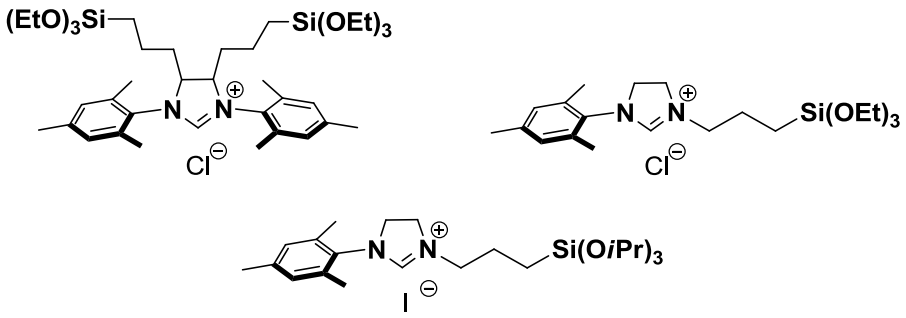

(*N*-heterocyclic carbene examples bearing functional groups for surface immobilization)

The functionalized *N*-heterocyclic carbenes were planned to be immobilized on the surface of silica nanoparticles, as shown in the figure below:

(–Si (OEt)$_3$ bearing *N*-heterocyclic carbene examples immobilized on silica nanoparticles)

Finally, it was planned to prepare the final ruthenium complex on the surface of the silica nanoparticles by introducing the Grubbs 1st generation type catalyst on the NHC modified silica nanoparticles as shown below:

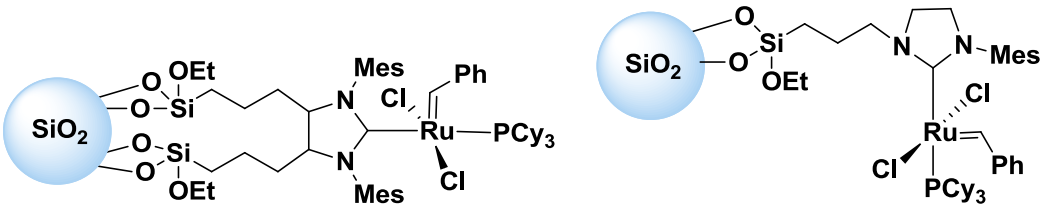

(Grubbs 2nd generation type catalysts immobilized on silica nanoparticles)

The modified substrates were planned to be used in ring opening metathesis reaction as well as ring closing metathesis reactions. Furthermore, the major aim of this work will be to obtain redox-switchable surfaces, which should be possible by switchable ferrocene moieties bearing polymers. The Grubbs 2nd generation

catalyst was planned to be codeposited with polyvinylferrocene polymers on the surface of silica nanoparticles as shown in the figure below, where the black stars represent the catalyst, and the orange layer represents the ferrocene polymers bound on the surface of silica nanoparticles.

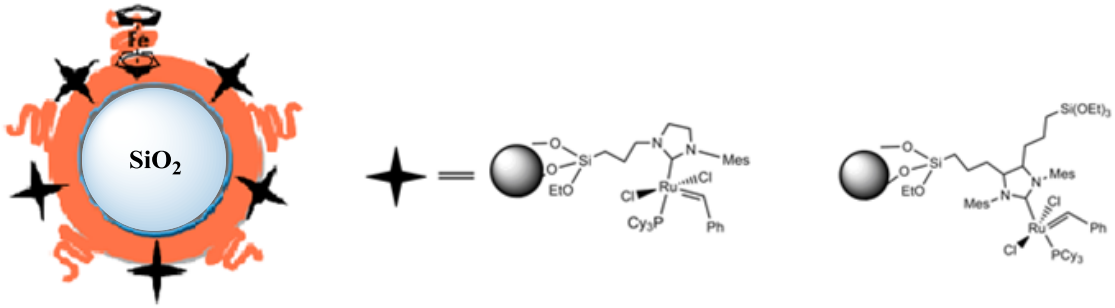

(Co-deposition of Grubbs 2nd generation type complexes and ferrocene bearing polymers on silica nanoparticles)

In order to show the switching properties of the modified silica surface, the particles will be oxidized where in this case polyvinylferrocene polymers are expected to show swelling behavior, while embedding the ruthenium catalyst inside the polymer layer, though making the catalyst inaccessible to olefin metathesis substrate.

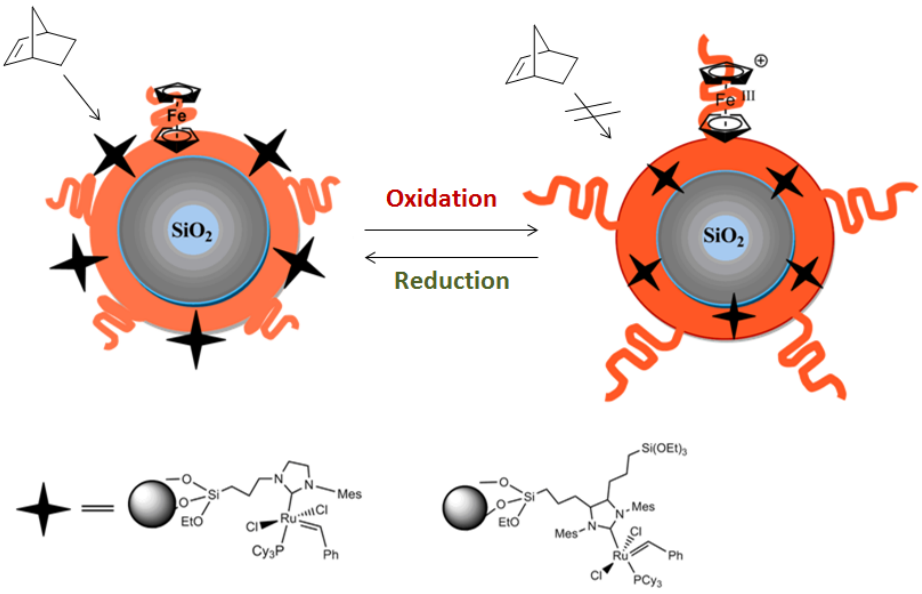

(Oxidation and reduction of polyvinylferrocene and ruthenium catalyst grafted silica nanoparticles)

On the other hand, when the polyvinylferrocene and ruthenium catalyst grafted silica nanoparticles will be reduced, the particle diameter is expected to reduce dramatically, showing that the polymer shrinks, while collapsing toward the surface of the silica nanoparticles. In this manner, the catalyst immobilized on the surface will be again accessible to the monomer molecule in order to perform ROMP reaction.

Aim 2: Immobilization of Ruthenium complex on mesoporous silica supported on indium tin oxide surface (ITO) and its application in surface initiated ROMP (SI-ROMP)

The second part of this work will be involving surface immobilization of Grubbs-Hoveyda 2nd generation type catalyst on mesoporous film for surface initiated ROMP, in cooperation with Fabio Krohm. Mesoporous silica thin films with 200 nm thickness, displaying organized pore arrays with high accessibility, which are going to be prepared by Fabio Krohm, research group of Jr. Prof. Dr. Annette Brunsen. The thin films are planned to be capped with benzophenone silane polymers as shown in the figure below, to ensure that no catalyst will be covalently bound on the surface of the film. The pores of the film are assumed to be enriched with hydroxyl groups where the Grubbs Hoveyda 2nd generation type complex, functionalized with ethoxy groups, will be covalently bounded.

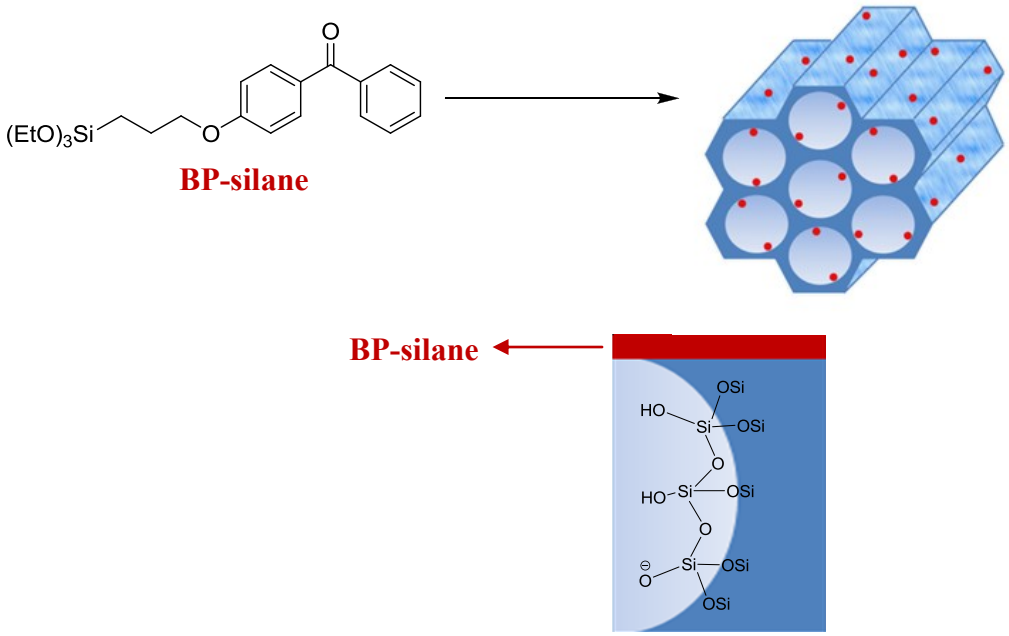

(Benzophenone-silane capping of mesoporous films)

Grubbs Hoveyda 2nd generation type complex bearing –Si(OEt)$_3$ groups is planned to be synthesized and covalently bound only in the pores of the mesoporous ITO, glass and Si-wafers films, as shown in the figure below.

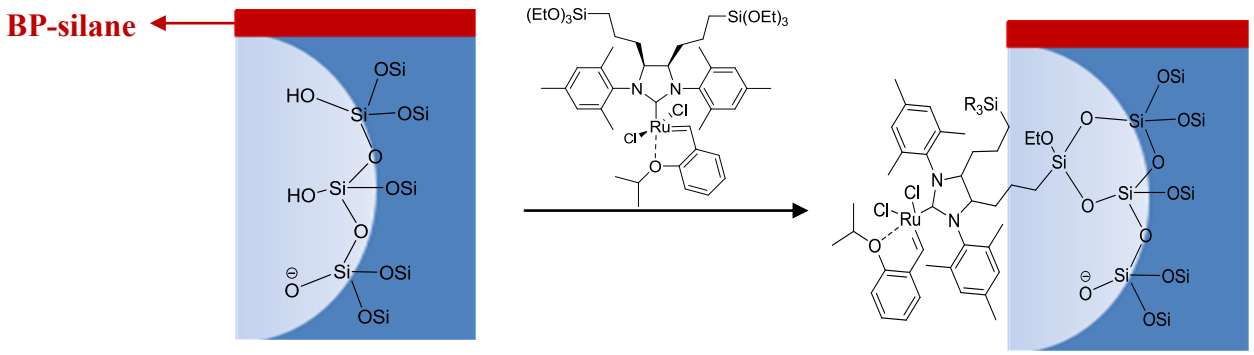

(Immobilization of Grubbs Hoveyda 2nd generation type complex on mesoporous substrates)

The catalyst modified indium tin oxide (ITO) substrates are planned to be used for surface initiated ring opening metathesis polymerization of norbornene derivative-ferrocene monomer as well as norbornene derivative-spiropyrane monomer as shown in the figure below. Furthermore, the polymers will be extracted from the mesopores and further characterized using GPC.

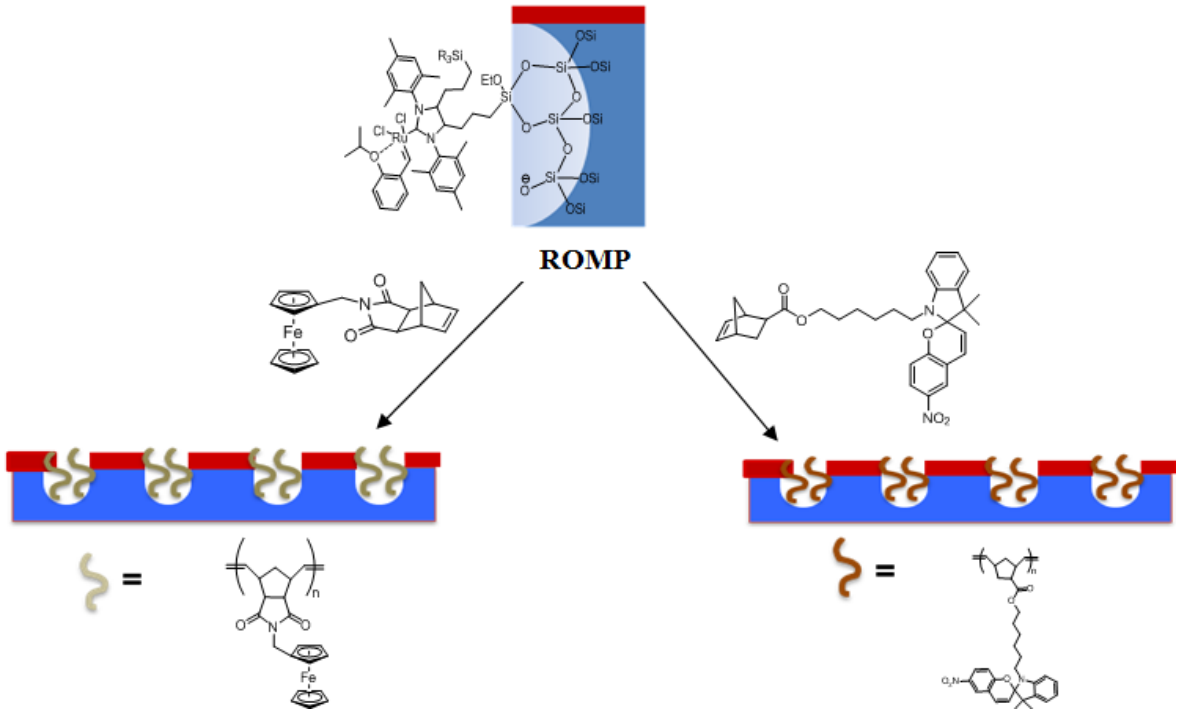

(Surface initiated ring opening metathesis polymerization of norbornene derivative-ferrocene monomer (left) and norbornene derivative-spiropyrane monomer (right))

Aim 3: Synthesis of [(NHC)AuCl] type complexes bearing $-NH_2$ and their immobilization on crystalline nanocellulose (CNC) and polymer modified filter paper.

The final aim of this work will be to synthesize [(NHC)AuCl] type complexes bearing amino groups as shown in the figure below, which complexes are planned to be immobilized on crystalline nanocellulose (CNC) (in cooperation with Dr. Kai Zhang) and polymer modified filter paper (in cooperation with Alexander Böhm, research group of Prof. Dr. Markus Biesalski) for the application in hydration reaction of alkynes as heterogenous catalysts. The supporting lingand will be chosen N-heterocyclic carbenes (NHCs) bearing amino groups ($-NH_2$) which will be used as anchoring groups to covalently bound on the surface.

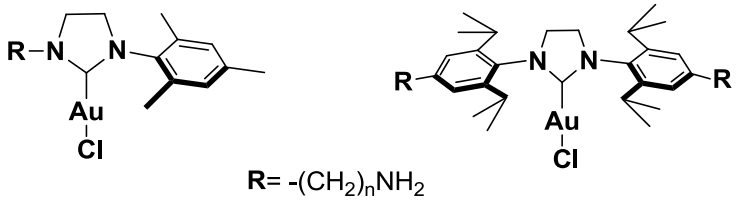

([(NHC) Au] type complexes with amino groups for surface immobilization)

For the immobilization of amino group functionalized catalyst nanocrystalline cellulose will be used bearing functional carbonyl groups. The crystalline nanocellulose (CNC) substrate will be synthesized by Dr. Kai Zhang from commercially available microcrystalline cellulose (MCC) as illustrated in the scheme below.

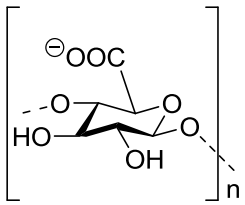

(Carbonyl groups bearing cellulose nanocrystals (CNC)))

The [(NHC)AuCl] gold will be then immobilized on cellulose nanocrystals via amino groups, in order to obtain a covalent binding of the catalyst on the surface of the cellulose.

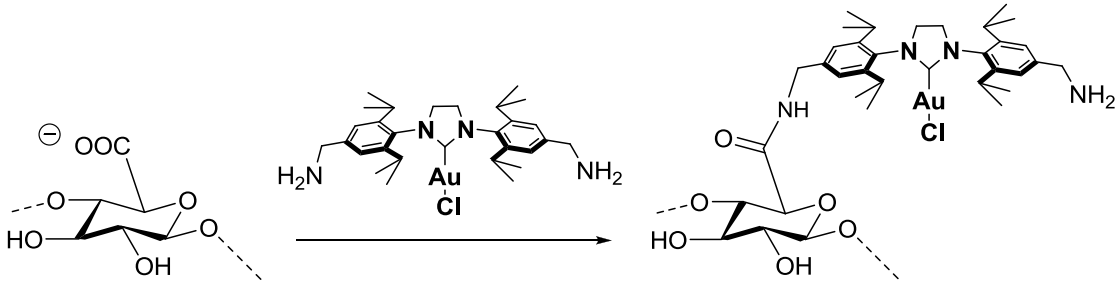

(Immobilization of [(NHC) AuCl] type complex on cellulose nanocrystals (CNC))

The catalyst modified crystalline nanocellulose ([(NHC)AuCl]@CNC) finally it is planned to be used for hydration reactions of alkynes as given in the scheme below.

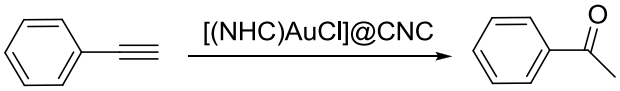

(Hydration of alkynes using [(NHC)AuCl]@CNC)

Another interesting substrate to be used for immobilization of [(NHC)AuCl] complexes bearing functional amino groups is polymer modified filter paper, in cooperation Alexander Böhm.

The standard filter paper it is planned to be chemically microstructured by photo-chemical attachment of functional polymers to cellulose microfibers, which will be performed by Alexander Böhm. The polymer network will be formed through three different types of copolymers as described in figure below where Methyl-methacrylate (MMA) will be chosen as the matrix monomer. The second monomer will be succinimide moieties bearing monomer which will be used for binding of the gold complex on the cellulose fibers. The third monomer will be containing benzophenone moieties which will have the function of the binder monomer as shown in the figure below.

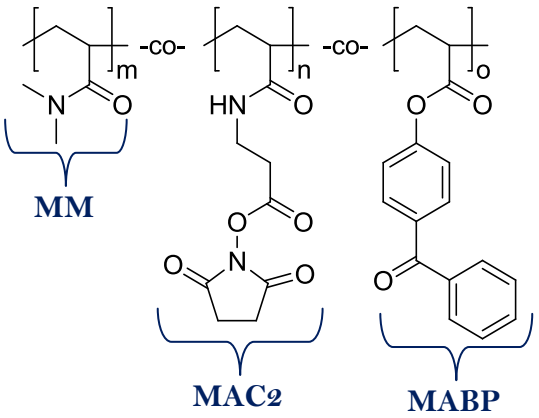

(P (DMAA-co-MAC2AE-co-MABP) modified filter paper)

After the polymer modification of the paper substrates, it was planned to immobilize the [(NHC)AuCl] type complexes bearing amino groups on the outer surface of the paper in order to obtain catalytically active paper as shown in the figure below.

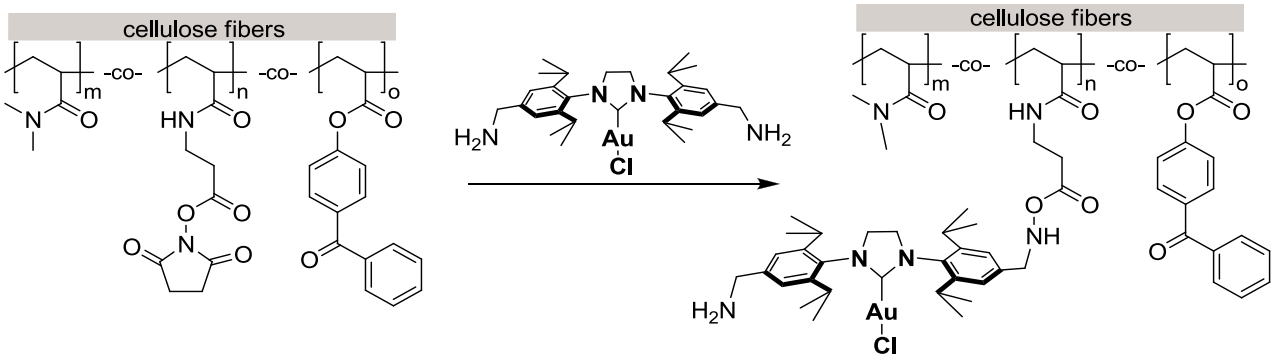

([(NHC) AuCl] type catalyst immobilization on polymer modified filter paper)

As a final step, the catalyst modified filter paper substrates ([(NHC)AuCl]@paper) are going to be tested in hydration reaction of alkynes as shown below.

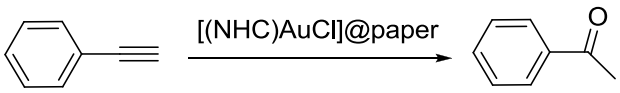

(Hydration reactions using [(NHC)AuCl]@paper substrates)

2. Aim 1 (Introduction)

2.1. Olefin metathesis

In the 1950's olefin metathesis was first discovered [1]. Since then, it has developed into a useful reaction that can be catalyzed by various transition metals [1]. This organic reaction which involves redistribution of fragments or parts of alkenes by scission and rearrangement of carbon-carbon double bonds as shown in the scheme 1 below [1].

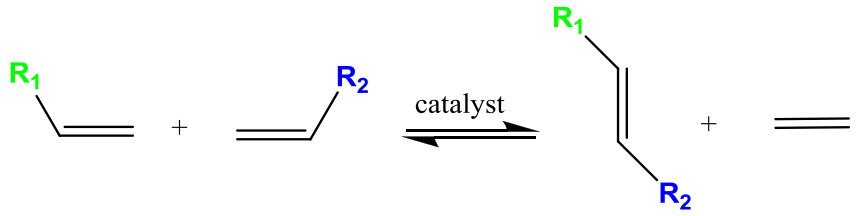

Scheme 1 Schematic representation of olefin metathesis reaction.

In order to shift the equilibrium to the product side, using the Le Chatelier's principle, one of the products (often ethene) is removed continuously from the reaction [1]. The catalysis of olefin metathesis is based on the so-called Chauvin mechanism which is given in the scheme 2 below.

Yves Chauvin (who has uncovered the mechanism of olefin metathesis), Richard Schrock and Robert Grubbs (who have developed highly active and well-defined catalysts for olefin metathesis reactions) were awarded the Nobel prize in chemistry in 2005 [2], [3].

The metal-catalyzed olefin metathesis reaction is characterized by mild reaction conditions and it is tolerant to many functional groups. Chauvin mechanism for olefin metathesis reaction involves the [2+2]-cycloaddition of an alkene double bond to a transition metal alkylidene to form a metallacyclobutane intermediate. The metallacyclobutane produced can then cyclorevert to give either the educts or a new alkene and alkylidene [2], [3]. If the reaction favors the product side then a new olefin with exchanged fragments, and a new metal carbene is formed. The course of the reaction is shown in scheme 2.

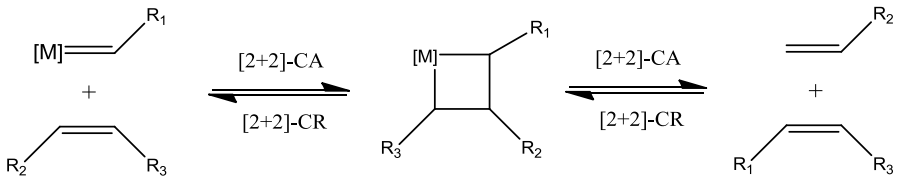

Scheme 2 Chauvin mechanism of olefin metathesis.

There are several types of olefin metathesis reactions, from which only two types are used for the application of the immobilized catalysts described in this work.

2.1.1. Ring closing metathesis (RCM)

In this type of metathesis, the acyclic dienes are reacted to form a cyclic alkene. The driving force of the reaction is the formation of highly volatile by-product that may escape from the reaction mixture. With this method, the formation of unstrained ring systems of different sizes is easily accessible as shown in scheme 3.

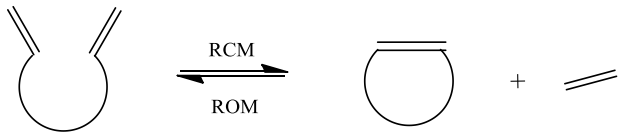

Scheme 3 Ring closing metathesis of an acyclic diene.

2.1.2. Ring opening metathesis polymerization (ROMP)

Ring-opening metathesis polymerization uses metathesis catalysts to generate polymers from cyclic olefins. Norbornene and norbornene derivatives are very good examples for such reactions, since they are strained cyclic olefins. Since the relief of the ring strain is a major driving force for the reaction, such monomers are widely appreciated for ring opening metathesis polymerization reactions as shown in the scheme below.

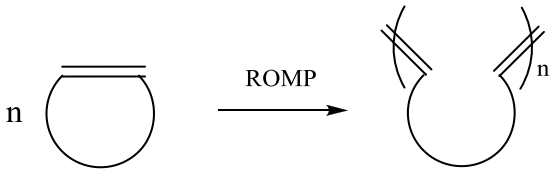

Scheme 4 Ring opening metathesis reaction of a cyclic olefin.

2.2. Catalyst for metathesis reactions

This part describes the most important catalysts used for olefin metathesis reactions. In the 1960s, $RuCl_3 \cdot H_2O$ was used as a catalyst for the ROMP reactions. The first experimenters, who have synthesized the data of the proposed mechanism for the appropriate alkylidene complex, were Schrock and Grubbs, where the development of well-defined catalysts, with high activity at moderate reaction temperatures and high functional group tolerance had then begun [2], [3], [4].

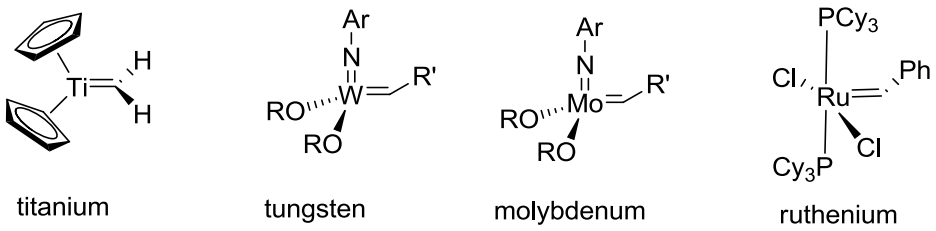

Figure 1 Development of alkylidene complexes for olefin metathesis.

The figure 1 above shows the complexes which are classified according to their tolerance of functional groups; from left to right decreasing sensitivity of precatalyst toward oxygen-containing functional groups. Molybdenum complex was developed by Schrock and already has a relatively high functional group tolerance, but the highest functional group tolerance is achieved with the ruthenium alkylidene complex-Grubbs catalysts. The main objective of the study on catalysts has been the development of stable, active and selective catalysts.

Through the diversified development of catalysts Robert Grubbs and his coworkers succeeded in developing the first water-and oxygen-resistant catalyst based on ruthenium [3].

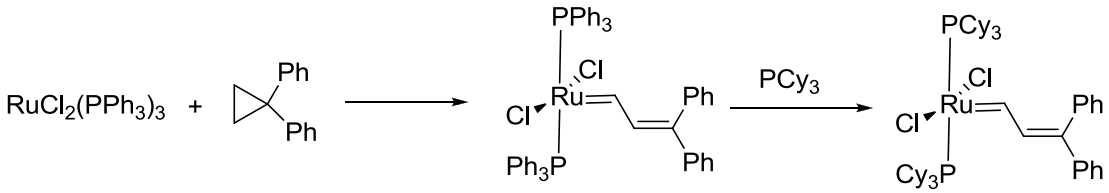

Figure 2 Schematic representation of the very first ruthenium complex.

As represented in figure 2, to dichlorotris(triphenylphosphine)ruthenium(II), cyclopropene derivatives were introduced, with the aim to finally form the target carbene complex. By introducing more basic and bulkier tricyclohexylphosphine ligands make the complex more stable, reactive and tolerant of functional groups. In the figure 3 below, Grubbs 1st generation catalyst and Grubbs 2nd generation catalysts are given, where the second generation catalyst has the same uses in organic synthesis as the first generation catalyst, but it is known for its higher activity. Furthermore, the catalyst is more stable toward moisture, air and it is easier to handle.

In the Grubbs 2nd generation catalysts, the PCy_3 group is exchanged with an *N*-heterocyclic carbene ligand (figure 3).

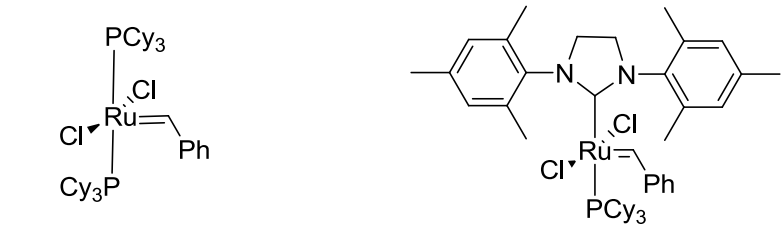

Figure 3 Grubbs 1st and 2nd generation complexes.

Complexes with improved stability are the Grubbs-Hoveyda catalyst, where the benzylidene ligand has a chelating isopropoxy group attached to the benzene ring. The chelating oxygen atom replaces a phosphine ligand, which for the 2nd generation catalyst gives a completely phosphine-free structure (figure 4) [5], [6].

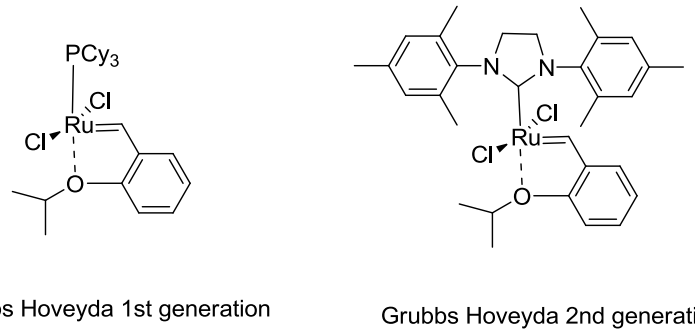

Figure 4 Grubbs-Hoveyda 1st generation and Grubbs-Hoveyda 2nd generation complexes.

2.2.1. Surface bound catalysts

Formation of by-products which contain ruthenium is the most undesirable feature of modern homogenous metathesis catalysts. These undesired products are very difficult to be removed from the reaction products. The level of the ruthenium in the desired product should be as low as possible (<10 ppm), since high contamination levels cannot be tolerated for pharmaceutical applications [7]. For this purpose, new catalytic architectures are designed: surface bound catalysts, which represent the heterogeneous catalysts for metathesis reactions [7]. Surface bound catalysts are more easily recovered from the reaction system as well as easily recycled. In addition, they are less prone to bimolecular decompositions which are common for homogenous catalysts for metathesis reactions.

Several ways of anchoring ruthenium complexes are reported in the literature such as: ruthenium complexes bound on solid support, dendric or soluble support or they are anchored on ionic tag [7].

The very first ruthenium catalyst bound on solid support was mentioned recorded by Barrett and co-workers, where the Grubbs 1st generation complex is attached to vinyl polystyrene as shown in the figure below.

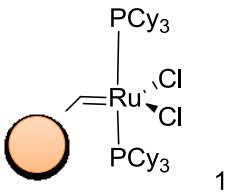

Figure 5 Grubbs 1st generation catalyst immobilized on vinyl polystyrene [8].

After the application of the immobilized complex in ring closing metathesis reactions, the conversion of the educt was 98%, whereas the residual ruthenium content was obtained as 500 ppm, which is too high for a product to be used for pharmaceutical applications.

Nolan and co-workers developed developed another catalyst immobilized on DVB (divinylbenzene), in which the tricyclohexylphosphine group is exchanged by an N-heterocyclic carbene ligand (L= SIMes, IMes), as shown in the figure 6 [9].

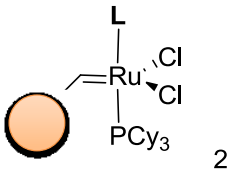

Figure 6 Grubbs 1st generation catalyst immobilized on vinyl polystyrene, where L= SIMes, IMes [9].

The immobilized Grubbs 2nd generation complex on divinylbenzene (complex 2) was later applied in ring closing metathesis reaction, where again high conversion was observed just as in the case with complex 1 above. The residual ruthenium was a disadvantageous feature since it was found to be even higher than complex 1, with a value of 2000 ppm [9].

Blechert [10], Hoveyda [11] and Dowden [12]. reported ruthenium catalysts, immobilized on solid polymers, bearing an isopropyl styrene fragment, which represented the first functionalized-boomerang-type catalysts. This type of solid-surface bound catalyst were also used metathesis reactions, which showed high conversion in ring closing metathesis reaction and low in residual ruthenium in the final desired product (figure 7).

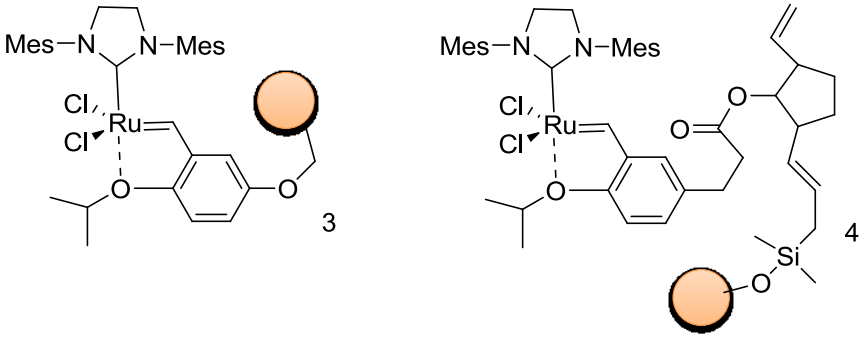

Figure 7 Blechert (3) and Downed (4) complex immobilized on solid polymer-supports [10, 12].

The complexes 3 and 4 showed the same recyclability whereas complex 2 showed higher activity in metathesis reactions than complex 3. The residual ruthenium content on the desired product, after the reactions, was not determined [10, 12].

2.2.2. Immobilization of ruthenium catalysts through N-heterocyclic carbene ligands

The first ruthenium catalyst immobilized via the N-heterocyclic carbene ligand was reported by Blechert et al [13], which was used in ring closing metathesis reactions and was shown to have improved reactivity compared to complexes mentioned above (3 and 4). In addition, this type of immobilized complexes are more stable and easy to be handled. Hoveyda et al [14] reported the immobilization of Grubbs 2nd generation catalysts (figure 8) as well as Grubbs-Hoveyda 2nd generation catalyst on monolith silica surface, which were anchored via the N-heterocyclic carbene ligand. In comparison to the other types of bonding on solid support, immobilization via NHC ligand led to improved recyclability of the catalyst [13].

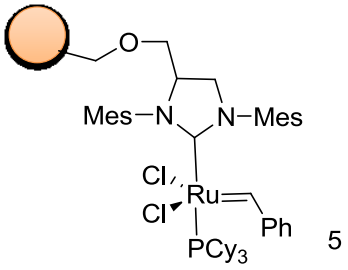

Figure 8 Grubbs 2nd generation type catalyst immobilized on monolithic silica rods [14].

In 2009, Grubbs and coworkers reported Grubbs-Hoveyda 2nd generation type catalyst, immobilized on silica nanoparticles using the backbone of the N-heterocyclic carbene. A $-Si(OEt)_3$ functionalized NHC ligand was prepared to synthesize the corresponding Grubbs-Hoveyda 2nd generation type complex. Finally, the complex was immobilized on the surface of silica particles, to be tested in olefin metathesis reactions (figure 9). These types of complexes (complex 4 and 5), bound via the backbone of the NHC ligand, were shown to compete for a wide variety of homogenous catalysts for the activity of olefin metathesis reactions. In addition, these complexes have shown true heterogeneity, which was tested with split test and finally the recyclability was tested. The complexes could be recycled several times and the ruthenium content in the final desired product after the metathesis reactions was found to be only 5 ppm.

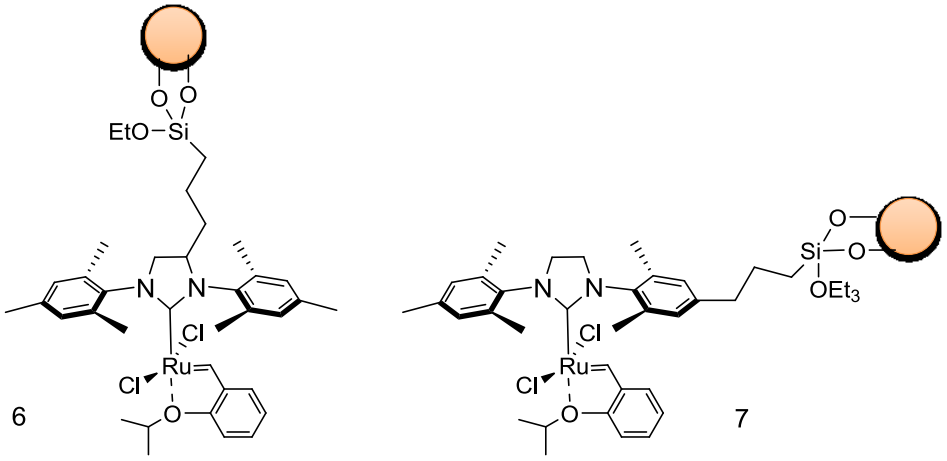

Figure 9 Grubbs-Hoveyda 2nd generation type catalyst immobilized via NHC ligand on silica particles [15].

Later on, in 2011, Lang and co workers reported an interesting application of immobilized ruthenium complex on solid surface. The functionalized NHC ligands are anchored on polysiloxanes and coated on the inner part of silica capillaries (figure 10). Using the techniques of solid state chemistry, the NHC ligands fused on silica microcapillaries were converted to metal complexes; gold as well as ruthenium complexes [16].

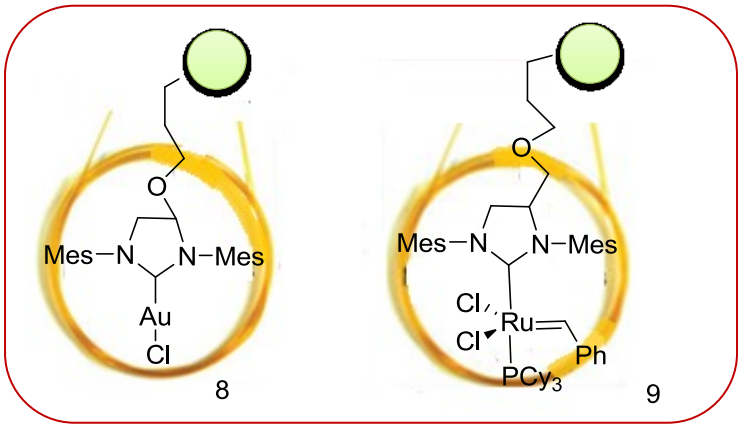

Figure 10 Immobilization of gold catalyst (8) and Grubbs 2nd generation type catalyst (9) using the backbone of the NHC ligand [16].

The complexes bound on silica capillaries were then used to perform olefin metathesis reactions, running on column.

In conclusion, immobilization of olefin metathesis catalysts has shown to be crucial for industrial applications due to the minimization of leaching of important metal catalysts. Immobilized catalysts then are known for their superior properties, while being highly active and usable in various reaction conditions.

2.3. Aim 1: Modulation of surface bound ruthenium catalyst by redox responsive ferrocene containing polymers

The primary target of this project is to obtain redox-switchable and surface immobilized catalysts for olefin metathesis reactions. First of all, in order to obtain ruthenium complexes which could covalently bind on the surface, N-heterocyclic carbene ligand bearing functional –Si $(OEt)_3$ are needed. In order to achieve this, it is planned to co-deposit Grubbs-type catalysts and ferrocene polymers on silica nanoparticles. Redox-reactions at the ferrocene polymers lead to an expansion or a contraction at the redox active polymers. After oxidation of the ferrocene polymers, the molecular environment increases dramatically in hydrophilicity and swelling of the resulting polyelectrolyte can be observed. In the expanded state the catalytic center buried in the polymer in the nanoparticle will not be accessible to olefin metathesis substrate. Alternatively, in the collapsed state of the ferrocene polymers, the substrate will be able to reach the catalytic center as shown in the figure below. Furthermore, after the reduction of the ferrocene moieties on the outer surface of silica nanoparticles the polymer chains were expected to collapse again towards the surface of the particles and in this case it was expected that the catalyst was available again for the continuation of ROMP of norbornene monomer as illustrated in the figure below.

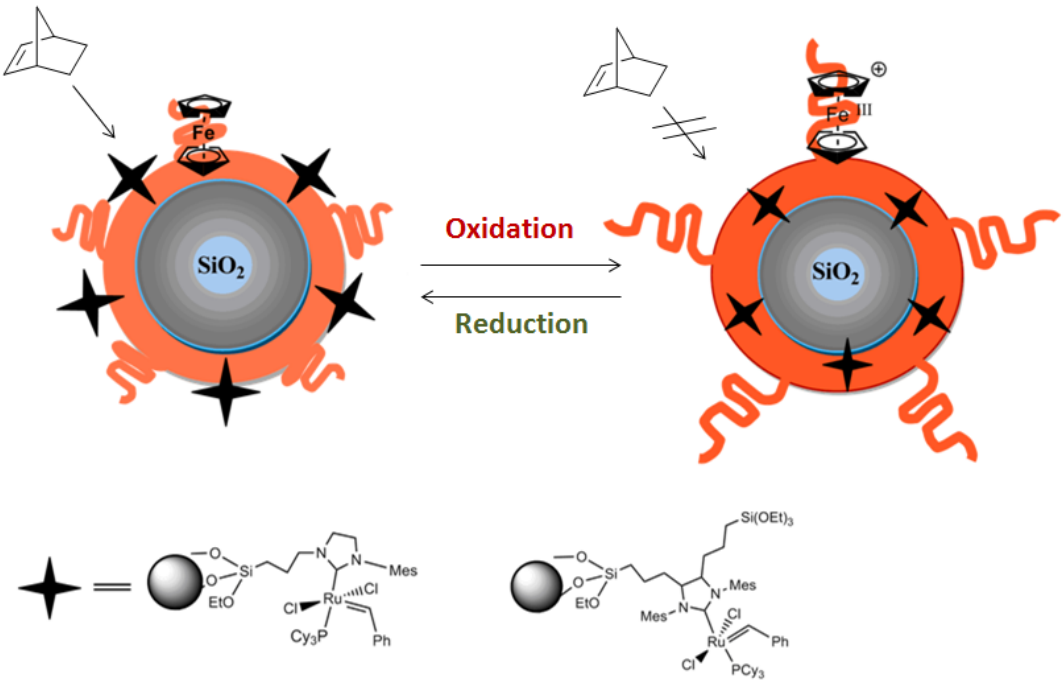

Figure 11 Modulating the activity of ruthenium catalyst via redox-responsive ferrocene containing polymers.

2.3.1. Redox responsive polymer brushes

The vast majority of reports about the stimuli responsive polymers deal with temperature, light or pH dependent changes of polymer chain conformation, but not enough examples are given about the redox-responsive systems [17]. Mazurowski et al in 2012 reported an interesting redox active micellar core-shell ferrocene containing polymer. The redox-stimulus ferrocene containing polymers were grafted on polystyrene particles and cyclic voltammetry was applied to obtain information about the reversibility via oxidation-reduction cylces [17].

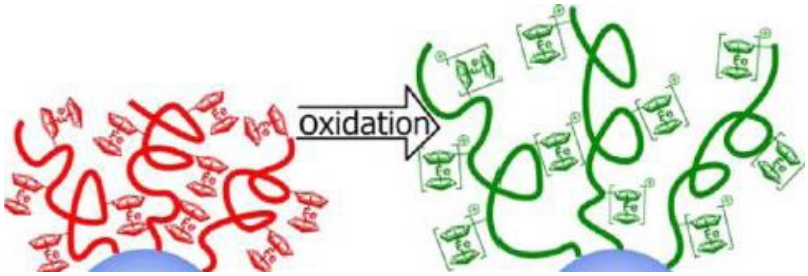

Figure 12 Poly (2-(methacryloyloxy)ethyl ferrocene carboxylate) brushes oxidized on the surface of polystyrene paticles [17].

The well defined redox responsive PFcMA brushes on the surface of the silica nanoparticles were synthesized by surface-initiated ATRP.

After the oxidation, the shell of the polystyrene particles had been observed to increase in shell thickness due to the ferrocene moiety caused by the polyelectrolyte effect. The increase in particle size had been also studied

via DLS (dynamic light scattering). Such switchable particles or surfaces could later be used for bio-organometallic applications, separation techniques, sensor applications or redox-responsive colloidal films [17]. Similar switchable polymer structures were used, as shown in the figure 12 above, in order to be co-deposited together with the Grubbs 2nd generation type catalyst on silica surface, in order to achieve the planned redox-switchable surfaces.

2.4. Results and discussion of Aim 1

2.4.1. Synthesis of symmetrical N-heterocyclic carbene ligands [18]

The diimine (1) is reacted with allylmagnesium chloride, in THF for 24 hours, to produce diamine (2) in 30% yield according to a procedure by Pleixats [18] (reaction scheme 5).

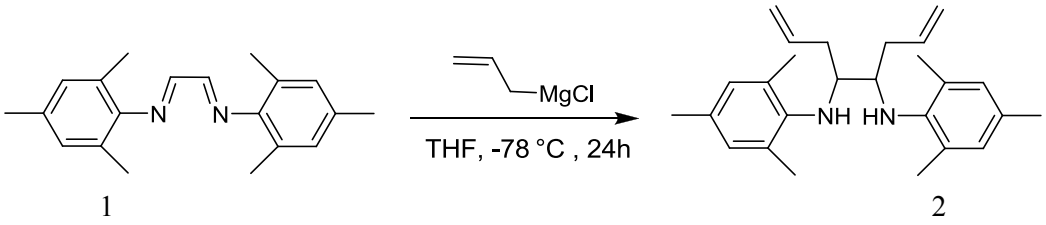

Scheme 5 Reduction of diimine to diamine using the Grignard reagent; Allylmagnesium chloride.

The diamine 2 is stirred at 140 °C for 5 hours in triethylorthoformate, in the presence of ammonium chloride to obtain imidazolium salt 3 in 60% yield. However, there were some problems regarding the synthesis of the imidazolium salt 3. Long reaction times, led to lower yield (30%) of the imidazolium salt 3. In the NMR spectrum an additional $-OCH_2CH_3$ signals were observed which might come from the residual $HC(OEt)_3$ of from some by-products derived by this compound. To eliminate this problem, the reaction time was reduced to 5 hours. After cooling the reaction vessel to room temperature, minimum amount of THF was added to precipitate the excess of ammonium chloride salt and the mixture is filtered. The product is washed several times with pentane to afford 3 in 60% yield as shown in the scheme below.

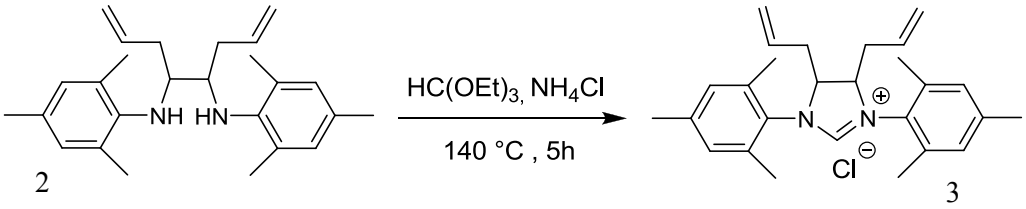

Scheme 6 Ring closing reaction of the diamine.

The imidazolium salt 3 was reacted with $HSiCl_3$ in a Pt-catalyzed hydrosilylation reaction to afford 4a. The product 4a was not isolated where excess ethanol was added to obtain 4b in 85% yield as shown in the scheme below.

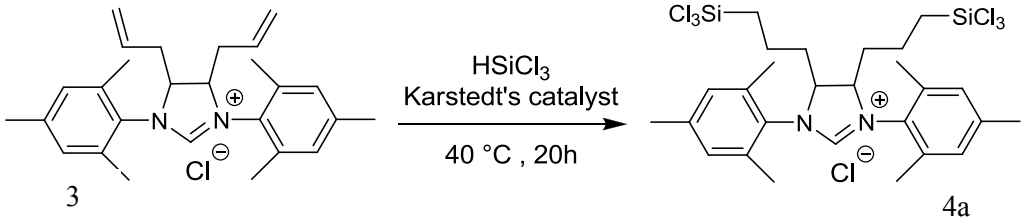

Scheme 7 Hydrosilylation reaction of imidazolinium salt 3.

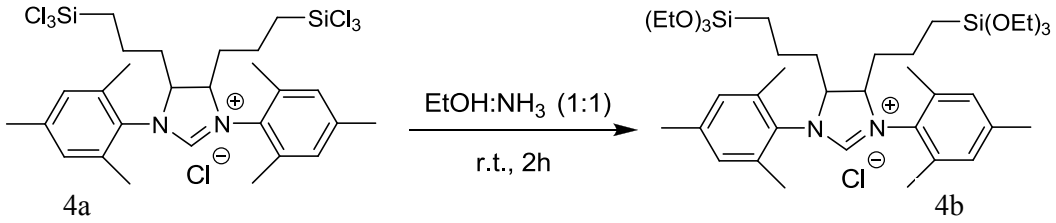

Scheme 8 Substitution of chloride groups with ethanolate groups to obtain the desired imidazolinium salt 4b.

2.4.2. Synthesis of unsymmetrical N-hetrocyclic carbene ligands [19]

Synthesis of unsymmetrical, functionalized NHC ligand was done by undergoing several reaction steps. First of all, 2,4,6-trimethylaniline was reacted with 2-bromoethylamine hydrobromide to give N- (2,4,6-trimethylphenyl)-1,2-diaminoethane 5 in 70% yield as shown in the shceme below.

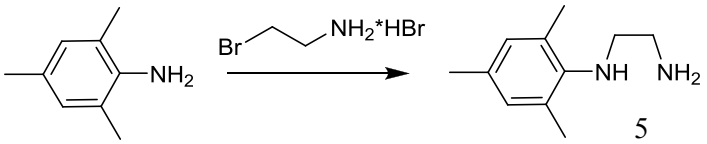

Scheme 9 Synthesis of N- (2, 4,6- Trimethylphenyl)-1,2-diaminoethane [19].

N- (2,4,6- Trimethylphenyl)-1,2-diaminoethane 5 was reacted with triethylorthoformate using PTSA as catalyst at 140 °C to afford 1-mesitylimidazole 6 in 73% yield (scheme 10).

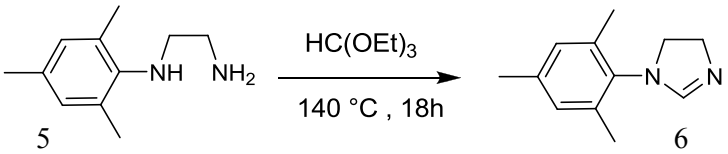

Scheme 10 Ring closing reaction of N- (2,4,6- Trimethylphenyl)-1,2-diaminoethane.

To obtain the desired, functionalized imidazolinium salt bearing –Si(OEt)$_3$ groups, 1-mesitylimidazole 6 was reacted with 3-chloropropyltriisopropoxysilane to afford compound 7 in 80% yield as shown in scheme 11 below.

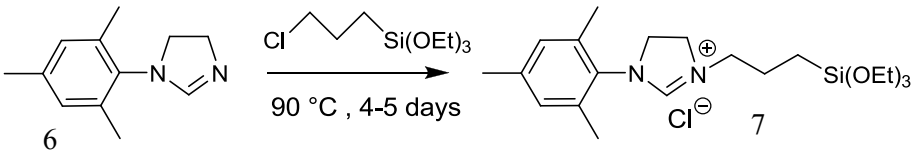

Scheme 11 Synthesis of imidazolinium salt 7: 1-Mesityl-3-(3-(triethoxysilyl)propyl)-4,5-dihydro-1H-imidazol-3-imidazolium chloride.

Another similar imidazolinium salt was synthesized bearing functional isopropoxy groups, which is believed to be more stable. Firstly, to afford compound 9, 3-Chlorpropyltriisopropoxysilane 8 was synthesized. The reaction was held in dry and degassed diethyl ether, at room temperature. In this case, the alkylation of mesityl imidazole 6 did not work in one step reaction, just in the case with trialkoxysilylalkylchloride as shown in scheme 11 above. Another reaction route was used, where the chlorine atom was exchanged to iodine to provide a more reactive alkyl chain. Finally, 3-Iodopropyltriisopropoxysilane 9 was reacted with 6 in dry toluene, and the reaction was refluxed for 48 hours to give 1-Mesityl-3-(3-(triisopropoxysilyl)propyl)-4,5-dihydro-1H-imidazol-3-imidazolium iodide 10 in 75% yield (scheme 12).

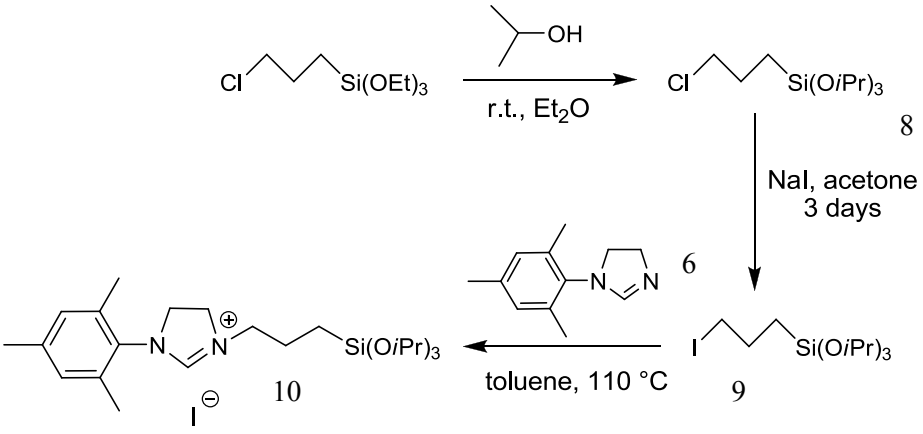

Scheme 12 Synthesis of imidazolinium salt 10: 1-Mesityl-3-(3-(triisopropoxysilyl)propyl)-4,5-dihydro-1H-imidazol-3-imidazolium iodide.

2.4.3. Synthesis of Grubbs Hoveyda 1st generation catalyst

Complex 11 was reacted with isopropoxy styrene, using amberlyst resin in dry form, to give Grubbs Hoveyda 1st generation catalyst 12 as a dark brown powder, in 93% yield. To achieve high yields, the reaction time was prolonged by 30 minutes in comparison to literature procedure as shown in the scheme 14 [20].

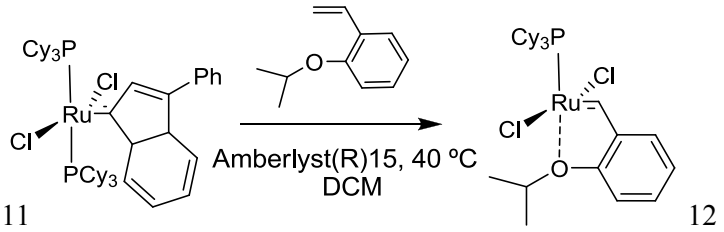

Scheme 13 Synthesis of Grubbs Hoveyda 1st generation catalyst 12.

2.4.4. Synthesis of functionalized Grubbs Hoveyda 2nd generation type catalyst [18]

Imidazolinium salt 4b was reacted with complex 12 to give Grubbs Hoveyda 2nd generation type catalyst 13 in poor yield. In addition, the catalyst 13 was not stable at room temperature and it was stored at -30 °C, under inert atmosphere. Grubbs Hoveyda 1st generation catalyst 12 was dissolved in toluene in a Schlenk flask under argon atmosphere and it was added via cannula to 4b, treated with KHMDS for 30 min at room temperature. The mixture is heated to 80 ºC and let to stir for 3 h to afford complex 13 in 20% yield as shown in the scheme below.

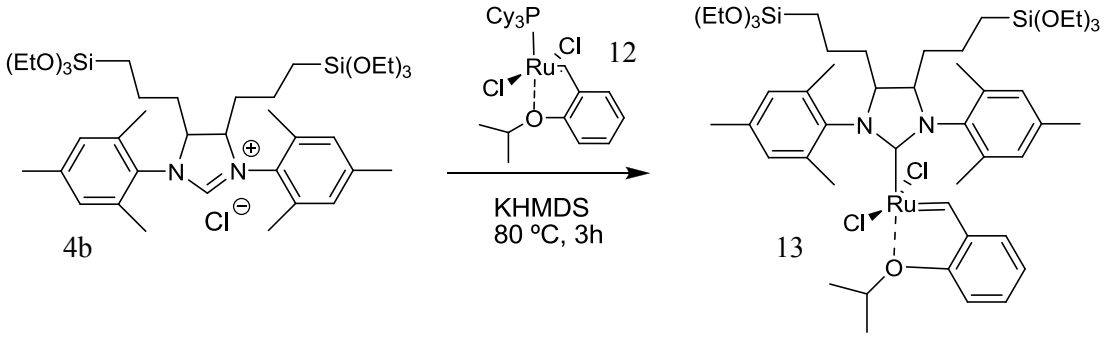

Scheme 14 Synthesis of functionalized Ruthenium catalyst 13.

Since complex 13 was decomposed via purification using column chromatography, the complex was purified using flash chromatography and the silica gel used was SiliCycle P60 R12030B of particle size 60.0 – 75.0 μm. The eluent used was a mixture of EtOAc : Cyclohexane. To avoid any decomposition of the complex from the water content in the used solvents, EtOAc was distilled before use, whereas cyclohexane was dried over molecular sieves. To scale up the product 13, the reaction was repeated several times, in small scales. Large scale reactions did not provide better yields. In the ^{1}H-NMR spectrum the characteristic peak of this complex appears at 16.50 ppm.

2.5. Preparation of catalytically active switchable surfaces

Functionalized NHC ligands in situ with ferrocene containing polymers, were anchored on solid support, silica particles, having a size in the range of 35-40 nm. Finally, Grubbs 1st generation catalyst was introduced to produce the desired complex on the surface of the particle.

2.5.1. Preparation of ruthenium immobilized silica supported catalyst

Firstly, the –Si(OEt)$_3$ bearing imidazolinium salts were immobilized on the surface of silica nanoparticles. The silica particles were dispersed in a solvent mixture of EtOH: NH_3: H_2O (1:1:1 by volume), characterized with a thick core shell of hydroxyl groups. The NHC ligands were bound on silica surface while occupying the silanol groups on the surface as shown in the figure below.

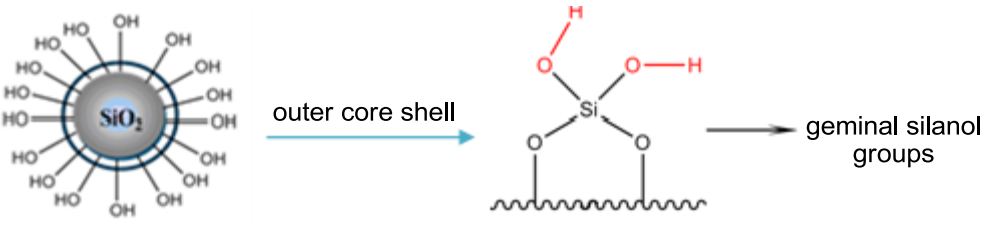

Figure 13 Silica particles with outer core shell, bearing functional –OH groups on the surface.

The NHC ligands were immobilized on the silica surface using two different methods:

Method 1: in this case, the NHC ligand was dissolved in the solvent mixture EtOH : NH_3 : H_2O, where the particles were dispersed. Later on, the system was left to reflux for 48 h. After this step, the particles were dried very well to ensure that there was no water content which could be a future obstacle in formation of the ruthenium complex on the surface.

Method 2: the solvent mixture EtOH : NH_3 : H_2O was evaporated and the particles were dried for 24 h under vacuum, at 50 °C. Higher temperature conditions were not taken into consideration since at higher temperatures the particles could agglomerate and lose their characteristic properties. Finally, the particles were dispersed in THF and were used for immobilization. The imidazolinium salt was immobilized on silica surface via both –Si(OEt)$_3$ groups, but for easier interpretation the immobilization is shown as in the figure 14 below.

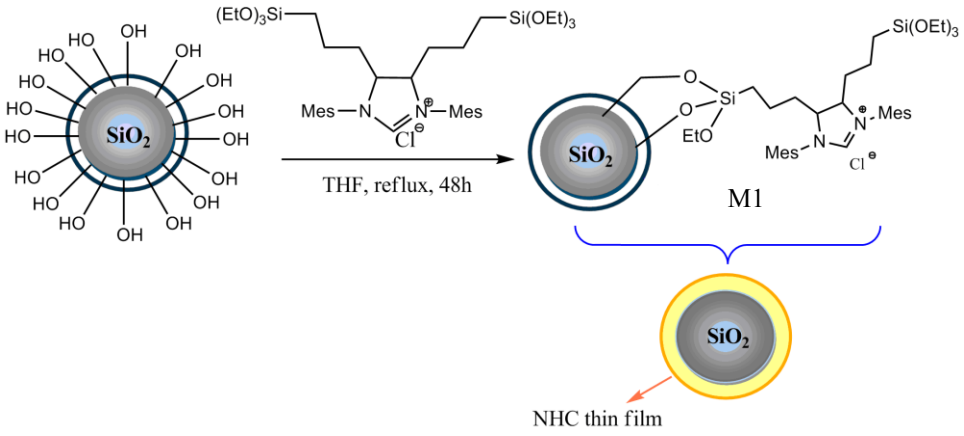

Figure 14 Immobilization of symmetrical NHC ligand on silica particles.

Silica particles were dispersed in dry THF under argon atmosphere. The NHC ligand was dissolved in THF, and this solution was added to the dispersed particles in THF, while continuous stirring. The system was left to reflux for 48 h under argon atmosphere. As the system was brought to room temperature, the particles were centrifuged out of the THF, and washed several times with THF, then with MeOH and finally with Et_2O, until a clear solvent was obtained after the washing (the first two washings result in beige-yellowish colored solvent).

The particles are then dried under vacuum at 100 ºC for 24 h, to make sure that they are free of water and ready to be used for the next immobilization step.

Material M1 was then used for further immobilization steps, to produce the final complex on the silica surface. The M1 particles were dispersed in dry toluene. Normal bare particles were partially dispersed in toluene, but in the case where the particles are modified, there is no difficulty regarding the dispersion in toluene. The dispersed particles were treated with 0.7 M KHMDS (Potassium bis (trimethylsilyl) amide, in toluene) solution which was used to generate the carbene anchored on the silica surface. After 30 min reaction time, Grubbs 1st generation catalyst, 0.049 mmol, (dissolved in a few ml of toluene in another schlenk flask) was added via cannula to the system of dispersed particles, in continuous stirring, under argon atmosphere. The system was left to stir at room temperature for 16 h as shown in the figure below.

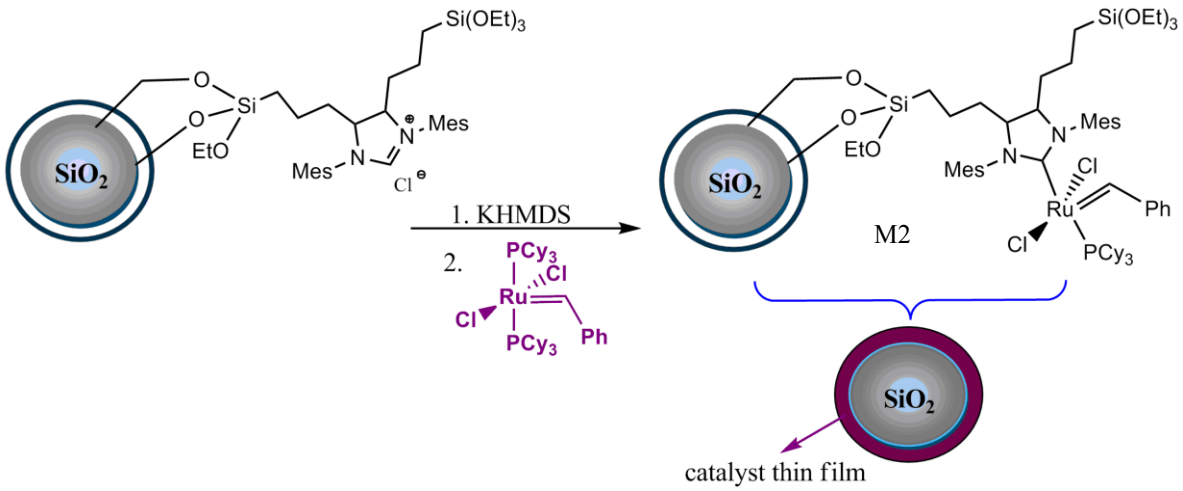

Figure 15 Formation of the symmetrical NHC-Ruthenium catalyst on the silica surface.

After 16 h of stirring, the particles were centrifuged and washed several times with toluene and finally with Et_2O, until a clear solvent was obtained after the centrifugation, in order to get rid of the physisorbed material on the particle surface. The unsymmetrical imidazolinium salts was immobilized on silica particles using the same procedure as in the case with symmetrical imidazolinium salt as shown in the figure 16.

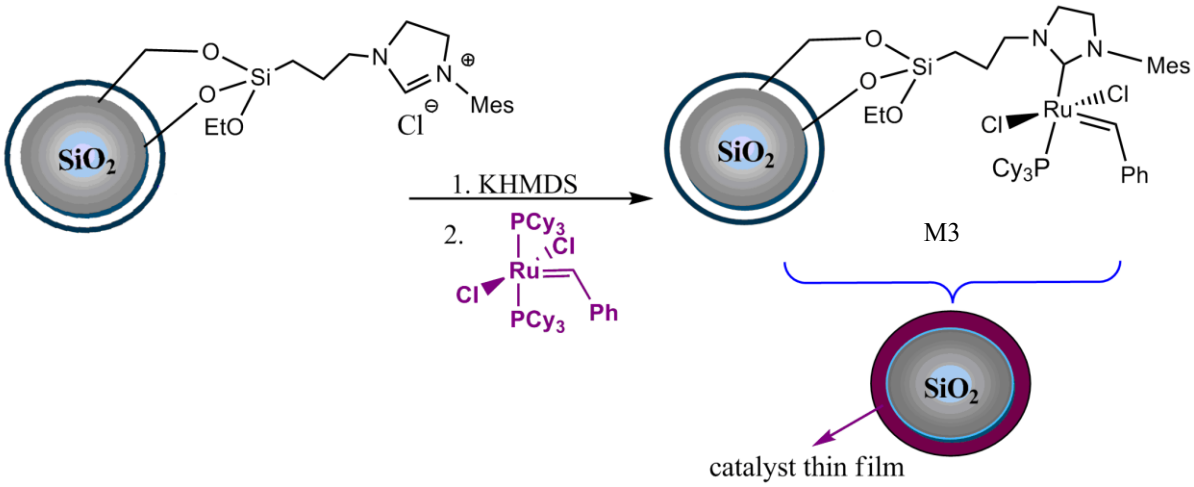

Figure 16 Formation of the unsymmetrical NHC-Ruthenium catalyst on the silica surface.

Grubbs Hoveyda 2nd generation type catalyst (as shown in figure 17) was immobilized on silica particles as well. The immobilization was done under argon atmosphere, using dry and degassed benzene. The silica particles were dried under vacuum at 50 ºC for 24 h. Unmodified silica particles were dispersed in dry benzene. In another Schlenk flask 0.0083 mmol of the Grubbs Hoveyda 2nd generation type catalyst was dissolved in 1 ml of dry benzene, and finally the catalyst was added to the dispersed silica in benzene, via cannula under argon atmosphere.

The mixture was left to stir for 48 h at room temperature. Finally, the modified silica particles were centrifuged and washed several times with benzene finally with Et_2O, and were left to dry under vacuum for 24 h before application in ring opening metathesis polymerization as shown in the figure below.

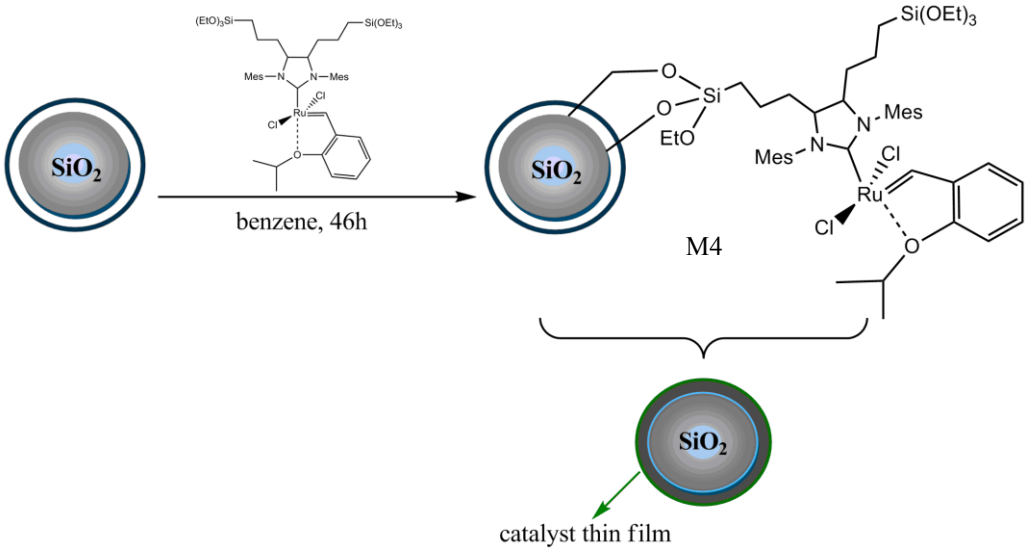

Figure 17 Immobilization of symmetrical NHC-Grubbs Hoveyda 2nd generation type complex on silica.

2.5.2. Codeposition of ferrocene containing polymers and ruthenium catalyst on silica particles

2.5.2.1. Codeposition of PvFc-TEOS polymer (polyvinylferrocene TEOS) and unsymmetrical/ symmetrical NHC-ruthenium catalyst on silica

Silica particles were dried under vacuum, were dirspersed in THF. Polyvinylferrocene-TEOS polymers used for co-deposition had a molecular weight of 1.51 kDa. The polymers together with the symmetrical imidazolinium salt were added to the dispersed silica particles in THF and the mixture was left to reflux for 48 h.

After cooling the system to room temperature, the particles were centrifuged out of the THF, and washed several times with THF finally with Et_2O, until a clear solvent was obtained after washing (the first two washings result in yellowish colored solvent). The particles (M5, figure 18) were then dried under vacuum at 100 °C for 24 h, to make sure that they were free of solvent and ready to be used for the next immobilization step.

Particle type M5 were dispersed in toluene in ultrasonic bath for a few minutes where they were treated with KHMDS and then Grubbs 1st generation catalyst was added and the reaction was left to stir at room temperature for 16 h. The reaction was held under argon atmosphere, at room temperature. Finally, the particles were centrifuged and washed several times with toluene, dichloromethane and finally with Et_2O, until a clear solvent was obtained after washing. Due to the small size of the particles, 40 nm, the particles were not Soxhlet extracted, since the particles could penetrate through the pores of the thimble. The final step included drying of particles under vacuum for 24 h, to obtain particles M6 as shown in the figure 18 below.

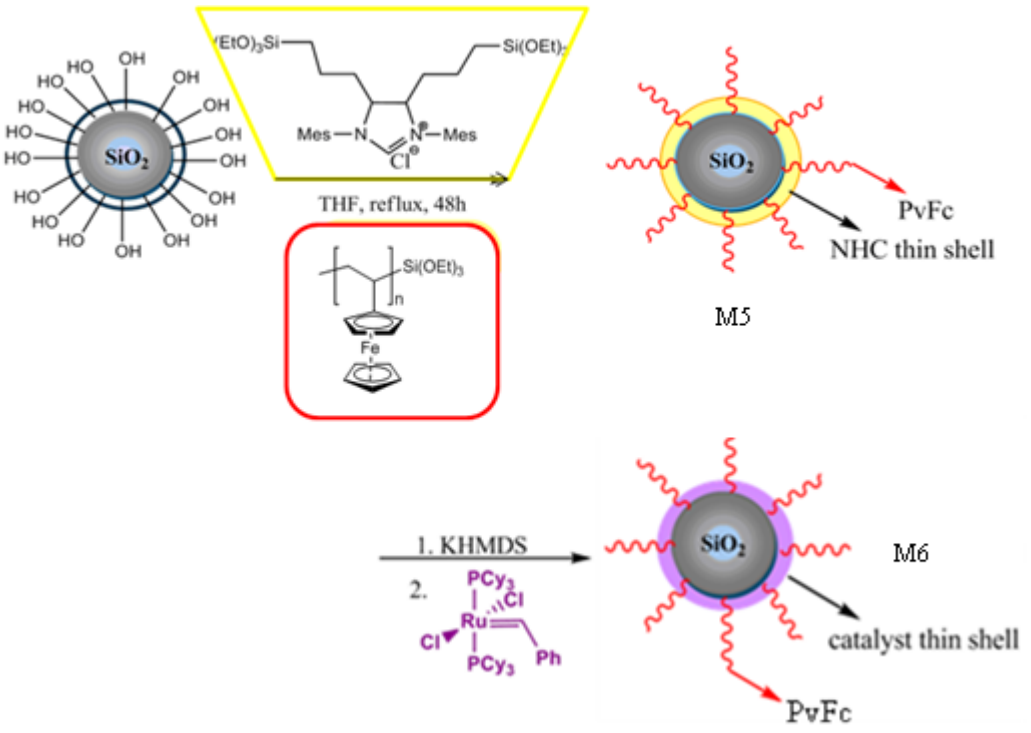

Figure 18 Co-deposition of polyvinylferrocene-TEOS and Ruthenium catalyst on silica articles.

The same procedure was used for the co-deposition of the unsymmetrical NHC-Ruthenium complex and polyvinylferrocene-TEOS on the silica particles.

Different from previously described immobilizations, in this case dry and degassed benzene was used as a solvent, so that the complex does not decompose during the long time stirring in solution. Dried silica particles were dispersed in the solvent benzene. The ruthenium catalyst was dissolved in benzene as well as PvFc-TEOS and the solutions were added under argon atmosphere via cannula to the dispersed particles. The mixture was mixed for 46 h, and finally the particles were centrifuged and washed with benzene, dichloromethane and finally with ether in order to get rid of the physisorbed material on the particles (M7 figure 19). Finally, M7 was dried under vacuum to be used in ring closing metathesis reactions.

2.5.2.2. Codeposition of PvFc polymer and symmetrical NHC-Grubbs Hoveyda 2nd generation type catalyst

Silica particles were dried under vacuum for a long time before used. As mentioned previously, high temperatures were not used for drying since at higher temperatures the particles can agglomerate and this can affect the characteristic properties of the particles. After drying, unmodified silica particles were dispersed in dry benzene, under argon atmosphere and they were left in ultrasonic bath so that the particles can disperse in the solvent. The Ruthenium catalyst (represented in green color-as thin shell on silica surface), was dissolved in minimum amount of benzene in a schlenk flask. The same was applied to polyvinylferrocene-TEOS (the red colored projections represented in figure 19), which was dissolved in another schlenk flask. Finally, the dissolved polymer and catalyst were added via cannula while vigorous stirring, to the dispersed particles in benzene.

The particles were left to stir at room temperature for 46 h. Afterwards, the particles were centrifuged and washed several times with benzene, then with dichloromethane and finally with ether.

To get rid of the physisorbed material, the silica particles are washed well, until a colorless solvent was obtained. The last step was particle drying, where they were dried at room temperature under vacuum for 24 h, to obtain material M7 as shown in the figure below.

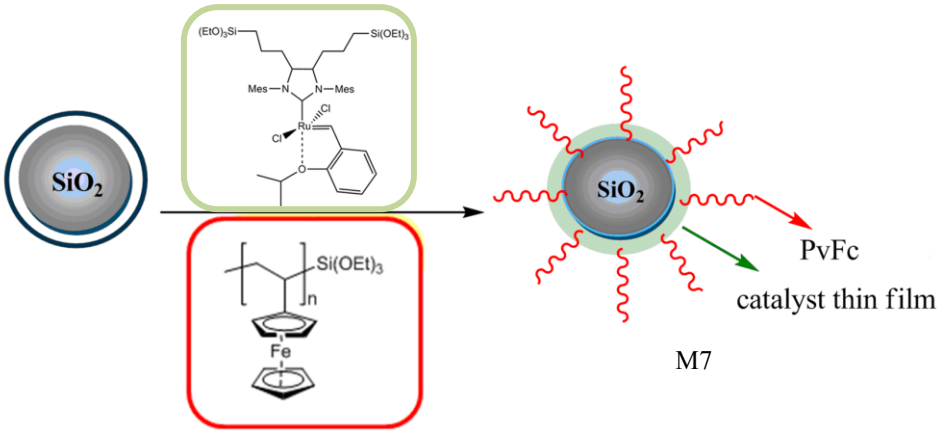

Figure 19 Co-deposition of polyvinylferrocene-TEOS and Grubbs Hoveyda 2nd generation type catalyst on silica surface.

2.5.3. Oxidation of functionalized silica nanoparticles with $[CpFe(C_5H_4Ac)]BF_4$

The primary target of the project was to co-deposit Grubbs-type catalysts and ferrocene polymers on silica nanoparticles. Secondly, the catalytic activity was going to be modulated via redox-reactions at the ferrocene polymers. Oxidation of immobilized ferrocene polymers was expected to lead to an expansion of the polymers. As a result, the catalytic center remains buried in the polymer on the nanoparticle and no more accessible to olefin metathesis substrate. To achieve this goal, the particles were oxidized with acetylferrocenium tetrafuoroborate, as represented in the figure 20 below. In the figure 20, the light orange colored layer on the particles (M6, figure 20) represents the ferrocene containing polymer layer, whereas the pancake like structures collapsed on the surface of the nanopartilces represent the polymer projections. The black stars represent the Grubbs 2nd generation type catalyst bound on the surface of the particles as well. After the oxidation of the ferrocene unit with acetylferrocenium tetrafluoroborate, the polymer chains are elongated due to swelling of the polymer layer (particle M8, figure 20). In this case it was expected that the catalyst (represented as black stars), were embedded in the polymer layer, though no more accessible to the olefin substrate to perform ring opening metathesis polymerization.

2.5.3.1. Oxidation of materials M3 and M6 with $[CpFe(C_5H_4Ac)]BF_4$

Materials M3 and M6 as represented in the earlier figures (16 and 18), were oxidized with an excess of acetylferrocenium tetrafluoroborate as shown in the figure below. Finally, the particles were dried for 24 h under vacuum before used in ring opening metathesis polymerization reactions.

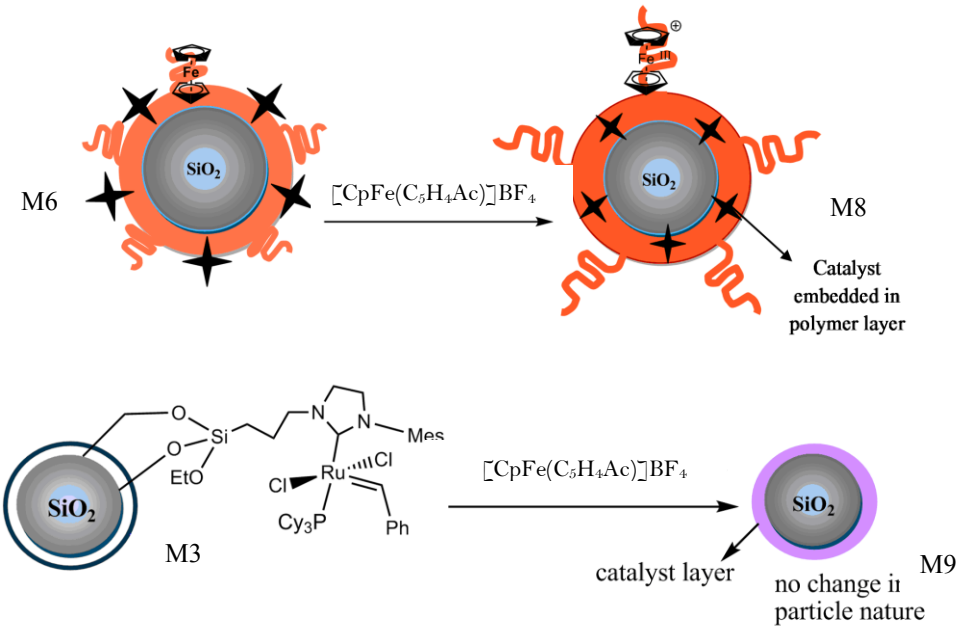

Figure 20 Oxidation of particles M6 and M3 with acetylferrocenium tetrafluoroborate.

Particles M3 represent the type of particles which are functionalized only with Ruthenium complex, without the polymer layer. Oxidation of such particles was done as a test reaction, to prove that the oxidizing agent

did not affect the ruthenium catalyst on silica surface and did not decrease the catalytic activity of the particles. To prove this, the particles were tested in ring opening metathesis reaction of the monomer norbornene. The figure below shown the oxidized particles dispersed in THF as well as the bare silica nanoparticles and the polyvinyl ferrocene-grafted silica nanoparticles as shown in the figure below.

Figure 21 Dispersion of particles in THF: oxidized particles (M8, left), bare SiO2 (middle) and PvFc-grafted particles (M6, right).

2.5.4. Olefin metathesis using supported ruthenium catalyst

2.5.4.1. Ring opening metathesis polymerization with surface bound catalysts

For the ring opening metathesis polymerization reactions, the monomer norbornene was used. The activity of particles M3, M6, M8 and M9 was tested. The particles were first dispersed in dichloromethane and kept for 2 min in ultrasonic bath. The monomer was dissolved in another schlenk flask and added via cannula to the dispersed particles. For this type of reactions, 0.6 M of norbornene was used and 20 mg of particles per milliliter solvent. After 1 h reaction time the polymers was cleaved from the reaction by a mixture of methanol:ethyl vinyl ether (MeOH:EVE), and the polymers were dried under vacuum.

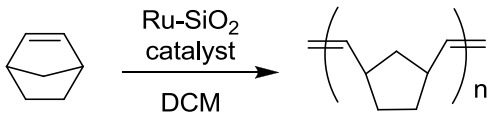

Scheme 15 Ring opening polymerization of norbornene using surface bound ruthenium catalysts.

sample	$[NB]_0$/ M	$[SiO_2]$/ mg ml^{-1}	observation
M2	0.6	20	Gel-like after 10 min
M6	0.6	20	Gel-like after 1 h
M8	-	-	No increase in viscosity after 1h
M9	-	-	Viscous after 30 min

Table 1 ROMP of norbornene using particles M2, M6, M8 and M9.

In table 1, the polymerization behavior of norbornene is described, depending on the sample type, at same monomer initial concentration. After 10 min, the final solution of the sample M3 was gel-like, where only Grubbs second generation type catalyst is immobilized on the silica surface. Sample M6, represents the in situ immobilization of polyvinylferrocene-TEOS and ruthenium Grubbs 2nd generation catalyst. After one hour the final solution from this sample was again gel-like, just like in the case with sample M3. Sample M9 represents the particles modified only with Grubbs 2nd generation type catalyst, oxidized with acetylferrocenium tetrafluoroborate. The final solution from this sample is viscous after 30 min. Finally, the behavior of the sample where in situ immobilization of polyvinylferrocene-TEOS and Ruthenium Grubbs 2nd generation catalyst was anchored on silica surface and the particles were oxidized with acetylferrocenium tetrafluoroborate. From this sample type, no increase of viscosity was observed even after one hour.

After the end of the polymerization, the polymer from each trial with different sample types was uncoupled with ethyl vinyl ether, so that it could be further characterized. From the sample solutions: M3, M6 and M9, polymer structure was obtained, whereas from the particles M8 the modified particles were reisolated via centrifugation and no polymer structure. The cleaved polynorbornene structures were characterized with size exclusion chromatography and its molecular weight was determined.

From the sample M6, the molecular weight of the polymer was found to be $1.8397 \cdot 10^6$ g/mol. The molecular weight of the polymer cleaved from the sample M3 was found to be $2.64 \cdot 10^5$ g/mol. Oxidized particles immobilized only with ruthenium catalyst, M9, also showed formation of polymerization where the molecular weight of the polymer was found to be $8.39 \cdot 10^4$ g/mol. Finally, M8 particles were characterized by size exclusion chromatography, but no signal was observed, indicating that no ROMP reaction had occurred. Particles M8 include the co-deposition of polyvinylferrocene-TEOS polymer and the ruthenium catalyst.

2.5.4.2. Reduction of material M8 with L-ascorbic acid

The oxidized particles (material M8), which did not show any ROMP reaction of norbornene monomer, were redirspersed in 1 ml of DCM solution and 56 mg of norbornene monomer was added via stirring. From the reaction mixture samples were taken after 10 min, 30 min as well as after 1 h and they were investigated by GPC but no polymer were obtained. The obtained molecular weights of the structures after ROMP with oxidized particles were: $5.1 \cdot 10^2$ g/mol (after 10 min), $3.2 \cdot 10^2$ g/ mol (after 30 min) and $5.5 \cdot 10^2$ g/ mol (after 1 h).

After this point, excess of L-ascorbic acid (20 mg) was added and the reaction was left to stir for another hour. After 1 h samples were taken for GPC analysis and this time polymer structure was obtained with molecular weight of $3.2 \cdot 10^6$ g/ mol which clearly indicated that the ferrocene moieties on the outer surface of the particles were reduced, though collapsed toward the surface while giving accessibility of the norbornene monomer to reach the catalyst on the surface and perform the ROMP reaction.

2.5.4.3. Ring closing metathesis with surface bound catalyst

For this type of olefin metathesis reactions, DEDAM (diethyldiallylmalonate) was used as educt, at 60 ºC, where the results are illustrated in table 2.

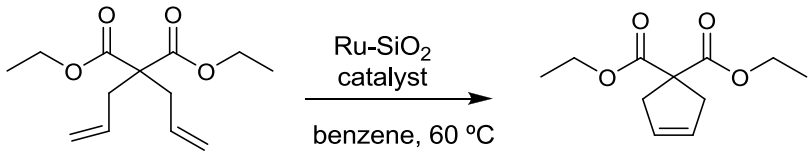

Scheme 16 Ring closing metathesis of DEDAM using surface bound ruthenium catalysts.

Samples; M2, M3, M4 and M7 were tested in RCM reaction, in benzene at 60 ºC. In a dry schelnk flask, 40 mg of particles were dispersed in 2 ml of benzene, and the particles are left in ultrasonic bath for 2 min. The solution was left to adapt to its temperature, 60 ºC, in oil bath for several minutes. Finally, the educt (DEDAM, 0.104 M, 49.7 mg) was added via micropipette, and samples were taken for 2 h, for gas chromatography analysis. The results are given in table 2 below.

sample	[DEDAM]$_0$/ [M]	[SiO2]/ mg ml^{-1}	Conversion (2h, %)
M7	0.104	40	97
M4	0.104	40	83
M3	-	-	8
M2	-	-	3

Table 2 Results of ring closing reaction of DEDAM using immobilized catalyst.

Sample M7 represents the particles where co-deposition of polyvinylferrocene-TEOS polymer and Grubbs Hoveyda 2nd generation type catalyst was done, which showed the highest conversion. M4 sample also showed high conversion, where in this case only the ruthenium catalyst (Grubbs Hoveyda 2nd generation type catalyst) was immobilized. The other samples: M3 and M2 showed relatively low conversion, where not enough amount of Ruthenium catalyst was immobilized.

The sample M3 represents the sample where the unsymmetrical NHC-ligand was immobilized on silica surface and then Grubbs 1st generation catalyst was introduced to form the final desired catalyst on surface: Grubbs 2nd generation type complex.

On the other hand, sample M2 involves the same immobilization process, where the symmetrical NHC-ligand was used for immobilization.

2.6. Characterization of modified particles

2.6.1. Solid state ^{29}Si-NMR measurements

To prove the immobilization of the functionalized NHC-ligand, solid state ^{29}Si-NMR was used. The idea was to see the difference in the types of silanol groups before and after immobilization. Two types of silanol groups are taken into consideration in these measurements: isolated silanol groups as well as vicinal groups. In the isolated silanol groups The Si atom is bound to four oxygen atoms which are bound to other silicon atom. In the case of vicinal silanol groups, the silicon atom is bound to one hydroxyl group and to three oxygen atoms which are bound to other silicon atoms as illustrated in the figure below.

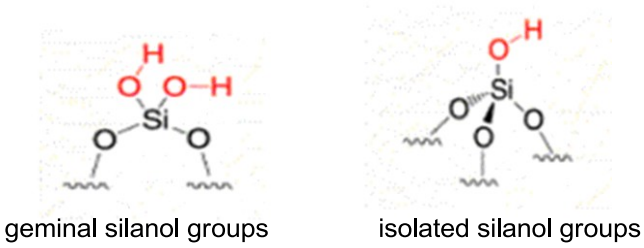

Figure 22 Types of silanol groups investigated on silicon solid NMR: germinal and isolated silanol groups.

These types of silanol groups are denoted as Q3 and Q4, where Q4 represents the vicinal silanol groups; Q3 represents the isolated silanol groups. The silicon NMR of the bare silica particles shows us that the vicinal silanols are dominant as seen in the spectrum below.

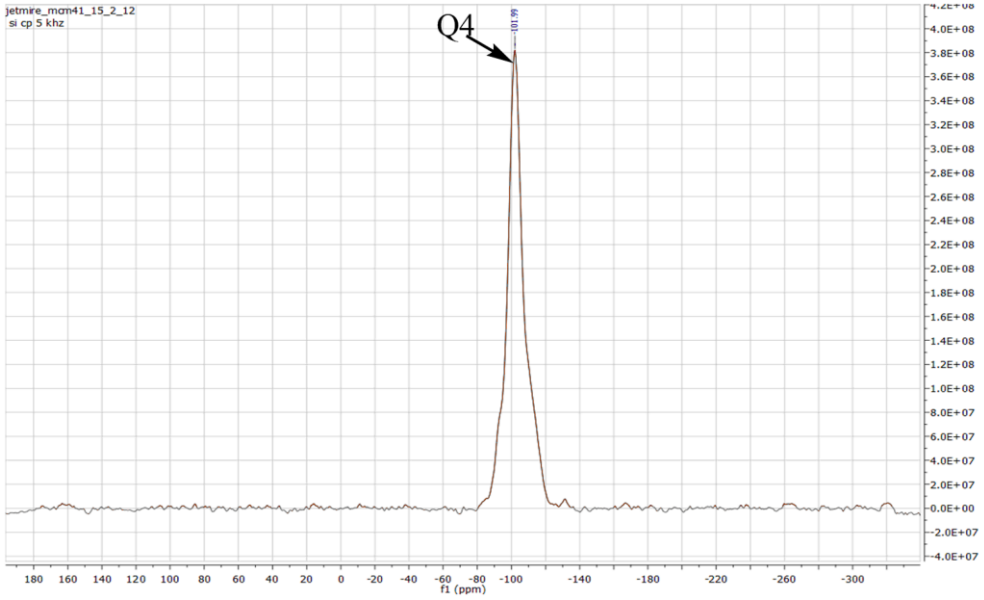

Figure 23 Solid state ^{29}Si-NMR of bare silica particles used for immobilization.

The above spectrum given in figure 12 represents the major peak which belongs to the vicinal silanol groups (Q4), which appear at around -101 ppm. As described in the "results" section, NHC-ligand is immobilized on silica particles. In this case it is expected that the vicinal silanol groups are gradually disappearing, while

being occupied by the NHC-ligand. In this situation, the peak which originates from the isolated silanol groups should increase, which is shown in the spectrum in figure 24.

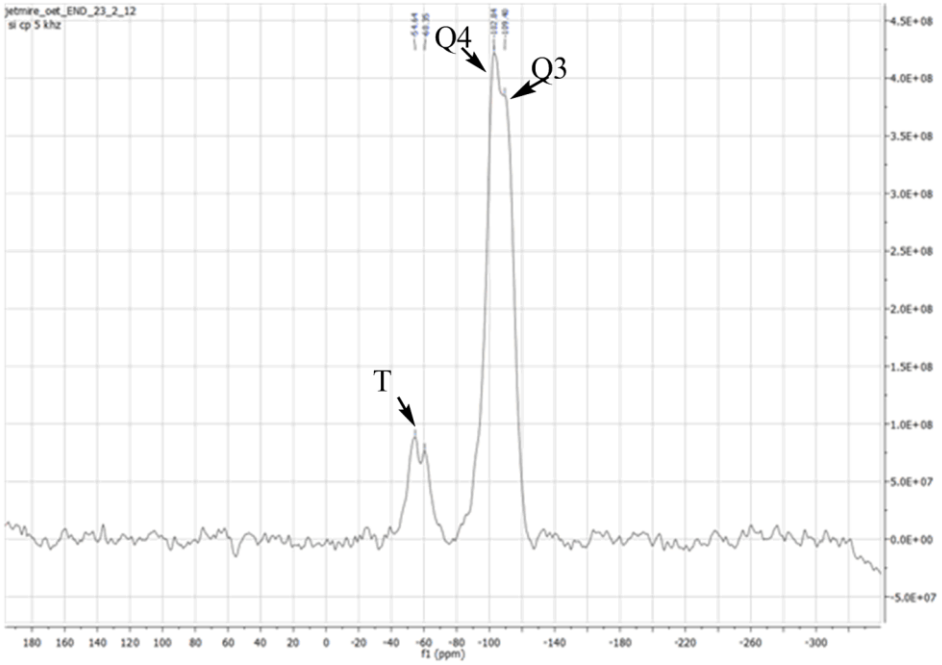

Figure 24 Solid state ^{29}Si-NMR of immobilized silica particles with NHC-ligand, material M1.

As shown in the spectrum above, a new peak shoulder is appearing at around -120 ppm which represents the increase in the isolated silanol groups, indicating that vicinal silanol groups are occupied by the NHC-ligand. In addition, the new appearing peaks (from the T-groups (trifunctional groups)), come from the -Si $(OEt)_3$ of the functionalized NHC-ligand, at around -40 and -60 ppm.

Solid state ^{29}Si-NMR is one of the most useful techniques to characterize the type of the silanol groups on silica particles. As long as the immobilization of the NHC-ligand was proved by solid NMR, for the particles M1 and M5, the Grubbs 1st generation catalyst was immobilized to form the final Grubbs 2nd generation catalyst on the silica surface.

After introducing the ruthenium complex, the presence of ruthenium on the particles was investigated by Secondary electron microscope (SEM) and Energy dispersive X-ray spectroscopy (EDS) to find the percentage of the elements on the scanned area of the modified silica particles.

2.6.2. Secondary electron microscopy (SEM) and Energy dispersive X-ray spectroscopy (EDS) measurements

Using the secondary electron microscope as well as energy dispersive X-ray spectroscopy, the silica particles were investigated before and after immobilization. SEM images were studied to see the any changes in the particle shape before and after immobilization, whereas the EDS measurements showed the elements abundant in the modified particles. First of all, the measurements with the bare silica particles were done in order to

differentiate them easily with the modified particles. The EDS results show peaks from two elements: silicon and oxygen as shown in figure 25.

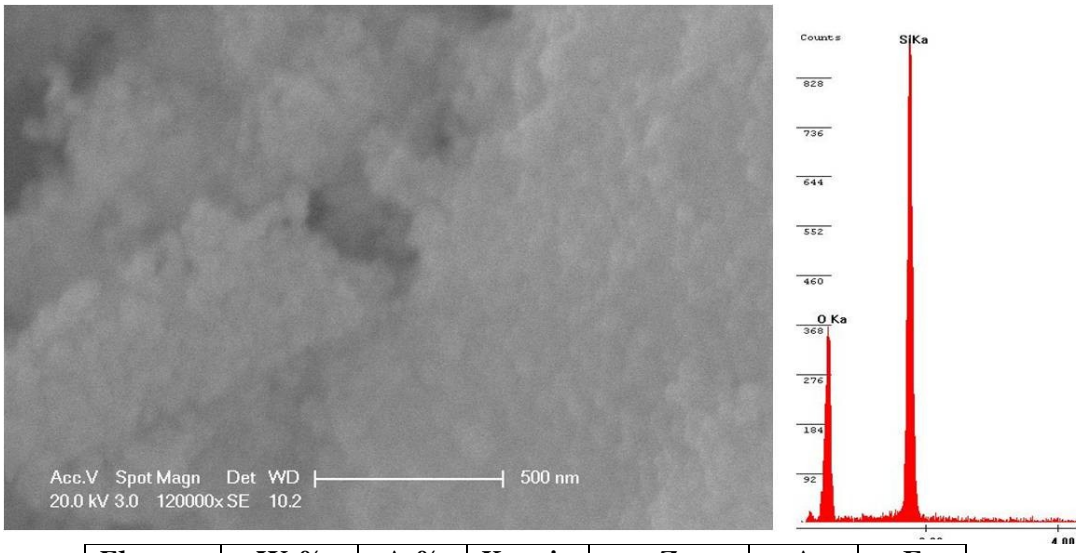

Element	Wt%	At%	K-ratio	Z	A	F
O K	54.18	67.49	0.1993	1.0192	0.3607	1.0005
Si K	45.82	32.51	0.3712	0.9769	0.8292	1.0000
Total	100.00	100.00				
Element	Net Inte.	Bkgd Inte.		Inte. Error	P/ B	
O K	110.56	1.08		2.03	102.71	
Si K	307.63	3.23		1.22	95.26	

Figure 25 SEM image and EDS measurements of the bare silica particles (SiO_2), scale bar 500 nm.

As seen in the EDS spectrum, figure 25, only two peaks are identified from the unmodified particles, which show the presence of the silicon and oxygen in the particles.

The modified silica particles with in situ immobilization of polyvinylferrocene-TEOS polymer as well as symmetrical NHC-ligand were also characterized by SEM/ EDS where at the same working distance (10.2) and at 500 nm, the silica particles were observed to be more globular in structure since as the polymer and NHC-ligand are immobilized the silica outer shell gets bigger, increasing the particle size. When it comes to EDS measurements it is expected to observe additional elements than silicon and oxygen. To prove the polymer immobilization on silica the iron peak should be seen on the EDS spectrum whereas, to prove the anchored NHC-ligand the chlorine peak should be seen.

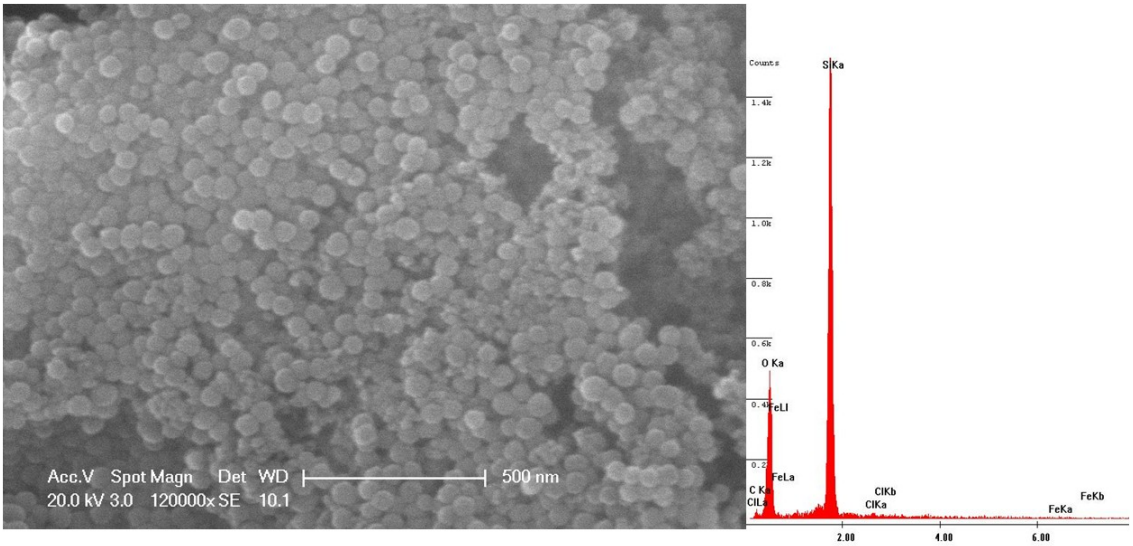

Element	Wt%	At%	K-ratio	Z	A	F
C K	13.10	20.18	0.0183	1.0328	0.1350	1.0005
O K	45.81	52.99	0.1359	1.0155	0.2920	1.0004
Si K	40.04	26.39	0.3282	0.9734	0.8419	1.0001
Cl K	0.48.	0.25	0.0034	0.9150	0.7740	1.0001
Fe K	0.57	0.19	0.0049	0.8572	1.0038	1.0000
Total	100.00	1.22				

Figure 26 SEM image and EDS measurements of the in situ immobilized particles with polymer and NHC-ligand (material M5), scale bar 500 nm.

As shown in the figure 26, the EDS measurements support the fact that both the polyvinylferrocene-TEOS polymers as well as the NHC-ligand are anchored on silica surface since iron and carbon are detected. Secondly, the size of the particles has increased, where we can see more definite, globular structures on the SEM image.

Particles M3 were also investigated by SEM/ EDS. These types of particles as described earlier contain the Grubbs 2nd generation catalyst, so by using EDS measurements, ruthenium content was expected to be detected in order to prove the catalyst anchored on silica particles. In addition, the SEM image, just like in the case where only the polyvinylferrocene-TEOS and NHC-ligand are immobilized, shows an increase in the particle size where at 200 nm scale we can clearly see the globular structure of silica particles. As mentioned earlier, in the case when we have bare silica particles, at 200 nm scale, in the SEM image only rough layers of silica particles could be observed but not globular structures, due to their smaller size than modified particles.

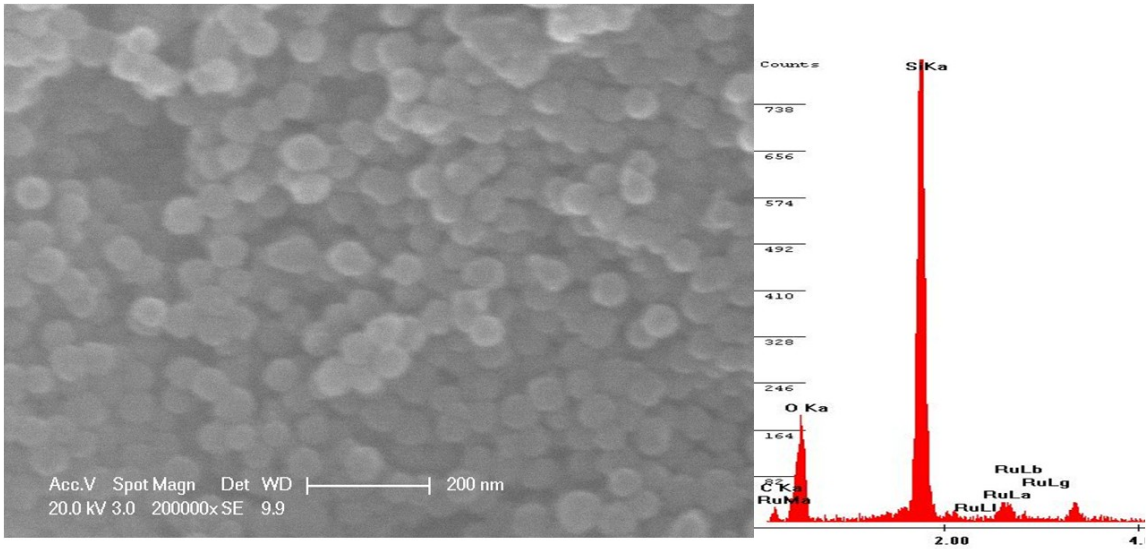

Element	Wt%	At%	K-ratio	Z	A	F
C K	19.13	29.70	0.0202	1.0392	0.1419	1.0003
O K	37.12	43.26	0.0904	1.0208	0.2386	1.0004
Si K	39.54	26.26	0.3289	0.9784	0.8492	1.0009
Ru L	4.21	0.78	0.0293	0.7712	0.9027	1.0000
Total	100.00	100.00				

Element	Net Inte.	Bkgd Inte.	Inte. Error	P/ B
C K	4.46	0.24	9.65	17.14
O K	44.77	0.60	2.93	74.94
Si K	243.66	2.69	10.08	90.71
Ru L	6.67	2.99		2.30

Figure 27 SEM image and EDS measurements of the silica particles immobilized with Grubbs 2nd generation catalyst (material M3), scale bar 200 nm.

As seen from the EDS results above, the particles contain ruthenium, as well carbon which support the presence of the ruthenium catalyst on the particles. Finally, the same measurements were carried for particles M6. Particles M6 represent the in situ immobilization of the polyvinylferrocene-TEOS and the symmetrical NHC-ligand, where afterwards the Grubbs 1st generation catalyst was introduced to the particles to form the Grubbs 2nd generation type complex on silica surface.

In comparison with the material M3, in this sample type, it was expected to detect the iron as an additional element, which result would support the immobilization of the polyvinylferrocene-TEOS polymer on silica particles as shown in figure 28.

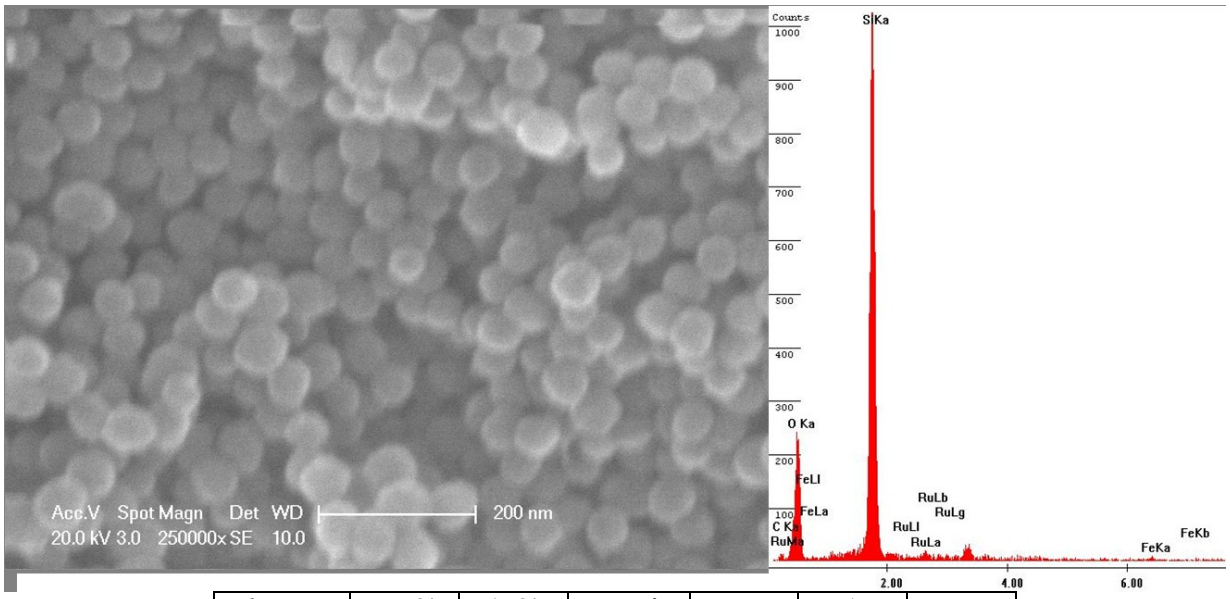

Element	Wt%	At%	K-ratio	Z	A	F
C K	13.74	21.73	0.0183	1.0361	0.1287	1.0004
O K	40.50	48.08	0.1118	1.0188	0.2709	1.0005
Si K	43.83	29.64	0.3627	0.9765	0.8472	1.0002
Ru K	0.73	0.14	0.0049	0.7693	0.8768	1.0000
Fe K	1.20	0.41	0.0104	0.8604	1.0014	1.0000
Total	100.00	100.00				

Figure 28 SEM image and EDS measurements of the silica particles immobilized with Grubbs 2nd generation catalyst as well as with polyvinylferrocene-TEOS polymer (material M6), scale bar 200 nm.

As shown in the figure above, both the Grubbs 2nd generation catalyst and the ferrocene containing polymer are immobilized on silica surface, as ruthenium and iron were detected by EDS measurements.

2.6.3. Transmission electron microscopy measurements (TEM)

Transmittion electron microscopy measurements were performed by Dr. Markus Gallei. For the TEM measurements the particles were dirspersed in THF solution (1mg/ ml) applying the drop-casting method on carbon coated copper grids. From the TEM images the diameter of the particles was revealed to be around 48 nm. The particle polydirsperdity was calculated out of the TEM images to be 1.01 (for 200 particles). The figure below shows the TEM images of particles of type M2 (silica nanoparticles grafted with imidazolium salt), where in comparison to the bare silica particles the images show the formation of newly formed shells of the immobilized imidazolium salt.

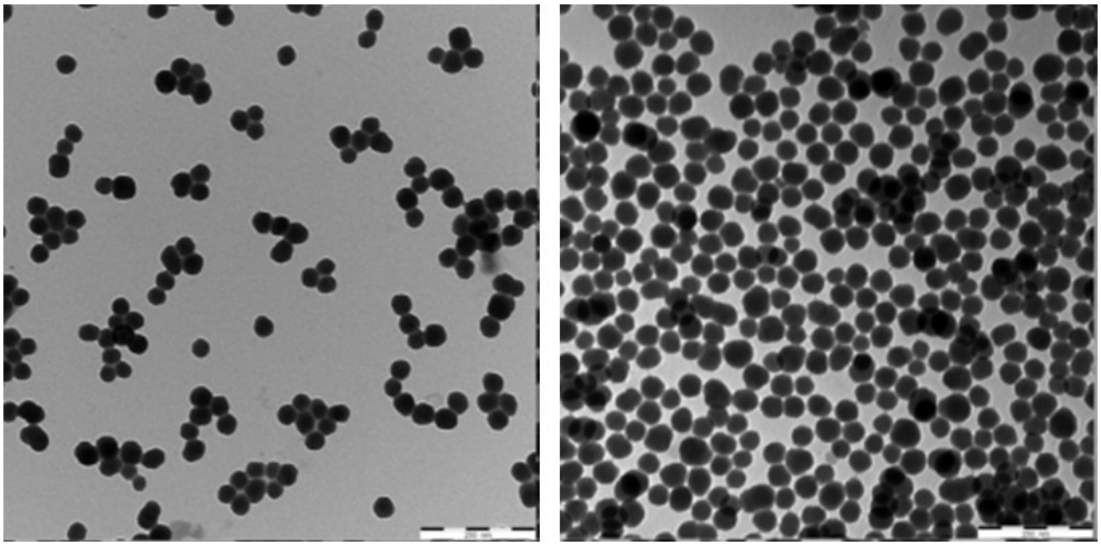

Figure 29 TEM images of bare silica nanoparticles (left) and M1 type particles grafted with imidazolium salt (right), scale bar 250 nm.

The particles of type M6 (grafted with PvFc+Grubbs cat.) were also studied before and after ring opening metathesis polymerization (ROMP) of norbornene. After ROMP reaction on the TEM image it was possible to observe the polymer agglomeration as shell on the outer surface of the particles, which indicates the successful immobilization of the Grubbs catalyst and successful ROMP reaction respectively.

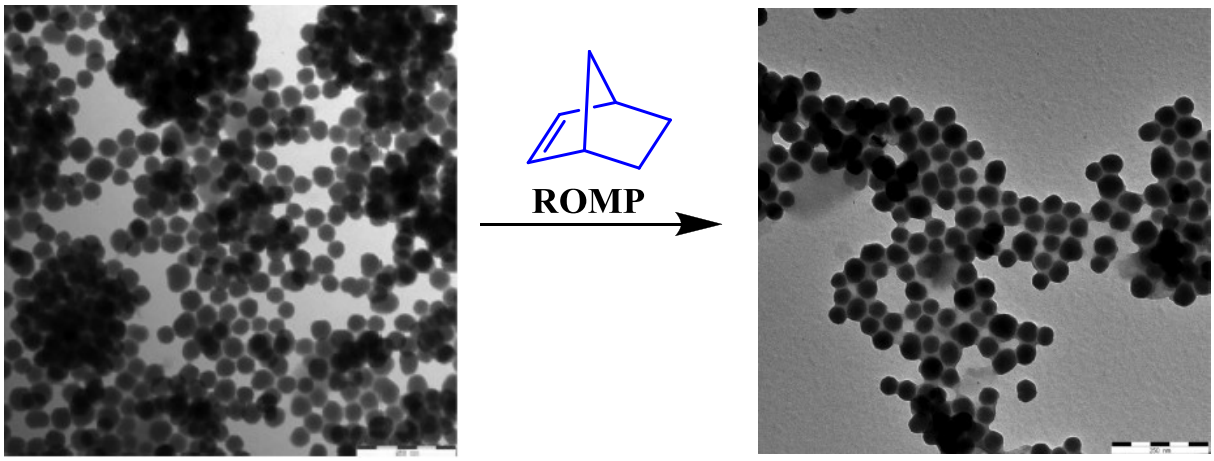

Figure 30 TEM images of bare silica nanoparticles (left) and M1 type particles grafted with imidazolium salt (right), scale bar 200 nm.

2.6.4. Cyclic Voltammetry measurements (CV)

Apart from SEM/ EDS and TEM, cyclic voltammetry studies of the modified silica particles were also carried out, which were done by Dr. Markus Galleri. For a better comparison of the CV results corresponding to modified particles particles, PvFc homopolymer and Grubbs second generation type catalyst were studied as shown in the figure 31, where 1:1 wt % mixture of both PvFc and Grubbs second generation type catalyst was prepared. The scan rate was chosen 100 mVs^{-1}.

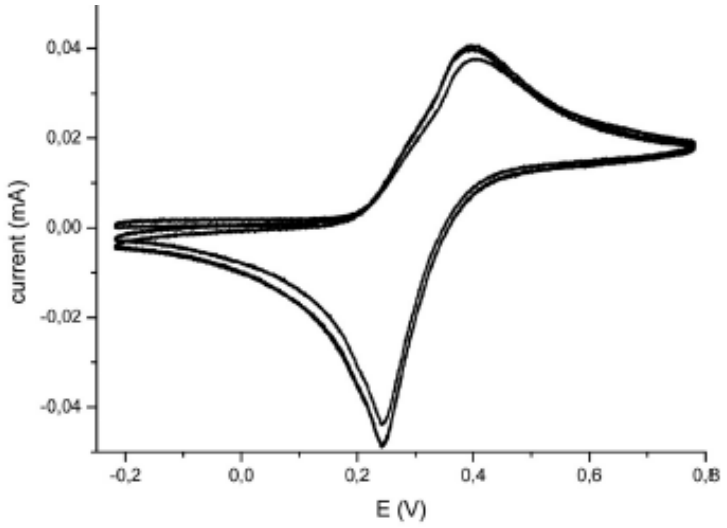

Figure 31 Cyclic voltammogram of PvFc and Grubbs second generation type catalyst (1:1 wt % mixture), at 100 mVs^{-1} scan rate.

As seen from the cyclic voltammogram of the mixture, in the figure above, the signals of both components were close. Cycic voltammoetry measurements of particle dispersion were influenced by diffusion which resulted in the broadening of the signals. For this reason it was decided that the particles were deposited on indium tin oxide surface (ITO) and then cyclic voltammetry measurements were carried out at different scan rates: 20 , 50, 100 and 200 mVs^{-1} as given in the figures below.

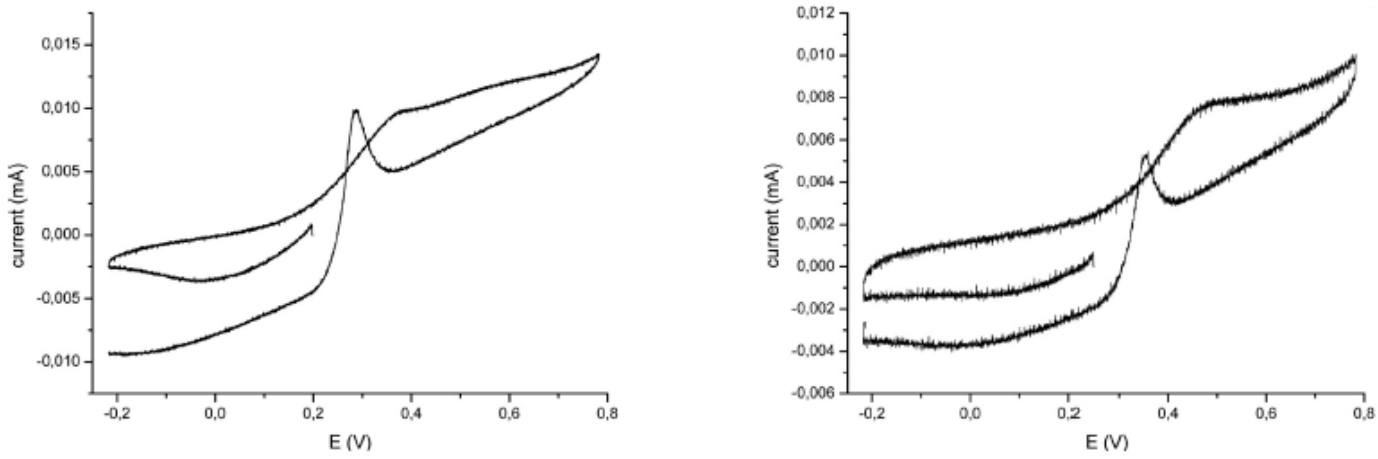

Figure 32 Cyclic voltammogram of PvFc and Grubbs catalyst modified silica nanoparticles, coated on ITO surface: at 20 mVs^{-1} (left) and 50 scan mVs^{-1} (right).

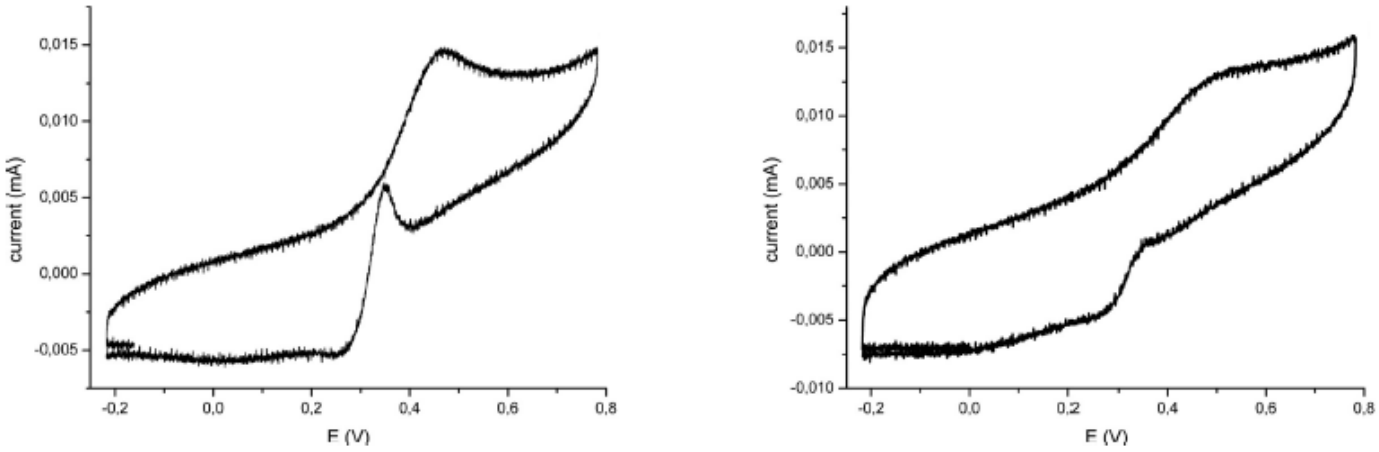

Figure 33 Cyclic voltammogram of PvFc and Grubbs catalyst modified silica nanoparticles, coated on ITO surface: at 100 mVs^{-1} (left) and 200 scan mVs^{-1} (right).

As can be seen in the cyclic voltammograms in the above figures, in comparison to the cyclic voltammogram of PvFc+Grubbs cat mixture, there was observed an additional oxidation signal. The variation of the scan rates (20-200 mVs^{-1}) led to decrease of this signal. The additional peak was observed in the case when both redox-responsive species were attached on the particle surface. As a result it was assumed that there was an electrochemical communication between the ferrocenium and the oxidized ruthenium during the reductive half cycle. To sum up, again from the cyclic voltammetry measurements we had a clue of the presence of both iron and ruthenium immobilized on the particle surface.

2.6.5. Dynamic light scattering measurements (DLS)

The dynamic light scattering measurements were done in cooperation with the institute of condensed matter physics, Technical University of Darmstadt, by Christina Lederle. As mention in the very beginning about the objective of this work, by oxidation of the particles the PvFc polymers on the surface are oxidized by showing swelling behavior though increasing the diameter of the particles. In this manner, as the polymer layer swells, they catalyst immobilized on the surface is embedded on the polymer layer and is no more accessible to the monomer molecule for ROMP reaction. On the other hand, when particles are reduced, the polymer layer shrink though decreasing in particle diameter.

In order to prove the above mentioned mechanism, dynamic light scattering (DLS) measurements were done in cooperation with the Physics department. Dynamic light scattering is a technique used in order to determine the size distribution profile of small particles in suspension.

Previous studies of surface attached PvFc-containing polymers showed a tremendous increase in hydrodynamic shell diameter after oxidation [17]. The DLS of bare silica particles, PvFc-polymer grafted silica particles as well as PvFc-oxidized particles was measured for comparison. In the figure 34, the measured intensity of the autocorrelation function (g2 (t, q) - 1) is given for the PvFc-grafted silica nanoparticles, where the autocorrelation function was found to be close to exponential, as seen from the observed polydispersities ranging from 1.6 % to 3.1 %.

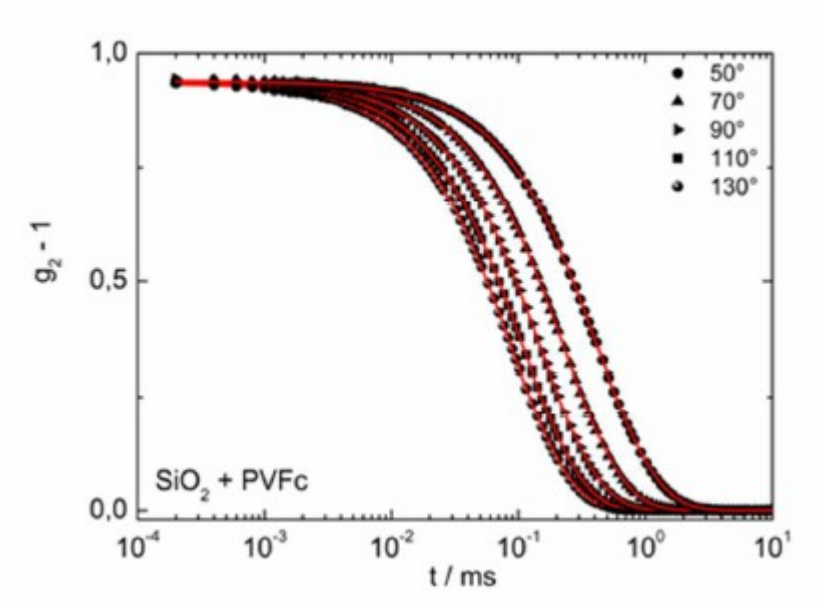

Figure 34 Intensity autocorrelation functions g2 (t, q) – 1, for PvFc-grafted silica nanoparticles. The fittings were done using cumulant method.

From the DLS results of nonmodified silica particles, PvFc-grafted particles as well as PvFc-oxidized silica nanoparticles, we could conclude that the bare silica particles had a dynamic radius of 45 nm. Even thoug, the particle aggregation could play a role in thid diameter, a swelling behavious of the PvFc corona chains could be obtained after oxidation. After particle grafting with PvFc-TEOS the radius of the particles increased by 6 nm. Furthermore, after oxidation of PvFc-grafted particles, the radius increase was increased by an additional of 10 nm of the hydrodynamic radius. The result are illustrated in the plot below.

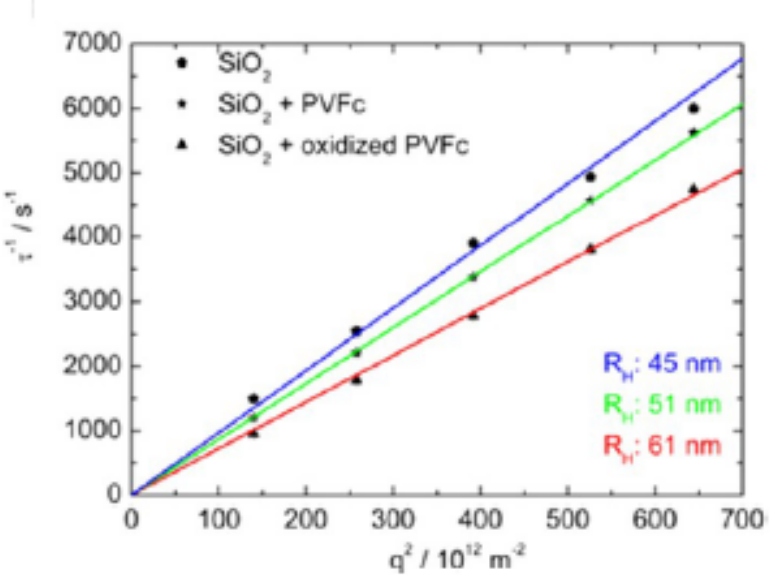

Figure 35 Dependency of inverse relaxation times on q2 to determine the diffusion coefficient and hydrodynamic radii for PvFc-particles: bare (blue line), PvFc-grafted (green line), oxidized PvFc-grafted (red line).

2.7. Summary and conclusion

In this study, ring opening metathesis polymerization was studied using surface immobilized Grubbs 2nd generation catalysts. The functionalized Grubbs 2nd generation catalysts were synthesized on the surface of silica nanoparticles. First of all, two different types of triethoxysilane-functionalized *N*-heterocyclic carbene ligands were synthesized; symmetrical and unsymmetrical NHC ligands, to give the respective Grubbs 2nd generation type catalyst on the surface of the silica nanoparticles as shown below (immobilized catalyst bearing symmetrical NHC ligand-left and the catalyst bearing the unsymmetrical NHC ligand-right):

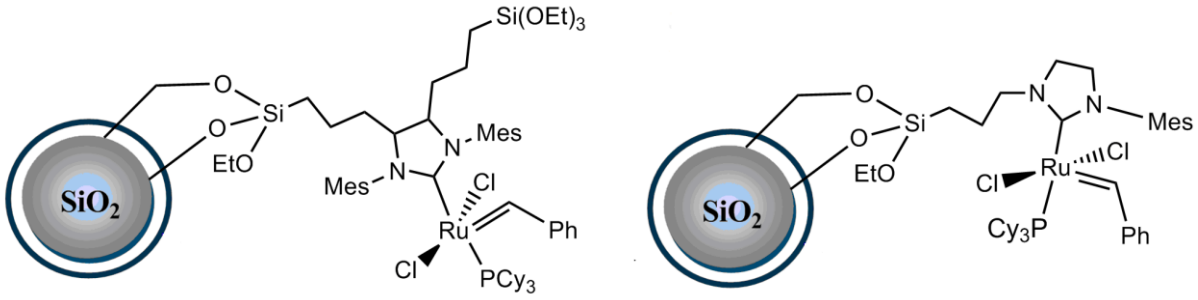

The catalyst was bound through the NHC ligand on the silica surface. These functionalized silica particles were then used in ring opening metathesis polymerization (ROMP) of the monomer norbornene. The polymer obtained was then cleaved from the reaction system and its molecular weight was determined using size exclusion chromatography.

Furthermore, co-deposition of redox-responsive ferrocene containing polymers and Grubbs 2nd generation type catalysts on silica nanoparticles was done as shown in the figure below:

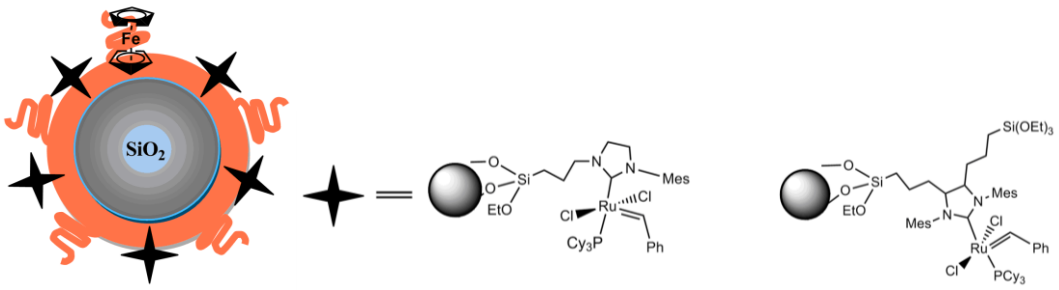

Redox-responsive polyvinylferrocene grafted silica particles were used in order to modulate the catalytic activity of Grubbs 2nd generation type catalyst, bound on silica surface, for ring opening metathesis polymerization of the monomer norbornene. The orange like colored layer on the silica particle as shown in the figure above, represents the polyvinylferrocene polymer chains immobilized via TEOS groups on the surface. The black-star like structures represent the Grubbs 2nd generation type catalyst, also immobilized on silica particles. Grafted silica particles were characterized using solid state ^{29}Si-NMR, scanning electron microscopy (SEM), as well as Energy dirspersive spectroscopy (EDS). This type of modified silica particles were then used in ring opening metathesis of norbornene. Polynorbornene was then cleaved from the reaction and further characterized using size exclusion chromatography. The molecular weight of the polymer obtained from the ROMP of these particles supported the formation of long polynorbornene chains.

The polyvinylferrocene polymers are so called stimuli-responsive polymers since they are able to change their conformation by external stimuli. The major aim was to be able cease the surface initiated ring opening metathesis polymerization of norbornene by oxidizing the ferrocene moiety of the polyvinylferrocene. As the modified particles were oxidized with acetylferrocenium tetrafluoroborane, the ferrocene polymers on silica surface were oxidized causing a dramatic increase in hydrophilicity and thus swelling (as illustrated in the figure below) due to the resulting polyelectrolyte effect.

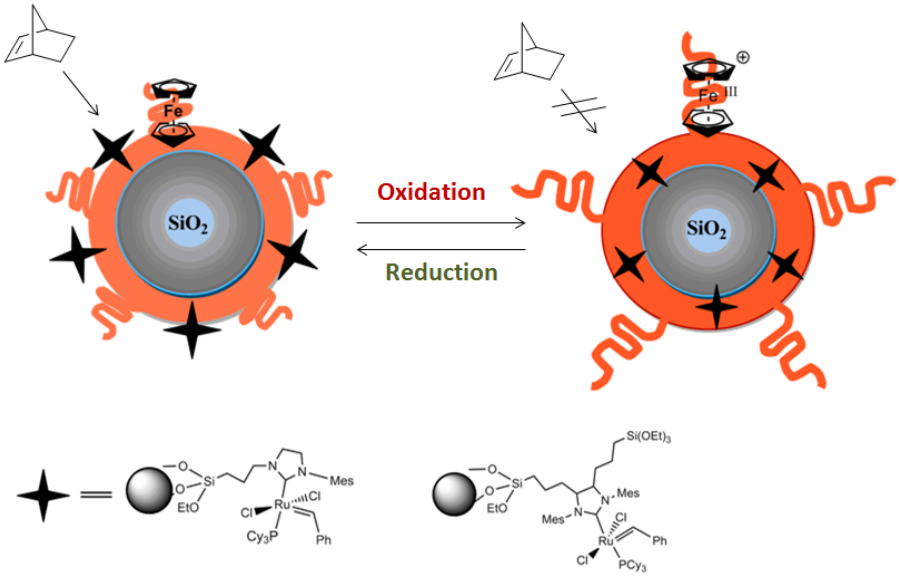

In this case, the Grubbs 2nd generation type catalysts which were on the surface of the particles, were later embedded into the polymer shell and are no more accessible to the monomer in the reaction environment to go on with ring opening metathesis polymerization. Samples were taken to be investigated using size exclusion chromatography, and the no SEC traces for the polynorbornene could be obtained after work up of the aliquots. Additionally TEM images of these oxidized particles revealed no surface attached polynorbornene. Notably, in situ reduction of the PvFc and Grubbs catalyst grafted particles were reduced by adding L-ascorbic acid to the dispersed catalytically inactive nanoparticles resulted to in initiated of the ROMP or norbornene monomer. In order to prove the proposed mechanism, dynamic light scattering (DLS) measurements were also carried out, to determine the change in the particle size before and after oxidation. In addition to SEM/ EDS, TEM, DLS, cyclic voltammetry (CV) measurements were also performed.

3. Aim 2 (Introduction)

3.1. Surface initiated ROMP (SI-ROMP)

Surface initiated ring opening metathesis polymerization (SI-ROMP) represents a continual addition of repeat units on the surface-tethered chains and represents a better method of preparing polymer films with different thickness [22]. SI-ROMP reactions are known to be catalyzed by metal alkylidenes, which is proven to be a very efficient method to control a polymer's size, bulk and structure [23]. This method has shown to polymerize a large variety of monomers, especially monomers (I) and (II) in a living fashion.

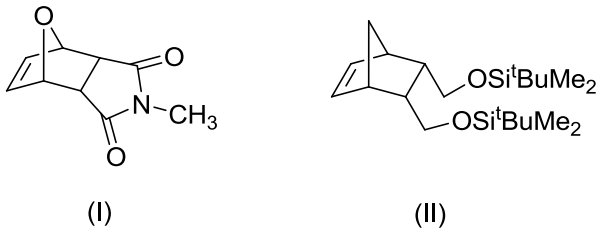

Figure 36 Example monomers used in ROMP reactions [23].

The very first SI-ROMP reaction was reported in 1999, by Grubbs et al, where they presented the first universal method for obtaining a large variety of chemically diverse polymer brushes on the surface of gold [24]. In this study a "molecular wire"-initiator unit was firstly synthesized (as given in the figure below) which was anchored on the surface of the gold substrate.

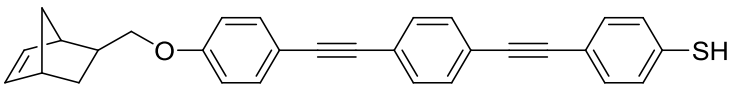

Figure 37 "Molecular wire"-type initiator unit [24].

The molecule could be self-assembled on a gold surface to initiate ROMP after addition of Grubbs first generation catalyst. The polymer layer on the surface was then characterized via SEM, STM and TMAFM [24]. In comparison to the standard ring opening metathesis polymerization, SI-ROMP limits load by allowing the grafting of multiple monomer units into an oligomeric chain from norbornene (Nb) tagged site on the surface of the given substrate, as given in figure below [25].

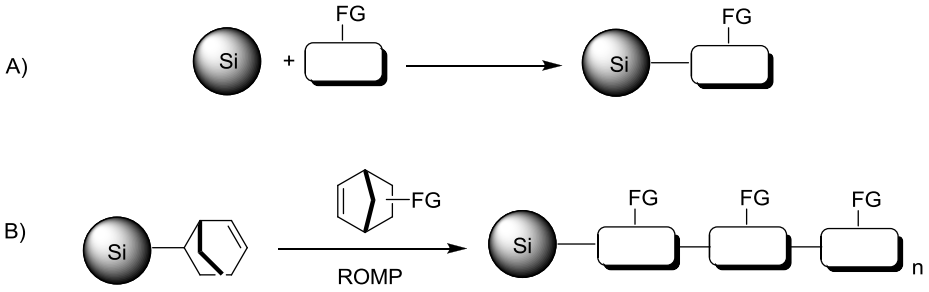

Figure 38 Standard functionalization of silica substrate (A), functionalization of Nb-tagged silica particles using SI-ROMP (B) [25].

Si-ROMP as a living, controlled polymerization, which also refers to "grafting from" technique, is useful in preparing uniform polymer brushes. In literature, surface initiated ROMP is reported for the grafting of organic polymers from inorganic nanopaticles, carbon nanotubes, resins etc [28], [29].

In 2003, Dai et al [29] have reported surface initiated ring opening metathesis polymerization on the surface of single walled carbon-nanotubes (SWCNTs). In this study for surface immobilization, two different pyrene-functionalized initiators were synthesized: the pyrene functionalized initiator (A) and the pyrene-substituted ruthenium alkylidene specie (B) [29].

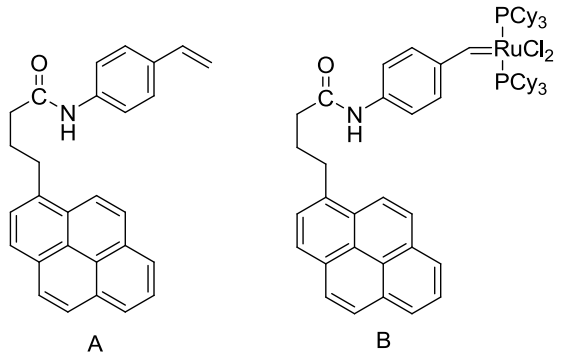

Figure 39 Pyrene functionalized initiator (A) and pyrene-substituted ruthenium alkylidene [29].

Two different pathways were then introduced for the functionalization of SWCNTs. The first pathway involved the functionalization of the pyridine initiator on the SWCNTs, followed by cross metathesis with a ruthenium alkylidine. In the second pathway, the pyrene-substituted ruthenium alkylidene was adsorbed on the side walls of SWCNTs for the ring opening metathesis polymerization of norbornene, as shown in the figure 40 below.

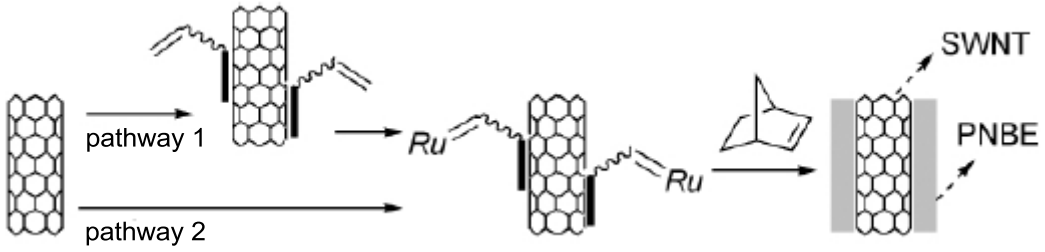

Figure 40 SI-ROMP on SWCNTs, pathway 1: non-covalent adhesion of pyridine functionalized initiator, pathway 2: adsorption of pyrene-substituted ruthenium alkylidene [29].

Finally, polynorbornene (PNBE) has been initiated and the characterization of the polymer layer on SWCNTs was done with transmission electron microscopy as well as atomic force microscopy, to detect the growth of the polymer on the surface [29].

In 2010, Advicula et al [30] reported SI-ROMP of norbornene monomer on electrode surface. In this study, Flechet-type olefin dendrons with terthiophene at the focal point were synthesized (as shown in the figure 41), to be electrochemically deposited on the surface of the conducting substrate (indium tin oxide).

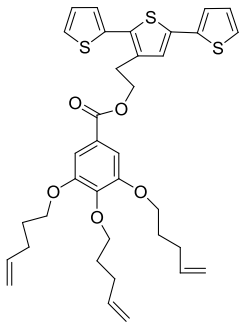

Figure 41 Fletcher-type olefin dendrons with terthiophene at the focal point [30].

The synthesized olefin dendrons with terthiophene at the focal point were then electrochemically polymerized on the surface of indium tin oxide (ITO). The electrografted polythiophene film was then followed by SI-ROMP of norbornene monomer after the activation by first generation Grubbs catalyst as shown in the figure below.

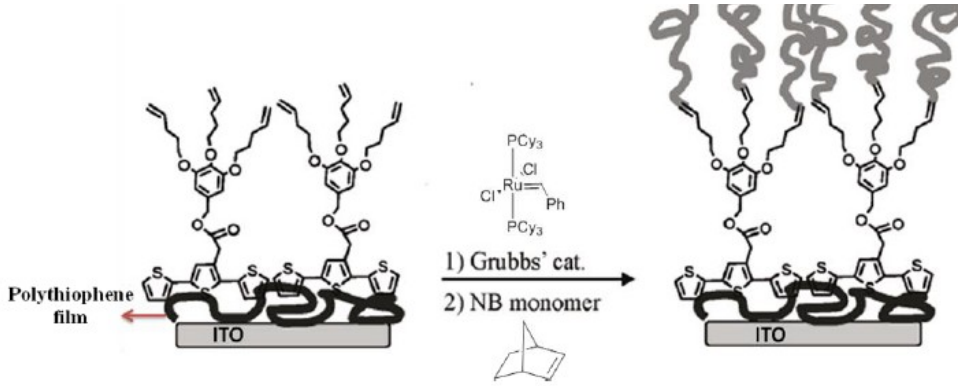

Figure 42 Polynorbornene brushes synthesized by SI-ROMP on the polythiophene film [30].

Surface initiated ROMP, in this study had offered the capability of preparing uniform polymer brushes and block copolymers by metathesis methods in mild conditions [30]. In 2012, Carlmark et al [31], reported for the first time surface initiated ROMP on cellulose fibers. Initially, Grubbs first generation catalyst was immobilized on filter paper, and then SI-ROMP of norbornene monomer was performed from the surface of the cellulose fibers, as shown in the figure below.

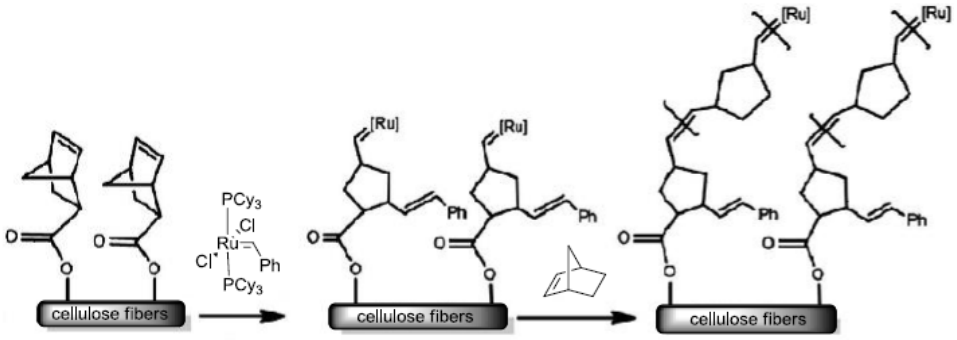

Figure 43 SI-ROMP from cellulose fibers [31].

Surface initiated ROMP in this study had shown a combination of the properties of cellulose and the properties of the grown polymers on cellulose surface to form a biocomposite which can be used as a component in advanced materials [31].

3.2. Aim 2: Immobilization of Grubbs Hoveyda type catalyst on mesoporous silica film on ITO surface for the application in SI-ROMP reactions

The second part of this work involved surface immobilization of Grubbs-Hoveyda 2nd generation type catalyst on mesoporous film for surface initiated ROMP. Mesoporous silica thin films with 200 nm thickness were obtained by Fabio Krohm, research group of Jr. Prof. Dr. Annette Brunsen, which displayed organized pore arrays with high accessibility. The thin films were capped with benzophenone silane polymers as shown in the figure below, to achieve a passivation of the outer film. The pores of the film were enriched with hydroxyl groups where the Grubbs Hoveyda 2nd generation type complex, functionalized with ethoxy groups, was going to be covalently bound.

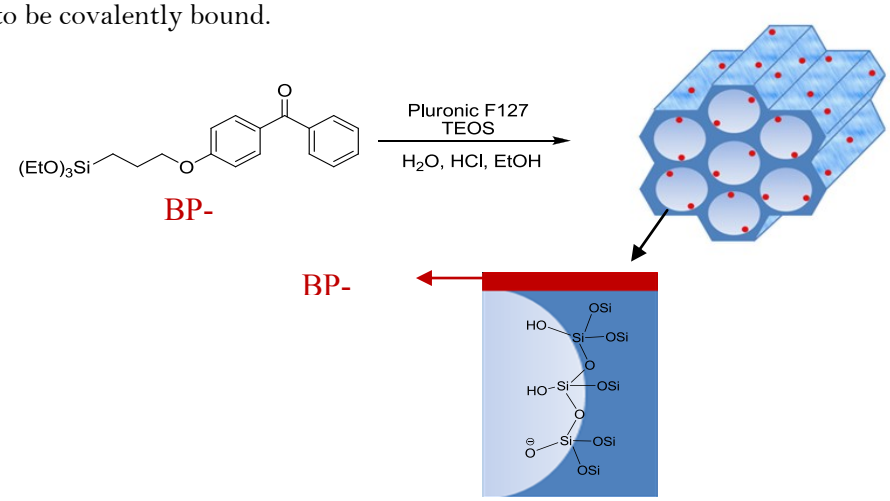

Figure 44 Benzophenone-silane capping of mesoporous films.

Grubbs Hoveyda 2nd generation type complex bearing –Si(OEt)$_3$ groups was synthesized and covalently bound only in the pores of the mesoporous ITO, glass and Si-wafers films, as shown in the figure below.

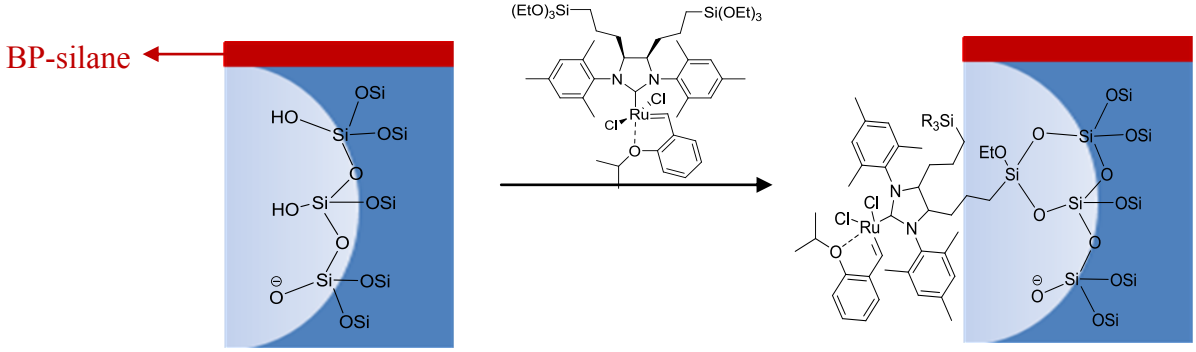

Figure 45 Immobilization of Grubbs Hoveyda 2nd generation type complex on mesoporous substrates.

The catalyst modified mesoporous silica thin film substrates were then used for surface initiated ring opening metathesis polymerization of norbornene derivative-ferrocene monomer as well as norbornene derivative-spiropyrane monomer as shown in the figure below (figure 46). The polymers were then extracted from the mesopores and further characterized using GPC.

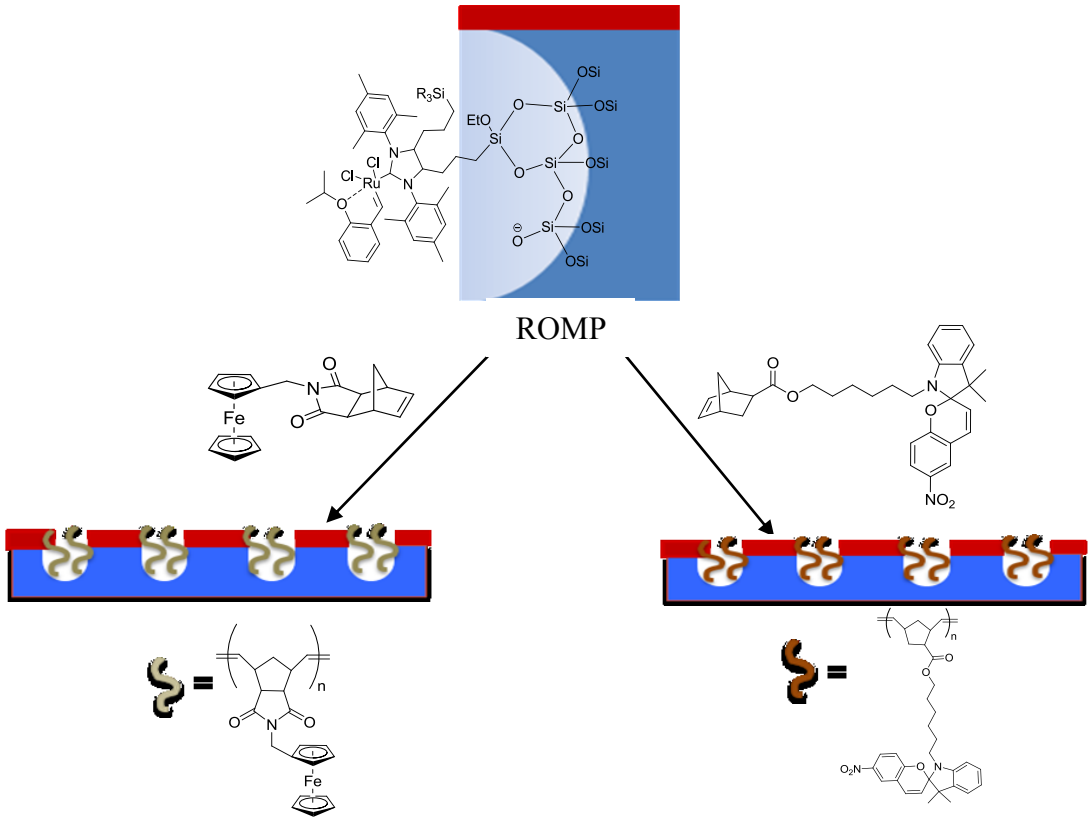

Figure 46 Surface initiated ring opening metathesis polymerization of norbornene derivative-ferrocene monomer (left) and norbornene derivative-spiropyrane monomer (right).

3.2.1. Switchable mesoporous polymer hybrid membranes

3.2.2. Modification of mesoporous silica films with dendrimers and polymer brushes

Mesoporous thin films, because of their complex cavity system, have a very broad application in optics, electronics, chemical sensing, catalysis, separation etc [33]. The introduction of different organic functions on the mesopores, gives the possibility of creation of complex chemical systems with tuned reactivity [33]. The organic functions are added in various ways; either by co-condensation of a functional inorganic precursor with another precursor in the presence of a template or by postsynthesis of a mesoporous material. Another possible method of introducing organic functional groups in mesopores is solution impregnation or exposure of volatile vapors [34]. Dendrimers, which are synthesized by step-by-step reactions, are known as macromolecular building blocks characterized by their branched structure [32]. The synthesis of dendrons inside the mesoporous system displays a high density of active sites, which are then useful for designing catalytic platforms [35]. In 2011, Soler-Illia et al, reported the synthesis of polyamidoamine dendrimers (PAMAM) which were functionalized on the inner pores of the mesoporous silica (MCM-41) [32].

The dendrimers were then used as nanostructured supports in order to bind with the rhodium catalyst on the surface of the mesoporous silica as shown in the figure below:

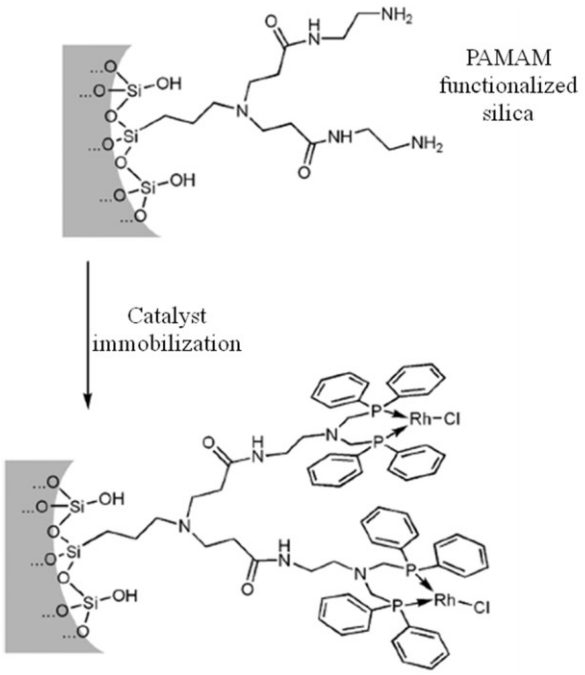

Figure 47 Immobilization of polyamidoamine (PAMAM) on mesoporous silica and complexation with rhodium catalyst [32].

Gonzàlez et al, in 2009 reported another strategy to introduce the dendrimers into the mesoporous network [36]. In this work, the dendrimers were introduced by a post-synthesis method using a novel amine precursor [32] as shown in the figure below. These precursors were used to covalently bound on pore walls, while reacting with the silanol groups on the pores [36]. Finally, cyanuric chloride was added in the presence of ethylene diamine to get the final amino modified mesoporous hybrid [36].

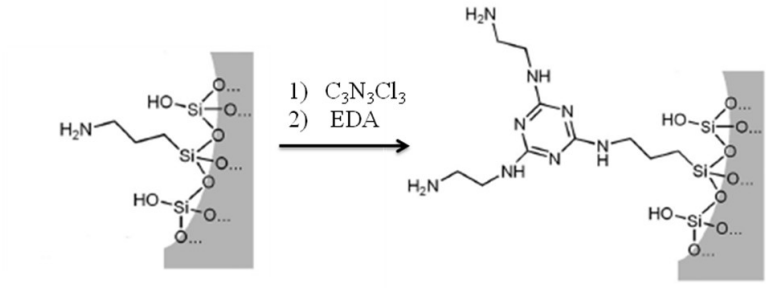

Figure 48 Post-grafting of dendrimers on amino modified mesoporous hybrids [36].

The above described route represented another modification pathway of mesoporous films in order to obtain surfaces with dense population of amino groups, while eliminating multistep reactions which are classical for dendric growth in the mesoporous films [36]. In 2006, Lenarda et al showed that polymerization chemistry can be used to build polymer-mesoporous hybrids [37]. Tetraethyl orthosilicate (TEOS)-based derivative (TEMPO (2′, 2′, 6′, 6′- tetramethyl-1′-piperidinyloxy)) was synthesized and covalently bounded on the walls of

mesoporous silica [37]. The modified mesoporous silica was then used as a perfect surface for controlled radical polymerization of styrene [37], as shown in the figure below.

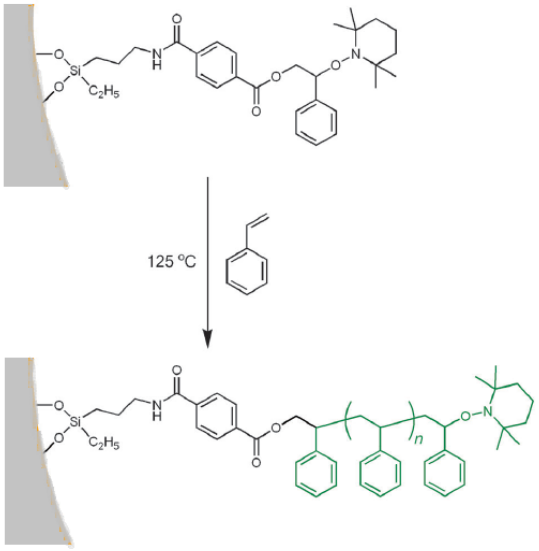

Figure 49 Controlled radical polymerization inside mesoporous frameworks using TEMPO-modified pore walls [37].

The polymerization of styrene, which occurred only in the pores of the mesoporous silica, occurred without affecting the structural and morphological features of the starting mesoporous silica [37].

In 2007, Zhou [38] and Fu [39] while using the same experimental procedure reported a strategy to build up a delivery system based on the stimuli-responsive poly (N-isopropylacrylamide) (PNIPAM) brushes synthesized inside a mesoporous matrix via atom transfer radical polymerization. In these studies, the control over drug release was investigated, where ibuprofen (IBU) was used as a probe molecule [38], [39]. In 2009,

Frey et al reported one pot deposition of conjugated polymers into mesostructured metal oxide films [40]. In this study, the conjugated polymer dissolved in xylene was added dropwise into the polar precursor solution including the metal oxide precursor species [40] as shown in the figure below.

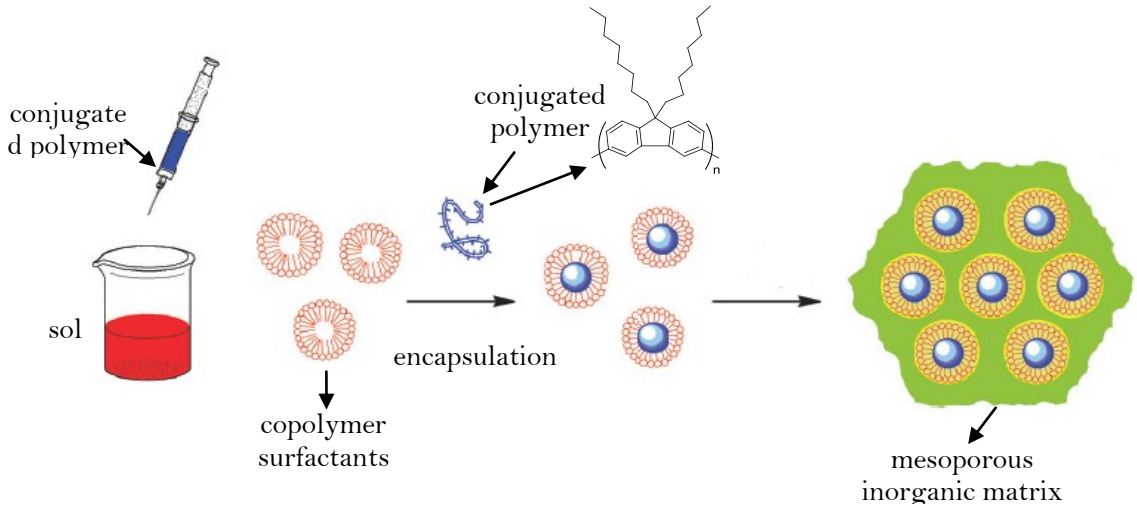

Figure 50 One-pot deposition of conjugated polymer-incorporated mesostructured metal oxide films [40].

The conjugated polymer-incorporated metal oxide films were demonstrated for optoelectronic devices, since the 3D-cubic silica film was while light emitting functional film [40]. Examples of controlled functionalization of mesoporous materials with polymer building blocks rely on the selective chemical derivatization of the inner and outer surface of the mesoporous system [41]. In 2007, Hong et al reported the functionalization of the outer surface of mesoporous silica, without changing the structure of the mesoporous silica, via reversible addition-fragmentation chain transfer (RAFT) polymerization [42]. A similar study reported on 2010 by Shantz et al, showed that amines and thiols can be grafted on the outer surface of mesoporous substrates (SBA-15) using a post-synthetic approach, where functionalization of the outer surface of the mesoporous matrix was achieved by reacting mesoporous silica (SBA-15) with the desired organosilanes before removing the template [43]. Growth of the polymer chains on the outer surface of the mesoporous films was also reported in 2008 by Lindèn et al [44]. Poly-(ethylene imine) (PEI) branches were grown on the outer surface of the mesoporous silica as shown in the figure below.

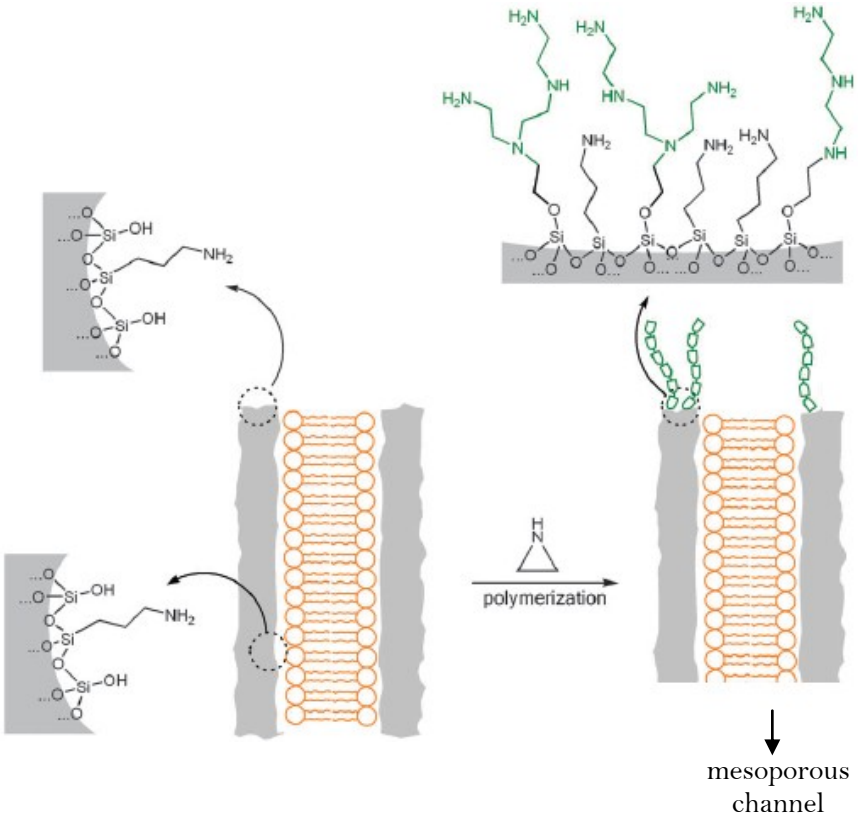

Figure 51 Functionalization of mesoporous silica with amino-terminated hyperbranched polymers on the outer surface of the porous film [44].

The functionalization of the mesoporous silica on the outer part of the surface with PEI (poly-(ethylene imine)) according to Lindèn, opens a gate to its application in cancer detection and though treatment [44]. The PEI modified silica can be further functionalized with with different types of biomolecules. In this case, the folic acid modified PEI-silica composite is endocytosed by cancer cells by indentification of the folate receptor [45].

3.2.3. Permselectivity and gate-like assembles based on mesoporous architectures

Mesoporous silica films are well known for their capability of designing controlled-release systems because of their special features like: biocompatibility, tunable and modifiable pore surface [46]. While taking into consideration these unique features in 2004 Lin and co-workers reported the covalent attachment of dendrimen on the surface of MCM-41 type mesoporous silica nanoparticles [46]. The structure of the mesoporous silica nanoparticles then allowed the encapsulation of pharmaceutical drugs inside the mesoporous silica channels where the amine terminated dendrimers were used as caps to trap the guest molecule inside [46]. In another study, in 2010, Sun and co-workers reported that pH responsive polymers can also be anchored on mesoporous silica nanoparticles to serve as a switch in order to control the opening and the closing of the pores [47]. The polymer brushes used in this study were based on poly- (2-(diethylamino) ethyl) methacrylate) (PDEAEMA) and the guest molecule was rhodamine B [47]. These authors reported that at low pH values the polymer brushes were swollen while resulting in the release of the guest molecule from the pores of the mesoporous silica. In basic conditions, the polymer brushes on the surface collapsed while closing the pores of the mesoporous silica though and trapping the guest molecule in the pores [47].

Interfaces which discriminate the transport of molecular species have increased a dramatic interest from the material science community. The passage of the molecular species in such interfaces is controlled via different types of stimuli [50]. There are many types of stimuli which can be used to initiate action, among which light-sensitivity is an attractive way of developing hybrid materials which are capable of external modulation of chemical changes in mesoporous materials [49]. In 2010, in another study by Lai and co-workers the combination of mesoporous films and polymeric building blocks created nanoscopic gate like assembly [48]. The light responsive copolymer brushes were covalently bounded on the surface of the mesoporous nanoparticles which led to the construction of light-responsive nano gates. The polymer brushes bearing photocleavable hydrophobic 2-nitrobenzyl moieties, collapsed at room temperature though making the polymer insoluble in collapsed state. After UV-irradiation the hydrophobic 2-nitrobenzyl acrylate moiety was photocleaved forming hydrophilic acrylate which resulted in increase of lower critical solubility temperature [48]. In this light triggered process, the polymer chains became hydrophilic resulting in the swelling of the polymers and opening the nano gate to release the host molecule trapped in the nano pores [48].

Brunsen et al, reported the construction of synthetic photoactive hybrid assemblies which displayed not only light-triggering gating functions but also photo-stimulated charge selectivity properties which leaded to control over the transport of the ionic species [51]. In this study, the polymer brushes were immobilized on the outer surface of mesoporous oxide thin films, in order to create photo-active light activated inorganic assemblies with permselective transport of the ionic species in the pores of the mesoporous thin film [51]. Mesoporous silica thin film supported on indium tin oxide (ITO) were functionalized with photolabile polymer brushes which were covalently bounded on the surface while reacting the surface amino groups with 2-bromoisobutyryl bromide in order to anchor the polymer initiators [51]. The polymer growth was latter initiated via surface-initiated atom transfer radical polymerization of 2-[(4,5-dimethoxy-2-nitrobenzoxy) carbonyl] aminoethyl methacrylate (NVOCAMA) monomer using the proper solvent mixture and catalyst

[52]. This process led to the growth of the polymer brushes on the surface of the mesoporous system as shown in the figure 52.

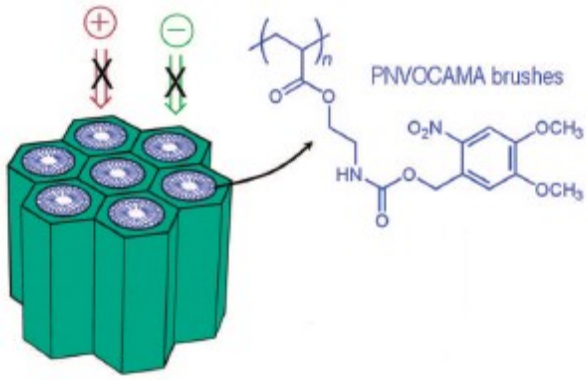

Figure 52 Modification of mesoporous silica films with PNVOCAMA brushes [51].

In the presence of the hydrophobic polymer brushes (PNVOCAMA) on the mesopores of the ITO film, the electrochemical response of both negative ($Fe(CN)_6^{3-}$) and positive ions ($Ru(NH_3)_6^{3+}$) at pH 3 respectively, was inhibited as shown in the figure below [51]. After the UV-irradiation of the mesoporous ITO films, the chromophore structure form the polymer brush was cleaved to form poly (2-aminoethyl methacrylate) (PAMA). Because of the presence of the NH^{3+} in the polymer structure, the pores became inaccessible for the positive ions. On the other hand, the polymer brushes became uncaged for the negative ions, and the negative ions could enter the pores as shown in the figure below:

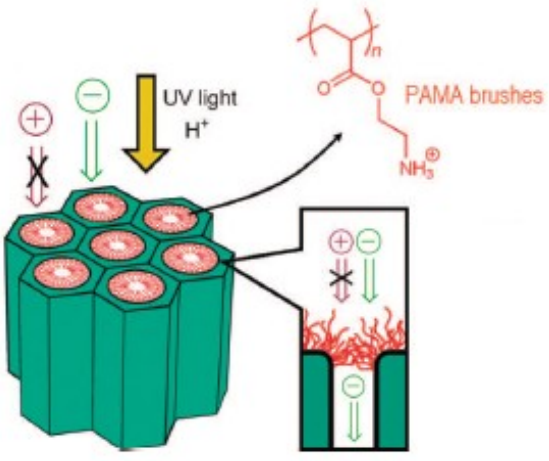

Figure 53 UV-irradiation of mesoporous ITO films and the uncaging of the polymer brushes for the accessibility of the positive ions in the porous system [51].

Voltammetric measurements were performed at a scan rate 100 mVs^{-1} with KCl solution as supporting electrolyte. As guest molecules were chosen negative and positive ions: ($Fe(CN)_6^{3-}$) and ($Ru(NH_3)_6^{3+}$) respectively. Before UV-irradiation, while the polymer brushes on the surface of mesoporous silica films give a hydrophobic nature to the surface, the cyclic voltammogram showed that there is no access for both the negative and positive ions on the pores of the mesoporous silica films as shown in the figure 54.

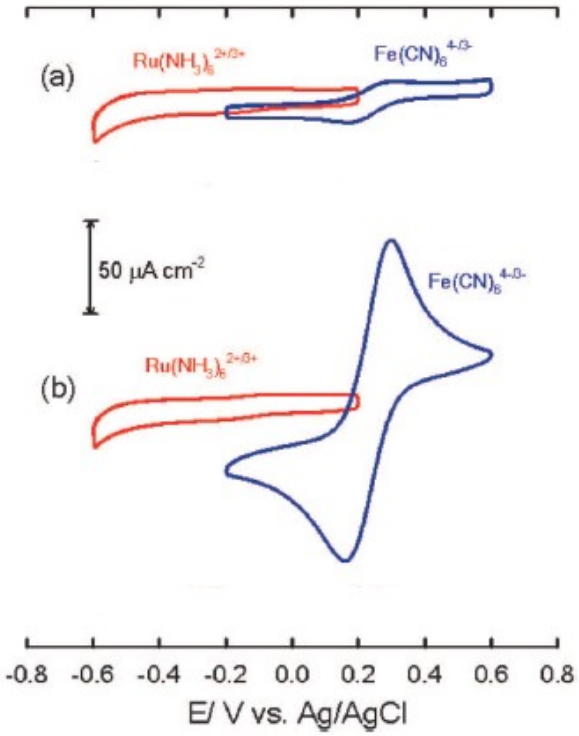

Figure 54 Cyclic voltammograms a) caged-polymer brushes b) uncaged-polymer brushes [51].

After the UV-irradiation, as the chromophore groups were cleaved leaving NH^{3+} groups on the structure of the polymer brushes. In these conditions, the surface of the mesoporous ITO films lost their hydrophobicity though uncaging the polymer brushes, in order to build up a permselective polycationic barrier to the outer region of the film [51]. As shown in the cyclic voltammogram the positive ions have no more access to the pores, whereas in the case of negative ions there is a significant response in the cyclic voltammogram indicating that the negative ions have access to the pores of the mesoporous ITO films [51].

Different approaches based on surface functionalization of mesoporous systems have been reported in recent years [54]. In most of the cases the ionic transport in the mesoporous systems has been studied, where in the majority of the studies the selectivity of the cations and anions is performed by adjusting the pH level of the environment in order to lead to the opening and closing of the pores of the mesoporous system [54]. Calvo et al in 2009 also described the preparation of mesoporous films with polyzwitterionic brushes, which films could discriminate the transport of cations and anions over a wide pH range [55]. In this study it was stated that even the surface-confined silanolate groups (-Si-O) with pKa value of 2, can show permselective properties for ionic species [55], where the transport of the ionic species through the mesoporous conductive ITO substrates was studied via cyclic voltammetry. The mesoporous ITO films were then modified by growing zwitterionic poly (methacrylol-L-lysine) (PML) brushes. The modification with polymer brushes was accomplished via surface-initiated radical polymerization of the monomer methacryloyl-L-lysine in the presence of adequate initiator [56]. As the modification of the mesoporous films was performed with zwitterionic polymer brushes, the transport of $Fe(CN)_6^{3-}$ anions and $Ru(NH_3)_6^{3+}$ cations was tested at different different pH level of the range from 1 to 8 [55]. At pH's 8 and 5 the modified mesoporous ITO films hindered the transport of anions and

enabled the transport of cations. On the other hand, at lower pH values, the mesoporous films hindered the transport of both the cations and anions as shown in the figure below:

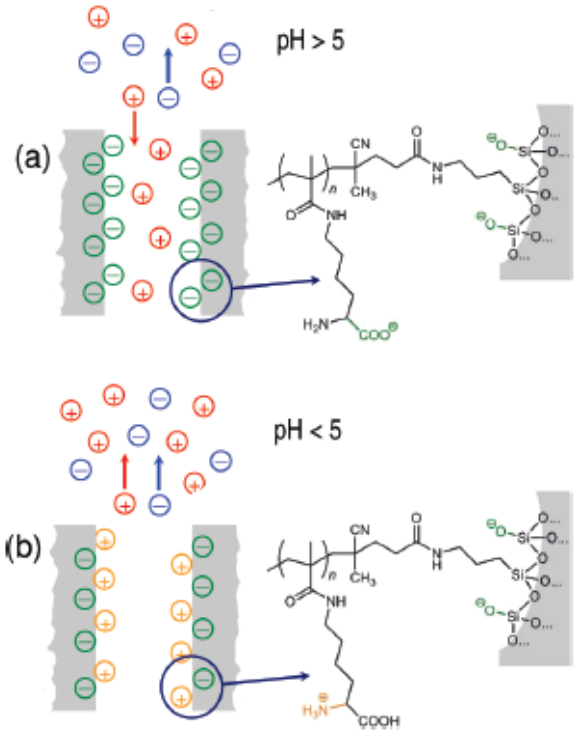

Figure 55 a) permselective transport of cations at pH > 5 b) ionic barrier, at pH < 5 [55].

In a similar study reported by Fattakhova et al, mesoporous layers of SiO_2 were functionalized with protonated amino groups, which showed very good permselective membrane properties [57]. In this study the transport of negative, positive ions as well as neutral molecules was studied: hexacyanoferrate $(Fe(CN)_6^{3-})$, hexaamino-ruthenium $(Ru(NH_3)_6^{3+})$ as well as ferrocene methanol molecules [57]. The selectivity and permselectivity of the guest molecules was controlled by changing the pH value, where depending on the charge, the flux of ions into the pores could be completely blocked or inhibited [57]. The mesoporous silica membranes were characterized with high porosity, which ensured better penetration of the ions into the pores in comparison to compact organic polymer layers which usually suffer from a number of drawbacks like poor porosity [58]. Such amino functionalized mesoporous silica films which can efficiently separate the charged species, are then used in medicine like in separation of blood, urine or other components [59].

3.3. Results and discussion

3.3.1. Synthesis of norbornene derivative ferrocene monomer

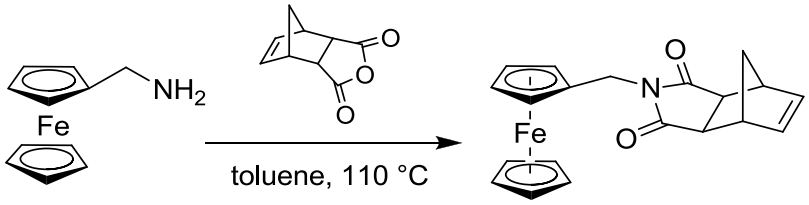

Scheme 17 Synthesis of norbornene derivative ferrocene monomer.

Ethyl amino ferrocene was dissolved in toluene then carbic anhydride was added and the mixture is left to reflux overnight. A dean start apparatus was used to collect the water liberated from the reaction. After the reaction time, the system is brought to room temperature and the solvent mixture was evaporated under reduced pressure. The product was purified by column chromatography, Cyclohexane:Ethyl acetate (2:1) to obtain the product as a light yellow powder in 87 % yield.

3.3.2. Preparation of mesoporous silica films on ITO [51]

Polymer modified mesoporous silica thin film supported on indium tin oxide films (ITO) were prepared by Fabio Krohm as shown in the figure below.

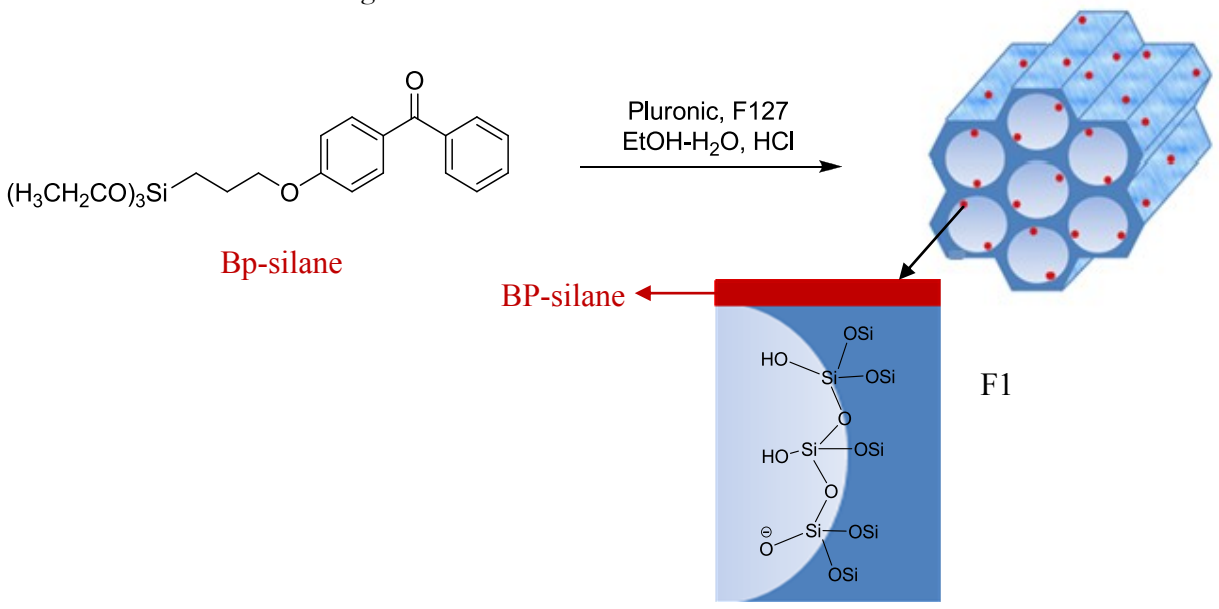

Scheme 18 Preparation of polymer modified silica films on indium tin oxide surface [51].

The morphology of the mesoporous silica films, modified with 4-propoxy-benzophenone (triethoxy) silane layer, was studied using secondary electron microscopy (SEM), which were measured by Fabio Krohm with the help of Dr. Jörg Engstler. As seen from the pictures below, the mesoporous system is clearly seen as the samples are scanned at a magnification of 200 nm and 100 nm as well.

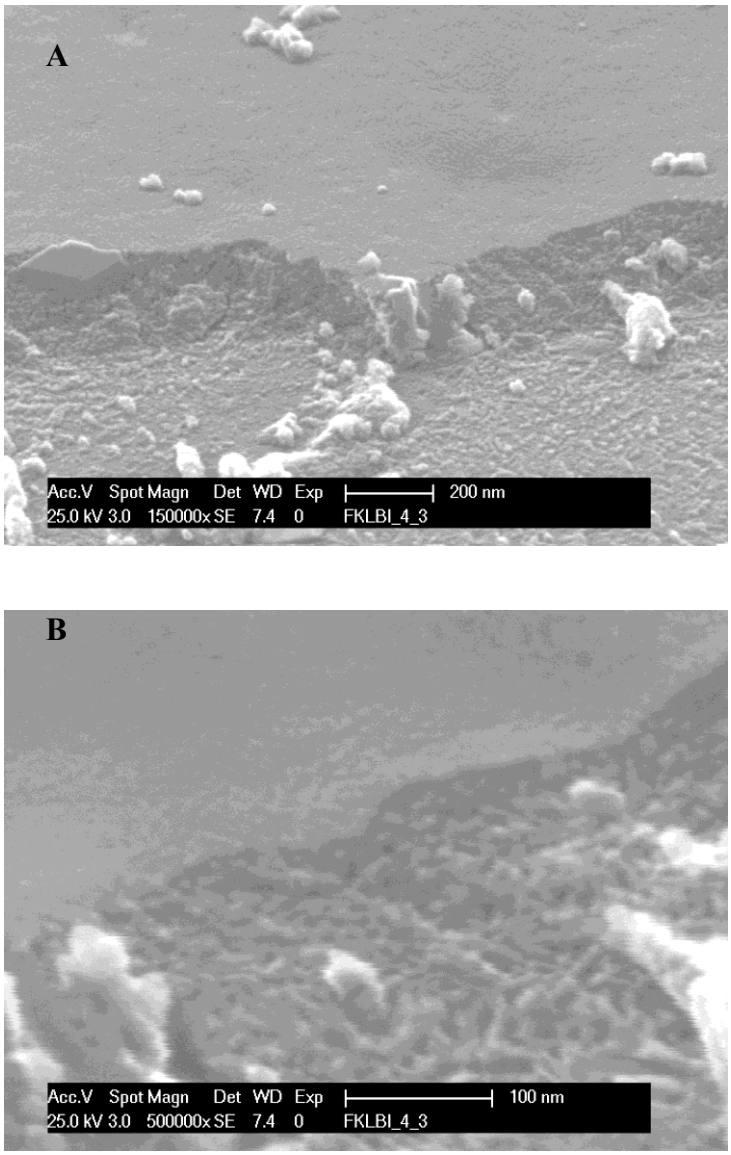

Figure 56 SEM images of benzophenone modified mesoporous indium tin oxide (ITO) substrates (substrates of type F1): A) image taken at 200 nm and B) image taken at 100 nm.

The initiator density as well as the polymer molecular weight could be varied and by varying these two parameters, the ion permselectivity in the pores could be controlled.

After the modification of the mesoporous silica thin films supported on indium tin oxide (ITO) the substrates were soxhlet extracted in EtOH overnight then dried under vacuum.

3.3.3. Immobilization of Grubbs Hoveyda 2nd generation type catalyst on the polymer modified mesopores silica films on ITO surface

After the preparation of the polymer modified mesoporous silica films on ITO substrates, Grubbs Hoveyda 2nd generation type catalyst was immobilized on the pores of the substrates. The –Si $(OEt)_3$ bearing Grubbs 2nd generation type catalyst was dissolved in dry dioxane in a schlenk flask (10 mg / ml). Finally, the modified films of type F1 and F2 were immersed in the catalyst solution under argon atmosphere and was left for 48 h at room temperature. After the reaction time, the slides were removed from the catalyst solution and washed several times with dioxane, methanol and finally with ether and dried under vacuum to obtain modified ITO substrates of type F3 as shown in the scheme below, which were later characterized by ellipsometry, contact angle measurements and cyclic voltammetry.

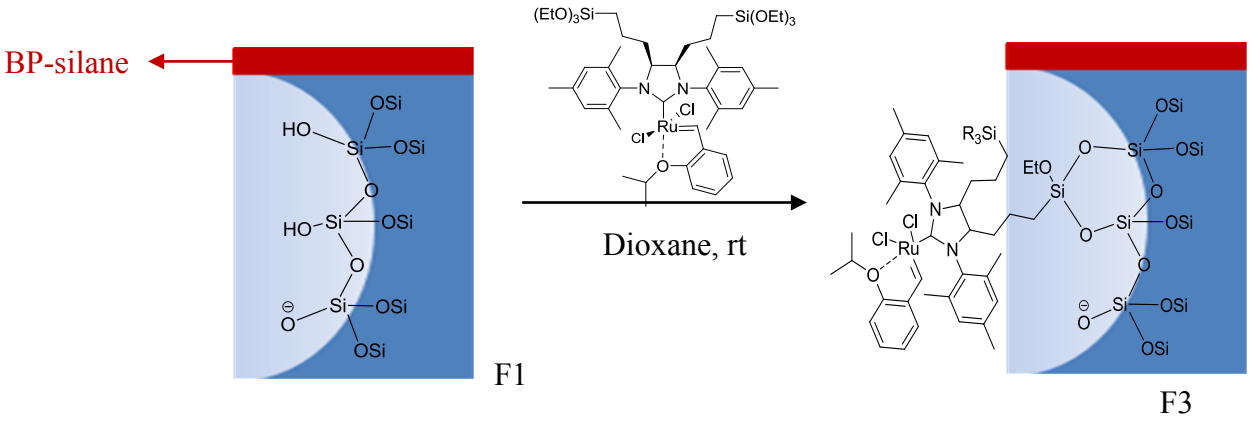

Scheme 19 Immobilization of Grubbs Hoveyda 2nd generation type catalyst on benzophenone-silane modified mesoporous silica films.

3.3.4. Permeation properties of mesoporous silica film on ITO surface (type F1 and F2 substrates)

3.3.5. Cyclic voltammetry measurements (type F1 and F2 substrates)

The permselective properties of mesoporous hybrid interface were characterized using redox probes that diffuse across the mesoporous film deposition on a conductive ITO-substrate. The selected redox probes were ferricyanide ($Fe(CN)_6^{3-}$) and hexaaminеruthenium(III) chloride. For the cyclic voltammetric studies, from both probes 1 mM concentration solutions were prepared. The scan rate was chosen to be 100 mVs^{-1} and as supporting electrolyte solution, 0.1 M KCl solution was used.

The measurements were done at different pH levels (3 and 8) to check the permselective properties of the thin film. First of all, the concentration of ferricyanide was tested at pH levels 3 and 8. The negative ferricyanide ions, at pH 3, have accessibility into the mesopores and this could be understood from the well defined electrochemical response (black solid line).

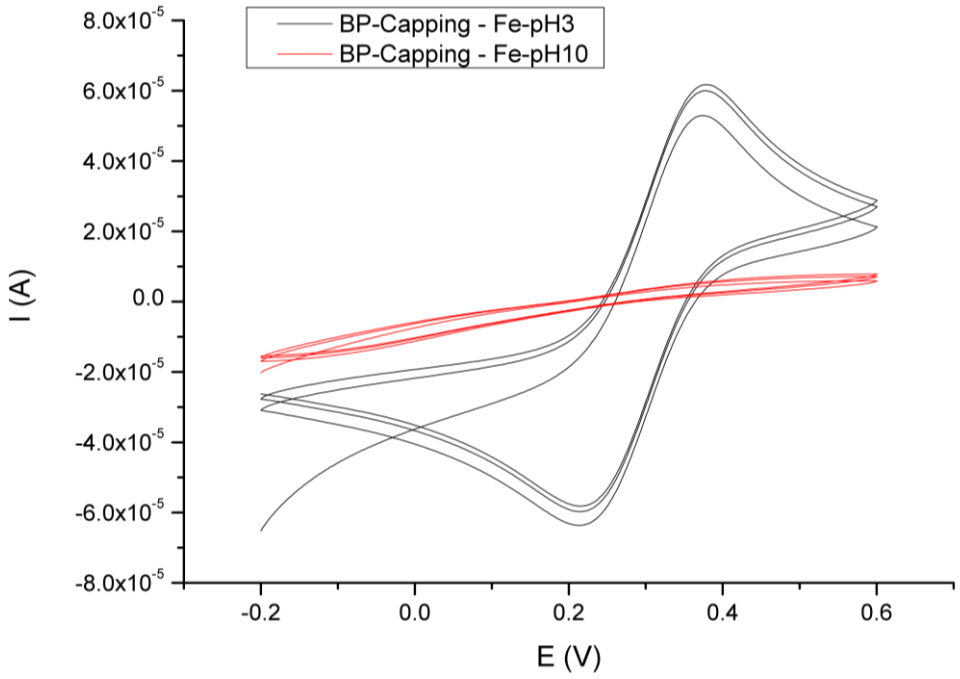

Figure 57 Cyclic voltammogram corresponding to benzophenone capped silica films, in the presence of 1mM Fe $(CN)_6^{3-}$, at pH 3 and 8, for substrates of type F1.

On the other hand, in basic conditions at pH 10, in the pores the generation of –Si-O$^-$ groups, the negatively charged ferricyanide ions underwent repulsion and though there was no access in the mesopores. This can be easily observed from the cyclic voltammogram where no electrochemical response was observed at high pH levels (red solid line) as shown in figure above.

Secondly, as positive ion to test perselective properties was chosen hexaaminеruthenium(III) chloride. At pH 3, the black solid line the figure 58 shows that the capping layer does not block the pores and that the mesoporous film still responds as expected for silica mesoporous films. On the other hand, at higher pH levels (8), because of the generation of the –Si-O$^-$ groups, the positively charged Ru $(NH_3)_6^{3+}$ ions were attracted into the mesopores of the ITO film. This could be easily seen from the great electrochemical response which could be easily seen in the cyclic voltammogram below (figure 58).

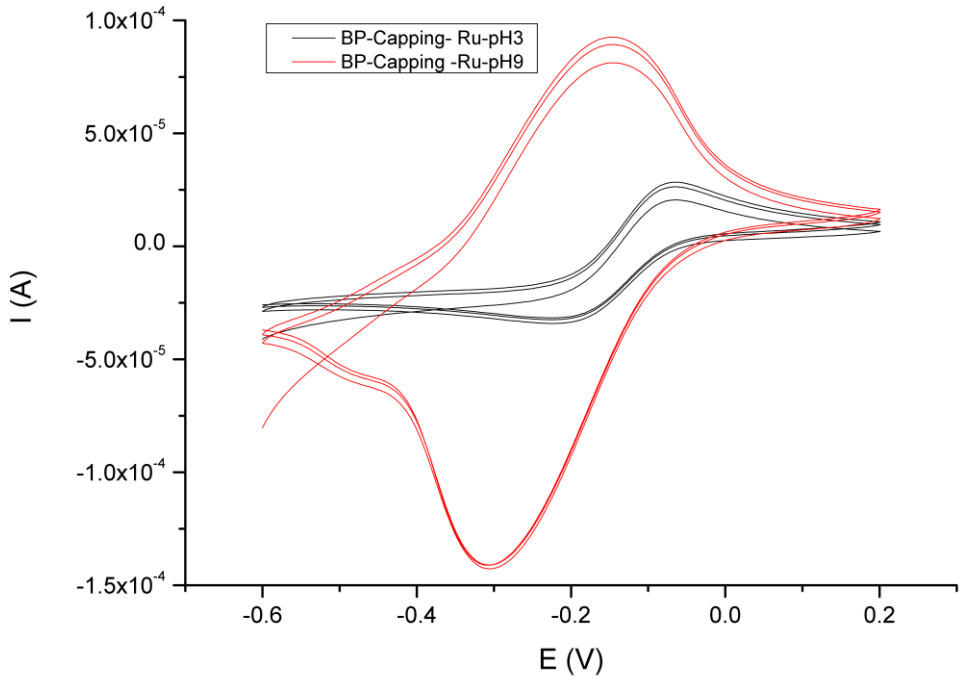

Figure 58 Cyclic voltammogram corresponding to benzophenone capped ITO films, in the presence of 1 mM Ru $(NH_3)_6^{3+}$, at pH 3 and 8, for substrates of type F1.

These trials were important to understand that the capping process was successfully achieved furthermore, that the conductive films possess permselective properties.

3.3.6. Contact angle measurements (type F1 substrates before and after capping)

Another surface characterization technique used to characterize the ITO substrates before and after modification were contact angle measurements. The angle formed between solid and the liquid interface represents the contact angle. The contact angle measurements were performed using static sessile drop method which was measured using a contact angle goniometer, where the amount of distilled water per drop was 13 · 2 µl. In order to study the effectiveness of the capping methods with benzophenone-silane, the contact angle of non modified mesoporous silica films (substrates without template) was measured then compared with the contact angle of the surface modified ITO substrates. In this case, it was expected that the contact angle increases as the outer layer of the ITO substrate is modified with benzephenone layer.

According to the literature [94] if the contact angle is equal to 0 ° then it is accepted that the surface or the substrate is hydrophilic and that the liquid drop is completely wetting the surface. When the contact angle is around 45 ° then it is accepted that the surface is partially hydrophilic and that the liquid drop is good wetting the surface. Finally, if the contact angle is 95 ° or higher, then it is accepted that the surface is hydrophobic and that the liquid drop is not wetting the surface.

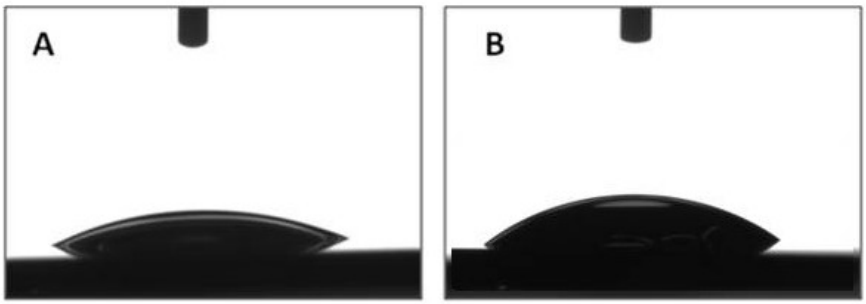

Figure 59 Contact angle measurement of ITO substrates: without template and before capping (A), after capping with benzophenone-silane (B).

As seen from the figures above, the contact angle showed a dramatic increase after the capping processes
The average value of contact angle measurements of the ITO substrate without template and before capping was found to be 10 °. As seen from the figure 49 above (A), the water drop was almost completely wetting the ITO surface since the surface is hydrophilic. The average contact angle after the benzophenone capping (capping process 1), was found to be 33 °. This increase in contact angle clearly shows that the capping process was successful and that the surface of the ITO was modified. As seen from the figure, case B, the water drop was not completely wetting the surface, though the surface had become more hydrophobic. From this increase of the contact angle we do understand that the surface of the mesoporous silica films on ITO has changed to hydrophobic and that the capping layer was not dense enough, otherwise a higher contact angle would be observed.

3.3.7. Ellipsometric measurements (type F1 substrates)

Imagining ellipsometry is a very useful technique which is used to characterize the material properties like: thickness, refractive index: n, extinction coefficient: k and many other properties [61].
The measured signal is the change in polarization as the incident radiation (in a known state) interacts with the material structure of interest (reflected, absorbed, scattered, or transmitted), as illustrated in the figure 60 below. The polarization change is quantified by the amplitude ratio, Ψ, and the phase difference, Δ [61]. The parameters give all relevant information about the polarization state of light at a given wavelength; measuring the complex reflectance ration:

$$\rho = \frac{r_p}{r_s} = \tan \Psi . e^{j\Delta} = f(n_i, k_i, T_i)$$

The tan Ψ gives the angle of the first diagonal of the rectangle in which the ellipse is enclosed and
cos Δ represents roughly how fat is going to be the ellipse (the shape).
In the figure 60 the working principle of the imaging ellipsometer is illustrated. An electromagnetic radiation is emitted by a light source and linearly polarized by a polarizer and the light falls into the sample. After reflection the radiation passes a second polarizer which is called the analyzer and the polarized light is

collected by the detector. The incident and the reflected beam extend across the plane of incidence and the light which is polarized is called p-polarized [61].

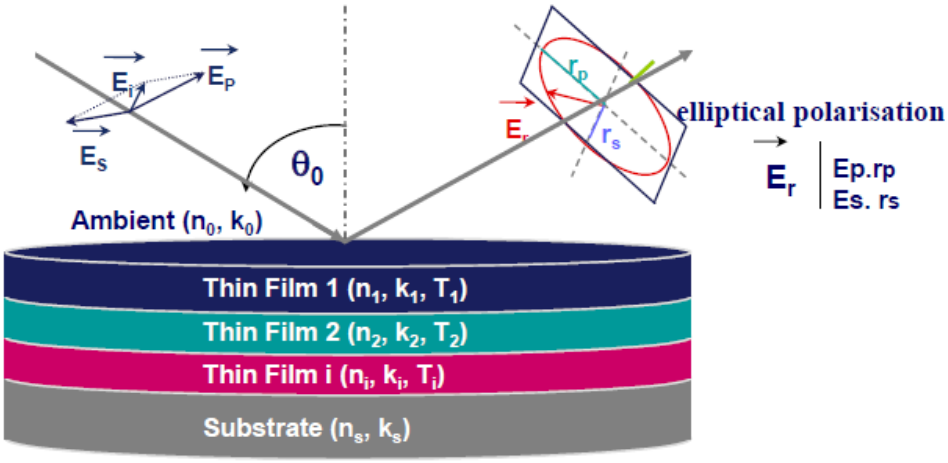

Figure 60 Working principals of spectroscopic ellipsometry [61].

Imaging ellipsometry was an important method in characterizing the ITO substrates before and after modification. The aim of the ellipsometric measurements was to study the change on the film thickness as well as the changes in the refractive index after surface modification. It was expected that the thickness of the silica film on ITO substrates will increase as the mesoporous silica is modified with bezophenone-polymer layer. In addition, the refractive index of the substrates is also expected to increase. The film thicknesses as well as the refractive indices of the silica films, before and after modification are illustrated in the table below.

Parameters	**ITO/ before capping (F2)**	**ITO/ after capping (F2)**
film thickness (nm)	192	225
refractive index	1. 269	1. 278

Table 3 Film thickness and refractive indices of indium tin oxide (ITO) substrates before and after modification.

As observed from the table 3 above, before beznophenone-silane modification, the film thickness of the mesoporous silica film was 192 nm, with a refractive index of 1. 296. After the modification of silica film with benzophenone polymer layer, the measured film thickness was increased by 33 nm. This clearly shows that the benzophenone modification of the surface was successful. As a conclusion we can say that by using the ellipsometric measurements, it was possible to measure the change in the film thickness and the change in refractive index, which results prove that from those significant change in values, the modification of the mesoporous ITO substrates was successful.

3.3.8. Application of substrates of type F2 in surface initiated ring opening metathesis polymerization (SI-ROMP) of norbornene derivative ferrocene monomer

3.3.9. Cyclic voltammetry measurements-SI-ROMP of norbornene derivative ferrocene monomer

A stock solution of the Fc-NB monomer was prepared with a concentration of 2.5 mM in THF. The electrolyte solution was prepared from tetrabutylammonium hexafluorophosphate ($TBAPF_6$, 0.1 M in THF). The catalyst modified ITO substrates of type F3, were used for surface initiated ring opening metathesis polymerization of norbornene derivative ferrocene monomer. The polymerization in the pores was followed by cyclic voltammetry where the flux of the monomer in the pores was studied by the voltammetric signal of the monomer and the intensity of the peak current.

After the characterization methods applied for the benzophenone capped mesoporous silica films on ITO surface as mentioned previously, we concluded that the pores of the mesoporous ITO substrates are accessible to the guest molecules. Before testing the SI-ROMP reactions in the pores with Fc-NB monomer, the crucial step was to test the accessibility of the ferrocene molecule, which is a similar neutral molecule to the norbornene ferrocene monomer, into the pores of the substrates. In this manner we could compare the difference in the electrochemical response both for ferrocene and Fc-NB monomer.

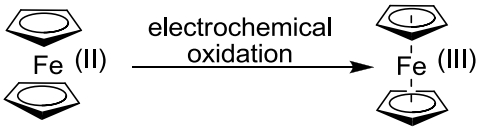

Figure 61 Electrochemical oxidation of ferrocene.

The cyclic voltammogram in the figure 62 represents the results of the permselective properties of the ITO substrates before and after modification for the ferrocene molecule. For better comparison, the reference ITO slides with no films were also used (green solid line). As seen from the electrochemical response which corresponds to the bare mesoporous ITO film (black solid line), the pores of the film are accessible to the ferrocene molecule. Finally, the electrochemical response of the modified mesoporous silica substrates with ruthenium catalyst was investigated. The catalyst was only immobilized in the pores of the mesoporous system, but still it was expected that the guest molecule has access on the pores of the substrates, since in further experiments the catalyst-modified substrates were going to be used in ring opening metathesis polymerization reactions, where the polymerization was expected to take place inside the pores. As seen from the cyclic voltammogram (figure 62), a well defined electrochemical responsewas observed in the case of catalyst-modified ITO substrate and 2.5 mM of ferrocene guest molecule. This results of cyclic voltammetry clearly showed that there was access for the ferrocene molecule in the pores of the mesoporous ITO substrate.

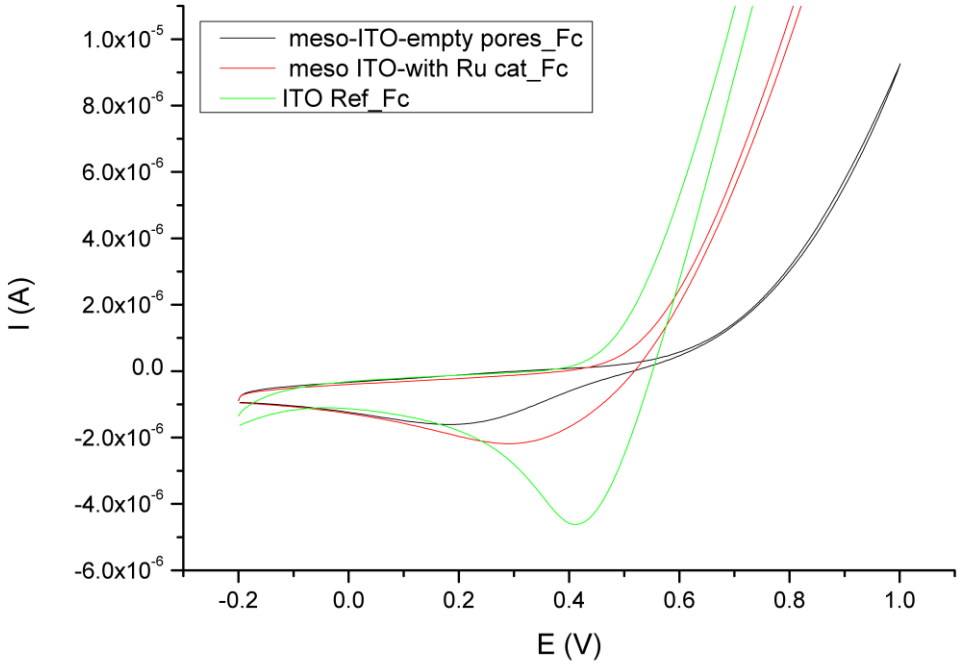

Figure 62 Cyclic voltammogram corresponding to benzophenone capped ITO films (black solid line), mesoporous ITO films with ruthenium catalyst (red solid line) and reference ITO slide (green solid line), in the presence of 2.5 mM ferrocene.

For the surface initiated ring opening metathesis polymerization of norbornene derivative ferrocene monomer, 2.5 mM of Fc-NB monomer solution was used in THF. The electrolyte solution used was tetrabutylammonium hexafluorophosphate ($TBAPF_6$, 0.1 M in THF). The catalyst modified ITO substrates of type F3, whereas as reference substrates were used blank ITO slides (without template) and mesoporous ITO slides without catalyst in the pores. The figure 63 represents the cyclic voltammogram from the surface initiated ring opening reaction (SI-ROMP) of Fc-NB monomer. The green solid line represents the electrochemical response for the blank ITO slide, without template. The black solid line represents the electrochemical response of the benzophenone capped ITO slide without catalyst in the pores in the monomer free environment, where there is no electrochemical response. The red solid line in the cyclic voltammogram corresponds to the catalyst modified mesoporous ITO substrate. The intensity of the electrochemical response was observed to be 1/30 of the intensity of the signal resulting from the bare ITO substrate. This clearly shows that the pores were filled with the polymer product after ROMP reaction of Fc-NB and there was no more accessibility for new monomer molecules to enter the pores of the ITO film.

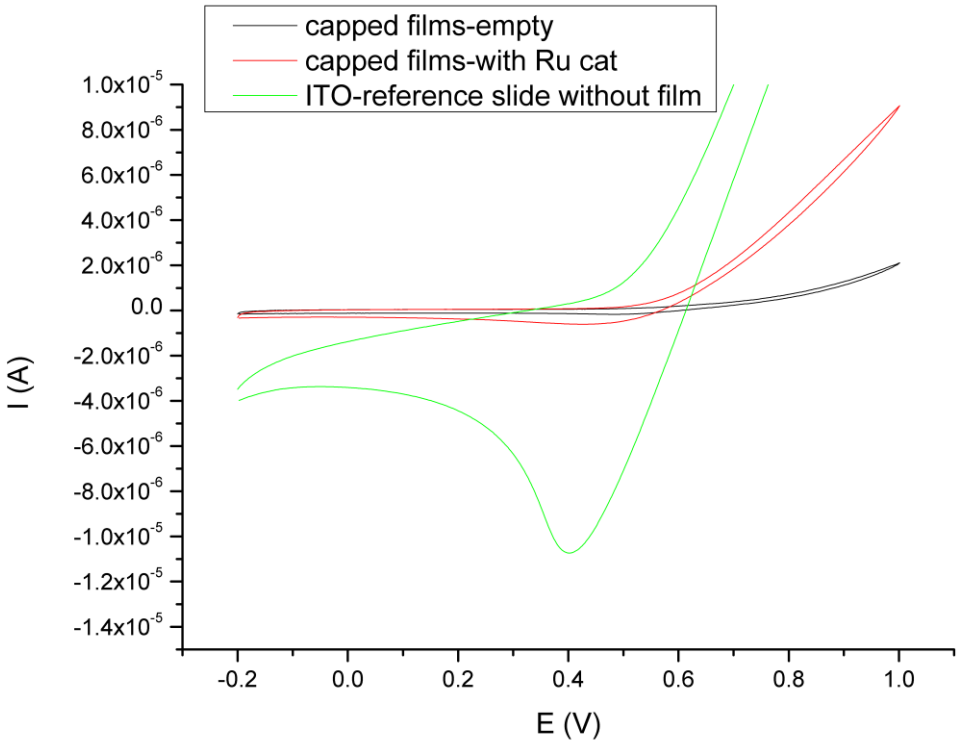

Figure 63 Cyclic voltammogram corresponding to empty benzophenone capped ITO films (black solid line), mesoporous ITO films with ruthenium catalyst (red solid line) and reference ITO slide (green solid line), in the presence of 2, 5 mM Fc-NB monomer.

The SI-ROMP of the norbornene derivative ferrocene monomer is expected to be performed by the ruthenium catalyst immobilized only in the pores of the silica film, supported on ITO, as illustrated in the figure below.

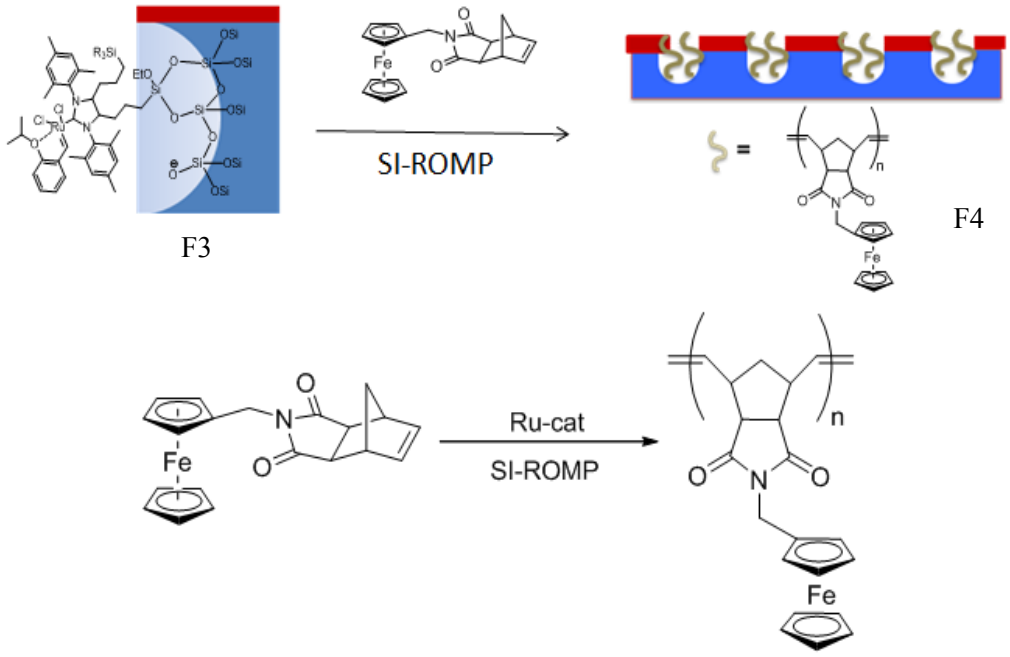

Figure 64 SI-ROMP of norbornene derivative ferrocene monomer in the pores of silica film.

3.3.10. Contact angle measurements (type F3 substrates-catalyst modified ITO and type F4 substrates after SI-ROMP reactions of norbornene derivative ferrocene monomer)

As mentioned previously, contact angle is also an interesting technique to study surface modifications and changes done on the surface of different types of substrates. The substrates of type F3 and F4 (before and after SI-ROMP respectively) were studied with a contact angle goniomteter again using static sessile drop method. As a reference substrate, the bare benzophenone capped ITO substrates were used. After the ruthenium catalyst immobilization inside the pores of ITO films it was expected that the ruthenium catalyst is immobilized only in the pores of the film and not on the surface of the benzophenone layer, therefore the contact angle of the substrates of type F3 should not show a dramatic increase in comparison to substrtaes of type F2 before modification. In addition, the substrates of type F4, ROMP reaction of the Fc-NB monomer, was expected to have a contact angle similar to substrates of type F2 and F3. The results from the contact angle measurements are represented in the figure below.

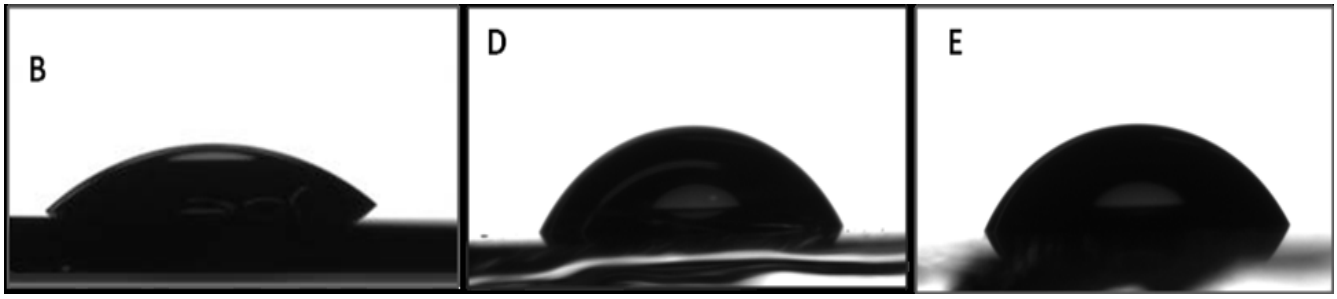

Figure 65 Contact angle measurement of ITO substrates: after capping with benzophenone-silane (B, F2) after the immobilization of ruthenium catalyst in the pores of ITO slides (C, F3) and after ROMP reaction of Fc-NB (E, F4).

The substrates of type F2, the picture B in the figure above, showed a contact angle of the value 33 °. After the ruthenium catalyst immobilization in the mesoporous ITO films, we only saw a small change in the contact angle by 12 ° (contact angle obtained was 50 °). As described previously, after the immobilization of the catalyst in the ITO films, the substrates of type F3 were use for SI-ROMP of the norbornene derivative ferrocene monomer. Since the polymerization took place in the pores of the film, the contact angle was expected that there was not a significant increase of the contact angle for the substrates of type F4. The average contact angle measured showed an increase by 5 ° (contact angle obtained was 55 °), as shown in the figure 65, case E. From the contact angle results it could be concluded that there was not a big increase in the contact angle, in this case only the pores of the ITO film are modified, where the water droplet can still well wet the surface.

In order to better characterize the modified ITO substrates and for better comparison with the unmodified ITO films (type F2 substrates), ellipsometry was used, in order to investigate other parameters like: change in film thickness and refractive index of the modified ITO films.

3.3.11. Ellipsometry measurements (type F3 substrates-catalyst modified ITO and type F4 substrates after SI-ROMP reactions of norbornene derivative ferrocene monomer)

Ellipsometric measurements were crucial in studying the change on the film thickness as well as the changes in the refractive index after surface modification. The benzophenone capped ITO substrates (type F2 substrates) were used as reference substrates. Substrates of type F3 and F4 were studied, after ruthenium catalyst immobilization and after SI-ROMP reaction in the pores of the mesoporous system.

Just like in the case of the contact angle measurements, it was expected that there is not such a dramatic change on the outer surface of the ITO films after modification of the pores of the mesoporous hybrid. For this reason, the film thickness of substrates of type F3 and F4 measured by ellipsometry, were expected to be similar in value with the substrates before modification (type F2 substrates). Ellipsometry was also useful in measuring the refractive index of the substrates as well. The measured refractive index for the benzophenone capped ITO substrates (type F2 substrates), was found to be 1.269. For the type F3 ITO films (modified with ruthenium catalyst) the refractive index was expected to be higher than substrates F2, because of the filled pores with catalyst. In addition, the refractive index of the substrates of type F4 (after SI-ROMP reaction) was expected to be higher than in the case of substrates F3.

The ellipsometry results concerning the film thickness as well as the refractive index are represented in the table below.

Parameters	**ITO/ after capping (F2)**	**ITO/ after ruthenium cat immobilization (F3)**	**ITO/ after SI-ROMP (F4)**
film thickness (nm)	225	225.1	225.3
refractive index	1.278	1.372	1.545

Table 4 Film thickness and refractive indices of indium tin oxide (ITO) substrates of type F2, F3 and F4, before and after modification.

As seen from the table 4 above, the film thickness of the substrates after catalyst immobilization (F3) and after SI-ROMP reactions (F4) did not show a significant change. This shows that there was no modification done on the surface of the ITO substrates. On the figure below, the refractive index results from ellipsometry measurements are presented.

For better comparison of results, the refractive index of benzophenone capped ITO substrates was measured (F2 substrates, before modification) and the average refractive index was found to be 1.278. After ruthenium catalyst immobilization n the pores of the ITO film, the average refractive index measured was 1.372. The increase in the refractive index showed that the pores of the film are modified, though filled with the catalyst. Finally, after ring opening metathesis polymerization of norbornene derivative ferrocene monomer, the average measured refractive index was found to be 1.545. This dramatic increase of the refractive index

showed that the polymerization was successful and that we have the polymerized product in the pores of the ITO film.

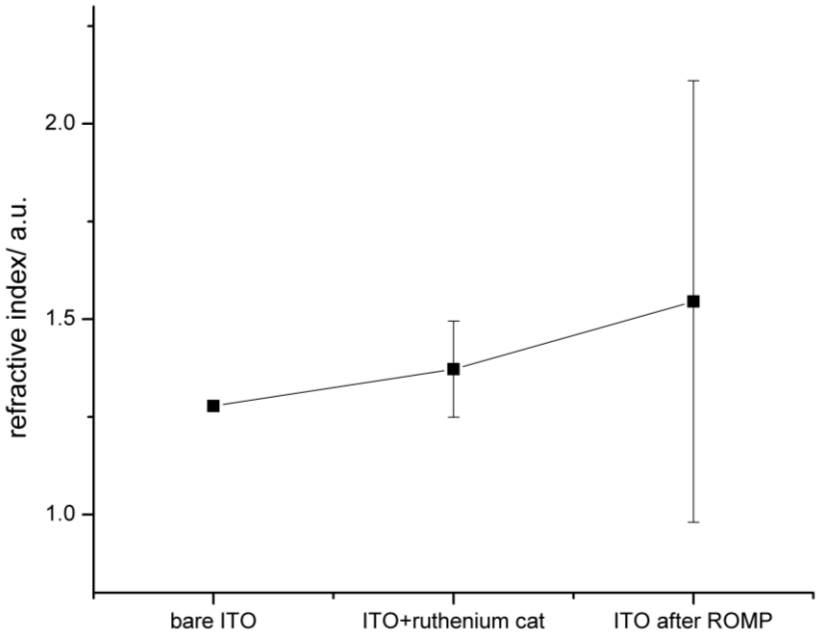

Figure 66 Increase of refractive index after immobilization of ruthenium catalyst and after SI-ROMP reactions in the pores of the mesoporous ITO substrates.

3.3.12. Application of substrates of type F2 in surface initiated ring opening metathesis polymerization (SI-ROMP) of norbornene derivative spiropyran monomer

3.3.13. Spiropyran polymer brushes and their photochemical properties

After the application of the ruthenium catalyst modified mesoporous ITO substrates in ROMP of norbornene derivative ferrocene monomer, the substrates were used for ROMP of a second monomer; norbornene derivative spiropyran monomer, which represented an interesting light-switchable organic molecule.

Samanta et al in claimed that the photochromism of spiropyrans includes photocleavage of the C-O bond. This property allows that the molecule can pass from its closed-colorless state (spiropyran = SP) to its open state (merocyanine = MC) as illustrated in the scheme below, which is characterized by a very intense color [62].

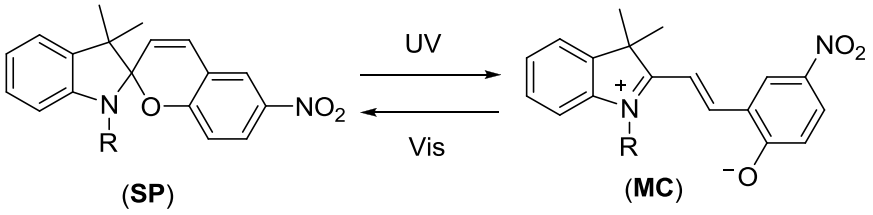

Scheme 20 Isomeric molecular structure of spiropyran irradiated with light, spiropyran (left, SP), merocyanine (right, MC) [62].

In the same study, photochromic polymer brushes bearing spiropyran moieties were grown via surface initiated opening metathesis polymerization (SI-ROMP) through a grafting-from approach [62]. The grown polymer brushes then had shown reversible photocontrol of surface properties and had shown changes in the surface morphology after irradiation in polar solvent [62].

Hauser et al, in 2012 reported a similar study related to SI-ROMP of norbornene derivative bearing spiropyran moieties [63]. Poly (norbornene) homo- and copolymers bearing spiropyran side groups were synthesized, where the switching between the apolar spiropyran form and the zwitterionic merocyanine form leaded to switchable wettability properties which were studied by contact angle measurements [63]. In the same year, Florea et al reported the growth of spiropyran groups bearing polymer brushes via SI-ROMP in the inner walls of fused silica-capillaries [60]. Since spiropyran has the freedom to respond the light, the functionalized silica capillaries were characterized via absorbance measurements as well as kinetic measurements. This interesting platform could then be applied in development of capillary sensors based on the properties of the spiropyran moieties [60].

Raymo et al, reported the development of three state molecular switch based on spiropyran derivatives which was synthesized from 2, 3, 3-trimethyl-3H-indole [64]. The aim of the study had been to understand the behavior of spiropyran derivative molecules in response to environmental stimulations. According to the study, it was necessary to reach molecular switches which can elaborate input signals and can respond in the form of measurable output signals [64]. As seen in the scheme below, spiropyran derivative were synthesized and the molecular responses at different conditions were studied.

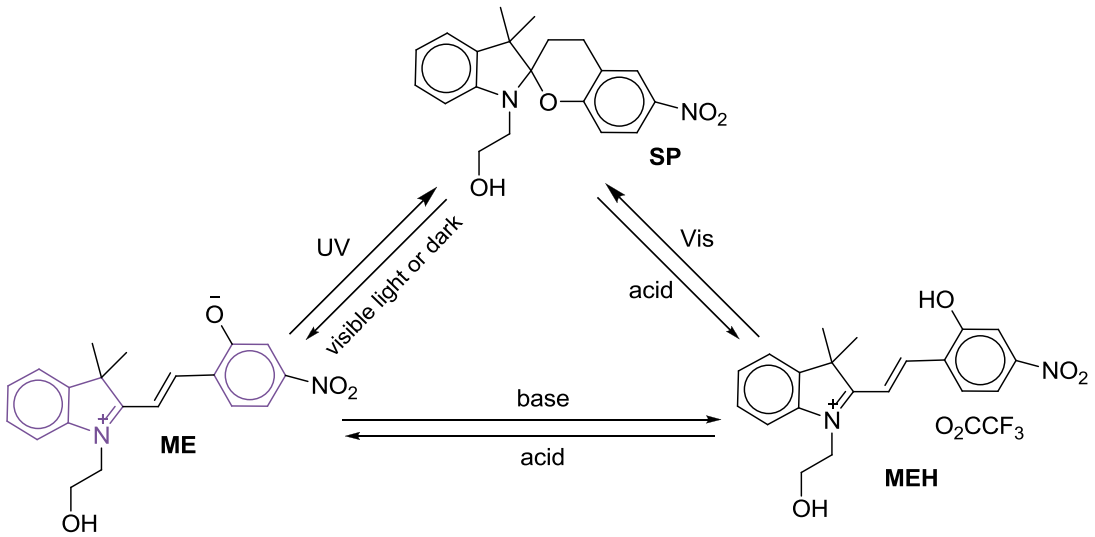

Scheme 21 The switching cycle corresponding to three states of spiropyran derivative: SP (spiropyran) and two merocyanine forms MC and MEH [64].

In this study, the switchable properties of spiropyrane moieties were studied under the following conditions: upon irradiation with ultraviolet light, the colorless SP switched to the purple ME form. After the addition of CF_3CO_2H the purple ME form then switched to the yellow-green form MEH.

The addition of CF_3CO_2H to a colorless solution of SP in the dark resulted to the yellow-green MEH. After the treatment of MEH with potassium carbonate to obtain basic conditions, resulted in complete switching to ME, giving an intense dark violet color [64].

The above mentioned study related to spiropyran molecule was conducted in order to show that the fabrication of artificial systems which could elaborate and transmit signals at the molecular level could be successfully achieved.

3.3.14. SI-ROMP of norbornene derivative of spiropyran monomer in the mesoporous silica films supported on ITO

For the surface initiated ring opening metathesis polymerization of the norbornene derivative spiropyran monomer which was synthesized and characterized by Fabio Krohm (monomer in figure 67, scheme 22), the substrates of type F2 were used (benzophenone capped mesoporous silica films). As mentioned previously, the ruthenium catalyst was immobilized inside the pores of the ITO films so that SI-ROMP reaction goes on only inside the pores of the film. In order to deactivate the physisorbed catalyst on the outer surface of the mesoporous film, the catalyst modified substrates of type F3 were plasma treated (CO_2-plasma at low pressure, low power and gas rate). After plasma treatment, the substrates were immersed in the monomer solution (4ml / ml of monomer in DCM) under inert atmosphere as illustrated in the figure 67. A batch of substrates was used and they were investigated at different polymerization times, from 2 min to 30 min. After the surface initiated ROMP, the reaction was quenched with ethyl vinyl ether and the modified substrates were then washed with DCM and then with methanol and finally dried under vacuum in order to obtain the substrates of type F5. As shown in the figure 67 below, the polymerization was expected to take place only in the pores of the mesoporous silica films. In order to prove the SI-ROMP in the pores of the films, further characterizations were carried out: ellipsometry measurements (film thickness measurements and refractive index measurements) as well as ATR-IR measurements.

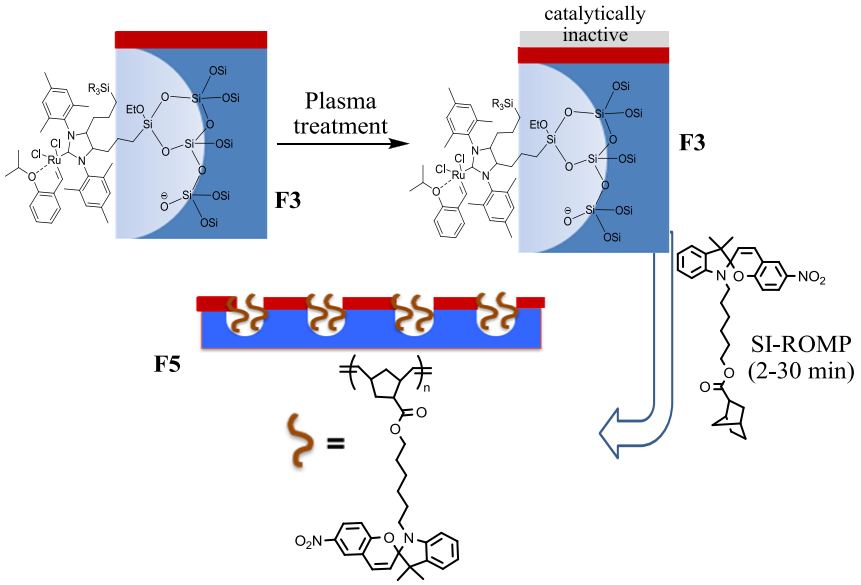

Figure 67 SI-ROMP of norbornene derivative spiropyran monomer in the mesoporous silica films, to obtain modified substrates of type F5.

After the ring opening metathesis polymerization reaction, the polymer product (norbornene derivative spiropyran polymer) was extracted with methanol solution from the pores of the ITO film. The dark violet norbornene derivative spiropyran polymer was further characterized via gel permeation chromatography (GPC) and UV-Vis measurements in solution.

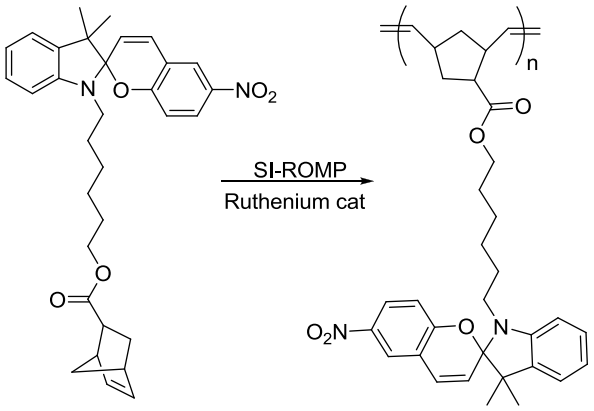

Scheme 22 Surface initiated ring opening metathesis polymerization (SI-ROMP) of norbornene derivative spiropyran monomer.

3.3.15. Ellipsometry measurements (type F5 substrates after surface initiated ring opening metathesis polymerization of norbornene derivative spiropyran, in mesoporous silica supported on ITO

Ellipsometry measurements were used in measuring the refractive index of the mesoporous ITO substrates after ruthenium catalyst immobilization and after SI-ROMP reaction of norborene derivative spiropyran monomer, in order to prove the pore filling. By a short plasma treatment it was possible to deactivate the ruthenium catalyst on the top of mesoporous film in order to obtain polymer only in the nanoconfined environment. As shown in the previous ellipsometry measurements, the layer thickness of the empty ITO substrates and catalyst immobilized ITO substrates did not show any significant increase. For this reason, during the ellipsometry measurements the layer thickness was set constant in all cases during the refractive index measurements, at the original value of empty mesoporous silica films (substrates of type F2). From the ellipsometry measurements, it was expected that the layer thickness of the substrates after catalyst immobilization and after SI-ROMP reaction does not show any significant increase. On the other hand, since after the mesoporous film modification the pores are filled, the refractive index of the surfaces was expected to increase gradually.

.

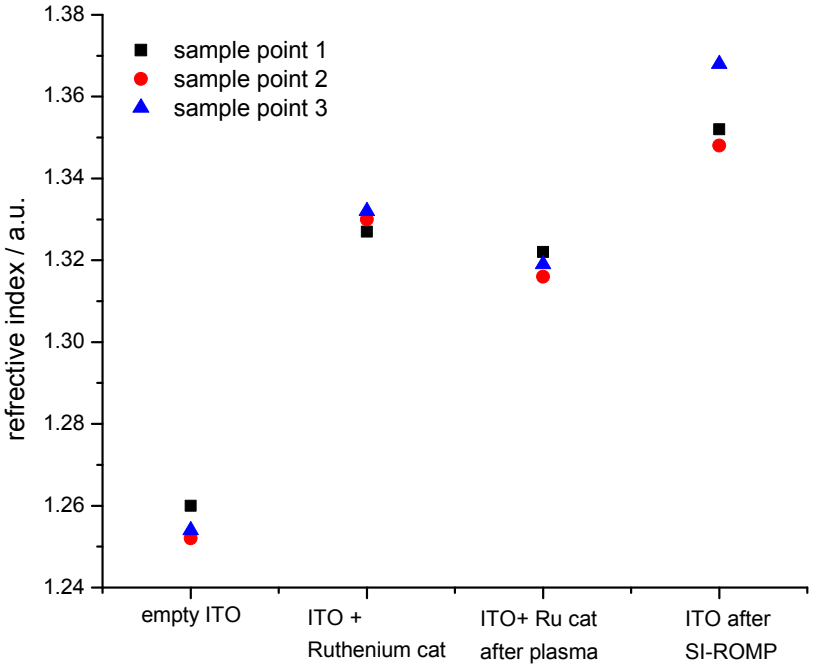

Figure 68 Ellipsometry measurements: refractive index results of ITO films: empty ITO, catalyst modified ITO, catalyst modified ITO-after plasma treatment, ITO after SI-ROMP of norbornene derivative spiropyran monomer.

The refractive index for each substrate was measured at three different points. The first measurements were carried out with the bare (empty) ITO substrates, where the average refractive index (measured at three different points) was observed to be 1.257. After the ruthenium catalyst immobilization in the pores of the mesoporous ITO substrates, there was a dramatic increase in the refractive index to 1.330. Plasma treatment was necessary to deactivate the physisorbed ruthenium catalyst on the outer surface of ITO films and it was expected that there was no significant change in the refractive index since the catalyst inside the pores of the film was not affected by this process. As seen from the graph in figure 59, the average refractive index measured from the samples after plasma treatment was 1.319, which was a value close to the refractive index of the substrates after ruthenium catalyst immobilization. Finally, the mesoporous ITO substrates after SI-ROMP of norbornene derivative spiropyran monomer were studied by ellipsometry. Because of polymer growth inside the pores of the film, the refractive index obtain was expected to be much higher than in all previous case before ROMP reaction. The average refractive index obtained was 1.356. This dramatic increase in the refractive index proved that the pores of the ITO substrates were filled with norbornene derivative spiropyran polymer, which was later extracted from the pores of the ITO substrates and further characterized by GPC as well as UV-VIS measurements.

For the GPC measurements, the polymer was extracted from several ITO slides in methanol and the molecular weight of the polymer was determined as shown in the table below after a short polymerization time.

Parameters	polymerization time (2.5 min)	polymerization time (5 min)
Mn [g/ mol]	7.0e^3	7.9e^3
Mw [g/ mol]	1.39e^4	1.41e^4
Polydispersity index (PDI)	2.0	1.8

Table 5 Molecula weight of spiropyran polymer after SI-ROMP on mesoporous ITO substrates.

3.3.16. ATR-IR (type F5 substrates-after surface initiated ring opening metathesis polymerization (SI-ROMP) of norbornene derivative spiropyran monomer)

The IR-spectroscopy of the polymer modified mesoporous ITO substrates was compared with the IR spectroscopy of the polymer which was results after ring opening metathesis polymerization reaction in DCM, which measurements were carried out by Fabio Krohm. The reaction time was much shorter, 2.5 min, which was more than enough to detect all the characteristic functional groups belonging to the norbornene derivative spiropyran polymer. The signals are also represented in the table 6.

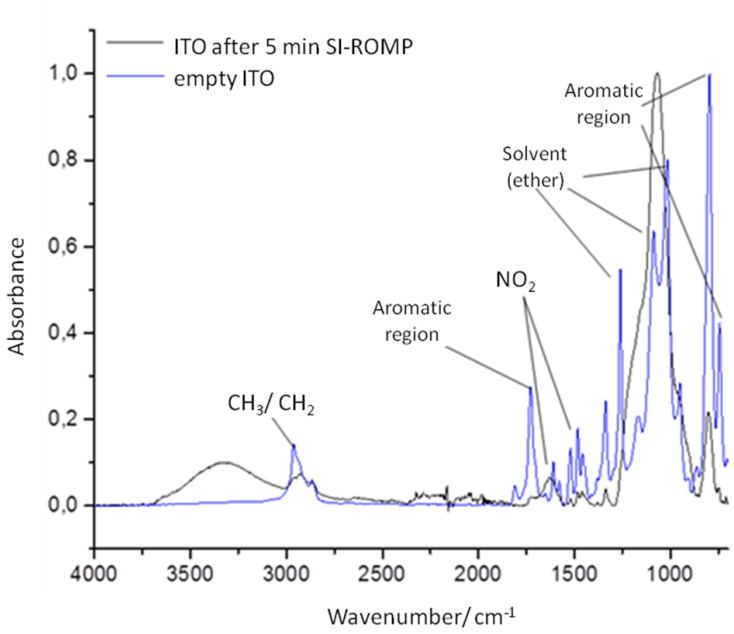

Figure 69 IR spectroscopy of ITO substrates: bare ITO (red solid line), modified ITO substrate after SI-ROMP (black solid line).

Frequency/ cm^{-1}	Functional groups
2955	CH_3 / CH_2
1720	Aromatic region
1610, 1460, 1425	C-NO_2
1260, 1075, 1005	C-O-C
1050	C-O-C
790	Aromatic region

Table 6 IR spectroscopy results after 2.5 min ROMP reaction of norbornene derivative spiropyran monomer solution (DCM).

To sum up, infrared spectroscopy was an important characterization technique to prove the SI-ROMP as well as ROMP reaction of norbornene derivative spiropyran monomer, by detecting the functional groups of the polymer. The polymer product which was extracted from the mesoporous ITO substrates after SI-ROMP was further characterized by UV-Vis spectroscopy and GPC.

3.3.17. UV-Vis spectroscopy of spiropyrannorbornene polymer

Polymer brushes bearing spiropyran moieties are characterized by their photochromism properties which involve photocleavage of the spiro C=O bond which allows reversible switching between a colorless closed form and a colored open form, merocyanine polymer form as shown in the scheme below.

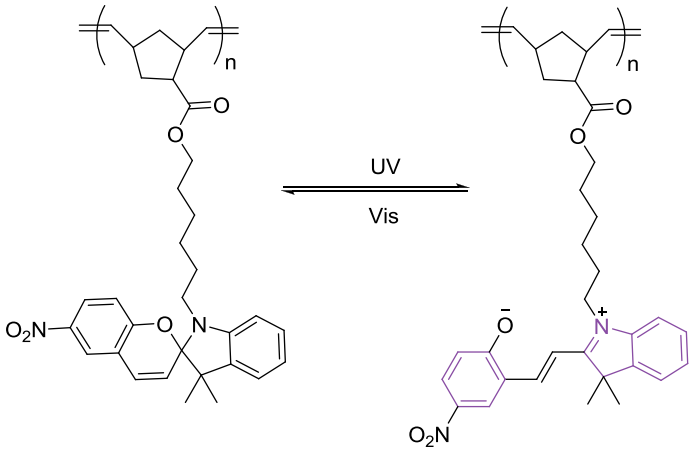

Figure 70 Isomeric molecular structure of spiropyrannorbornene polymer irradiated with light, spiropyran, closed form (left, SP), merocyanine, open form (right, MC).

The UV-Vis measurement were provided by Fabio Krohm, which were carried out in two different solvents, DCM and DMF, where the concentration of the polymer was in all cases 5.095 µM (0.071 mg/ ml where the molecular weight of the polymer was found to be 14100 g/ mol).

The spiropyrannorbornene polymer used for UV-Vis measurements was extracted from the ITO substrates after 5 min SI-ROMP reaction. The closed form of the polymer form (spiropyran form, SP) gave a colorless solution, whereas the open form of the polymer (merocyanine form, MC) gave an intense violet color upon UV irradiation as shown in the figure below.

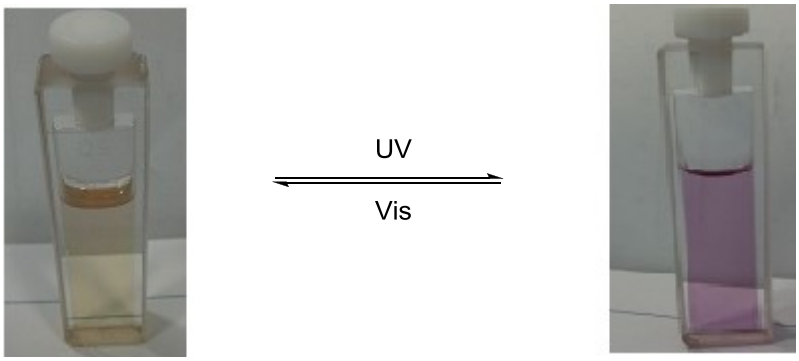

Figure 71 Spiropyranenorbornene polymer (0.071 mg/ ml in DCM or DMF).

The UV-Vis measurements were performed in two different solvents: DCM and DFM respectively and the absorbance spectra are given in the figure below. At 373 nm wavelength in DCM the maximum absorption was observed to be 0.55, whereas in DMF at 380 nm the maximum absorption was 0.53.

As can be observed from the UV-Vis results, the switching efficiency of the spiropyran polymer in DCM decreases after 0.3, while the switching efficiency at this at 0.3 absorption unit increases in the case of DMF solvent.

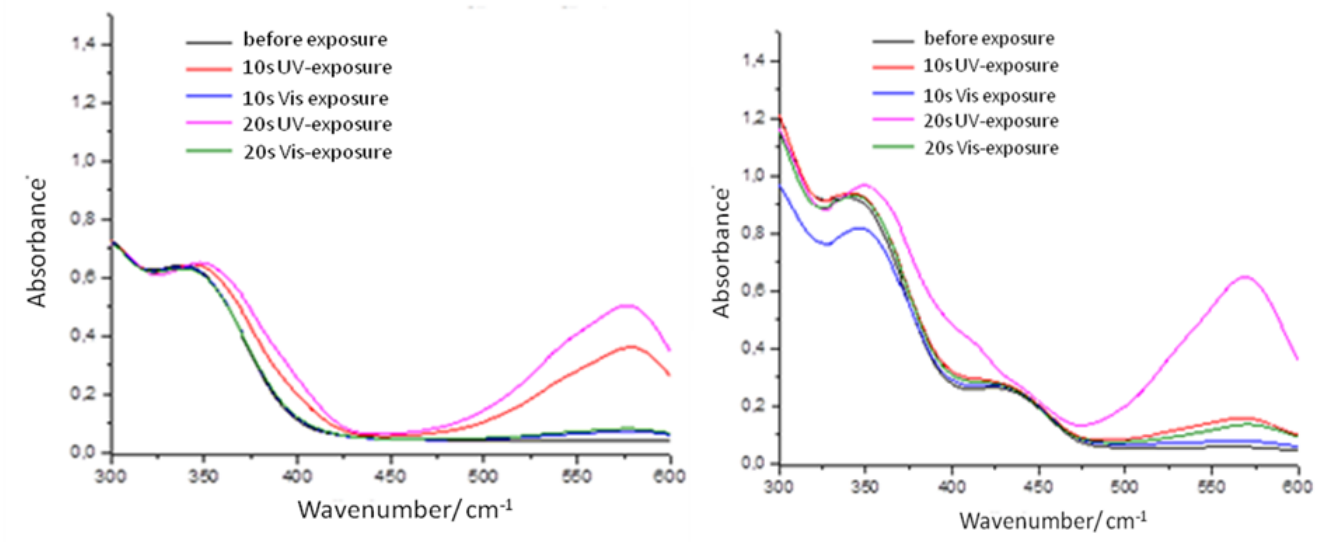

Figure 72 UV-Vis spectrum of spiropyran polymer ($7.1 \cdot 10^{-2}$ mg/ ml, Mw= 14100 g/ mol) after 5 min ROMP, in DCM (left) and DMF (right).

3.4. Summary and conclusion

In this study, surface initiated ring opening metathesis polymerization (SI-ROMP) inside the pores of mesoporous silica films supported on intium tin oxide (ITO) substrates, which substrates were prepared by Fabio Krohm, was studied. Grubbs Hoveyda 2nd generation type catalyst bearing functional –Si $(OEt)_3$ groups which could be covalently bound on the surface.

Secondly, silica mesoporous substrates were prepared capped with benzophenone polymer on the surface for the passivation of the surface of silica film. After the removal of the template, ITO substrates were obtained with benzophenone (BP) polymer layer on the outer surface whereas the pores of the ITO substrates were bare with functional –Si-OH groups. The accessibility of the guest molecules, negatively and positively charged respectively $(Fe(CN)_6)^{3-}$ and $Ru(NH_3)_6^{3+}$ in the ITO pores was tested at different pH conditions in order to prove that the pores of the hybrid system are available for the immobilization of the –Si $(OEt)_3$ groups bearing ruthenium complex. Finally, Grubbs Hoveyda 2nd generation type complex was immobilized on the pores of the ITO films as shown below. The functionalized ITO substrates before and after modification were characterized by ellipsometry, ATR-IR, contact angle, cyclic voltammetry (CV) as well scanning electron microscopy (SEM).

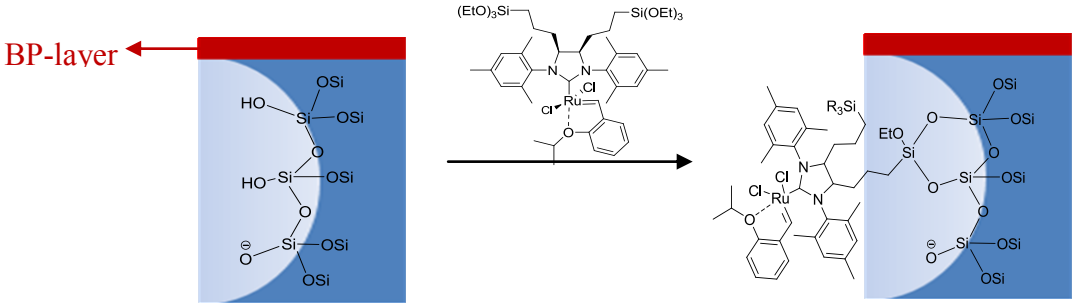

The catalyst modified ITO substrates were then used for the surface initiated ring opening metathesis polymerization (SI-ROMP), but these were some problems regarding the catalysts in terms of polymer stability in the presence of solvents. Two different types of monomers were used for ROMP reactions: norbornene derivative ferrocene monomer (Fc-NB) as well as norbornene derivative spiropyran monomer as shown below.

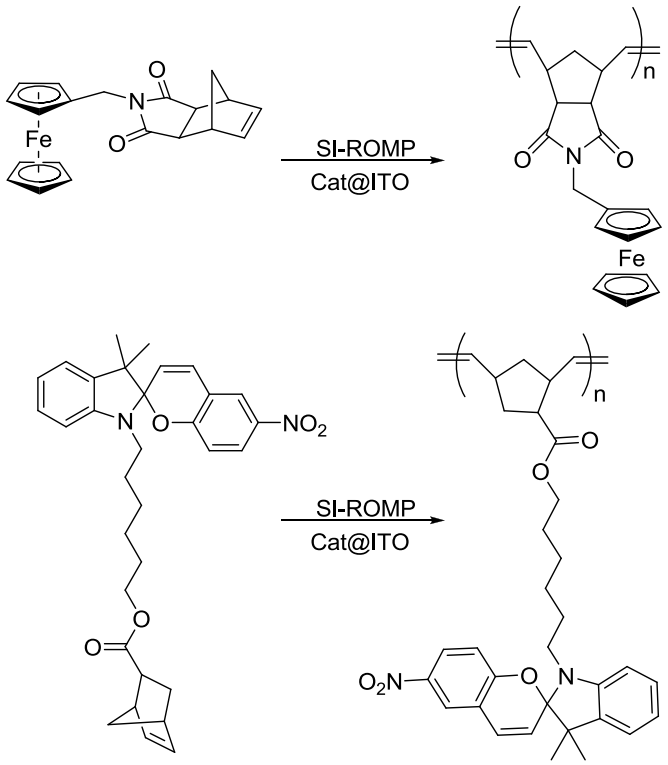

The ring opening metathesis polymerization of the above mentioned monomers (Fc-NB and spiropyran-NB), were carried out only inside the pores of the mesoporous silica substrates as shown in the fugure below, which was also one of the most important goals of this work.

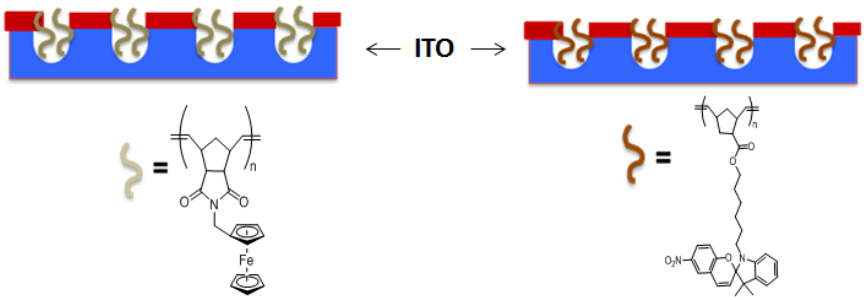

Again, to prove that the polymerization of the monomer has taken part only inside the pores of the mesoporous ITO films, several characterization techniques were performed with for the substrates before and after SI-ROMP reactions: ellipsometry (for the measurement of the film thickness as well as refractive index measurement), contact angle measurements, ATR-IR as well as UV-VIS in the case of norbornene derivative spiropyran monomer in order to study its switchable properties.

4. Aim 3 (Introduction)

4.1. Alkyne hydration reactions catalysed by organometallic gold compounds

The hydration of alkynes is known to be mediated by addition of large excess of acidic reagents. On the other hand, milder conditions can be used for hydration reactions for alkynes, where transition metals have been used to catalyze these reactions, where the alcohols are added across the triple bond [65]. Transition metal complexes containing Ru(III), Rh, Pd(II), Cu(II) or Ag(I) have been used. For many years the gold compounds in catalysis have been avoided because of the opinion that it is expensive. However, gold salts even in very small amounts are known to do display high catalytic activity [65]. In 1998 Teles et al reported the addition of methanol to alkynes in mild conditions catalyzed by Au(I) [66]. In 2003, the activity of Au(III) organometallic complexes was tested in addition of water and alcohol to alkynes in neutral media where it was also possible to identify the possible intermediates by spectroscopic methods [65]. In this study, the catalystic activity of gold(III) ionic compounds with one or two pentafluorophenyl (C_6F_5) or mesityl (2, 4,6-$(CH_3)_3C_6H_2$) radicals was tested in hydration reaction of phenylacetylene, in mild conditions as shown in the scheme below.

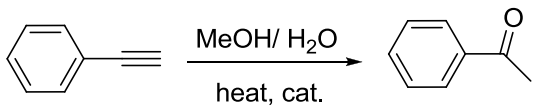

Scheme 23 Hydration of phenylacetylene with gold(III) complexes [65].

For the hydration of phenylacetylene, Na[AuCl] (2 mol %, 1h) was used where the resulting product (phenyl methyl ketone) in 91 % yield [65].

Tanaka et al tested the catalysis of [(Ph_3P)AuMe]/ H^+ in the hydration reaction of 1-octyne, which showed really high turnover frequency (TOF) [67]. The drawbacks of this reaction had been the use of high loadings of strong acids. In 2008, Nolan and coworkers developed [(L)Au] based complexes to be used in hydration reactions of alkynes, where the choice of supporting ligands had been *N*-heterocyclic carbenes, since they lead to the development of highly efficient systems at low catalytic loadings [68]. Gold complexes bearing different types of NHC ligands were synthesized, as shown in the figure below.

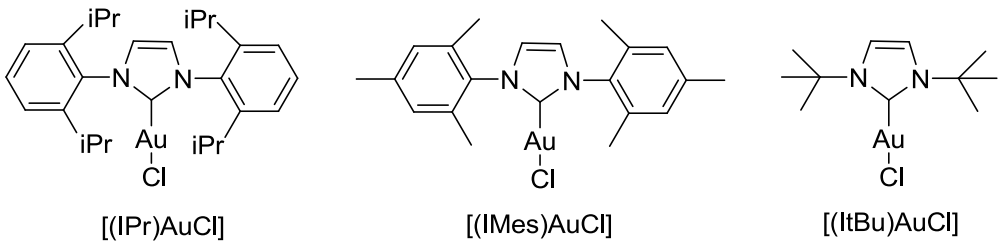

Figure 73 Gold complexes used in hydration of alkynes [68].

After testing all the complexes in the hydration of alkynes, [(NHC)AuCl]/ $AgSbF_6$ catalytic system (used in part per million loadings) had shown the biggest conversion (97 %) in 1,4-dioxane or methanol [68]. The scheme for the optimization of hydration conditions is given in the scheme 24 below.

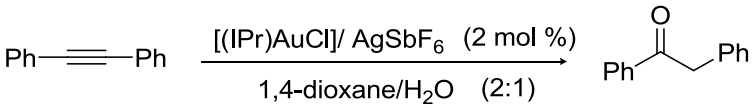

Scheme 24 Optimized conditions for hydration of alkynes [68].

Gold complexes have experienced a fast growth recently because of their activity in water media as well as their effective catalysis in reactions like; hydroamination of alkenes and alkynes, polymerization, enyne cycloisomerisation etc [69]. For this reason, further research was done on improving the synthesis of [(NHC)AuX] (X= Cl, Br, I) complexes and their application in hydration reactions. In 2013, Nolan and coworkers represented a one step synthesis of gold complexes, using relatively mild conditions and technical grade solvents, where they could apply the conditions to both imidazolium and imidazolinium salts [70].

Even though homogenous catalysis has shown a very important role in the world of modern catalysis [71], a very interesting approach would be able to recycle the complexes and eliminate the metal contamination of the products. For this reason, the homogenous catalysis, including the gold complexes, have been heteogenized where the gold complex is anchored on a solid substrate [72].

Li and coworkers, in 2013 reported the very first *N*-heterocyclic carbene gold(I) complex immobilized on porous organic polymer (POP) because of their porous nature and high surface area [72]. In this work, Au-NHC@POPs with varying NHC's were synthesized via Sonogashira chemistry as shown in the figure below.

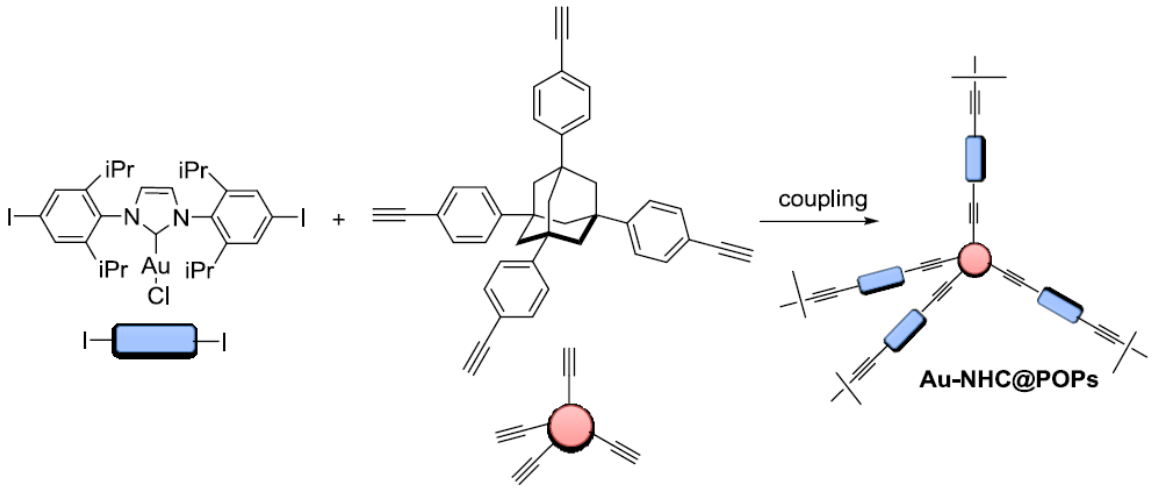

Figure 74 Synthesis of Au-NHC@POPs using the Pd catalyzed Sonogashira coupling [72].

As seen in the scheme above, first of all the iodine functionalized *N*-heterocyclic gold(I) building block was synthesized, then it was polycondensed with the alkyne monomer linker in order to form the desired system

Au-NHC@POPs [72]. The synthesized heterogeneous gold catalysis was then used for hydration reactions of alkynes where the optimized conditions for these reactions are given in the scheme below.

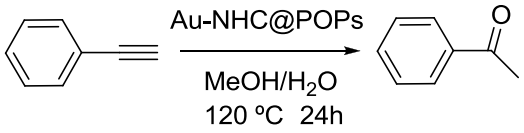

Scheme 25 Optimized conditions for hydration reaction of phenylacetylene coupling [72].

The gold catalyst immobilized on porous organic polymers (POP), was found to be a very effective catalytic system for hydration reactions, with good tolerance of substrate and without a significant loss of catalytic efficiency [72].

After observing the application of gold complexes in several valuable processes and their ability to perform reactions in water, the idea of the third project was to synthesize heterogeneous *N*-heterocyclic carbene gold(I) complexes and test them in hydration reactions of alkynes for effective catalysis.

4.2. Objective of the project: Synthesis and Immobilization of amino group bearing [(NHC)AuCl] complexes on cellulose nanocrystals (CNC) and polymer modified filter paper and their application in hydration reactions of alkynes

The third part of this work was synthesis of [(NHC)AuCl] complexes as illustrated in figure 75 and their immobilization on cellulose nanocrystals (CNC) and polymer modified filter paper. The heterogenous gold catalyst system was then applied in hydration reactions of alkynes. The supporting lingand were chosen *N*-heterocyclic carbenes (NHCs) bearing amino groups (-NH_2) which were used as anchoring groups to covalently bind on the surface.

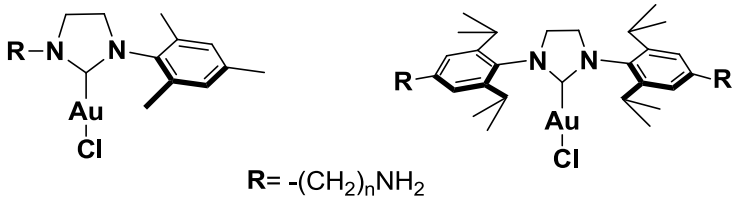

Figure 75 [(NHC) AuCl] type complexes with amino groups for surface immobilization.

For the immobilization of amino group functionalized catalysts, nanocrystalline cellulose was used bearing functional carbonyl groups. The nanocrystals were obtained from oxidation of commercially available microcrystalline cellulose (MCC) as described in the scheme 26 below and the cellulose nanocrystals were dispersed in water.

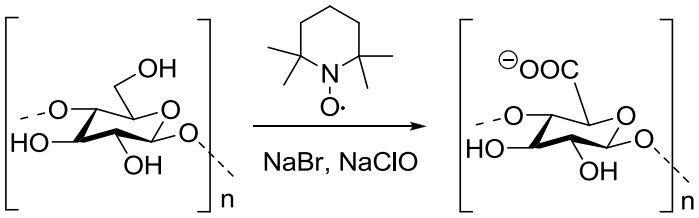

Scheme 26 Synthesis of cellulose nanocrystals (CNC) from microcrystalline cellulose (MCC).

The prepared cellulose nanocrystalls (CNC), dispersed in (DMSO/H_2O), were then used for the immobilization of [(NHC) AuCl] complex, as illustrated in the scheme below.

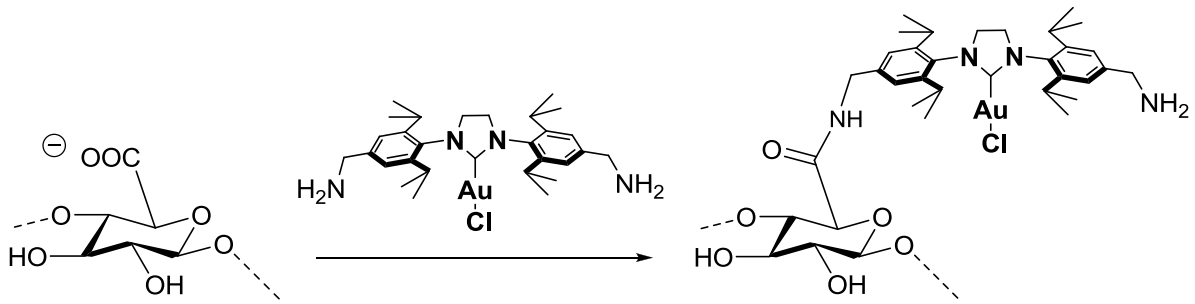

Scheme 27 Immobilization of [(NHC)AuCl] type complex on cellulose nanocrystals (CNC).

The catalyst modified crystalline nanocellulose ([(NHC)AuCl]@CNC) was then used for hydration reactions of alkynes as given in the scheme below.

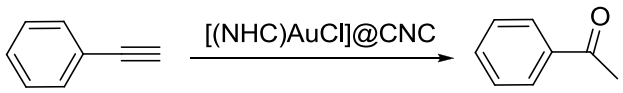

Scheme 28 Hydration of alkynes using [(NHC)AuCl]@CNC.

Another target substrate for immobilization of gold complexes was polymer modified filter paper. The standard filter paper was chemically microstructured by photo-chemical attachment of functional polymers to cellulose microfibers. The polymer network was formed through three different types of monomers as described in figure 76. Methyl-methacrylate (MMA) was chosen as the matrix monomer. The second monomer was succinimide moieties bearing monomer which was used for covalently binding of the gold complex on the cellulose fibers. The third monomer was containing benzophenone moieties which were used as binder monomers.

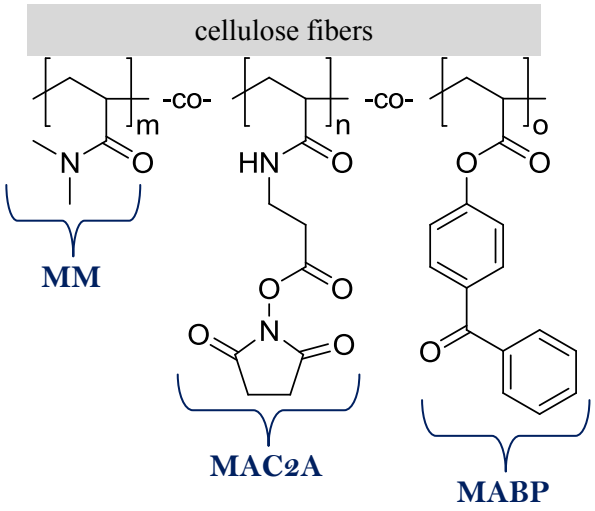

Figure 76 P (DMAA-co-MAC2AE-co-MABP) modified filter paper.

The next crucial step was the immobilization of the [(NHC)AuCl] type complexes on the previously mentioned polymer modified filter paper substrates as illustrated in scheme below.

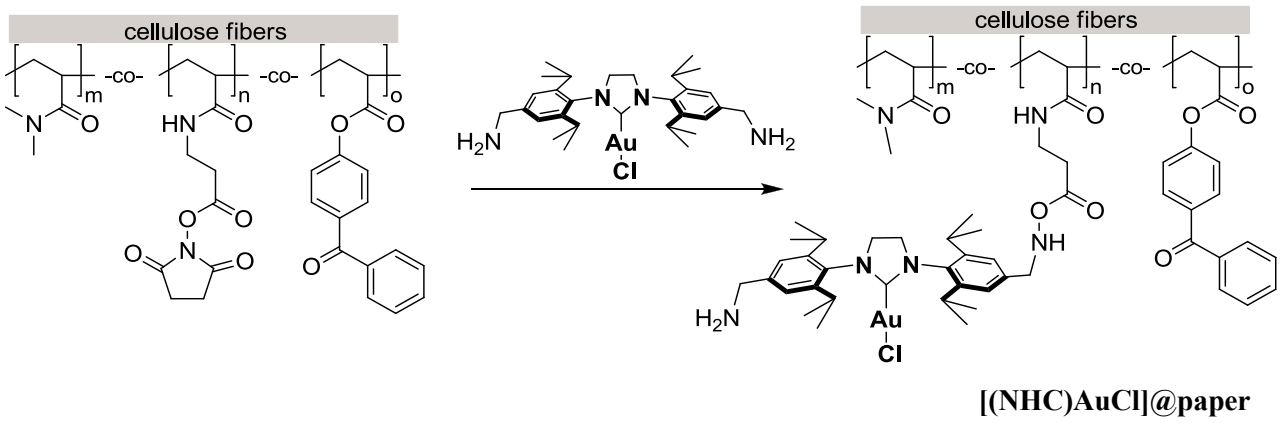

Scheme 29 Immobilization of [(NHC)AuCl] complex on polymer modified filter paper.

The catalyst modified filter paper substrtaes ([(NHC)AuCl]@paper) was then use for hydration reaction of alkynes as shown in scheme 30.

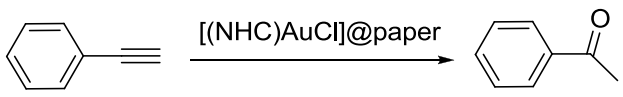

Scheme 30 Hydration reactions using [(NHC)AuCl]@paper substrates.

4.3. Selective synthesis of cellulose products and polymer functionalization of cellulose fibers (filter paper)

4.3.1. Selective synthesis of cellulose products

Cellulose is considered as one of the most common organic polymer which represents almost unlimited source of raw material for the increasing demand for the environmental friendly products [73]. The figure below represents the molecular structure of cellulose, which is a linear-chain polymer in which the chain length is the number of constituent anhydroglucose (degree of polymerization DP), with a large number of hydroxyl groups [73].

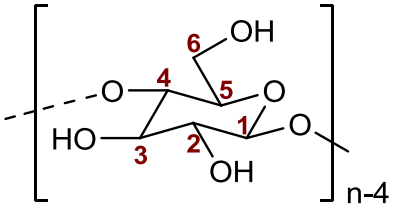

Figure 77 Molecular structure of cellulose, n= DP, degree of polymerization [73].

Cellulose as well as cellulose derivatives can be characterized by various methods like: X-ray diffraction, electron microscopy, solid ^{13}C-NMR and most importantly liquid state ^{1}H and ^{13}C NMR, which makes it simpler to understand cellulose reactivity and functionalization [74]. Since the reactivity of the OH groups are determined by hydrogen bond breaking step, it makes it more difficult to perform normal organic reaction with cellulose. Nevertheless, cellulose activation can be controlled and heterogeneous type reactions permit ideal cellulose derivatives [75]. The solubility of cellulose and cellulose derivatives has been studied for many years to make the homogenous synthesis possible. Ciacco et al, reported that tetrabutylammonium fluoride trihydrate in DMSO (DMSO/ TBAF) was a good solvent system for the solubility of cellulose in order to advance in homogenous synthesis regarding the functionalization of cellulose [75]. After those investigations, it has been possible to synthesize new types of cellulose derivatives. In additios, the knowledge about the reaction mechanisms, reaction control as well as structure-properties has been increased [75].

The properties of cellulose can be tuned by introducing different types of functional groups. One example of this preparative study involves the study of cellulose with reduced functionality.

In 2000, Redl and coworkers reported the synthesis of cellulose with optoelectronic properties and reduced functionality at O_2 and O_3 as ether protected substrates for the consequent reactions at O_6-OH groups, as illustrated in the scheme 31 below [76]. To the free O_6-OH group then any functional group can be introduced, eg. covalently bound dyes, in order to obtain cellulose derivative bearing optoelectronic properties [76].

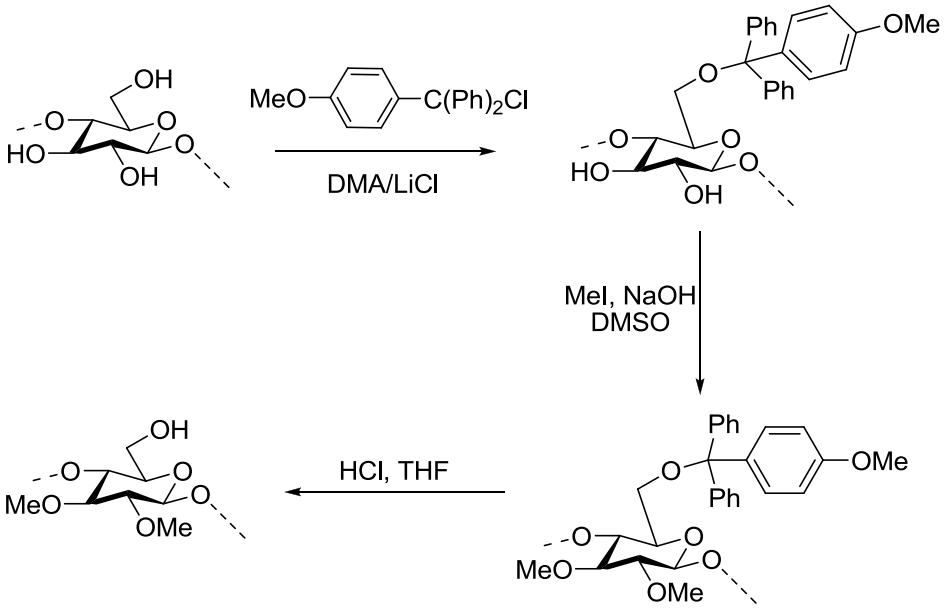

Scheme 31 2, 3-Methyl ether as regioselective element in preparation of cellulose derivatives with reduced functionality [76].

In 2003, Henze and coworkers reported further reactions regarding functionalization of cellulose and characterization of cellulose products [77]. They claimed that through the activation of free acids in situ with tosyl chloride, *N*, *N'*-carbonyldiimidazole under homogenous acylation with DMA/ LiCl or DMSO/ TBAF mixture, as shown in the scheme below.

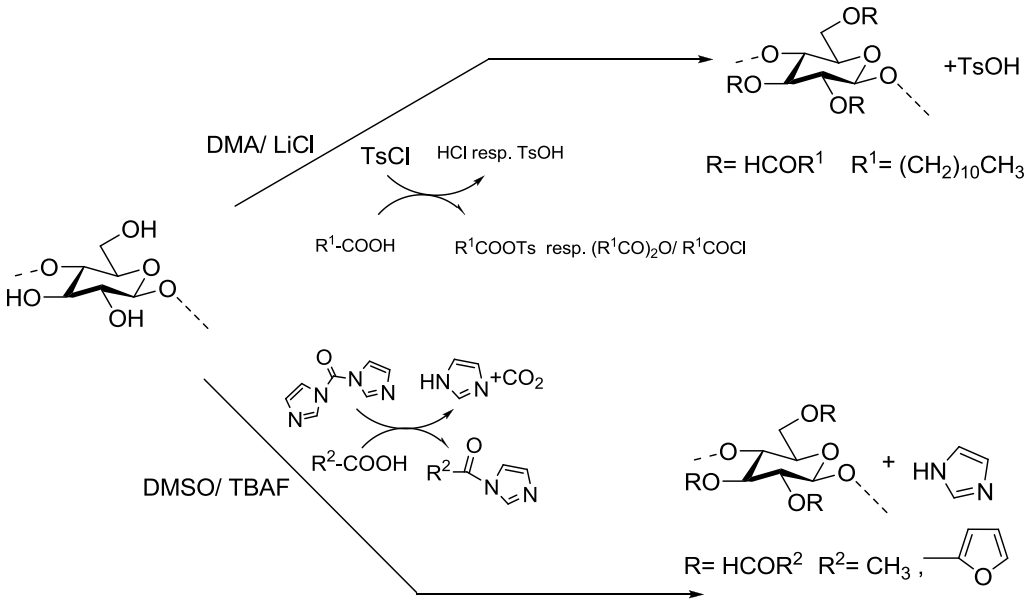

Scheme 32 Esterification of cellulose by activation of carboxylic acid by: tosyl chloride and by *N*, *N'*-carbonyldiimidazole [77].

As observed in the scheme 32, many different types of cellulose products, esters of aliphatic, aromatic and functionalized carboxylic acids are synthesized, which clearly refers to a wide range in degree of substitution is possible [77].

Among several organic reactions and cellulose derivatives, aminocellulose derivatives was reported by Tiller and coworkers, where they refer to aminodeoxy derivatives that bear the nitrogen function to the cellulose skeleton [78]. They reported the synthesis of aminocellulose through cellulose starting materials designed with tosyl functional groups, as illustrated in the scheme below.

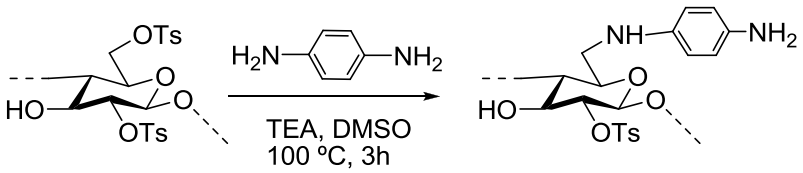

Scheme 33 Synthesis of aminocellulose from tosyl cellulose [78].

Cellulose derivatives bearing amino groups have shown to be very good substrates for surface immobilization. In a given example, aminocellulose has been used as substrates for immobilization of proteins. As seen in the scheme above, these typical aminocellulose derivatives were synthesized from tosyl cellulose (DP= 2.3), which reacted with 1,4-diphenyldiamine (PDA) in DMSO in the presence of triethylamine [78].

Another study related to diphenyldiamine cellulose derivatives was carried out by Tiller and coworkers in 2001 [79]. In their report they showed that aliphatic diamino group can be anchored to the cellulose surface using diaminoalkanesas represented in the scheme below.

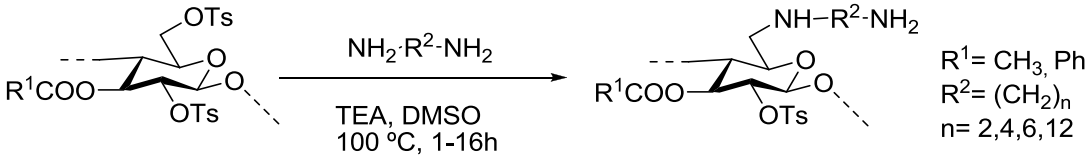

Scheme 34 Aminocellulose synthesis from tosyl amine derivatives [79].

The aminocellulose derivative products were then used in film formation, which films were applied in immobilization of enzymes on surface [79]. Another example representing the surface immobilization through cellulose derivatives was reported by Diekmann and coworkers, regarding protein fixation [80]. First of all, nitrilotriacetic acid (NTA) was covalently bound on cellulose. The NTA-cellulose derivative dissolved in DMSO was used for the formation of thin films on glass substrates. The films were later treated with solution of histidine and fluorescently labeled proteins as shown in the figure below. The immobilized substrates were then rinsed in order to get rid of the unbound protein [80]. As illustrated in the figure 78, the protein unit was bound through the metal center to the NTA-modified cellulose anchored on glass substrates [80].

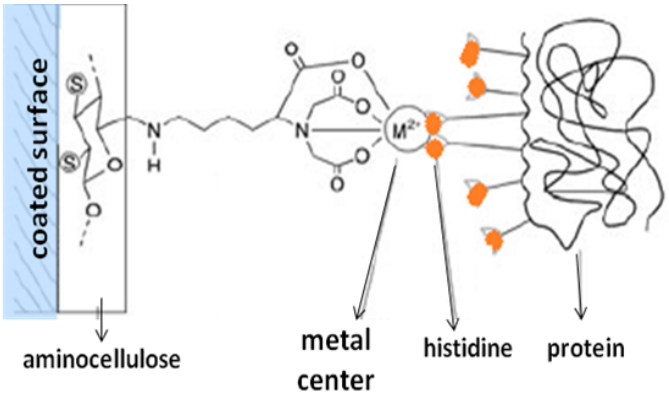

Figure 78 Immobilization of histidine and fluorescently labeled proteins into NTA (nitrilotriacetic acid) modified cellulose films by metal complex [80].

As observed from the literature studies, cellulose and its derivatives are becoming more important in the development and application of polymer materials. Furthermore, the knowledge obtained about the possible synthetic routes of cellulose derivatives has been important for the application in the chemistry of low molecular weight carbohydrates as well as polymer chemistry.

In addition to microcrystalline cellulose and its derivatives, filter paper could be also modified and used for surface immobilization.

4.3.2. Polymer functionalization of cellulose fibers (filter paper)

Paper is considered as another interesting substrate for surface immobilization. Chemically modified paper has gained a great interest in industrial and academic research, because of its wide application in microelectronics, preparation of "intelligent papers" for example magnetic papers as reported by Shen and coworkers in 2011 [81]. The paper properties can be changed by surface modification to micro-patterned paper, mm-scale channeled (for control of fluid penetration) for the application in lab-on paper devices [82]. For instance, in preparation of microfluidic paper devices, a huge amount of hydrophobic materials are applied on the paper surface in order to change the paper properties with respect to control the fluid flow inside the paper [82]. In another work reported in 2008 by Li et al, the modification of filter paper was done by emerging the paper substrates in alkylketene dimer solution and then later reacted with hydroxyl groups on the cellulose fibers using thermal conditions [83]. On the paper surface hydrophilic micro patterns were generated by plasma removal of some alkylketene dimer parts, using a metal mask in order to control the fluid transport on the cellulose fibers [83].

Roy and coworkers showed that not only small molecules can be covalently bound on cellulose fibers, but also functional macromolecules can be anchored in order to change the properties of the paper substrates [84]. For the polymer immobilization on cellulose fibers, either a polymer bearing functional groups can be introduced

on the paper surface, or the cellulose fibers can be prepared with functional groups which can bind on the polymer introduced [84].

Growing polymer on papers where the microfibers are modified with functional groups represents the "grafting from" approach of paper modification. On the other hand, "grafting to" approach is the case where the polymer bearing functional groups are anchored on cellulose fibers [84].

A recent research by Citterio et al showed that paper substrates could be microstructures using in situ photo-polymerization of cross linkable hydrophobic monomers [85]. Nevertheless, in this study it was concluded that the polymer gel formed inside the cellulose fibers was not formed in a defined way with respect to cross linking density amount of the polymer [85].

Another approach for paper modification with polymer structures was been reported by Toomey et al, where photo-reactive polymer structures were used [86]. The polymer structures bearing benzophenone moieties could be surface attached by UV-irradiation, in which case benzophenone moieties are excited by the UV light and form radicals. The radicals then could react with alkyl groups by hydrogen abstraction and finally bind the polymer structure covalently on the surface of cellulose fibers [86].

Murata and coworkers reported that benzophenone bearing monomers can be combined with other monomers which result in polymers which can be immobilized on any substrate like; glass slides and plastic surfaces [87]. Such modified surfaces were used in application for bioanalytical devices [87].

In a recent work reported by Biesalski et al, functional polymers bearing benzophenone moieties were used to modify the filter paper substrates [88]. In this report three different types of polymers were prepared as shown in the figure below.

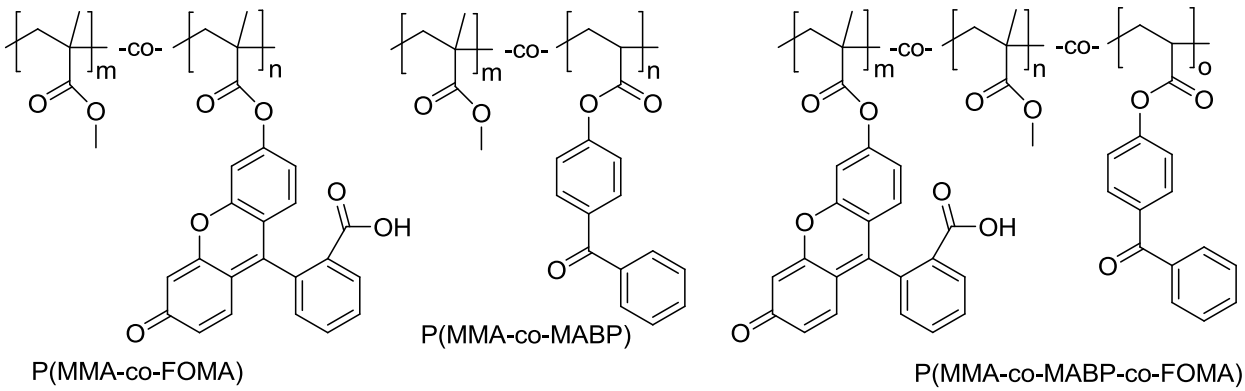

Figure 79 Copolymers used for paper modification: fluorescently labeled copolymer (P(MMA-co-FOMA) left), photoreactive copolymer (P(MMA-co-MABP) middle), fluorescently labeled and photoreactive copolymer (P(MMA-co-MABP-co-FOMA) right) [89, 90].

As illustrated in the figure 79 above, the three different types of copolymers were the following: the fluorescently labeled copolymer (P(MMA-co-FOMA)), the photoreactive copolymer (P(MMA-co-MABP) as well as the fluorescently labeled and photoreactive copolymer (P(MMA-co-MABP-co-FOMA)) where the MMA was chosen as matrix monomer. The resulting polymers on the paper surface were hydrophobic which leaded to a change in the paper properties, for instance wetability [88].

The copolymers were attached photochemically on the cellulose fibers. The bare paper substrates were immersed in a solution of copolymers. The paper substrates treated with polymer solution were then irradiated with UV-light [88]. After the UV-irradiation, the beznophenone moieties on the polymer structure form radical, which then react with the aliphatic C-H groups of the cellulose fibers as well as with the other polymer branches on the surrounding as shown in the figure below [88], where the blue dots represent benzophenone moieties attached on the cellulose fibers, the orange spots represent the benzophenone groups which have reacted with other polymer segments in order to form the polymer matrix on the outer surface of the paper.

Figure 80 Polymer structure anchored on cellulose fibers via UV-irradiation [88].

The paper substrates before and after modification were characterized with scanning electron microscopy (SEM) as well as fluorescence microscopy where the results showed that the polymer could be anchored on the paper surface in a homogenous way, without changing the structure of the cellulose fibers [88]. In addition to these characterization techniques, contact angle goniometer was used in order to measure the contact angle of water droplets on the surfaces of the paper before and after modification of paper with polymers, as shown in the figure below [88].

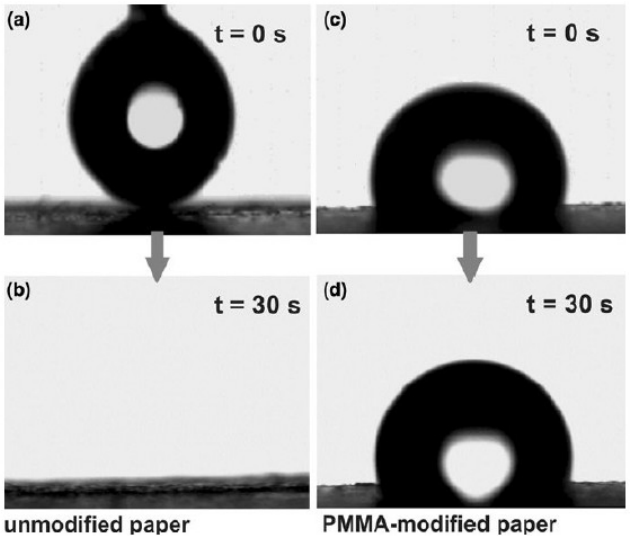

Figure 81 Contact angle measurements of paper before and after polymer immobilization [88].

As observed in the figure above, in the case of unmodified paper, the water droplet is penetrating rapidly into the surface of paper (case a and b). On the other hand, the PMMA modified paper exhibited a contact angle of 103 ° which clearly showed that the surface of the paper had changed to hydrophobic, into a non-wetting state [88].

Furthermore, a chemical microstructuring of the paper was studying using lithography. In order to make the micro patters on the paper surface, first of all, the paper was treated with copolymer solution mixture of P (MMA-co-MABP-co-FOMA). The illumination with UV light was done after placing a lithographic mask on the surface of the paper, which could expose spots on the paper with diameter of 3 mm [88]. The modified paper characterization was done with fluorescent spectroscopy. As observed from the fluorescent micrograph below, a well defined chemical micro pattern can be formed on the surface of paper by UV-irradiation [88].

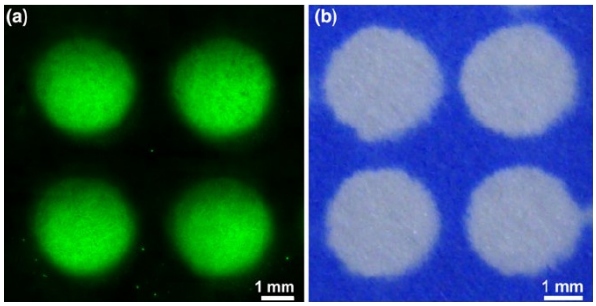

Figure 82 Florescent micrograph of P(MMA-co-MABP-co-FOMA) after UV-irradiation through a lithographic mask (a), paper immersed in blue ink after UV-irradiation (b) [88].

To sum up, there are various ways which lead to surface immobilization of cellulose fibers while changing the properties of the paper. Two possible ways are known for covalently bonding of materials on the cellulose fibers: either by "grafting from" or by "grafting to" method and the resulting paper can have a wide application as "smart paper" substrates both in academic and industrial research.

4.4. Results and Discussion

4.4.1. Synthesis of symmetrical azolium-$(CH_2NH_2)_2$ salts for surface immobilization

For the surface immobilization on carboxyl group bearing crystalline nanocellulose as well as on polymer modified filter paper with succinimide moieties, it was necessary to synthesize azolium salts with $-NH_2$ and the respective complexes to be covalently bound on the surface.

Both symmetrical and unsymmetrical NHC ligands were synthesized bearing amino groups.

First of all, for the synthesis of symmetrical amino group bearing NHC ligand bearing amino groups was synthesized by following several steps. The first five steps leading to 1,3-bis(4-(chloromethyl)-2,6-diisopropylphenyl)-4,5-dihydro-1H-imidazol-3-ium chloride were synthesized as described in the procedure given by Sashuk et al [91], as shown in the scheme 35.

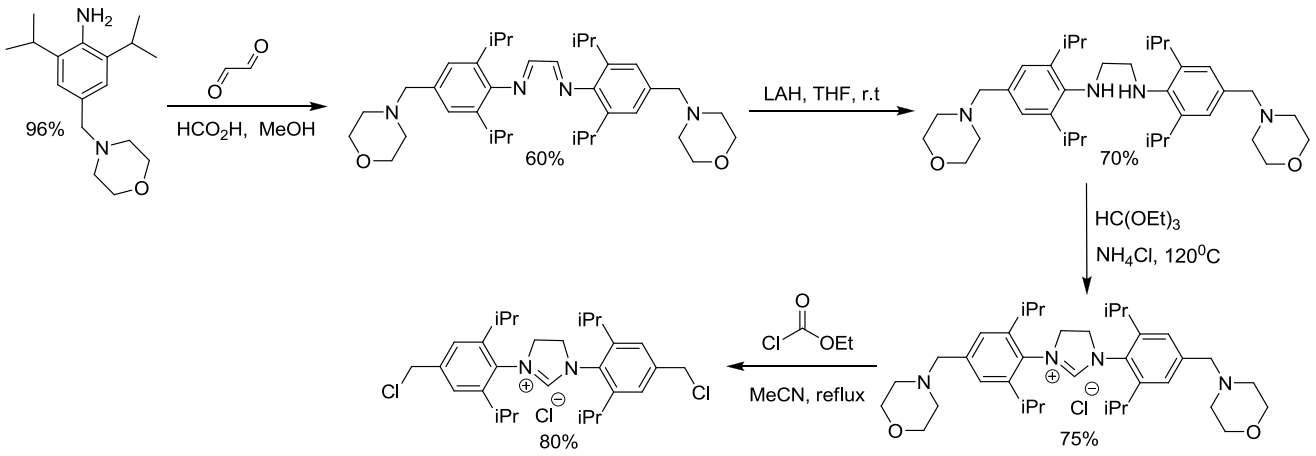

Scheme 35 Synthesis of diimine from 1,3-bis(4-(chloromethyl)-2,6-diisopropylphenyl)-4,5-dihydro-1H-imidazol-3-ium chloride.

The next step involved the preparation of azolium-$(CH_2N_3)_2$ salt. For this following step, the azolium-$(CH_2Cl)_2$ salt was dissolved in technical grade MeOH solution and excess of sodium azide was added to the reaction mixture and it was left to reflux overnight. After cooling the reaction mixture to room temperature, water was added to precipitate the product. Usually, during this step the solution was stored in the -40 °C fridge for 15 min, and the precipitate was filtered and the product was dried under vacuum to give the product as a white powder in 65 % yield.

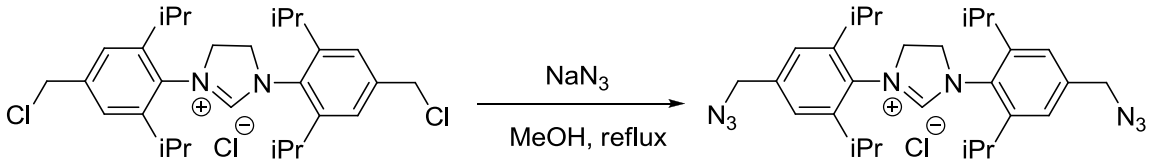

Scheme 36 Synthesis of 1,3-bis(4-(azidomethyl)-2,6-diisopropylphenyl)-4,5-dihydro-1H-imidazol-3-ium chloride.

The final step involved the preparation of azolium-$(CH_2NH_2)_2$ from azolium-$(CH_2N_3)_2$ which was done as described in the scheme below.

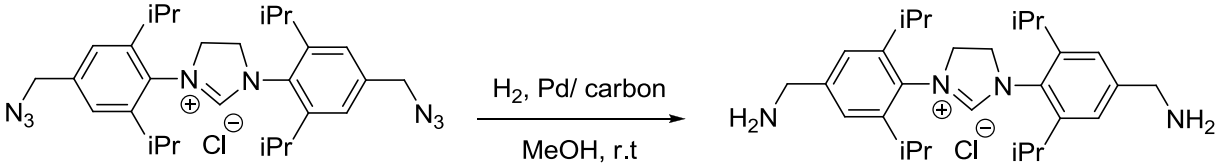

Scheme 37 Synthesis of 1,3-bis(4-(aminomethyl)-2,6-diisopropylphenyl)-4,5-dihydro-1H-imidazol-3-ium chloride.

First of all, azolium-$(CH_2N_3)_2$ salt was dissolved in technical methanol and Pd/ C (5 % Pd) was added to the reaction mixture. Finally, H_2 gas was bubbled through the solution at room temperature and the reaction progress was checked via ^{1}H-NMR. After 8 h, the reaction was stopped and filtered through a filter paper to get rid of Pd/ C. The filtrate was the evaporated to obtain the product as a white-yellowish colored powder in 85 % yield.

4.4.2. Synthesis of unsymmetrical azolium-$(CH_2)_nNH_2$ salts for surface immobilization

For surface immobilization it is adequate that there is only one functional group which will react with the terminal groups on the outer surface of the substrates. For this reason, it was planned to synthesize unsymmetrical azolium-$(CH_2)_nNH_2$ salt with long alkyl chains and then to prepare the respective gold complexes for hydration reactions in water. The longer the alkyl chain it is predicted to have a more flexible complex immobilized on the outer surface of the substrate.

Unsymmetrical azolium-$(CH_2)_nNH_2$ salts with different chain length were synthesized, where an example is illustrated in the scheme 38.

First of all, azolium-$(CH_2)_{10}I$ salt was synthesized from 1-mesityl-4,5-dihydro-1H-imidazole which was mixed with 1,10-diiododododecane in a schlenk flask under inert atmosphere. The reaction mixture was heated to 90 °C. After two days, the viscous mixture had turned to a hard solid residue. The residue was brought to room temperature and chilled ether was added. The solid residue was scratched out of the schlenk flask and it was left to stir in ether for some minutes. The solid residue was filtered and washed with ether several times. Finally, the product was dried under vacuum to obtain the azolium-$(CH_2)_{10}I$ salt as a white powder in 86 % yield.

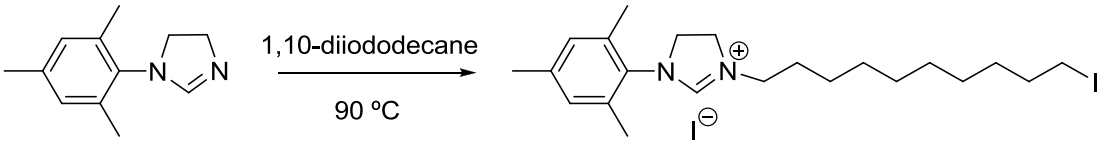

Scheme 38 Synthesis of 3-(10-iododecyl)-1-mesityl-4,5-dihydro-1H-imidazol-3-ium iodide.

The next step was the synthesis of azolium-$(CH_2)_{10}N_3$ salt. For this step, the same procedure which was followed during the preparation of the symmetrical azolium-$(CH_2N_3)_2$ salt was followed as shown in the scheme below.

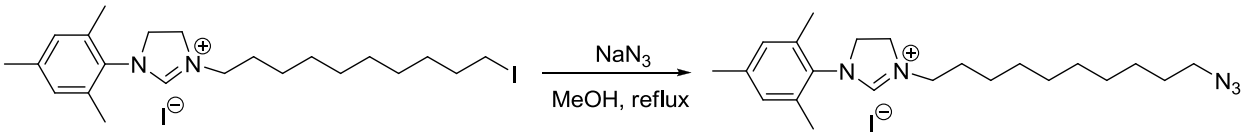

Scheme 39 Synthesis of 3-(10-azidodecyl)-1-mesityl-4,5-dihydro-1*H*-imidazol-3-ium iodide.

Azolium-$(CH_2)_{10}I$ salt was dissolved in technical grade methanol and sodium azide was added. The mixture was left to reflux overnight. After the reaction time, water was added to the reaction mixture to precipitate the product. The reaction mixture was stored in fridge for 15 min, and then the precipitate was filtered, washed several times with water and dried under vacuum to obtain the product as a white solid in 70 % yield.
The final step, after the azido substituted product involves the synthesis of azolium-$(CH_2)_{10}NH_2$ salt. During this step, azolium-$(CH_2)_{10}N_3$ was dissolved in technical grade methanol and then Pd/ C (5 % Pd) was added as shown in the scheme below.

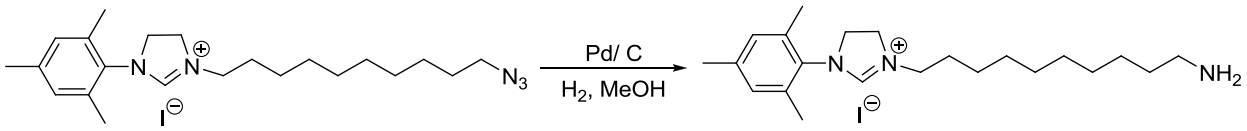

Scheme 40 Synthesis of 3-(10-aminodecyl)-1-mesityl-4,5-dihydro-1H-imidazol-3-ium iodide.

Hydrogen gas was bubbled continuously via stirring and the reaction progress was tested via ^{1}H-NMR. In this case, these wasn't observed any difference in the ^{1}H-NMR spectrum before and after reaction, for this reason thin layer chromatography was performed for the staring material (azolium-$(CH_2)_{10}N_3$) and the reaction system where the TCL plates were then immersed in ninhydrin solution. The TLC plate belonging to the product turned to dark blue which shows the evidence of primary amines. On the other hand, the TLC plate with the starting material did show any coloration to blue. After 8 h of hydrogen gas bubbling the reaction mixture was filtered through filter paper to get rid of Pd/ C and the filtrate was evaporated to obtain the product as a light beige colored solid in 85 % yield.

4.4.3. Synthesis of symmetrical and unsymmetrical [(NHC)AuCl] complexes bearing amino group for surface immobilization

After the synthesis of symmetrical and unsymmetrical azolium salts bearing $-NH_2$ groups, gold complexes were synthesized as shown in the figure below.

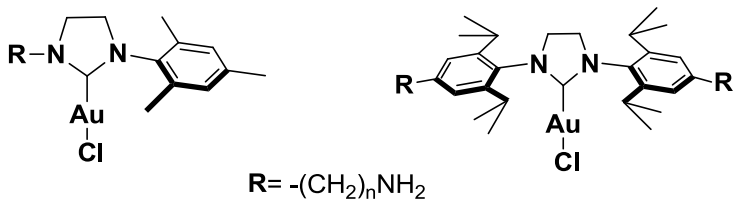

Figure 83 Types of [(NHC)AuCl] complexes.

For the synthesis of [(NHC)AuCl] complexes the free NHC route was not successful. In order to obtain the gold complex the transmetalation route was used, where the [(NHC)AgCl] was synthesized and transferred to [(NHC)AuCl] complex.

As illustrated in the example, scheme 41, for the synthesis of silver complexes, azolium-$(CH_2NH_2)_2$ was dissolved in dry and degassed DCM in a schlenk flask under argon atmosphere.

Finally, Ag_2O was added and the mixture stirred for 12 h under inert atmosphere with exclusion of light, using similar reaction conditions as described by Yahnke et al [92]. The reaction mixture was filtered through silica plug and the filtrate evaporated to obtain a residue, which was washed with pentane to provide the product as a white solid in 50 % yield. As shown in shceme 41.

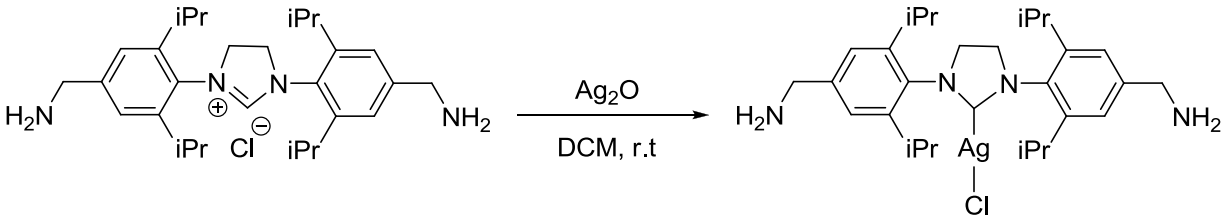

Scheme 41 Synthesis of (1,3-bis(4-(aminomethyl)-2,6-diisopropylphenyl)imidazolidin-2-yl)silver(II) chloride.

After the isolation of the silver complex, the [(NHC)AuCl] complex was synthesized as shown in the scheme 42 below. The [(NHC)AgCl] salt was dissolved in dry and degassed DMC and $AuCl(Me_2S)$ was added. The reaction mixture was stirred for 2 h at room temperature with light exclusion. As soon as $AuCl(Me_2S)$ was added, a white precipitate falling out of the reaction system was observed, which was the –AgCl precipitate. When the reaction was left longer than 2 h stirring the product obtained contained a lot of impurities. After the 2 h reaction time, the mixture was filtered through celite. The celite was washed with DMC and the filtrate was evaporated under reduced pressure. The obtained residue was washed with pentane in order to obtain the product as a white, fluffy powder in 60 % yield.

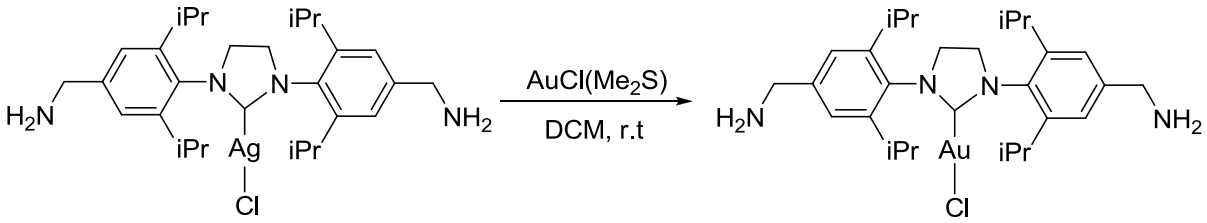

Scheme 42 Synthesis of (1,3-bis(4-(aminomethyl)-2,6-diisopropylphenyl)imidazolidin-2-yl)gold(II) chloride.

Using the same experimental procedures, the unsymmetrical [(NHC)AgCl] was synthesized and the respective complexes were then immobilized on the surface of crystalline nanocellulose and polymer modified filter paper, via $–NH_2$ groups, as described in the following chapters of this work.

4.5. Preparation of cellulose substrates for the immobilization of [(NHC)AuCl] complexes

4.5.1. Preparation of crystalline nonocellulose substrates (CNC)

Crystalline nanocellulose was synthesized by Dr. Kai Zhang and coworkers [93] as described in the scheme below.

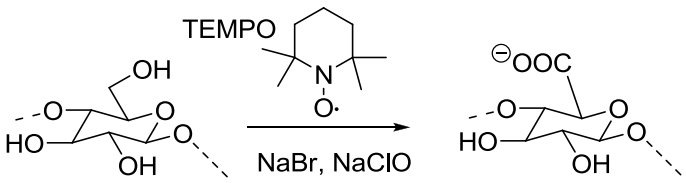

Scheme 43 Synthesis of crystalline nanocellulose (CNC) from microcrystalline cellulose (MCC) [93].

Microcrystalline cellulose used had a granule size of size of 50 µm, which was suspended in water under vigorous stirring. For the oxidation of microcrystalline cellulose and the generation of the functional carboxylic groups (2,2,6,6-Tetramethylpiperidine-1-yl)oxy was used (TEMPO). In addition, NaBr was added and the suspension was left to stir for 30 min. After this reaction time, NaClO was added to the suspension at pH 10. Finally, the pH value was dropped to 7.5 and the oxidized cellulose product was isolated by centrifugation. The cellulose product was re-dispersed in water and sonicated at room temperature. The last step involved the dialysis of the product, until the conductivity reached ~1 µS/cm and its volume was adjusted to 200 mL.

The figure below represents the schematic representation of the synthesis of CNCs from MCCs from TEMPO mediated oxidation.

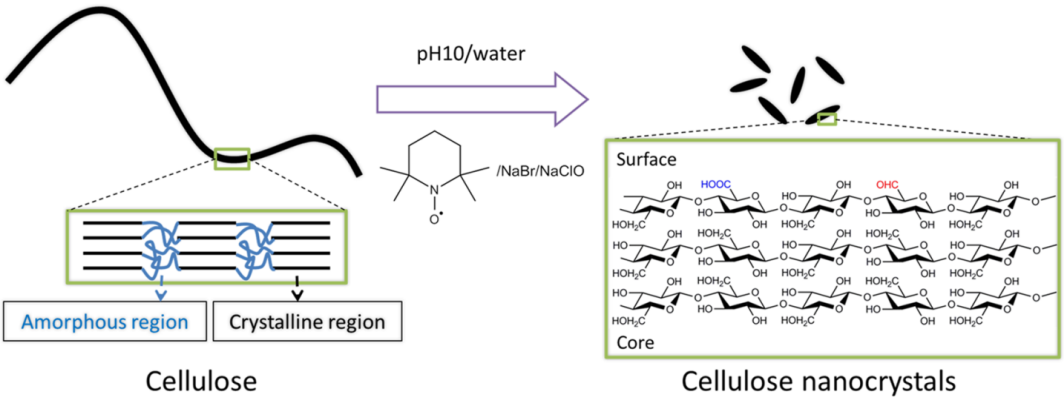

Figure 84 Schematic representation of synthesis of CNCs from MCCs.

The structure of the crystalline nonocellulose was studied by atomic force spectroscopy (AFM), which was provided by Dr. Kai Zhang, for a nice two dimensional projection of a single CNC as shown in the AFM image below. From the AFM measurements it was possible to get information about the diameter of the crystalline cellulose, which was found to be 7 nm, whereas the length of a single CNC was around 300 nm.

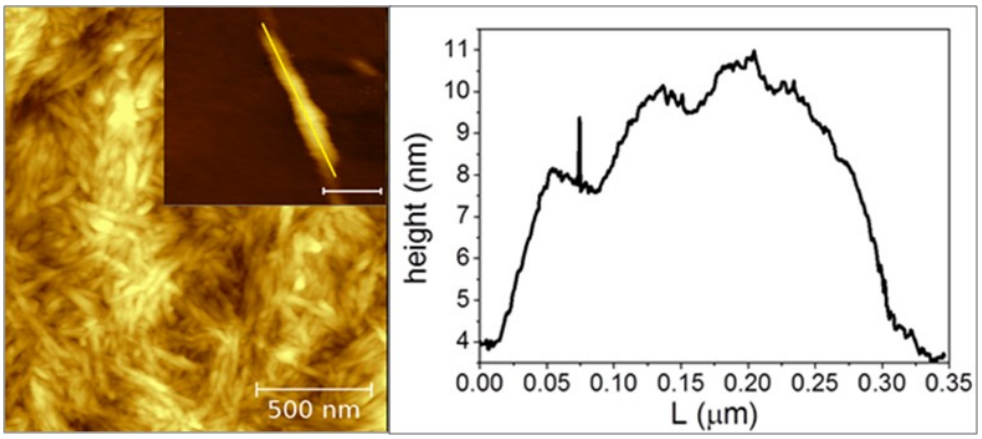

Figure 85 AFM image (500 nm and 100 nm, left), height profile (right) [93].

The advantage of using cellulose nanocrystals as substrates for immobilization was the large surface are that they provide, the ease of preparation from renewable sourse, cellulose, chemically modified yielding in surfaces with exposed functional groups. Furthermore, the easy of characterization made it an ideal substrate for catalyst immobilization, as these substrates were soluble in solvents and ^{13}C-NMR was possible to be measured as shown in the spectrum below.

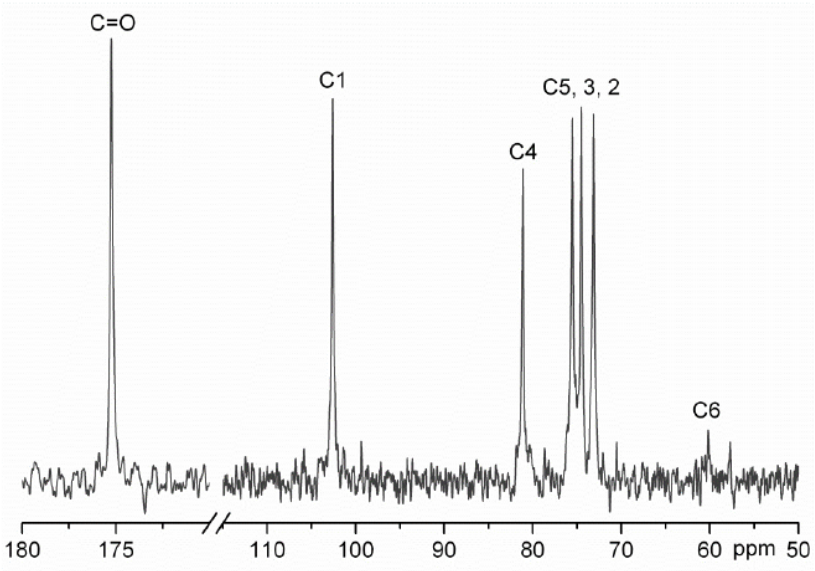

Figure 86 ^{13}C NMR spectrum (180-50 ppm) of water-soluble CNC in D_2O at room temperature.

Another important characterization technique used was the electric conductivity titration, which was necessary in order to determine the ration of the surface-exposed carboxylic to carbonyl groups of CNC. The

content of carboxylic groups was evaluated using a few milliliters of CNC suspension where the pH value was adjusted to 2 with 0.1 M HCl. The solution was titrated using 665 Dosimat (Metrohm) at the dosing rate of 0.01 ml/s, while the conductivity was recorded using 865 Conductivity Module (Metrohm).

In order to determine the content of aldehyde groups, the CNC suspension was oxidized with $NaClO_2$ at ambient temperature and pH 4-5. Finally, the total carboxylic groups were titrated again. As a result, the difference between pre-oxidized and oxidized CNC was calculated, which was equal to the content of aldehyde groups. In the figure below the conductivity plot vs NaOH base used is shown, where according to the results the contents of carboxyl and aldehyde groups were determined to be 1.386 mmol/ g and 0.072 mmol/ g respectively.

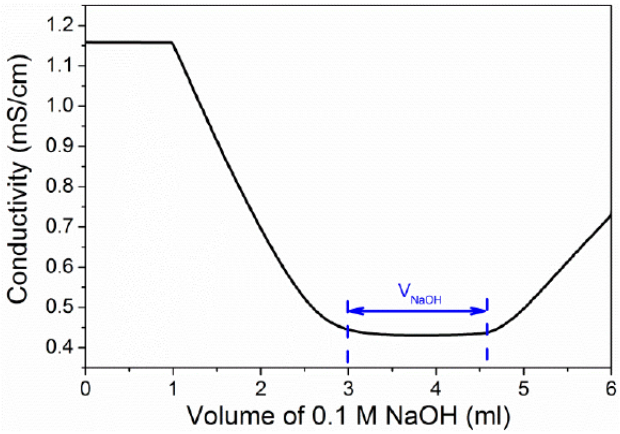

Figure 87 Conductive vs V(NaOH) graph of aqueous CNC suspension for the determination of the carboxylic and aldehydic content [93].

After the characterization of crystalline nanocellulose (CNC), these substrate with functional carboxylic groups was later used as surface for immobilization of [(NHC)AuCl] type complex to form heterogeneous catalysis for hydration reactions of alkynes as will be described in the later chapters.

.

4.5.2. Preparation of chemically modified filter paper

Another interesting substrate for the immobilization of [(NHC)AuCl] type complexes was chosen modified filter paper which was prepared by Alexander Böhm, research group of Prof. Dr. Markus Biesalski [88]. The polymer modified and chemically microstructured paper substrates were obtained by a photo-chemical attachment of functional polymers to cellulose microfibers inside filter paper.

First of all, the photo reactive polymers we synthesized. All the polymers were by statistical free radical copolymerization and characterized with respect to molar mass and composition by size exclusion chromatography. The chemical structure of the copolymers and their synthesis is represented in the scheme 44.

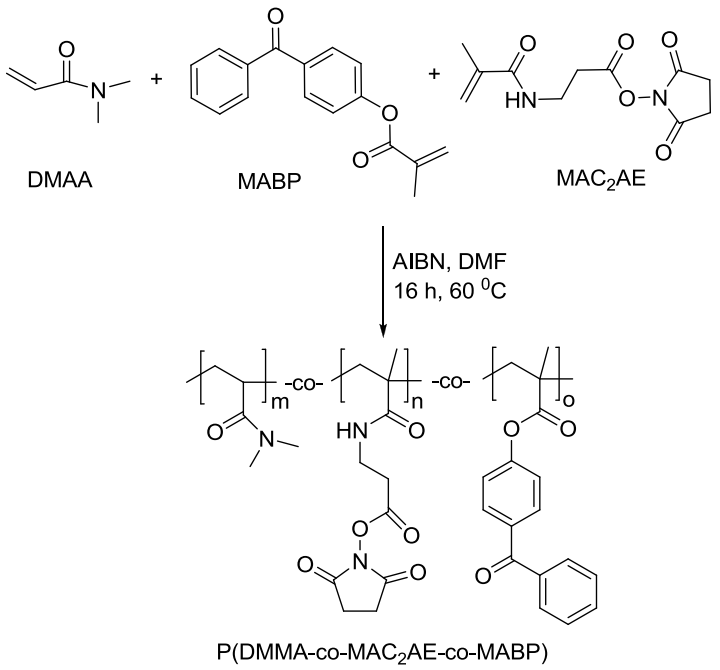

Scheme 44 Synthesis of P(DMMA-co-MAC2AE-co-MABP)

As seen in the reaction scheme above, for the synthesis of P (DMMA-co-MAC2AE-co-MABP), in a Schlenk flask under inert atmosphere, 1,3-simethylamylamine (DMAA), N-methaclyloyl-β-alanine succinimide ester (MAC_2AE) as well as 4-methaclyloyloxybenzophenone (MABP) as well as the initiator azobisisobutyronitrile (AIBN) were mixed in dry DMF and the reaction mixture was stirred at 60 °C in thermostated bath for 16 h for polymerization.

After the reaction time, the polymer was precipitate with methanol and was dried under vacuum. For purification, the polymer was purified by reprecipitation from THF in methanol and then characterized by ^{1}H-NMR as well as by size exclusion chromatography.

The next important step following the copolymer synthesis was the modification of the filter paper with the copolymer. For this step, the copolymer P(DMMA-co-MAC2AE-co-MABP) was dissolved in THF at a concentration of 30 mg/ ml. The filter paper was cut into pieces of 2.5 x 2.5 cm and then the paper was submerged into the polymer solution for a short time, like 20 s, then the papers were pulled out at a constant velocity 1 cm/ min (using dip coating), and air dried for at least 30 min. After this step, the paper substrates were irradiated with UV-light (λ= 364 nm, E= 16 J cm^{-2}). During this process, the benzophenone moieties in the copolymer structure were excited. In order to get a more homogenous polymer layer on the surface of filter paper, the paper substrates were illuminated from both sides.

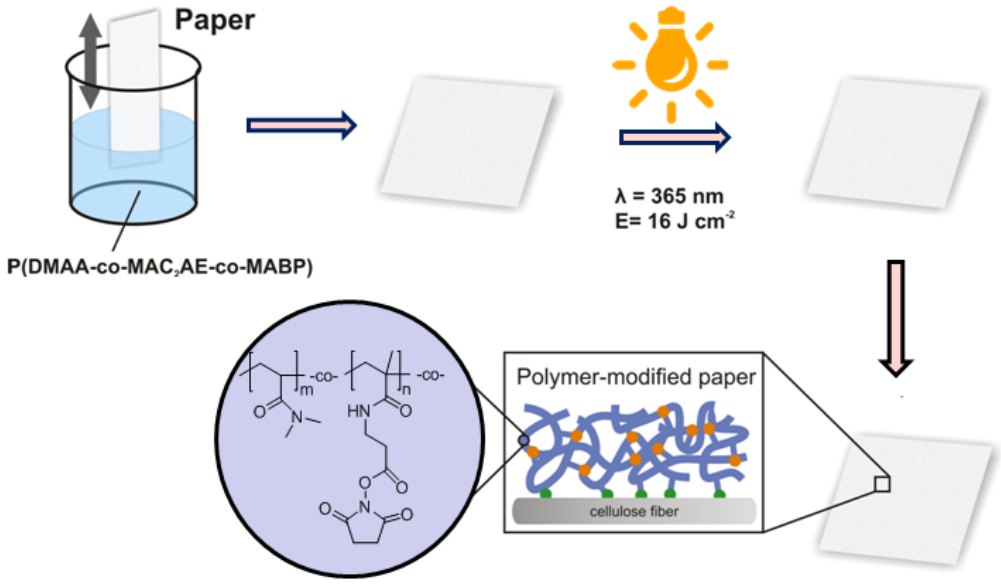

Figure 88 Paper coating and photochemical attachment of polymers to cellulose microfibers by UV-irradiation.

As described in the figure above, during the illumination process the beznophenone groups react with the surface of the cellulose fibers (the green dots in the figure) as well as with the polymer chains (the orange dots in the figure). The polymer which was physisorbed on the paper substrates were removed by soxhlet extraction.

After the polymer modification of the paper, the substrates were ready to be used for the immobilization of the [(NHC)AuCl] type complexes as will be described in the following chapters and then the catalyst modified paper substrates were used for hydration reaction of alkynes.

4.6. Immobilization of [(NHC)AuCl] type complexes on crystalline nanocellulose (CNC) and polymer modified paper substrates

4.6.1. Immobilization of [(NHC)AuCl] type complexes on crystalline nanocellulose (CNC)

As described previously, crystalline nanocellulose (CNC) was synthesized from microcrystalline cellulose (MCC) where during this process the hydroxyl groups on the surface of MCC at -C_6 position were transferred to carboxylic group by TEMPO mediated oxidation. Crystalline nanocellulose was then used for surface immobilization of [(NHC)AuCl] type complexes bearing –NH_2 groups, whose synthesis was described in the earlier chapters as well.

As shown in the scheme 45, crystalline nanocelulose (CNC) first of all was dissolved in ellythenedichloride (EDC), then *N*-hydroxysuccinimide was added as an activationg reagent for carboxylic group on the CNC surface. As the CNC crystals were isolated, they were redispersed in DMSO/ H_2O mixture so that the nanocellulose particles do not aggregate.

After this step the $-NH_2$ groups bearing gold catalyst ([(NHC)AuCl]) was introduced to NHS-containing crystalline nanocellulose, which is an ideal surface for reaction with amines. The suspension was stirred under basic conditions at room temperature for 72 h. The final product [(NHC)AuCl] @ CNC as shown in the scheme below was then isolated by centrifugation and purified from the physisorbed catalyst by dialysis.

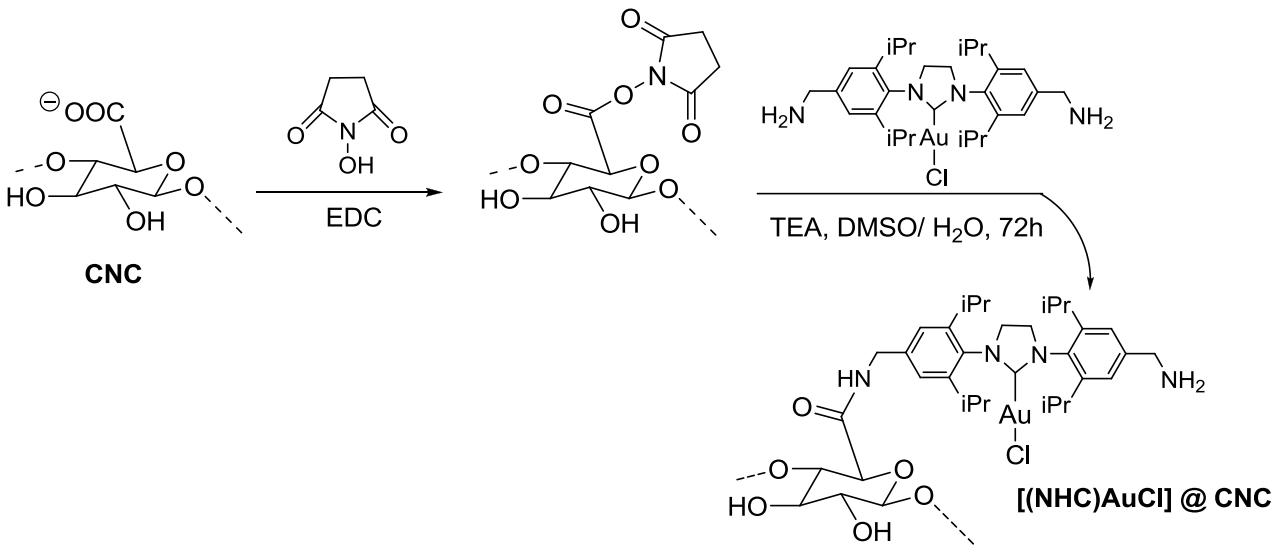

Scheme 45 Immobilization of [(NHC)AuCl] complex on the surface of CNC.

The final functionalized crystalline nanocellulose particles, which had a characteristic violet color as shown in the figure below, were redirspersed in water to prevent particle aggregation.

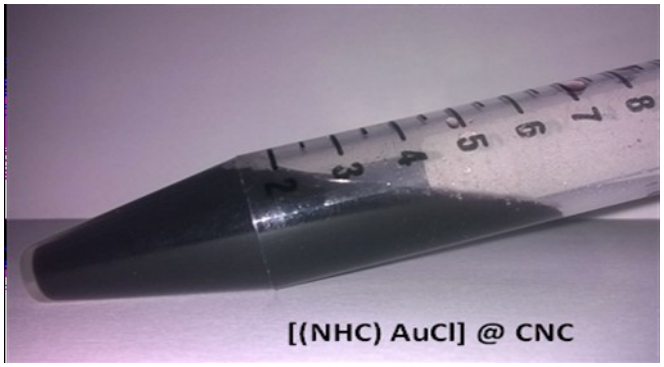

Figure 89 [(NHC)AuCl@CNC particles dirspersed in water.

The functionalized crystalline nanocellulose (CNC) was characterized by elemental analysis where the content of the catalyst was calculated. The elemental analysis is given in the table 7, per 100 g of functionalized CNC.

Element type	Amount per 100 g CNC
N	2.023
C	40.35

Table 7 Elemental analysis of [(NHC)AuCl@CNC.

From elemental analysis it was possible to calculate the content of the catalyst per 100 g of CNC, based on the amount of nitrogen as following: (2.023/ 14/ 3) =0.0482 mol/100 g sample.
The synthesized substrates [(NHC)AuCl] @ CNC, dispersed in water, were then used in hydration reactions of alkynes as will be described in the following chapters.

4.6.2. Immobilization of [(NHC)AuCl] type complexes on polymer modified paper substrates

The polymer modified filter papers as described previously, were also used as substrates for immobilization of $-NH_2$ groups bearing [(NHC)AuCl] type complex. The copolymer anchored on the cellulose fibers by photo-chemical attachment containing NHS-ester, as shown in the figure below, were very prone to react with the gold catalyst bearing amino groups.

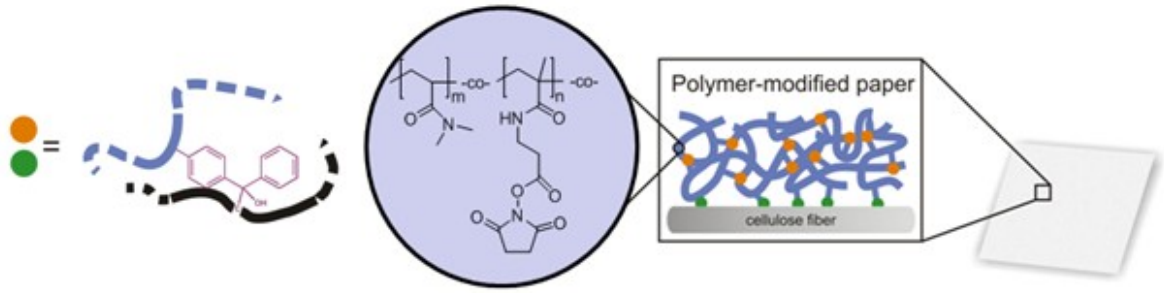

Figure 90 Benzophenone groups (green and orange dots), NHS-ester containing polymer chains.

First of all, for the immobilization of the [(NHC)AuCl] complex on paper, 10 mg/ ml solution of the complex was prepared in ethanol. The polymer modified paper substrates of size 2.5 x 2.5 cm were then immersed in the catalyst solution, as shown in the figure below and they were kept at 5 °C for 24 h. This procedure is known to be as a general procedure for the immobilization of proteins on the NHS-ester containing paper substrates.

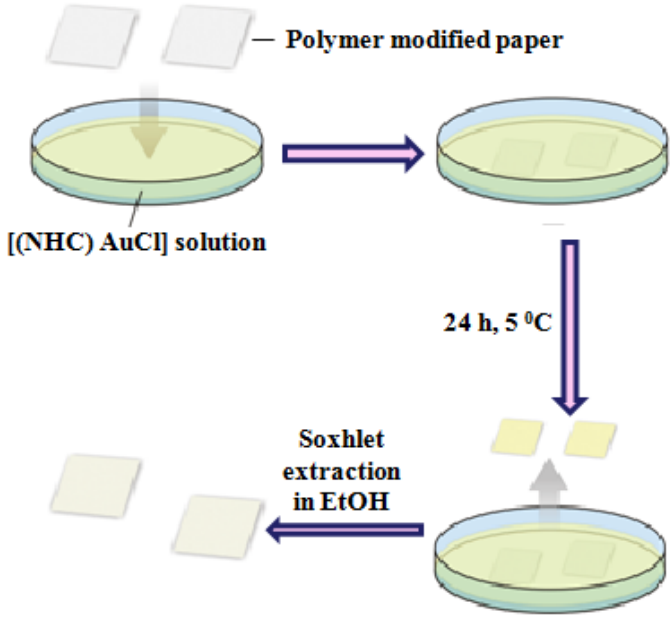

Figure 91 Immobilization of [(NHC) AuCl] on polymer modified filter paper.

After the reaction time as illustrated in the figure above, the paper substrates were removed from the catalyst solution, air dried and then they were soxhlet extracted in ethanol for 150 min in order to get rid of the physisorbed catalyst on the cellulose fibers. After this process, the paper substrates were dried and then further characterized for the catalyst content on the surface.

The figure below represents the schematic representation of the reaction of amino group bearing [(NHC) AuCl] catalyst with the NHS-groups on the paper surface.

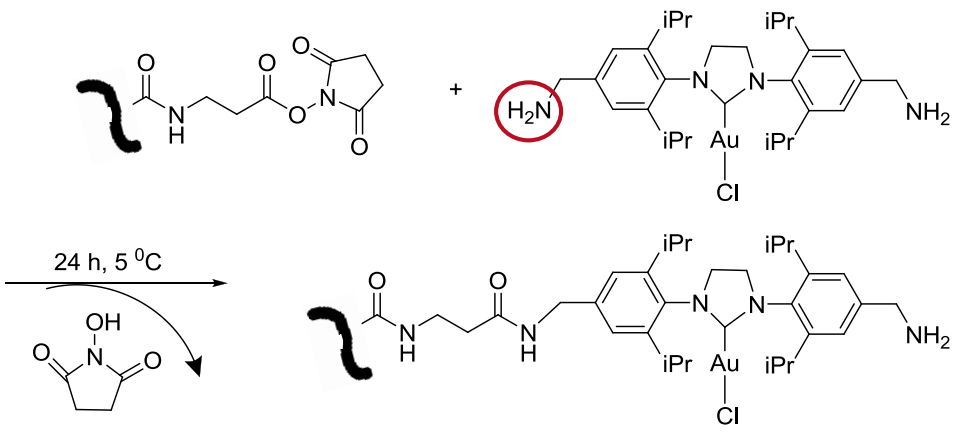

Scheme 46 Reaction of NHB-ester bearing polymers with amino groups bearing [(NHC)AuCl] complex.

The catalyst modified paper substrates ([(NHC)AuCl]@paper) were characterized using ninhydrin (2,2-dihydroxyindane-1,3-dione) solution. Ninhydrin solution was prepared in ethanol solution, 10 mg/ ml then the catalyst modified paper substrates were immersed in ninhydrin solution and left to stay for 24 h at room

temperature. After this process, the paper substrates were removed from the ninhydrin solution and soxhlet extracted with ethanol for 150 min for 24 h as illustrated in the figure below.

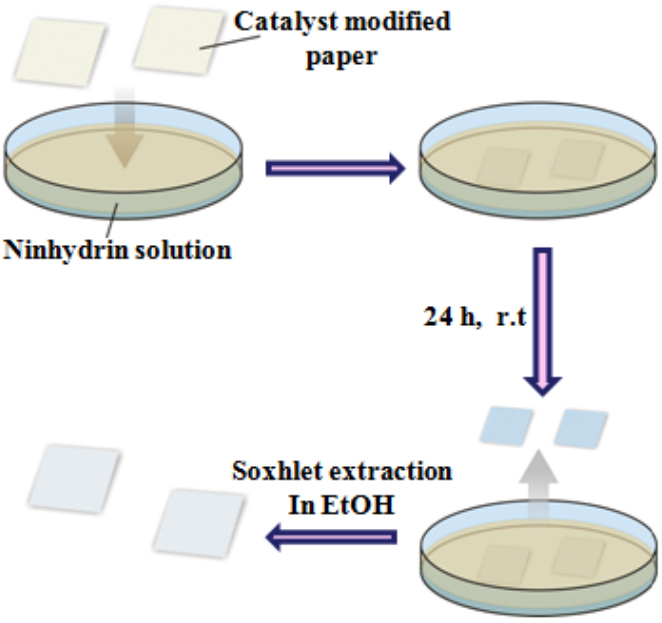

Figure 92 Treatment of [(NHC)AuCl]@paper substrates with ninhydrin solution.

The ninhydrin was used to detect the primary or secondary amines on the surface of the paper substrates, which would prove the reaction of the NHS-ester containing polymers on the paper with the amino groups from the gold catalyst. As ninhydrin reacts with amines, as shown in the scheme below, a deep blue color is produced which is known as Ruhemann's color.

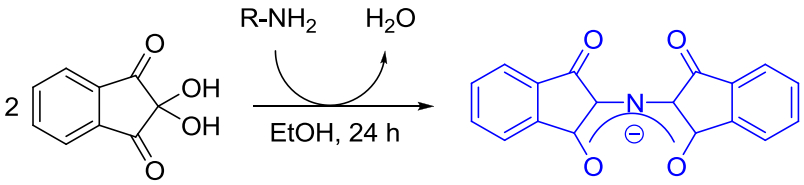

Scheme 47 Reaction of ninhydrin with primary amines.

Three different types of paper substrates were treated with ninhydrin solution, in the same manner as described in the figure 41 above: [(NHC) AuCl]@paper substrates, unmodified filter paper (bare paper) and P(DMAA-co-MABP) modified paper substrates (reference paper). According to the the unmodified paper substrates as well as the reference paper did not show any color change after ninhydrin treatment. On the other hand, the catalyst modified paper substrates after ninhydrin treatment were obtained as dark blue colored, as shown in the figure 93, which shows the presence of amino groups on the cellulose fibers.

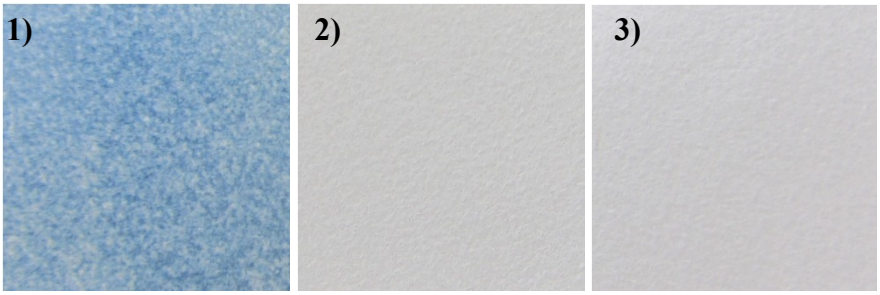

Figure 93 Paper substrates after ninhydrin reaction: [(NHC)AuCl]@paper (1), P(DMAA-co-MABP)@ PAPER (2), bare filter paper (3).

Regarding the catalyst content immobilized on paper substrates, a rough calculation was performed. Taking into the consideration the amount of NHS-esters on the surface of cellulose fibers which was 1.2 mg on paper of size 2.5 x 2.5 cm, which corresponds to 0, 005 mmol, the amount of catalyst was found to be 2.96 mg on the 2.5 x 2.5 cm paper surface.

After the catalyst immobilization on paper substrates, the [(NHC)AuCl]@paper were then used as heterogeneous catalysts for hydration reactions of alkynes as will be described in the following chapter.

4.7. Application of [(NHC)AuCl]@paper and the [(NHC)AuCl@CNC substrates in hydration reactions of alkynes

The cellulose immobilized gold catalysts, as heterogenous catalysts, were used for hydration reactions of alkynes. These reactions have gained a large interest because such reactions are relatively easy and they require really small amount of catalytic loading. In this work, two different surface immobilized gold catalysts were used for hydration reaction as shown in the figure below.

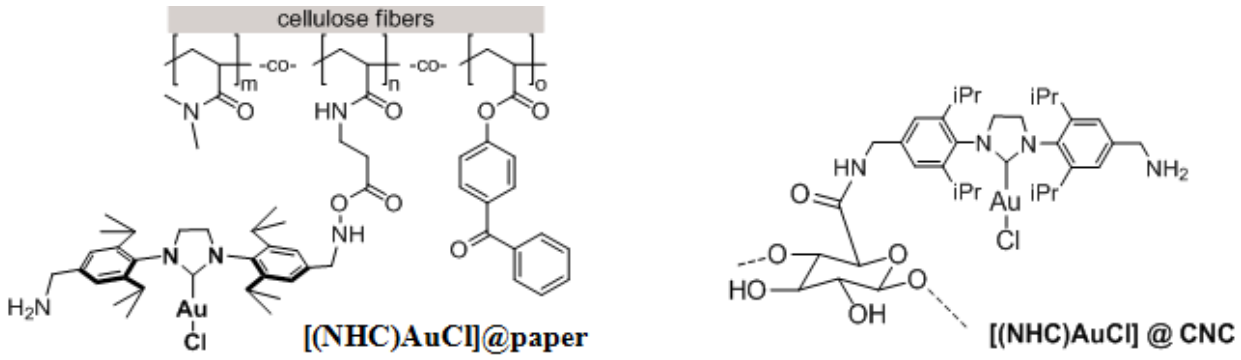

Figure 94 Substrates used for hydration reaction of alkynes: [(NHC)AuCl]@paper (left), [(NHC)AuCl]@CNC (right).

Phenylacetylene was used as a substrate and the catalysts used were either [(NHC)AuCl]@paper or [(NHC)AuCl]@CNC as shown in the scheme 48.

*[(NHC) AuCl]@paper or [(NHC) AuCl]@CNC

Scheme 48 Hydration reaction of phenylacetylene.

Different reaction conditions were tested for the hydration reaction of phenylaldehyde as shown in the table 8. The general conditions for this reaction, at the same time the best results obtained were as the reaction was performed in MeOH : H_2O (2:1) mixture. First of all, the solvent mixture was prepared and only 1 ml of the solvent mixture was used for the reaction. In the case of [(NHC)AuCl]@paper substrates, the paper (2.5 x 2.5 cm) was cut into very small pieces, and placed in the reaction vessel. After this step, phenylacetylene (20 mg, 0.196 mmol) was added and then $AgBF_4$ (tip of spatula, 11 mol %) was added as cocatalyst. Since the reaction progress was analysed by gas chromatography, mesitylene was also added in the reaction system as an internal standard (10 mg, 0.0832 mmol). The reaction mixture was left to stir at 100 °C for 15 h. The amount of gold in the paper size of 2.5 x 2.5 cm was calculated as 0.985 mg, which obviously showed that there was a very small amount of catalyst immobilized on paper surface.

After the reaction time, the mixture was left to cool to room temperature. To the reaction mixture 10 ml of water was added and then the aqua phase was extracted with ether several times. The organic phase was dried over $MgSO_4$ and the solvent was evaporated under reduced pressure. The oily residue obtained was then submitted to GC in order to calculate the GC yield.

In the case of [(NHC)AuCl]@CNC substrates used in hydration reactions of phenylacetylene, the same reaction conditions were used. The [(NHC)AuCl]@CNC particles were dispersed in water therefore the amount of water coming from the particle-environment was also taken into consideration when trying to adjust the MeOH: H_2O ration (2:1). The more water was used, the lower the conversion was obtained. In the case of catalyst modified crystalline nanocellulose substrates, it was possible to know the amount of particles dispersed in water but not the catalyst content on the surface of cellulose. The table 8 described the conditions tried for the hydration reaction of phenylacetylene, and the GC yield calculated.

Entry no.	Substrate	Educt (mg)	$AgBF_4$ (mol%)	solvent	T (°C)	Rxn time	Conversion (%)
1	**Paper** (1x1cm²)	30	1	MeOH:H_2O (2:1)	80	15 h	20
2	**Paper** (1x1cm²)	30	2	MeOH:H_2O (2:1)	100	15 h	49
3	**Paper** (2.5x2.5cm²)	20	5	MeOH:H_2O (2:1)	100	15 h	73
4	***Paper** (2.5x2.5cm²)	20	tip of spatula (11)	MeOH:H_2O (2:1)	100	15 h	96
5	**CNC-Aucat** (165µl-1.07mg)	20	5	MeOH:H_2O (2:1)	100	15 h	30
6	**CNC-Aucat** (495µl-3.218mg)	20	tip of spatula (11)	MeOH:H_2O (2:1)	100	15 h	99
7	**CNC-Aucat** (700µl-5 mg)	20	0	MeOH:H_2O (2:1)	100	15 h	50
8	**SiPr-AuCl** 5 mol %	20	0	MeOH:H_2O (2:1)	100	15 h	99

Table 8 Catalytic performance of [(NHC)AuCl]@CNC and [(NHC)AuCl]@paper for the hydration reaction of phenylacetylene.

4.8. Summary and Conclusion

This work was concentrated on the synthesis of $-NH_2$ groups bearing [(NHC)AuCl] type complexes and their immobilization on two different type of surfaces: crystalline nanocellulose (CNC) and polymer modified filter paper.

First of all, two type of amino groups bearing *N*-heterocyclic carbene ligands were synthesized; symmetrical and unsymmetrical NHCs, and then their respective silver and gold complexes were synthesized (unsymmetrical [(NHC)AuCl] complex left and symmetrical [(NHC)AuCl] complex right).

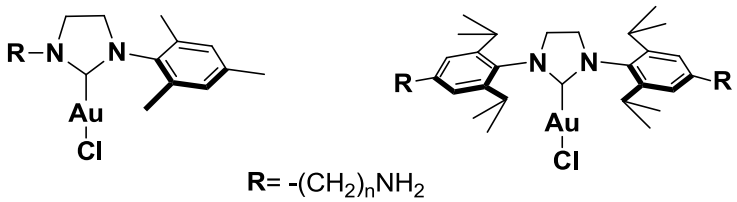

Secondly, two different types of substrates with functional groups were prepared which could be used for the covalent attachment of the gold complex on the outer surface of the substrates. The surfaces prepared were:

NHS-ester bearing polymer modified filter paper (left) and crystalline nanocellulose with functional carboxylic groups (CNC).

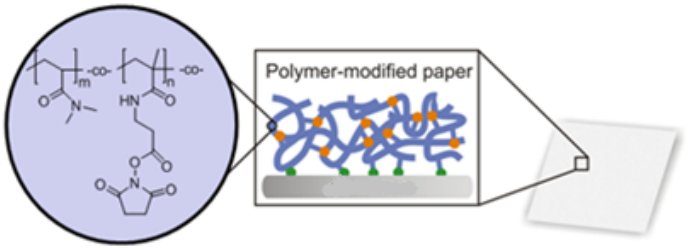

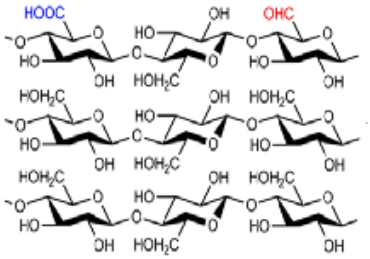

Finally, the catalyst was reacted with the surface of the substrate in order to give the heterogeneous gold catalysts: [(NHC)AuCl]@paper (left) and [(NHC)AuCl]@CNC (right). The catalyst modified paper substrates were characterized by ninhydin treatment and the catalyst content was calculated relying on the amount of the NHS-ester groups on the surface of the paper. The CNC samples were characterized by ^{13}C-NMR, AFM and conductive titration (for the determination of the content of the carboxylic groups). After the catalyst immobilization the CNC samples were characterized by elemental analysis.

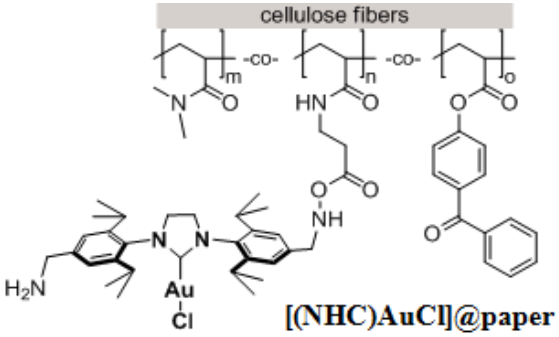

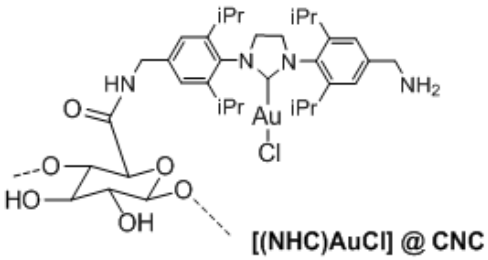

The catalyst modified substrates were then used to perform hydration reaction of alkynes and the product yield was determined by gas chromatography.

*[(NHC) AuCl]@paper or [(NHC) AuCl]@CNC

5. Zusammenfassung

Diese Arbeit konzentrierte sich auf die Synthese von Komplexen des [(NHC)AuCl]-Typs mit $-NH_2$ Gruppen sowie deren Immobilisierung auf zwei verschiedenen Arten von Oberflächen: kristalliner Nanocellulose (CNC) und polymer-modifiziertem Filterpapier.

Zuerst wurden zwei verschiedene *N*-heterozyklische Carbene (symmetrische und unsymmetrisch) mit Amino-Gruppen synthetisiert, die anschließend zu den entsprechenden Silber und Gold Komplexen umgesetzt wurden (links der unsymmetrische [(NHC)AuCl] und rechts der symmetrische [(NHC)AuCl]-Komplex).

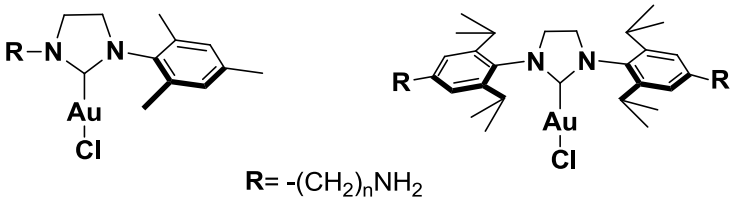

Zwei verschiedene Arten von Oberflächen (mit funktionellen Gruppen) wurden vorbereitet, welche eine kovalente Bindung zu den jeweiligen Gold-Komplexen ausbilden können. Die Oberfläche des Filterpapiers, die mit NHS-Ester-modifizierten Polymeren ausgestattet sind (siehe linke Abbildung) und die der kristallinen Nanocellulose, die mit Carboxy-Gruppen (CNC) ausgestattet ist (siehe rechte Abbildung), wurde mit diesen Komplexen umgesetzt.

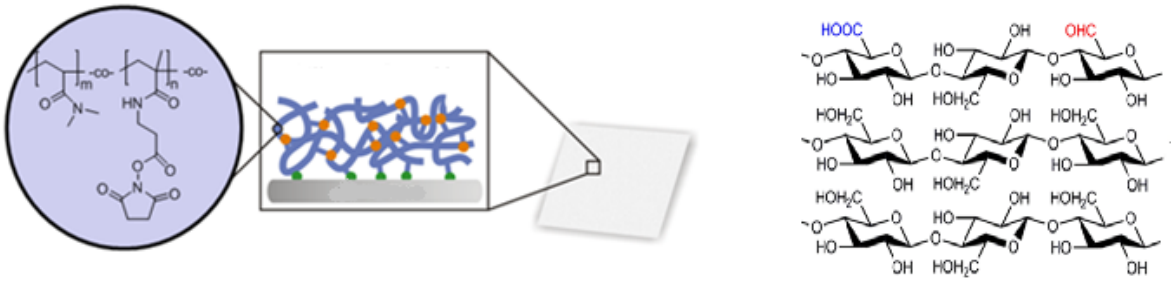

Letztendlich reagierte der Katalysator mit der Oberfläche und bildet dabei den heterogenisierten Gold-Katalysator: [(NHC)AuCl]@Filterpapier (Abbildung links) und [(NHC)AuCl]@CNC (Abbildung rechts). Das Katalysator-modifizierte Filterpapier wurde zur Charakterisierung mit Ninhydrin behandelt. Der Gehalt an Katalysator beruht auf der Menge an NHS-Ester-Gruppen auf der Filterpapieroberfläche. Die CNC-Proben wurden mit ^{13}C-NMR, Rasterkraftmikroskopie und Elementaranalyse charakterisiert (um den Gehalt an Katalysator zu bestimmen, der auf der Oberfläche immobilisiert ist).

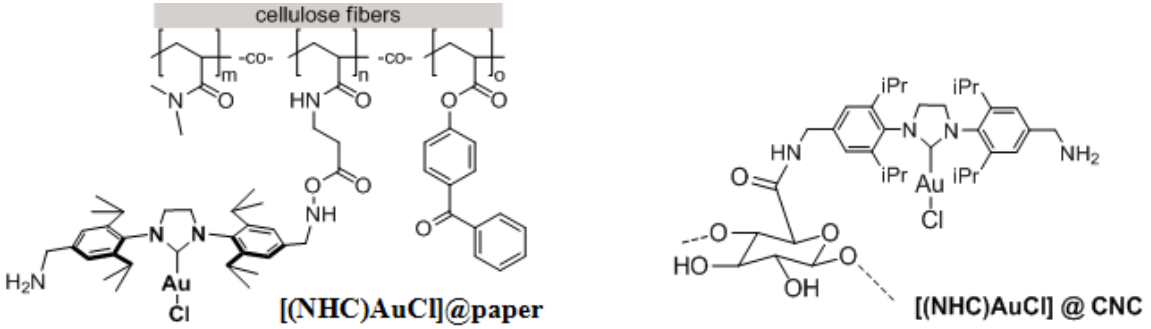

Die mit Katalysatoren modifizierten Oberflächen wurden anschließend für die Hydratisierung von Alkinen verwendet und die Ausbeute des Produktes mittels Gaschromoatographie bestimmt.

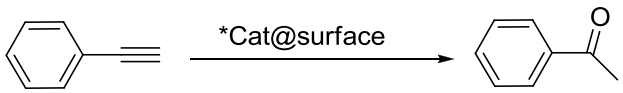

*[(NHC) AuCl]@paper or [(NHC) AuCl]@CNC

6. Experimental

6.1. General part

All chemicals were purchased as reagent grade from commercial suppliers and used without further purification unless otherwise noted. Grubbs I and and Grubbs-Hoveyda catalyst were synthesised according to literature procedures with minor modifications. Solvents were dried by passing over Al_2O_3 and/or by storing over molecular sieves unless otherwise noted. Flash column and preparative thin layer chromatography were performed using silica gel 60 (0.063-0.20 mesh ASTM). TLC was performed by using silica gel 60 F254 (0.2 mm) on alumina plates. NMR spectra were recorded on Bruker DRX500 and Bruker DRX300. The chemical shifts are given in ppm relative to TMS, coupling constants J are in Hz. GC experiments were run on a Clarus 500 GC with autosampler and FID detector. Column: Varian CP-Sil 8 CB (l = 15m, diam. = 0.25mm, dF = 1.0 µm), N2 (flow: 17 cm/sec; split 1:50); Injector-temperature: 200 °C, detector temperature: 270 °C. Temperature program: isotherm 60 °C for 5min, heating to 300 °C with 25 °C/min, isotherm for 5min. The spectroscopic data (1H NMR) of the isolated products are identical to those reported in the literature. Standard SEC was performed with THF as the mobile phase (flow rate 1 mL min^{-1}) on a SDV column set from PSS (SDV 1000, SDV 100000, SDV 1000000) at 30 °C. Calibration was carried out using PS standards (from Polymer Standard Service, Mainz). Electron microscopic characterization was performed by SEM (Philips XL 30 FEG) that is equipped with a LaB6 electron gun, a vacuum SE detector, an elevated pressure SE detector, a backscattering electron detector (BSD), and a Bruker AXS XFlash 4010 detector. SEM images were obtained using a vacuum SE detector where electron acceleration voltage of the incident beam was varied within 10-20 kV and the samples were kept typically at 5×10^{-5} Torr inside the SEM chamber. All of the EDX data were collected using an electron acceleration voltage of 20 kV and a working distance of 10 mm. TEM experiments were carried out on a Zeiss EM 10 electron microscope operating at 80 kV. CV measurements for the modified silica nanoparticles were carried out on a multipotentiostat VMP2 (Princeton Applied Research) with a custom-made cell in dry methylene chloride with tetrabutylammonium hexafluorophosphate (TBAHFP) as electrolyte (0.1 M) and ferrocene as standard under a nitrogen atmosphere. Ag/AgCl reference electrode and Pt counter electrodes were chosen and scan rates from 20 to 200 mV s^{-1} in a range of 0−1.0 V were applied. Dynamic light scattering (DLS) experiments were carried out with a setup based on a He−Ne laser (λ = 632.8 nm) as the light source.

6.2. Synthesis of symmetrical NHC-ligands bearing $-S(OEt)_3$ groups

6.2.1. Synthesis of N^4, N^5-dimesitylocta-1,7-diene-4,5-diamine [18] (2)

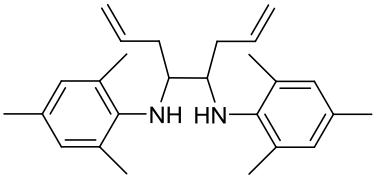

In a dry 250 ml Schlenk flask under argon atmosphere, 16.56 g (0.0566 mol, 1eq) of N, N'-bis, (2,4,6-trimethylphenyl) ethandiimin was added and dissolved in 10 ml of dry toluene. The reaction solution was cooled in an ice bath to at -78 ° C. Allyl magnesium chloride, 100 ml, (0.17 mmol, 9 eq), was added to the cooled reaction solution slowly. The reaction solution was warmed to room temperature and stirred overnight. For the work up, the reaction solution was cooled to 0 ° C and quenched using NH_4Cl. The phases are separated and the aqueous phase was extracted three times with diethyl ether. The organic phases were combined, dried over $MgSO_4$, filtered, and the volatiles were removed under reduced pressure. A yellowish oil was obtained which was left under vacuum for 2 days in order to solidify. The brown-yellowish solid residue obtained is suspended in methanol, filtered and finally washed well in methanol to obtain a white solid. Diamine 1 was obtained in 30 % yield.

Yield: 6.39 g (30 %)

^{1}H-NMR (300 MHz, $CDCl_3$): δ = 6.80 (s, 4-H), 5.82-5.68 (m, 2-H), 5.10-5.01 (dd, 4-H), 3.70 (bs, 2-H), 2.25 (s, 12-H, CH_3), 1.23 (s, 6-H, CH_3)

^{13}C-NMR (300 MHz, $CDCl_3$): δ = 141.77, 135.96, 130.14, 129.78, 128.54, 58.34, 35.55, 20.47, 19.24, 19.08

6.2.2. Synthesis of cis-4,5-diallyl-1,3-bis-(2,4,6-trimethylphenyl)-4,4-dihydro-3,4-imidazol-1-ium chloride [18] (3)

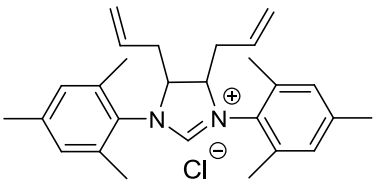

Diamine **2** (6.0 g, 15.93 mmol) and ammonium chloride (988 mg, 18.48 mmol) were stirred in triethyl orthoformate (4.45ml, 30.06 mmol) at 140 °C for 5 hours. After cooling the reaction vessel to room temperature, a small amount of THF was added to precipitate the excess of ammonium chloride salt. The

mixture is filtered and the product is washed five times with pentane, diethyl ether and dried in vacuum. Imidazolinium salt **7** is obtained in 60 % yield.

Yield: 3.88 g (60 %)

^{1}H NMR (300 MHz, $CDCl_3$) δ = 10.54 (s, 1-H), 6.95 (s, 2-H, 2H), 6.92 (s, 2-H, 2H), 5.49-5.41 (m, 2-H), 5.06-4.94 (m, 6 H), 2.47 (m, 10-H, CH_2, CH_3), 2.37 (s, 6-H, CH_3), 2.27 (s, 6-H, CH_3)

^{13}C-NMR (300 MHz, $CDCl_3$): δ = 160.52, 140.23, 135.55, 134.78, 131.92, 130.34, 129.36, 118.83, 65.53, 31.40, 21.03, 19.44, 19.27, 18.71

6.2.3. Synthesis of 1,3-Dimesityl-4,5-bis(3-(triethoxysilyl)propyl)-4,5-dihydro-1H-imidazol-3-ium chloride (4b) [18]

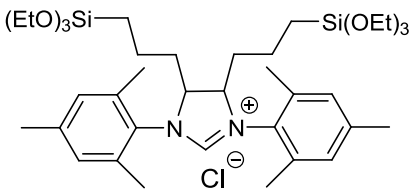

In a dry 50 ml Schlenk flask, under argon atmosphere 1.79 g of 4,5-diallyl-1, 3 - dimesityl-4 ,5-dihydro-1H-imidazol-3-ium chloride **(3)** (4.24 mmol, 1 eq) was dissolved in dry and degassed dichloromethane. Trichlorosilane (12 ml, 118.61 mmol, 28 eq) and Karstedt catalyst (1.53 mL, 1.4 g, 0.165 mmol) are added and the reaction mixture is left to stir at 40 ° C for 20 h. After the reaction time, the volatiles were removed under reduced pressure. The residue is dissolved in 20 ml dichloromethane and cooled to 0 ° C. A 1:1 mixture of ethanol and triethylamine (15 ml: 15 ml) was added and the solution was left to stir for 2 h at room temperature. After two hours the volatiles were removed under reduced pressure. The residue was washed with toluene, and the precipitate filtered. The filtrates were evaporated and the residue was washed several times with pentane, filtered and dried under vacuum to obtain the product as a white powder.

Yield: 2.71 g (85 %)

^{1}H-NMR (300 MHz, $CDCl_3$): δ = 10.71 (s, 1-H), 6.95 (s, 2-H), 6.91 (s, 2-H), 3.73-3.66 (q, J= 3.69, 12-H), 2.47 (s, 6-H, CH_3), 2.35 (s, 6-H, CH_3), 2.26 (s, 6-H, CH_3), 1.92-1.66 (m, 4H, CH_2) 1.22-1.33 (m, 4H) 1.17-1.12 (t, J= 1.15, 18-H), 0.54-0.48 (t, 4-H)

^{13}C NMR (300 MHz, $CDCl_3$): δ = 10.8, 18.4, 18.9, 19.3, 20.7, 21.1, 30.2, 58.5, 66.1, 130.0, 130.4, 130.5, 134.6, 135.8, 140.0, 160.4

6.3. Synthesis of unsymmetrical NHC-ligands

6.3.1. Synthesis of N- (2,4,6- Trimethylphenyl)- 1,2- diaminoethane [19] (5)

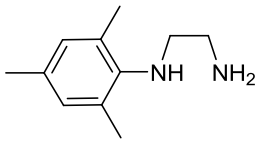

In a 250 ml round bottom flask, 25 g (0.1848 mol, 2 eq.) of 2,4,6 - trimethylaniline was diluted with 100 ml toluene. 18.94 g (0.0924 mol, 1 eq.) of bromoethylamin-hydrobromide was added in the same flask and the mixture was left to reflux at 110 ° C overnight. After cooling to room temperature, the mixture was treated with 300 ml of potassium hydroxide solution (6.67 M) and stirred. The organic phase was separated from the aqua phase, and dried under magnesium sulfate. The volatiles were evaporated, and finally the product ***5*** was obtained after distillation in 70 % yield.

Yield: 11.52 g (70 %)

^{1}H-NMR (300 MHz, $CDCl_3$): δ = 6.85 (s, 2 H), 3.00 (t, J= 3.00, 2 H), 2.90 (t, J= 2.91, 2 H), 2.29 (s, 6 H, CH_3), 2.24 (s, 3 H, CH_3)

6.3.2. Synthesis of 1- (2,4,6- Trimethylphenyl)- 4,5- dihydro- 1H- imidazole [19] (6)

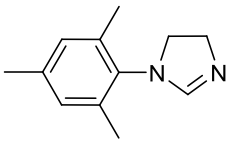

In a dry Schlenk flask, 11.50 g (0.0645 mol, 1 eq.) of N-(2, 4, 6) - trimethylphenyl) - 1,2 – diaminoethane, ***5***, was added to 37.97 g (42 ml, 0.1935 mol, 3 eq.) of triethyl orthoformate. PTSA (paratoluenesulfonic acid). 219 mg (1.2707 mmol, 0.0197 eq.) was finally introduced and the reaction was left to reflux at 140 ° C for 18 hours. Finally, the reaction system was cooled to room temperature, and the crude material was dissolve in 200 ml of water and extracted twice with diethyl ether, dried over $MgSO_4$ and the volatiles were evaporated. The product was obtained as white crystals after distillation with Buchi glass furnace (Kugelrohr apparatus) at 200 ° C under vacuum.

Yield: 9.10 g (75 %)

^{1}H NMR (300 MHz, $CDCl_3$): δ = 6.90 (s, 1H), 6.89 (s, 2H), 4.06 (t, 2H), 3.57 (t, 2H), 2.28 (s, 3H), 2.22 (s, 6H)

^{13}C NMR (300 MHz, $CDCl_3$): δ = 155.99, 137.52, 136.76, 134.5, 129.38, 54.65, 48.93, 20.89, 18.05

6.3.3. Synthesis of 1-Mesityl-3-(3-(triethoxysilyl)propyl)-4,5-dihydro-1H-imidazol-3-ium chloride [95] (7)

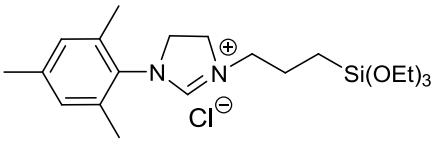

The synthesis of 7 was performed using a silimal procedure to the literature [95]. In a dry 100 ml Schlenk flask under an argon atmosphere, 1.2 g of mesityl-4, 5 - dihydro-1H-imidazole (6.37 mmol, 1eq) **6** and 1.7 mL (3-chloropropyl) triethoxysilane (7.07 mmol, 1.70 g, 1.11 eq) was added. The reaction was heated to 90 ° C and stirred for 4-5 days.
After the reaction time, a solid residue was formed, which was washed with petroleum ether and filtered. The light brownish product was then dried under vacuum to obtain imidazolinium salt **7** in 80 % yield.

Yield: 2.18 g (80 %)

^{1}H-NMR (300 MHz, $CDCl_3$): δ = 9.64 (s, 1-H) 6.85 (s, 2-H), 4.16-4.13 (m, 4H), 3.91 (t, 2H), 3.76-3.72 (q, J= 3. 77, 6-H), 2.24 (s, 6H, CH_3), 2.20 (s, 3H, CH_3) 1.13 (t, J= 1. 16, 9H, CH_3), 0.62-0.57 (t, 2H)

6.3.3.1. Synthesis of 3-Chlorpropyltriisopropoxysilane [96] (8)

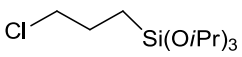

In a dry Schlenk flask under argon atmosphere, 6 ml (8.16 g, 0.0385 mol, 1 eq) of trichloro (3-chloropropyl) silane was added and diluted with 30 ml of degassed ether. Thereafter, the mixture was added dropwise to a solution of 31 ml (2.28 mg, 0.2309 mol, 6 eq.) triethylamine and 24 ml (1.8475 mol, 8 eq.) of isopropanol which was further diluted with 100 ml diethyl ether and cooled to 0 ° C. The reaction mixture was stirred at room temperature. Finally, the volatiles are removed under reduced pressure, the residue filtered, washed with 50 ml of propanol, and finally distilled.

Yield: 7.9 g (73 %)

^{1}H NMR (300 MHz, $CDCl_3$): δ = 4.21 (sep, 3H), 3.53 (t, 2H), 1.87 (M, 2H), 1.19 (d, 18H, CH_3), 0.69 (m, 2H)

6.3.3.2. Synthesis of 3-Iodopropyltriisopropoxysilane (9) [95]

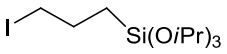

In a dry Schlenk flask, 8 g (0.0293 mol, 1 eq.) of 3-Chlorpropyltriisopropoxysilane **8** and 6.358 g (0.0586 mol, 2 eq.) of sodium iodide were added and dissolved in 40 ml of dry and degassed acetone. The mixture was stirred at 56 ° C for three days under reflux. The solvent was removed under vacuum and the residue stirred in 15 ml of pentane. The mixture was filtered and the filtrate was concentrated on a rotary evaporator. The oily residue was then distilled to obtain 70% of the product 9.

Yield: 7.67 g (70%)

^{1}H NMR (300 MHz, $CDCl_3$): δ = 4.19 (sep, 3H), 3.21 (t, 2H), 1.90 (M, 2H), 1.19 (d, 18H, CH_3), 0.66 (m, 2H)

6.3.4. Synthesis of 1-Mesityl-3-(3-(triisopropoxysilyl) propyl)-4,5-dihydro-1H-imidazol-3-ium iodide [95] (10)

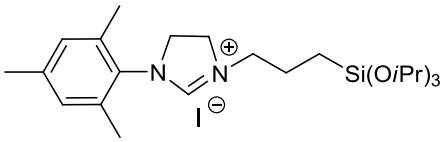

In a dry Schlenk flask under argon atmosphere, 0.997 g of 6 (5.296 mmol, 1 eq.) 1-(2,4,6 - trimethylphenyl) - 4,5 - dihydro-1H-imidazole was mixed with 1.748 g (5.296 mmol, 1eq.) of 3 - iodopropyl-triisopropoxysilane. The mixture is then stirred in 60 ml of dry toluene at 110 ° C for two days under reflux. After the reaction time, the mixture is cooled to room temperature and the solvent is evaporated under reduced pressure. The residue is washed with ether, filtered, and the the solvent is removed on a rotary evaporator and the residue washed with 30 ml of ethyl ether, filtered and the brownish powdered product is dried under vacuum.

Yield: 2.37 g (80 %)

^{1}H NMR (300 MHz, DMSO-d6): δ = 8.72 (s, 1-H), 7.04 (s, 2-H), 4.18 (sept, 3H), 4.09-4.14 (m, 4H), 3.53 (t, 2H), 2.27 (s, 3H, CH_3), 2.25 (s, 6H, CH_3), 1.71 (m, 2H), 1.17 (d, 18H, CH_3), 0.53 (m, 2H)
^{13}C NMR (300 MHz, DMSO-d6): δ = 158.73, 139.19, 135.46, 131.19, 129.32, 64.53, 50.36, 49.91, 48.30, 25.41, 20.54, 17.15, 8.02

6.4. Synthesis of ruthenium complexes

6.4.1. Synthesis of Grubbs-Hoveyda 1st generation catalyst using Amberlyst resin [20] (11)

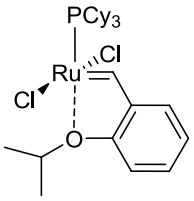

In a 100ml Schlenk flask, 993 mg (1.076 mmol, 1 eq) of [$RuCl_2$ (Ind) (PCy_3)$_2$], was weighted, and 1.10 g (4.0 mmol, 4 eq) of Amberlyst resin was added under argon atmosphere. The complex was dissolved in 50-60 ml of dry and degassed dichloromethane. Finally, 2-isopropoxystyrene (196 µl, 183 mg, 1.13 mmol, 1.05 eq) was added, and the reaction mixture was left to stir at 40 ° C for 95 min. The color of the reaction solution changed from reddish to dark brown. The progress of the reaction was followed by means of thin layer chromatography. Finally, the reaction mixture was filtered to get rid of the Amberlyst resin, and the volatiles were removed under vacuum.

The dark brownish residue was washed with cold pentane, and dried under vacuum to obtain product **12** in 93 % yield.

Yield: 616 mg (93 %)

^{1}H-NMR (300 MHz, $CDCl_3$): δ = 17.43 (s, 1-H), 7.68-77.58 (dd, J= 7.64, 2-H),7.09-7.04 (t, 2-H), 5.28 (sept, 1H), 2.39-2.27 (m, 3-H, Cy), 2.08 (m, 6-H, Cy), 1.82-1.71(m, 24-H, Cy), 1.28 (s, 6H, CH_3)
^{13}C-NMR (300 MHz, $CDCl_3$): δ = 143.97, 129.62, 122.85, 122.51, 113.38, 75.57, 35.87, 35.54, 30.12, 27.84, 26.29, 22.11.

6.4.1.1. Synthesis of functionalized Grubbs-Hoveyda 2nd generation-type complex [18] (12)

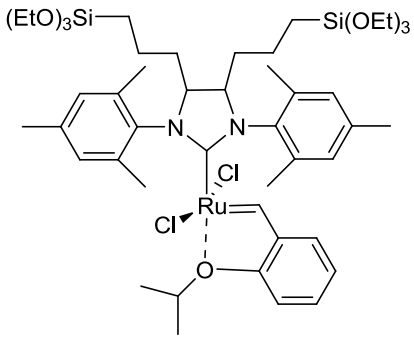

Complex **12** was synthesized according to the literature procedure given by Pleixats et al [18], but with a few modification of the procedures. In a dry 100 ml Schlenk flask under argon atmosphere, 1,3-dimesityl-4 ,5-bis (3 - (triethoxysilyl) propyl) -4,5-dihydro-1H-imidazol-3-ium chloride **4b** (113 mg, 0.15 mmol, 1.5 eq) was suspended in 10 ml of toluene. 0.5 M KHMDS (in toluene) (0.10 mmol, 2.3 eq) was added under argon atmosphere, and the reaction mixture was left to stir at room temperature for 15 minutes to generate the carbene. Grubbs Hoveyda 1st generation complex (0.10 mmol, 61.56 mg, 1 eq) was dissolved in 10 ml of dry toluene in another flask and added via cannula, under argon atmosphere to the NHC-suspension mixture. The reaction was left to stir at 80 °C for 3 h. The reaction progress was monitored by thin layer chromatography. After 3 h reaction time, the reaction system was cooled to room temperature and the volatiles were removed under reduced pressure. At the time of removing the volatiles, the residue changed color from violet to dark green. Pleixats et al [18] reports that the residue was treated with chloroform and left to stir overnight before purification with column chromatography. Different from the literature procedure, the final step was skipped, since no better yields were observed as the residue was left to stir in chloroform overnight. The complex was purified by flash chromatography, using a special silica gel: SiliCycle P60 R12030B particle size of 60.0 – 75.0 µm. The eluent used was a mixture of Pentane: EtOAc (6:1). Pentane was distilled in the rotovap before use, whereas ethyl acetate was stirred over molecular sieves and degassed with argon. The yield of complex **13** was never more than 20 %. The product was not stable at room temperature, therefore was stored under inert atmosphere at -30 ^{0}C. The complex obtained was a dark green, sticky solid.

Yield: 20.70 mg (20 %)

^{1}H-NMR (300 MHz, $CDCl_3$): δ = 16.61 (s, 1H), 7.50-7.44 (dt, 1H), 7.09-7.04 (m, 4-H), 6.-691 (t, 1H), 6.86-6.83 (t,1H) 6.77-6-74 (d, 1H), 4.90-4.81 (sept, 1H), 4.89-4.85 (sept 1H), 3.76-3.69 (q, J= 3.73, 12H), 2.63 (s, 3H, CH_3), 2.52 (s, 3H, CH_3) 2.43 (s, 3H, CH_3), 2.32 (s, 9H, CH_3), 1.82 (s, 3- H), 1.80 (s, 3H), 1.20-1.15 (t, J= 1.18, 18H, CH_3), 0.55 (m, 4H).

^{13}C-NMR (300 MHz, $CDCl_3$): δ = 300.00, 211.00, 152.33, 146.00, 140.29, 140.40, 140.00, 130.40, 130.00, 123.10, 122.6, 113.3, 75.10, 68.90, 66.90, 58.70, 32.10, 23.10, 21.32, 18.70, 11.31.

6.5. Synthesis of symmetrical NHC-ligands bearing $-NH_2$ groups

6.5.1. Synthesis of *N, N'*-Bis(2,6-diisopropyl-4-(morpholinomethyl)phenyl)ethylenediamine [91] (13)

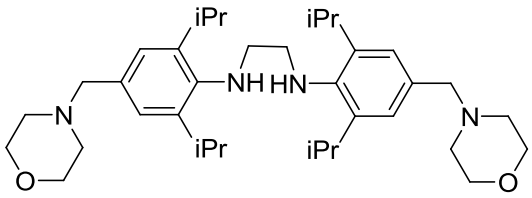

Synthesis of N, N'-Bis(2,6-diisopropyl-4-(morpholinomethyl)phenyl)ethylenediamine was done according to the literature procedure reported by Sashuk [91] but with a few modification regarding the purification of the obtained product.

In a Schlenk flask 20 g of N,N'-Bis(2,6-diisopropyl-4-(morpholinomethyl)phenyl)ethylenediimine (0.035 mol, 1 eq.), which was synthesized according to literature procedure [91], was dissolved in 100 ml of dry THF. Lithium aluminium hydride 2.66 g (0.07 mol, 2 eq.) was added slowly within a time interval of 30 min, at 0 ° C and the mixture was stirred overnight. The exess of $LiAlH_4$ was quenched with ice/ HCl mixture then the mixture was basified to pH level of 9-10 using NaOH solution. The product was extracted with ether several times, to obtain yellowish highly viscous oil. According to the literature, the viscous oil was used for the next reaction steps without purification, but in this case the ring closed product was obtained with impurities. For this reason, the diamine was purified by column chromatography Cyclohexane:EtOAc (4:1) before using for the next reaction steps.

Yield: 14.21 g (70 %)

^{1}H-NMR (300 MHz, $CDCl_3$): δ = 7.04 (s, 4H), 3.72-3.74 (m, 8H), 3.47 (s, 4H), 3.35 (heptet, *J*= 6.9 Hz, 4H), 3.15 (s, 4H), 2.44 (m, 8H), 1.26 (d, *J*= 6.6 Hz, 24H).

^{13}C-NMR (300 MHz, $CDCl_3$): δ = 142.66, 132.99, 124.85, 67.52, 63.94, 53.99, 52.75, 28.16, 27.32, 24.67

6.5.2. Synthesis of 1,3-bis(4-(azidomethyl)-2,6-diisopropylphenyl)-4,5-dihydro-1H-imidazol-3-ium chloride (14)

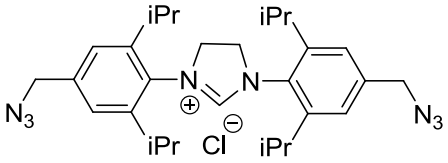

In a round bottom flask 7 g of 1,3-Bis(2,6-diisopropyl-4-(chloromethyl)phenyl)-4,5-dihydro-1H-imidazol-3-iumchloride (0.013 mol, 1 eq.) was dissolved in 50 ml of technical grade MeOH.. Sodium azide 3.38 g (0.052

mol, 4 eq.) was added and the mixture was refluxed for 18 h. After cooling the mixture to room temperature, water was added to form a white precipitate. The precipitate was filtered, washed with water and dried under vacuum to give the product as a white powder.

Yield: 4.53 g (65 %)

^{1}H-NMR (300 MHz, DMSO): δ = 9.47 (s, 1H), 7.43 (s, 4H), 4.54 (s, 8H), 3.10 (heptet, *J*= 6.8 Hz, 4H), 1.36 (d, *J*= 6.7 Hz, 12H), 1.21 (d, *J*= 6.8 Hz, 12H).

^{13}C-NMR (300 MHz, DMSO): δ = 160.16, 146.58, 138.82, 129.49, 124.72, 53.67, 53.15, 28.27, 24.85, 23.24

6.5.3. Synthesis of 1,3-bis(4-(aminomethyl)-2,6-diisopropylphenyl)-4,5-dihydro-1H-imidazol-3-ium chloride (15)

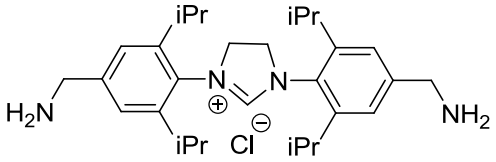

In a round bottom flask 4 g of **14** (7.45 mmol, 1 eq.) was dissolved in 20 ml of technical grade MeOH. Pd on carbon 2 g (5 % Pd, 56. 6 %) was added and H_2 gas was bubbled for 8 h at room temperature. The reaction progress was followed with ^{1}H NMR. After the reaction time, the mixture was filtered thru a filter paper and the filtrate was evaporated to give the product as a light brownish solid.

Yield: 3.40 g (85 %)

^{1}H-NMR (300 MHz, DMSO): δ = 9.38 (s, 1H), 7.38 (s, 4H), 4.49 (s, 4H), 3.76 (s, 4H), 3.06 (heptet, *J*= 6.8 Hz, 4H), 1.39 (d, *J*= 6.7 Hz, 12H), 1.22 (d, *J*= 6.8 Hz, 12H).

^{13}C-NMR (300 MHz, DMSO): δ = 160.23, 147.25 145.33, 127.90, 123.21, 53.58, 45.45, 28.25, 24.91, 23.34

6.5.4. Synthesis of (1, 3-bis(4-(aminomethyl)-2,6-diisopropylphenyl)imidazolidin-2-yl)silver(II) chloride (16)

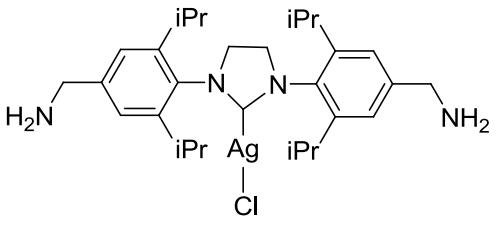

In a Schlenk flask 3 g of **15** (6.20 mmol, 1 eq.) was dissolved in 20 ml of dry DCM. Silver (I) oxide 4.31 g (18.6 mmol, 3 eq.) was added and the mixture was stirred under inert atmosphere in the dark at room temperature, overnight. After the reaction time, the mixture was filtered through silica plug. The filtrate was evaporated to obtain a crude residue, which was washed with pentane to give the product as a white solid.

Yield: 1.84 g (50 %)

^{1}H-NMR (300 MHz, $CDCl_3$): δ = 7.15 (s, 4H), 4.01 (s, 4H), 3.87 (s, 4H) 3.00 (heptet, *J*= 6.9 Hz, 4H), 1.26-1.28 (dd, *J*= 6.9, 4.5 Hz, 24H).

^{13}C-NMR (300 MHz, $CDCl_3$): δ = 146.48 144.81, 132.94, 124.13, 123.22, 53.81, 46.33, 28.83, 25.25, 23.92

6.5.5. Synthesis of (1,3-bis(4-(aminomethyl)-2,6-diisopropylphenyl)imidazolidin-2-yl)gold(II) chloride (17)

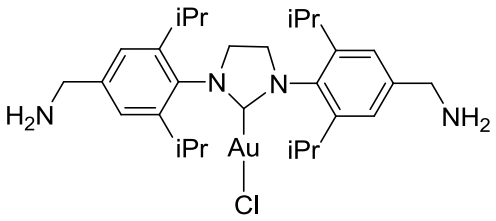

In a Schlenk flask 500 mg of **16** (0.734 mmol, 1 eq.) was dissolved in 10 ml of dry and degassed DCM. Me_2SAuCl 216 mg (0.734 mmol, 1 eq.) dissolved in 5 ml dry DCM and it was added to the silver salt and was left to stir for 2h. After the reaction time the mixture was filtered through celite and the filtrate was evaporated under reduced pressure. A white residue was obtained which was washed with pentane to give the product as a white powder.

Yield: 300 mg (60 %)

^{1}H-NMR (300 MHz, $CDCl_3$): δ = 7.19 (s, 4H), 4.04 (s, 4H), 3.92 (s, 4H), 3.02-3.04 (m, *J*= 6.80 Hz, 4H), 1.54 (d, *J*= 6.70 Hz, 24H).

^{13}C-NMR (300 MHz, $CDCl_3$): δ = 160.23, 147.25 145.33, 127.90, 123.21, 53.58, 45.45, 28.25, 24.91, 23.34

6.6. Synthesis of 2-vinylphenol [97] (18)

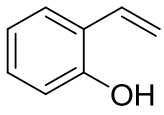

In a Schlenk flask 11, 5 g of PPh_3MeI^- (28.30 mmol, 2.3 eq) was dissolved in dry THF and sodium tert-petoxide 11 ml (28.30 mmol, 2.3 eq) was added and the mixture is left to stir for 30 min at room temperature. Finally, 1, 5 g of 2-hydroxybenzaldehyde (12.30 mmol, 1 eq.) was added and the mixture was left to stir overnight at room temperature. A white precipitate was formed which was filtered and the filtrate was evaporated under reduced pressure. The product ***23*** was obtained as colorless oil.

Yield: 1.26 g (85 %)

^{1}H-NMR (300 MHz, $CDCl_3$): δ = 7.43 (dd, *J*= 7.7, 1.7 Hz, 1H), 7.18 (dt, *J*= 7.7, 1.7 Hz, 1H), 6.98 (m, 2H), 6.82 (dd, *J*= 7.7, 1.0 Hz, 1H), 5.78 (dd, *J*= 16.15, 1.14 Hz, 1H), 5.39 (dd, *J*= 13.48, 1.65 Hz, 1H), 5.25 (s, 1H).

6.6.1. Synthesis of triethoxy (11-(2-vinylphenoxy) undecyl) silane (19)

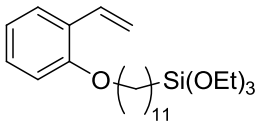

In a Schlenk flask 600 mg of **18** (4.99 mmol, 1 eq.) was dissolved in 10 ml of dry acetonitrile. 1, 69 g (5.49 mmol, 1.1 eq.) of (11-bromoundecyl)triethoxysilane, 3.25 g (9.98 mmol, 2.0 eq.) of Cs_2CO_3 and 828 mg (4. 99 mmol, 1 eq.) of KI was added and the mixture was left to stir overnight at 60 ° C. After the reaction time the volatiles were evaporated under reduced pressure, the residue was washed with hexane and filtered. The filtrate was concentrated under reduced pressure to give the product as colorless oil.

Yield: 1.00 g (67, 6 %)

^{1}H-NMR (300 MHz, $CDCl_3$): δ = 7.46 (d, 1H), 7.19 (m, 1H), 7.12-7.01 (m, 1H), 6.94-6.84 (m, 2H), 5.77 (d, 1H), 5.77 (d, 1H), 5.52 (d, 1H), 3.98 (t, 2H), 3.86 (q, *J*= 19. 33 Hz, 6H), 1.81 (m, *J*= 12. 30 Hz, 2H), 1.50-1.26 (m, 18H), 1.23 (t, *J*= 19. 33 Hz, 9H), 0.6 (m, *J*= 2.00 Hz, 2H).

6.6.2. (SIPr)Ru(Py)(Ind)Cl_2 [98] (20)

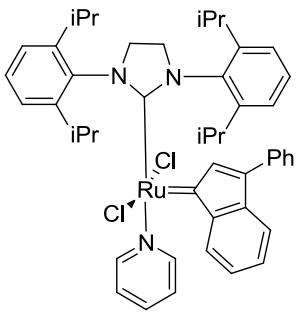

In a Schlenk flask 300 mg of (SIPr)(PPh_3)Cl_2Ru (0.296 mmol, 1 eq.) was dissolved in 2 ml of dry pyridine and the mixture was left to stir at room temperature for 1 h. After the reaction time 20 ml of cold pentane was added to precipitate the product. The mixture was stirred for 15 min then stored at -40 ° C for 15 min. The precipitate was then filtered and washed with pentane and dried under vacuum to obtain the complex as a reddish-brown powder.

Yield: 172 mg (72 %)

^{1}H-NMR (300 MHz, C_6D_6): δ = 8.75 (d, *J*= 7. 0 Hz, 1H), 8.26 (d, *J*= 5. 0 Hz, 2H), 7.82 (d, *J*= 7. 0 Hz, 2H), 7.48-7.46 (m, 4H), 7.11 (t, 1H), 6.98 (t, *J*= 1. 0 Hz, 2H), 6.70 (d, t, *J*= 1. 0 Hz, 1H), 6.51 (t, *J*= 1. 0 Hz, 1H), 6.22 (t, *J*= 1. 00 Hz, 2H), 4.29-3.94 (m, 4H), 3.70-3.04 (m, 4H), 1.96 (s, 3H), 1.92 (s, 3H), 1.56 (s, 3H), 1.37 (s, 3H), 1.26 (s, 3H), 1.02 (s, 3H), 0.97 (s, 3H).

^{13}C-NMR (300 MHz, C_6D_6): δ = 217.42, 153.45, 142.34, 142.29, 142.03, 141.16, 140.98, 140.13, 137.80, 137.60, 136.38, 136.21, 130.44, 129.94, 129.74, 128.88, 128.06, 128.06, 126.80, 124.60, 123.25, 117.56, 55.22, 54.29, 30.09, 29.91, 28.86, 27.98, 27.72, 27.49, 26.94, 26.67, 24.63, 23.83, 23.46, 22.34.

6.6.3. Synthesis of (1,3-bis(2,6-diisopropylphenyl)imidazolidin-2-yl)(2-(11 (triethoxysilyl)undecyloxy)benzylidene)ruthenium(V) chloride (21)

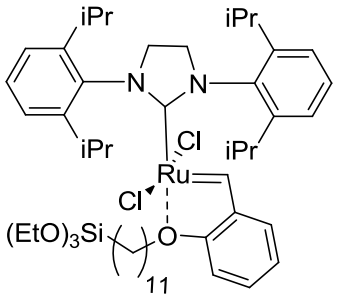

In a Schlenk flask 100 mg of **20** (0.139 mmol, 1 eq.) was dissolved in 2 ml of dry and degassed toluene. 63 mg (0.144 mmol, 1.2 eq.) of **19** was added and the reaction was left to stir for 2 h at 65 ° C. After the reaction time all the volatiles were evaporated and the residue was purified with flash chromatography, cyclohexane : ethyl acetate (4:1) to obtain the product as a dark green powder.

Yield: 60.9 mg (60 %)

^{1}H-NMR (300 MHz, C_6D_6): δ = 16.26 (s, 1H), 7.45-7.36 (m, 3H), 7.27-7.25 (m, 5H), 6.75-6.66 (m, 2H), 4.07 (s, 4H), 3.70 (m, 2H), 3.50 (m, 4H), 1.71 (m, 2H) 1.33-1.14 (m, 36H), 0.56 (m, 2H).

6.6.4. Synthesis of (1,3-bis(2,6-dimethylphenyl)imidazolidin-2-yl)(2-(11 (triethoxysilyl)undecyloxy)benzylidene)ruthenium(V) chloride (22)

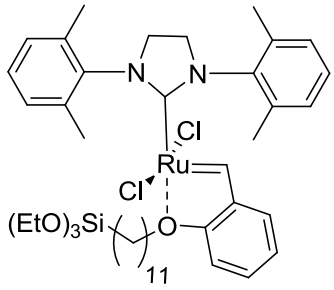

In a Schlenk flask 100 mg of (IMes)Ru(Py)Cl_2 (0.139 mmol, 1 eq.) was dissolved in 2 ml of dry and degassed toluene. 63 mg (0.144 mmol, 1.2 eq.) of **19** was added and the reaction was left to stir for 2 h at 65 ° C. After the reaction time all the volatiles were evaporated and the residue was purified with flash chromatography, cyclohexane: ethyl acetate (4:1) to obtain the product as a dark green powder.

Yield: 51 mg (50 %)

^{1}H-NMR (300 MHz, C_6D_6): δ = 16.44 (s, 1H), 7.37 (m, 1H), 6.96 (s, 4H), 6.79 (m, 3H), 4.02 (m, 4H), 3.73 (m, 2H), 2.37 (s, 12H), 2.30 (s, 6H) 1.33-1.12 (m, 27H), 0.53 (m, 2H).

6.7. Synthesis of 1,3-bis(2,6-dimethyl-4-((methyl(pyridin-3-ylmethyl)amino)methyl)phenyl)-4,5-dihydro-1H-imidazol-3-ium (23)

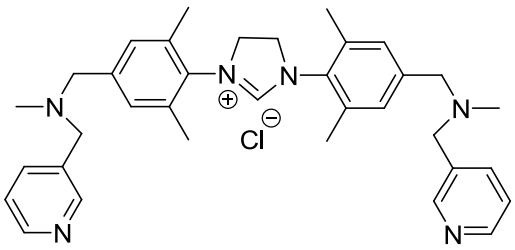

In a Schlenk flask 170 mg of 1,3-Bis(2,6-diisopropyl-4-(chloromethyl)phenyl)-4,5-dihydro-1H-imidazol-3-iumchloride (0.413 mol, 1 eq.) was dissolved in 5 ml of dry DMF N-methyl-1-(pyridin-3-yl)methanamine 509 µl (4.130 mol, 10 eq.) and NaI 613 mg (4.130 mmol, 10 eq.) was added and the mixture was stirred at 80 ° C for 12 h. After cooling the mixture to room temperature 100 ml of DCM and 100 ml of water was added to the reaction mixture and the organic layer separated and washed several times with water. The collected organic layers were then dried over $MgSO_4$ the solvent was evaporated under reduced pressure.
A brownish highly viscous residue was obtained which was solidified by washing with Et_2O and drying under vacuum to obtain the product as a light brownish powder.

Yield: 192.7 g (80 %)

^{1}H-NMR (300 MHz, DMSO-d6): δ = 9.00 (s, 1H), 8.55 (m, 2H), 8.49-8.46 (m, 2H), 7.78-7.75 (m, 2H), 7.38-7.36 (m, 2H), 7.26 (s, 4H), 4.46 (s, 4H), 3.56 (s, 4H), 3.50 (s, 4H), 2.39 (s, 12H), 2.09 (s, 6H).

^{13}C-NMR (300 MHz, DMSO-d6): δ = 160.20, 149.87, 148.34, 141.10, 136.35, 135.60, 134.14, 132.09, 128.83, 123.46, 60.27, 58.31, 50.87, 41.58, 17.33

6.7.1. Synthesis of [(NHC-27)RhCl(cod)] (24)

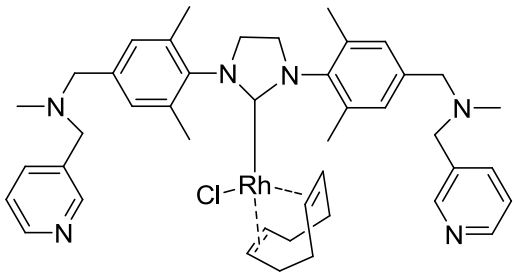

In a Schlenk flask 40 mg of [Rh-(μ-Cl)(cod)]$_2$ (0.081 mmol, 1 eq.) was dissolved in 5 ml of dry THF and KO^{t}Bu 22 mg (0.195 mmol, 2.2 eq.) was added and the mixture was left to stir at room temperature for 45 min. Finally, salt ***23,*** 105 mg (0.195 mmol, 2.2 eq.) dissolved in 10 ml of dry THF was added to the reaction mixture via cannula. The mixture was left to stir at room temperature for another 2 h. After the reaction time, the solvent was evaporated under reduced pressure and the residue was recrystallized in DCM / pentane mixture to obtain the product as a yellow powder.

Yield: 56.76 mg (85 %)

^{1}H-NMR (300 MHz, CDCl$_3$): δ = 8.62 (m, 2H), 8.53 (m, 2H), 7.22 (m, 2H), 7.30 (m, 2H), 7.20 (s, 2H), 7.15 (s, 2H), 4.73 (bs, 2H), 3.93-3.87 (m, 4H), 3.60-3.50 (m, 10H), 2.67 (s, 6H), 2.44 (s, 6H), 2.24 (s, 6H), 1.80-1.67 (m, 4H), 1.49-1.32 (m, 4H).

^{13}C-NMR (300 MHz, CDCl$_3$): δ = 150.59, 148.75, 139.02, 136.74, 135.84, 130.23, 128.34, 123.50, 95.84, 61.68, 58.98, 51.80, 42.43, 32.39, 29.10, 22.45, 18.82.

6.7.2. Synthesis of [(NHC-27)RhCl(CO)$_2$] (25)

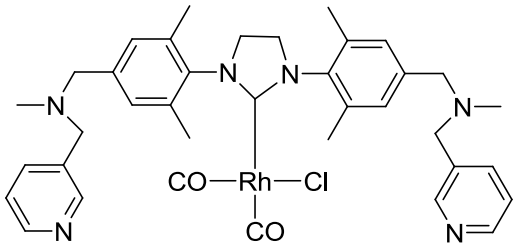

In a round bottom flask 50 mg of 1,3-bis(2,6-dimethyl-4-((methyl(pyridin-3-ylmethyl)amino)methyl)phenyl)-4,5-dihydro-1H-imidazol-3-ium (0.0607 mmol) was dissolved in 10 ml of dry DCM and CO gas was bubbled into the solution for 30 min. The reaction progress was followed by thin layer chromatography. After the reaction time, the solution was concentrated to 2 ml and chilled pentane was added. The precipitate was filtered, washed several times with pentane. After the reaction time, the solvent was evaporated under reduced pressure and the residue was recrystallized in DCM / pentane mixture to obtain the product as a yellow powder.

Yield: 36.14 mg (80 %)

^{1}H-NMR (300 MHz, $CDCl_3$): δ = 8.59 (m, 2H), 8.51 (m, 2H), 7.72-7.69 (m, 2H), 7.51 (m, 2H), 7.11 (s, 4H), 4.03 (s, 4H), 3.54-3.49 (m, 8H), 2.49 (s, 6H), 2.37 (s, 12H).

^{13}C-NMR (300 MHz, $CDCl_3$): δ = 160.20, 149.87, 148.34, 141.10, 136.35, 135.60, 134.14, 132.09, 128.83, 123.46, 60.27, 58.31, 50.87, 41.58, 17.33

6.7.3. Synthesis of 1,3-bis(4-((benzylamino)methyl)-2,6-diisopropylphenyl)-4,5-dihydro-1H-imidazol-3-ium chloride (26)

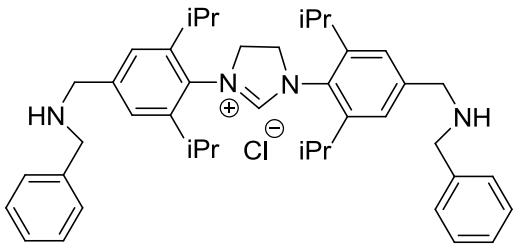

In a Schlenk flask 500 mg of 1,3-Bis(2,6-diisopropyl-4-(chloromethyl)phenyl)-4,5-dihydro-1H-imidazol-3-iumchloride (0.954 mmol, 1 eq.) was dissolved in 20 ml of dry DMF/acetone mixture (1:1). Phenylmethanamine 1.02 g (9.54 mmol, 10 eq.) and NaI 1.43 g (9.54 mmol, 10 eq.) was added and the mixture was stirred at 80 ° C for 12 h. After cooling the mixture to room temperature 100 ml of DCM and 100 ml of

water was added to the reaction mixture and the organic layer separated and washed several times with water. The collected organic layers were then dried over $MgSO_4$ the solvent was evaporated under reduced pressure to obtain a viscous residue. The residue was solidified by washing with Et_2O and drying under vacuum to obtain the product as a beige colored powder.

Yield: 476 mg (75 %)

^{1}H-NMR (300 MHz, DMSO-d6): δ = 9.39 (s, 1H), 7.35-7.34 (m, 14H), 4.52 (s, 4H), 3.61 (s, 4H), 3.07 (m, 4H), 1.36 (bs, 12H), 1.19 (bs, 12H).

^{13}C-NMR (300 MHz, DMSO-d6): δ = 160.00, 148.00, 140.02, 140.00, 137.80, 137.40, 135.80, 133.00, 128.50, 127.90, 127.00, 124.30, 124.10, 59.30, 58.40, 57.80, 56.80, 29.80, 29.00, 23.3.

6.7.4. Synthesis of 1,3-bis(4-((allylamino)methyl)-2,6-diisopropylphenyl)-4,5-dihydro-1H-imidazol-3-ium chloride (27)

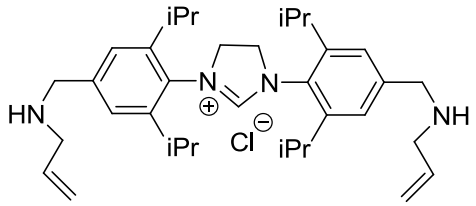

In a Schlenk flask 500 mg of 1,3-Bis(2,6-diisopropyl-4-(chloromethyl)phenyl)-4,5-dihydro-1H-imidazol-3-iumchloride (0.954 mmol, 1 eq.) was dissolved in 5 ml of dry DMF. Allylamine 545 mg (9.540 mmol, 10 eq.) and NaI 1.431 g (9.540 mmol, 10 eq.) were added and the reaction was left to stir at 80 ° C for 18 h. After the reaction time the mixture was left to cool to room temperature and 100 ml of DCM and 100 ml of water was added to the reaction mixture and the organic layer separated and washed several times with water. The collected organic layers were then dried over $MgSO_4$ the solvent was evaporated under reduced pressure to obtain a viscous residue. The residue was solidified by washing with Et_2O and drying under vacuum to obtain the product as a brownish powder.

Yield: 431.42 g (80 %)

^{1}H-NMR (300 MHz, DMSO-d6): δ = 9.38 (s, 1H), 7.35 (s, 4H), 5.87 (m, 2H), 5.12 (dd, *J*= 14.1, 2.0, 4H), 4.50 (s, 4H), 3.71 (s, 4H), 3.16 (m, 4H), 3.05 (m, *J*= 6.8, 4H), 1.33 (d, 4H, *J*= 6.7, 12H), 1.19 (d, 4H, *J*= 6.7, 12H)

6.7.5. Synthesis of 1,3-bis(4-((allyl(ethyl)amino)methyl)-2,6-diisopropylphenyl)-4,5-dihydro-1H-imidazol-3-ium chloride (28)

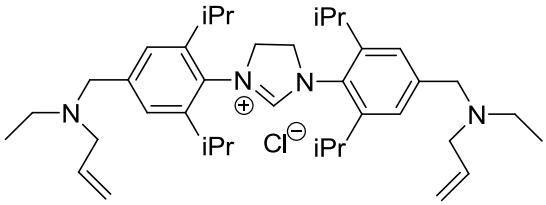

In a Schlenk flask 280 mg of **27** (0.495 mol, 1 eq.) was dissolved in 5 ml of dry DMF. Triethylamine 138 µl (0.1991 mmol, 2 eq.) and the reaction was cooled to 0 ° C. Finally, triethyloxonium tetrafluoroborte 188 mg (0.991 mmol, 2 eq.) was added and the mixture is left to stir at room temperature overnight. After the reaction time, the mixture was quenched with water and the organic phase was washed several times with water. The organic phase was dried over $MgSO_4$ was evaporated under reduced pressure. The residue was washed several times with pentane to obtain the product as a white solid.

Yield: 172.24 mg (56 %)

^{1}H-NMR (300 MHz, DMSO-d6): δ = 9.40 (s, 1H), 7.35 (s, 4H), 5.50 (m, 2H), 5.18 (dd, *J*= 14.1, 2.0, 4H), 4.52 (s, 4H), 3.61 (s, 4H), 3.43 (m, 4H), 3.09 (m, 8H), 1.36 (d, *J*= 6.6, 12H), 1.22 (d, *J*= 6.6, 12H), 1.01 (t, *J*= 7.1, 4H)

^{13}C-NMR (300 MHz, $CDCl_3$): δ = 157.84, 146.02, 144.28, 136.68, 135.95, 127.61, 125.52, 125.16, 124.73, 117.35, 116.48, 67.12, 57.56, 56.55, 54.73, 29.26, 25.41, 23.98, 12.24.

6.7.6. Synthesis of N^4, N^5-bis (2,6-diisopropylphenyl)octa-1,7-diene-4,5-diamine (29)

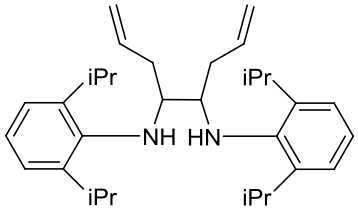

In a Schlenk flask 21.35 g of N, N'-Bis(2,6-diisopropylphenyl)ethanediimine (0.057 mol, 1 eq.) was added and dissolved in 200 ml of dry toluene. The reaction solution was cooled in an ice bath to -78 ° C. Allyl magnesium chloride, 100 ml, (0.171 mol, 3 eq), was added to the cooled reaction solution slowly. The reaction solution was warmed to room temperature and stirred overnight. After the reaction time the mixture was cooled to 0 ° C and quenched with NH_4Cl. The phases were separated and the aqueous phase was extracted three times with diethyl ether. The organic phases were combined, dried over $MgSO_4$, filtered, and the volatiles were removed under reduced pressure. Yellowish oil was obtained which was left under vacuum for 2 days to solidify. The

brown-yellowish solid residue obtained was suspended in methanol, filtered and finally washed well in methanol to obtain the product as a white solid.

Yield: 10.50 g (40 %)

^{1}H-NMR (300 MHz, $CDCl_3$): δ = 7.12-7.10 (m, 4H), 7.06-7.00 (m, 2H), 5.73 (m, 2H), 5.04 (m, *J*= 1.3 Hz, 4H), 3.58 (t, 2H), 3.37 (heptet, 4H), 2.32 (t, *J*= 6.3 Hz, 4H), 1.27 (d, *J*= 6.9 Hz, 12H), 1.24 (d, *J*= 6.3 Hz, 12H).

6.7.7. Synthesis of N^4, N^5-bis (2,6-diisopropylphenyl)octa-1,7-diene-4,5-diamine (30)

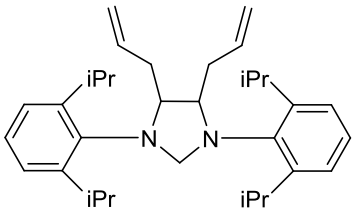

In a round bottom flask 500 mg of N^4, N^5-bis (2,6-diisopropylphenyl)octa-1,7-diene-4,5-diamine (1.085 mmol, 1 eq.) was dissolved in 10 ml of ethanol. Acetic acid 100 µl (1.085 mmol, 1 eq.) was added and finally 33 mg of paraformaldehyde (1.085 mmol, 1 eq.) was added and the reaction was left to stir at 75 ° C overnight. After the reaction time, the mixture was cooled to room temperature, the solvent was evaporated and the product was obtained after recrystalization with EtOH.

Yield: 436.65 g (85 %)

^{1}H-NMR (300 MHz, $CDCl_3$): δ = 7.23 (d, *J*= 7.6 Hz, 2H), 7.13 (m, 4H), 5.82 (m, *J*= 6.6 Hz 2H), 4.97 (m, 4H), 4.48 (s, 1H), 4.28 (s, 1H), 4.03 (m, 2H), 3.89 (m, 2H), 3.32 (m, 2H), 2.39-2.37 (m, 2H), 2.29-2.27 (m, 2H), 1.31-1.25 (dd, *J*= 12.2, 6.8 Hz, 12H), 1.23-1.17 (dd, *J*= 10.4, 6.8 Hz, 12H).

^{13}C-NMR (300 MHz, $CDCl_3$): δ = 157.84, 146.02, 144.28, 136.68, 135.95, 127.61, 125.52, 125.16, 124.73, 117.35, 116.48, 67.12, 57.56, 56.55, 54.73, 29.26, 25.41, 23.98, 12.24.

6.7.8. Synthesis of 4,5-diallyl-1,3-bis(2,6-diisopropylphenyl)-4,5-dihydro-1H-imidazol-3-ium 2,3,5,6-tetrachloro-4-hydroxyphenolate (31)

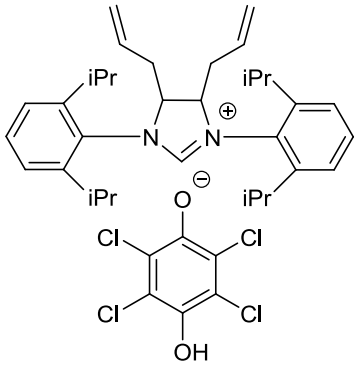

In a round bottom flask 320 mg of ***30*** (0.694 mmol, 1 eq.) was dissolved in 10 ml of benzene and chloranil 322 mg (1.31 mmol, 2 eq.) was added. The reaction was left to stir at room temperature overnight. After the reaction time the precipitate was filtered and the solid was washed with benzene and dried under vacuum to obtain the product as a dark redish powder.

Yield: 448.97 g (90 %)

^{1}H-NMR (300 MHz, DMSO-d6): δ = 9.39 (s, 1H), 7.55 (t, 2H), 7.43-7.41 (m, 4H), 5.42 (m, 2H), 5.18 (s, 2H), 5.07-4.94 (m, 4H), 3.11-3.01 (m, 4H), 2.85 (m, 2H), 2.43 (m, 2H), 1.36-1.34 (dd, *J*= 6.6, 4.3 Hz, 12H), 1.19-1.15 (dd, *J*= 6.6, 4.3 Hz, 12H).

^{13}C-NMR (300 MHz, DMSO-d6): δ = 159.21, 148.96, 146.43, 146.32, 144.03, 133.22, 131.24, 128.52, 125.10, 124.87, 120.69, 119.95, 118.13, 67.16, 30.64, 28.62, 28.35, 25.57, 24.84, 23.13, 22.69.

6.7.9. Synthesis of 1,3-bis(2,6-diisopropylphenyl)-4-(3-(triethoxysilyl)propyl)-4,5-dihydro-1H-imidazol-3-ium chloride (32)

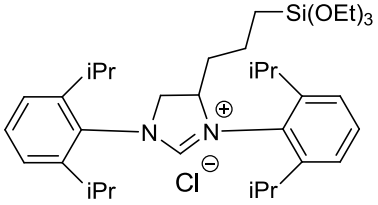

In a Schlenk flask, under argon atmosphere 300 mg of 4-allyl-1,3-bis(2,6-diisopropylphenyl)-4,5-dihydro-1H-imidazol-3-ium chloride (0.642 mmol, 1 eq.) was dissolved in dry and degassed dichloromethane. Trichlorosilane 972 µl (9.63 mmol, 15 eq.) and Karstedt catalyst 200 µl (0.0211 mmol Pt, 0.033 eq.) are added and the reaction mixture is left to stir at 40 ° C for 20 h. After the reaction time, the volatiles were removed under reduced pressure. The residue is dissolved in 20 ml dichloromethane and cooled to 0 ° C. A 1:1 mixture of ethanol and triethylamine (1.25 ml: 1.25 ml) was added and the solution was left to stir for 2 h at room

temperature. After two hours the volatiles were removed under reduced pressure. The residue was washed with toluene, and the precipitate filtered. The filtrates were evaporated and the residue was washed several times with pentane, filtered and dried under vacuum to obtain the product as a white powder.

Yield: 344 mg (85 %)

^{1}H-NMR (300 MHz, $CDCl_3$): δ = 10.90 (s, 1-H), 7.47 (m, 3H), 7.29 (m, 2H), 7.24 (m, 1H), 4.87 (s, 1H), 3.82 (m, 2H), 3.71 (q, *J*= 7.0 Hz, 6H), 3.08 (m, 4H) 2.89 (m, 2H) 1.84 (m, 2H), 1.38 (dd, J=1.4 Hz, 1.4 Hz, 24H), 1.14 (t, 9H)

6.7.10. Synthesis of 4,5-diallyl-1,3-bis(2,6-diisopropylphenyl)-4,5-dihydro-1H-imidazol-3-ium chloride (33)

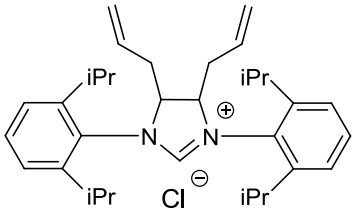

In a round bottom flask 400 mg of ***31*** (0.557 mmol, 1 eq.) was dissolved in 5 ml of THF. HCl in dioxane 1 ml (4 mmol, 7.2 eq.) was added dropwise to the solution via stirring until the solution turned into yellow from dark red. The volatiles were then evaporated under reduced pressure and the residue was washed with ether several times and dried under vacuum, to obtain the product as a light yellowish solid.

Yield: 268 mg (95 %)

^{1}H-NMR (300 MHz, DMSO-d6): δ = 9.39 (s, 1H), 7.55 (t, 2H), 7.43-7.41 (m, 4H), 5.42 (m, 2H), 5.18 (s, 2H), 5.07-4.94 (m, 4H), 3.11-3.01 (m, 4H), 2.85 (m, 2H), 2.43 (m, 2H), 1.36-1.34 (dd, *J*= 6.6, 4.3 Hz, 12H), 1.19-1.15 (dd, *J*= 6.6, 4.3 Hz, 12H).

^{13}C-NMR (300 MHz, DMSO-d6): δ = 159.21, 148.96, 146.43, 146.32, 144.03, 133.22, 131.24, 128.52, 125.10, 124.87, 120.69, 119.95, 118.13, 67.16, 30.64, 28.62, 28.35, 25.57, 24.84, 23.13, 22.69.

6.7.11. Synthesis of (4,5-diallyl-1,3-bis(2,6-diisopropylphenyl)imidazolidin-2-yl)silver(II) chloride (34)

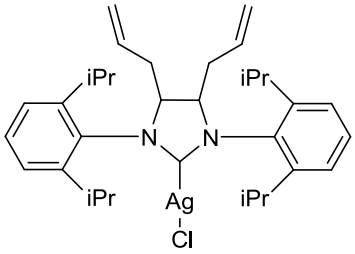

In a Schlenk flask 100 mg of ***33*** (0.197 mmol, 1 eq.) was dissolved in 10 ml of dry DCM. Ag_2O 437 mg (0.591 mmol, 3 eq.) was added and the mixture was left to stir at room temperature overnight. After that, the reaction mixture was filtered through silica plug to remove the excess of silver oxide. The filtrate was then evaporated under reduced pressure to obtain a beige colored residue which was washed with pentane to obtain the desired product as a white powder.

Yield: 97 mg (80 %)

^{1}H-NMR (300 MHz, $CDCl_3$): δ = 7.52 (m, 2H), 7.31-7.28 (m, 2H), 7.25-7.22 (m, 2H), 5.55 (m, 2H), 5.09-4.97 (m, 4H), 3.19-3.12 (m, 2H), 3.04 (m, 2H), 2.79-2.32 (m, 4H), 1.41 (d, *J*= 9.8 Hz, 6H), 1.36-1.22 (m, 18H).

^{13}C-NMR (300 MHz, $CDCl_3$): δ = 159.21, 148.96, 146.43, 146.32, 144.03, 133.22, 131.24, 128.52, 125.10, 124.87, 120.69, 119.95, 118.13, 67.16, 30.64, 28.62, 28.35, 25.57, 24.84, 23.13, 22.69.

6.8. Synthesis of 2-(5-bromopentyl)isoindoline-1,3-dione [99] (35)

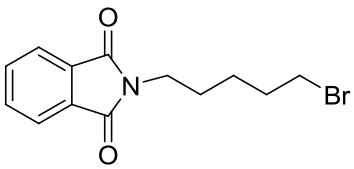

In a round bottom flask 7.45 g of 1,5-dibromopentane (0.032 mol, 3 eq.) and 100 ml of acetone were mixed and 2 g of potassium phthalamide (0.0109 mol, 1 eq.) was added potion wise within 15 min at room temperature. The mixture was then refluxed overnight. After the reaction time, the mixture was cooled to room temperature and filtered. The filtrate was evaporated under reduced pressure and the residue was purified by column chromatography pentane:cyclohexane (14:1) to give the product as viscous colorless liquid.

Yield: 2.45 g (76 %)

^{1}H-NMR (300 MHz, $CDCl_3$): δ = 7.52 (m, 2H), 7.31-7.28 (m, 2H), 7.25-7.22 (m, 2H), 5.55 (m, 2H), 5.09-4.97 (m, 4H), 3.19-3.12 (m, 2H), 3.04 (m, 2H), 2.79-2.32 (m, 4H), 1.41 (d, *J*= 9.8 Hz, 6H), 1.36-1.22 (m, 18H).

^{13}C-NMR (300 MHz, $CDCl_3$): δ = 159.21, 148.96, 146.43, 146.32, 144.03, 133.22, 131.24, 128.52, 125.10, 124.87, 120.69, 119.95, 118.13, 67.16, 30.64, 28.62, 28.35, 25.57, 24.84, 23.13, 22.69.

6.8.1. Synthesis of 2-(5-bromopentyl)isoindoline-1,3-dione (36)

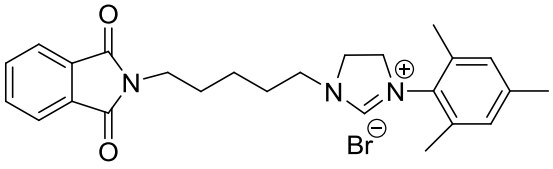

In a Schlenk flask 554 mg (2.94 mmol, 1.0 eq) of 1-(2,4,6-Trimethylphenyl)-4,5-dihydro-1*H*-imidazole and 970 mg of (3.28 mmol, 1.1 eq) *N*-(5-bromopentyl)-phthalimide were dissolved in 15 mL of dry toluene and stirred overnight under argon-atmosphere at 90 °C. After cooling down the reaction mixture to ambient temperature, toluene was evaporated under reduced pressure. The crude solid was treated with Et_2O, filtered and dried under vacuum to obtain the product as a white-yellowish powder.

Yield: 712 mg (50 %)

^{1}H-NMR (300 MHz, DMSO-d6): δ = 8.82 (s, 1H), 7.85 (m, 4H), 7.00 (s, 2H), 4.14 (s, 4H), 3.58 (m, 4H), 2.29 (s, 3H), 2.25 (s, 6H), 1.69 (m, 4H), 1.31 (m, 2H).

^{13}C-NMR (300 MHz, DMSO-d6): δ = 158.60, 135.49, 134.43, 133.55, 131.19, 129.30, 123.01, 50.36, 48.31, 47.44, 37.19, 27.47, 25.78, 23.08, 20.52, 17.13.

6.8.2. Synthesis of 3-(5-aminopentyl)-1-mesityl-4,5-dihydro-1H-imidazol-3-ium bromide (37)

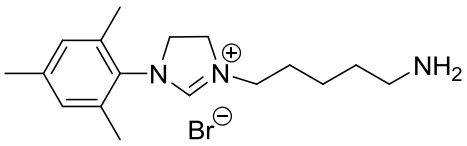

In a round bottom flask 200 mg (0.41 mmol, 1 eq) 1-(2,4,6-Trimethylphenyl)-3-(phthalimide-*N*-pentyl)-4,5-dihydro-1*H*-imidazol-3-ium-bromide was dissolved in 30 ml of 4 M hydrochloric acid and refluxed overnight. After cooling down the reaction mixture to room temperature, the precipitate was filtered off. The filtrate was neutralized with saturated $NaHSO_4$-solution and extracted three times with DCM (3 x 50 ml). The combined

organic phases were concentrated under reduced pressure to obtain a sticky residue which was washed several times with Et_2O to obtain the product as a white solid.

Yield: 113 mg (78 %)

^{1}H-NMR (300 MHz, DMSO-d6): δ = 8.76 (s, 1H), 7.01 (s, 2H), 4.12 (s, 4H), 3.62-3.50 (m, 4H), 2.26 (m, 4H), 2.19 (s, 6H), 1.68 (m, 4H), 1.33 (m, 2H).

^{13}C-NMR (300 MHz, DMSO-d6): δ = 158.62, 139.15, 135.46, 134.40, 131.54, 50.30, 48.24, 47.40, 37.16, 27.44, 25.74, 22.99, 20.49, 17.12.

6.8.3. Synthesis of 3-(6-iodohexyl)-1-mesityl-4,5-dihydro-1H-imidazol-3-ium iodide (38)

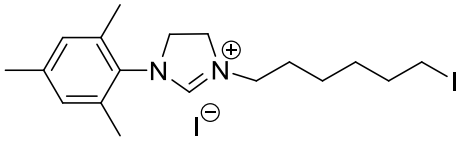

In a Schlenk flask under an argon atmosphere, 2 g of mesityl-4, 5 - dihydro-1H-imidazole (10.62 mmol, 1eq) **6** and 3, 98 g of 1,6-diiodohexane (11.78 mmol, 1.11 eq) was added. The reaction was heated to 90 ° C and stirred overnight. After the reaction time, a solid residue was formed, which was washed with petroleum ether and filtered. The beige colored solid was then dried under vacuum to obtain the desired product.

Yield: 4.47 g (80 %)

^{1}H-NMR (300 MHz, DMSO-d6): δ = 8.73 (s, 1H), 7.03 (s, 2H), 4.14 (s, 4H), 3.53 (t, *J*= 7.1 Hz, 2H), 3.29 (t, *J*= 7.1 Hz, 2H), 2.26 (s, 3H), 2.24 (s, 6H), 1.78 (m, 2H), 1.68 (m, 2H), 1.43-1.34 (m, 4H).

^{13}C-NMR (300 MHz, DMSO-d6): δ = 159.00, 141.90, 129.46, 128.70, 126.00, 59.70, 51.10, 56.70, 30.00, 26.60, 21.90, 18.50.

6.8.4. Synthesis of 3-(6-azidohexyl)-1-mesityl-4,5-dihydro-1H-imidazol-3-ium iodide (39)

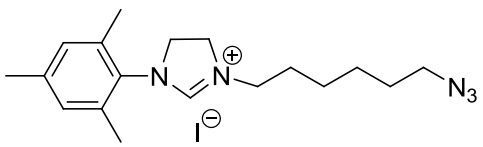

In a round bottom flask 600 mg of 3-(6-iodohexyl)-1-mesityl-4,5-dihydro-1H-imidazol-3-ium (1.14 mmol, 1 eq.) was added and dissolved 10 ml of DMF. 222 mg of sodium azide (3.42 mmol, 3 eq.) was then added and the reaction mixture was left to stir overnight at room temperature. After the reaction time 50 ml of water was added and the precipitate was filtered, washed with Et_2O and dried under vacuum to obtain the product as a white solid.

Yield: 352 mg (70 %)

^{1}H-NMR (300 MHz, DMSO-d6): δ = 8.73 (s, 1H), 7.03 (s, 2H), 4.14 (s, 4H), 3.53 (t, *J*= 7.1 Hz, 2H), 3.29 (t, *J*= 7.1 Hz, 2H), 2.26 (s, 3H), 2.24 (s, 6H), 1.78 (m, 2H), 1.68 (m, 2H), 1.43-1.34 (m, 4H).

^{13}C-NMR (300 MHz, DMSO-d6): δ = 160.00, 141.90, 129.47, 128.72, 126.01, 59.71, 51.12, 56.71, 30.01, 26.61, 21.91, 18.51.

6.8.5. Synthesis of 3-(6-aminohexyl)-1-mesityl-4,5-dihydro-1H-imidazol-3-ium iodide (40)

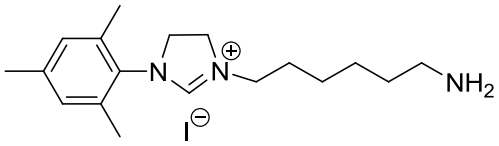

In a round bottom flask 300 mg of ***39*** (0.679 mmol, 1 eq.) was dissolved in 15 ml of technical grade MeOH. Pd on carbon 150 mg (5 % Pd, 56.6 %) was added and H_2 gas was bubbled for 8 h at room temperature. The reaction progress was followed with ^{1}H NMR. After the reaction time, the mixture was filtered thru a filter paper and the filtrate was evaporated to give the product as a light yellowish solid.

Yield: 240 mg (85 %)

^{1}H-NMR (300 MHz, DMSO-d6): δ = 8.81 (s, 1H), 7.08 (s, 2H), 4.17 (s, 4H), 5.56 (m, 2H), 3.31 (m, 2H), 2.25 (s, 9H), 1.69 (m, 2H), 1.55 (m, 2H), 1.35 (m, 4H).

^{13}C-NMR (300 MHz, DMSO-d6): δ = 158.56, 139.16, 135.44, 131.17, 129.28, 50.49, 50.32, 48.38, 47.44, 28.03, 26.09, 25.49, 25.12, 20.46, 17.14.

6.8.6. Synthesis of 3-(10-iododecyl)-1-mesityl-4,5-dihydro-1H-imidazol-3-ium iodide (41)

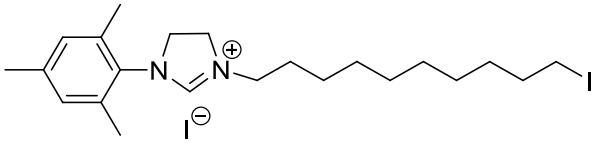

In a Schlenk flask under an argon atmosphere, 3 g of mesityl-4, 5 - dihydro-1H-imidazole (15.93 mmol, 1eq) **6** and 6.97 g of 1,10-diiododecane (17.68 mmol, 1.11 eq) was added. The reaction was heated to 90 °C and stirred for 2 days, until a solid residue was formed. After the reaction time, the solid residue was washed several times with Et_2O and dried under vacuum to obtain the product as a white solid.

Yield: 7.98 g (86 %)

^{1}H-NMR (300 MHz, DMSO-d6): δ = 8.76 (s, 1H), 7.03 (s, 2H), 4.16 (s, 4H), 3.52 (m, 2H), 3.29 (m, 2H), 2.28 (s, 3H), 2.26 (s, 6H), 1.73 (m, 4H), 1.31 (m, 12H).

^{13}C-NMR (300 MHz, DMSO-d6): δ = 158.57, 139.18, 135.46, 131.19, 129.31, 50.33, 48.35, 47.52, 32.81, 29.80, 28.79, 28.70, 28.30, 27.82, 26.19, 25.58, 20.50, 17.17, 9.12.

6.8.7. Synthesis of 3-(10-azidodecyl)-1-mesityl-4,5-dihydro-1H-imidazol-3-ium iodide (42)

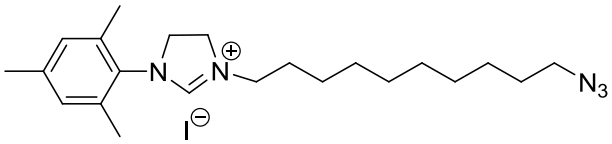

In a round bottom flask 2 g of 3-(10-iododecyl)-1-mesityl-4,5-dihydro-1H-imidazol-3-ium iodide (3.43 mmol, 1 eq.) was added and dissolved 10 ml of DMF. 669 mg of sodium azide (10.29 mmol, 3 eq.) was then added and the reaction mixture was left to stir overnight at room temperature. After the reaction time 100 ml of water was added and the precipitate was filtered, washed with Et_2O and dried under vacuum to obtain the product as a white solid.

Yield: 1.19 g (70 %)

^{1}H-NMR (300 MHz, DMSO-d6): δ = 8.76 (s, 1H), 7.04 (s, 2H), 4.15 (s, 4H), 3.54 (m, 2H), 3.31 (m, 2H), 2.27 (s, 3H), 2.25 (s, 6H), 1.68 (m, 2H), 1.53 (m, 2H), 1.29 (m, 12H).

^{13}C-NMR (300 MHz, DMSO-d6): δ = 158.55, 139.16, 135.45, 131.18, 129.30, 50.58, 50.33, 48.36, 47.52, 28.75, 28.47, 28.31, 28.18, 26.19, 26.09, 25.59, 20.48, 17.17.

6.8.8. Synthesis of 3-(10-aminodecyl)-1-mesityl-4,5-dihydro-1H-imidazol-3-ium iodide (43)

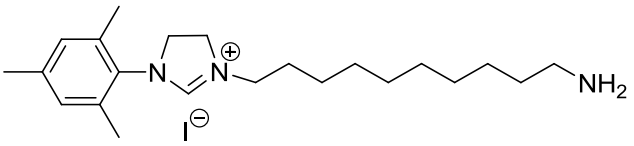

In a round bottom flask 1 g of **42** (2.01 mmol, 1 eq.) was dissolved in 25 ml of technical grade MeOH. Pd on carbon 500 mg (5 % Pd, 56. 6 %) was added and H_2 gas was bubbled for 8 h at room temperature. The reaction progress was followed with ^{1}H NMR. After the reaction time, the mixture was filtered thru a filter paper and the filtrate was evaporated to give the product as a beige colored solid.

Yield: 806 mg (85 %)

^{1}H-NMR (300 MHz, DMSO-d6): δ = 8.75 (s, 1H), 7.04 (s, 2H), 4.14 (s, 4H), 3.53 (m, 2H), 3.34 (m, 2H), 2.27 (s, 3H), 2.24 (s, 6H), 1.67 (m, 2H), 1.53 (m, 2H), 1.29 (m, 12H).

^{13}C-NMR (300 MHz, DMSO-d6): δ = 158.55, 139.16, 135.45, 131.18, 129.30, 50.58, 50.33, 48.36, 47.52, 28.75, 28.47, 28.31, 28.18, 26.19, 26.09, 25.59, 20.48, 17.17.

6.8.9. Synthesis of (1-(10-aminodecyl)-3-mesitylimidazolidin-2-yl)silver(II) iodide (44)

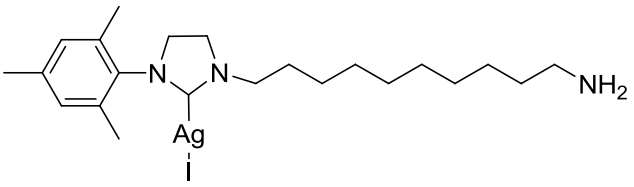

In a Schlenk flask 800 mg of 3-(10-aminodecyl)-1-mesityl-4,5-dihydro-1H-imidazol-3-ium iodide (1.69 mmol, 1 eq.) was dissolved in 20 ml of dry DCM. Ag_2O 1.17 g (5.07 mmol, 3 eq.) was added and the reaction was left to stir overnight at room temperature. After the reaction time, the mixture was filtered through a silica plug to remove the excess of silver oxide. The filtrate was evaporated under reduced and the solid residue was washed with pentane, dried under vacuum to obtain the product as a white solid. .

Yield: 979 mg (80 %)

^{1}H-NMR (300 MHz, DMSO-d6): δ = 6.94 (s, 2H), 3.79 (s, 4H), 3.30 (m, 4H), 2.28 (s, 3H), 2.04 (s, 6H), 2.04 (s, 6H), 1.54 (m, 4H), 1.27 (m, 12H)

6.9. Synthesis of [(NHC-20)RhCl(cod)$_2$] (45)

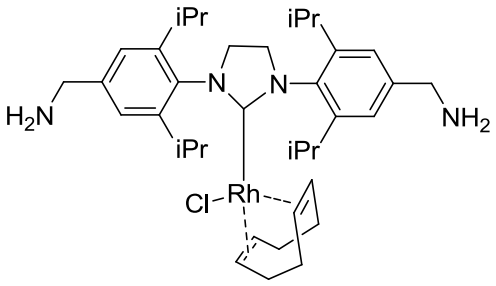

In a Schlenk flask 60 mg of (1, 3-bis(4-(aminomethyl)-2,6-diisopropylphenyl)imidazolidin-2-yl)silver(II) chloride (0.100 mmol, 1 eq.) was dissolved in 10 ml of dry DCM. [Rh-(μ-Cl)(cod)]$_2$ 50 mg (0.100 mmol, 1 eq.) was added and the mixture was left to stir at room temperature for 2 h. After the reaction time, the solvent was concentrated under reduced pressure. Pentane was added to precipitate the final complex and the yellow complex was filtered, washed with pentane and dried under vacuum.

Yield: 61.71 mg (85 %)

^{1}H-NMR (300 MHz, CDCl$_3$): δ = 7.18 (s, 4H), 4.05 (s, 4H), 3.93-3.75 (m, 4H, CH-COD), 3.89 (s, 4H), 3.03 (pentet, *J* = 6.9 Hz, 4H), 1.76 (m, 8H, CH$_2$-COD), 1.34 (dd, *J*= 6.8, 5.3 Hz, 24H).

6.10. Synthesis of 2,2-dimethyl-1-(piperazin-1-yl)propan-1-one (46)

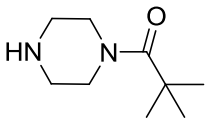

In a round bottom flask 4.31 g of piperazine (0.050 mol, 5 eq) and di-*tert*-butyl dicarbonate (2.18 g, 0.010 mol, 1 eq.) were dissolved in 50 ml dioxane-water mixture (1:1). The reaction mixture was cooled down to 90 °C and NaOH (400 mg, 0.010 mol, 1 eq.) was added. The reaction was stirred left to stir overnight at room temperature. After the reaction time the reaction mixture was poured into a 5wt % K_2CO_3 solution and the product was extracted with $CHCl_3$. The organic phase was dried over $MgSO_4$ and the solvent was evaporated under reduced pressure. The product was obtained as yellowish oil.

Yield: = 6.59 g (85 %)

^{1}H-NMR (300 MHz, CDCl$_3$): δ = 3.29 (m, 4H), 2.73 (m, 4H), 1.37 (s, 9H).

6.10.1. Synthesis of 2,2-dimethyl-1-(4-(undec-10-enyl)piperazin-1-yl)propan-1-one [100] (47)

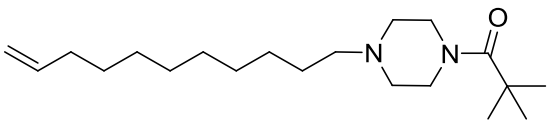

In a Schlenk 2,2-dimethyl-1-(piperazin-1-yl)propan-1-one (799 mg, 4.29 mmol, 1 eq.), 11-bromoundec-1-ene (1.00 g, 4.29 mmol, 1 eq.) and K_2CO_3 (712 mg, 5.15 mmol, 1.2 eq.) were mixed in 10 ml of CH_3Cl and the mixture was left to stir at 90 °C overnight under argon atmosphere. After the reaction time the mixture is concentrated under reduced pressure, 50 ml of water was added and the crude product was obtain after extraction with chloroform. The product was then purified with column chromatography, $CHCl_3$:MeOH (10:1).

Yield: = 1.96 g (93 %)

^{1}H-NMR (300 MHz, $CDCl_3$): δ = 5.75 (m, 1H), 4.91 (m, 2H), 3.41 (m, 4H), 2.33 (m, 4H), 1.98 (m, 2H), 1.42 (s, 9H), 1.33-1.24 (m, 14H).

6.10.2. Synthesis of 1-(undec-10-enyl)piperazine (48)

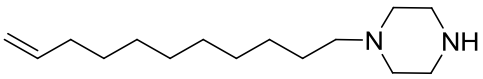

In around bottom flask 2,2-dimethyl-1-(4-(undec-10-enyl)piperazin-1-yl)propan-1-one (1.36 g, 4.02 mmol, 1 eq.) was dissolved in 20 ml of MeOH and HCl in dioxane (10.4 ml, 58.25 mmol, 14.5 eq.) was added. The reaction mixture was stirred overnight at room temperature. After the reaction time the volatiles were removed under reduced pressure and the solid residue was washed with ether and dried under vacuum to obtain the product as a white solid.

Yield: = 623 mg (65 %)

^{1}H-NMR (300 MHz, $CDCl_3$): δ = 5.78 (m, 1H), 4.54 (m, 2H), 3.76 (m, 4H), 2.03 (m, 2H), 1.84 (m, 2H), 1.33-1.27 (m, 14H).

6.10.3. Synthesis of 1,1'-(4,4'-(4,4'-(ethane-1,2-diylbis(azanediyl))bis(3,5-dimethyl-4,1-phenylene))bis(piperazine-4,1-diyl))bis(2,2-dimethylpropan-1-one) (49)

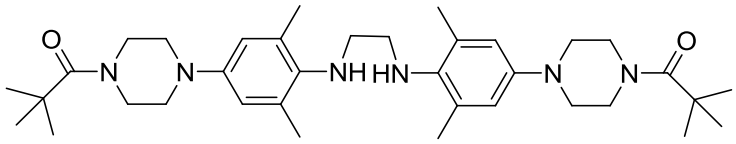

In a Schlenk flask N^1, N^2-bis (4-bromo-2,6-dimethylphenyl)ethane-1,2-diamine (256 mg, 0.60 mmol, 1 eq.), 2,2-dimethyl-1-(piperazin-1-yl)propan-1-one (336 mg, 1.80 mmol, 3 eq.), $Pd(OAc)_2$ (5.4 mg, 0.024 mmol, 4 mol%), (9-Ethyl-9-fluorenyl)dicyclohexylphosphonium tetrafluoroborate (23 mg, 0.048 mmol, 8 mol%) were dissolved all together in 20 ml of dry toluene under argon atmosphere. After 5 min of stirring, sodium tert-butoxide (720 µl, 1.8 mmol, 3 eq.) was added and the reaction mixture was left to stir at 100 °C overnight. After the reaction time, the mixture was cooled to room temperature and water was added. The phases were separated and the aqua phase was extracted with ether. The organic layers were combined, dried over $MgSO_4$ and the solvent was evaporated under reduced pressure. The product was purified by column chromatography, Cyclohexane:Ethyl acetate solvent mixture (4:1).

Yield: = 182 mg (50 %)

^{1}H-NMR (300 MHz, $CDCl_3$): δ = 6.63 (s, 4H), 3.57 (t, 8H), 3.11 (s, 4H), 3.03 (t, 8H), 2.30 (m, 12H), 1.49 (s, 18H).

6.10.4. Synthesis of 1,1'-(4,4'-(4,4'-(ethane-1,2-diylbis(azanediyl))bis(3,5-diisopropyl-4,1-phenylene))bis(piperazine-4,1-diyl))bis(2,2-dimethylpropan-1-one) (50)

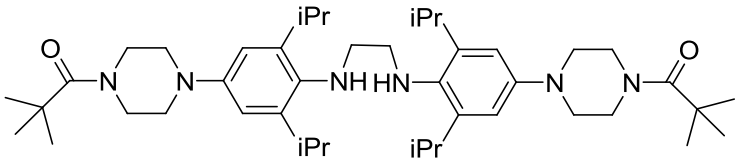

In a Schlenk flask N^1, N^2-bis (4-bromo-2,6-diisopropylphenyl)ethane-1,2-diamine (1 g, 2.35 mmol, 1 eq.), 2,2-dimethyl-1-(piperazin-1-yl)propan-1-one (1.31 g, 7.05 mmol, 3 eq.), $Pd(OAc)_2$ (30.76 mg, 0.14 mmol, 4 mol%), (9-Ethyl-9-fluorenyl)dicyclohexylphosphonium tetrafluoroborate (130, 58 mg, 0.27 mmol, 8 mol%) were dissolved all together in 50 ml of dry toluene under argon atmosphere. After 5 min of stirring, sodium tert-butoxide 4.10 ml, 10.24 mmol, 3 eq.) was added and the reaction mixture was left to stir at 100 °C overnight. After the reaction time, the mixture was cooled to room temperature and water was added. The phases were separated and the aqua phase was extracted with ether. The organic layers were combined, dried over $MgSO_4$ and the solvent was evaporated under reduced pressure. The product was purified by column chromatography, Cyclohexane:Ethyl acetate solvent mixture (4:1).

Yield: = 182 mg (50 %)

^{1}H-NMR (300 MHz, $CDCl_3$): δ = 6.71 (s, 4H), 3.60 (m, 8H), 3.37 (septet, 4H), 3.14 (m, 8H), 3.07 (s, 8H), 1.49 (s, 24H), 1.25 (s, 18H).

6.11. Synthesis of ferrocene –CHNOH (51)

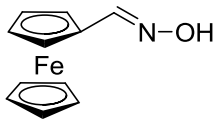

In a round bottom flask, ferrocenecarboxaldehyde (5 g, 0.02 mol, 1 eq.) was dissolved in 100 ml of technical grade EtOH then hydroxylammonium chloride (2.78 g, 0.04 mol, 2 eq.) and NaOH (5.12 g, 0.128 mol, 6.4 eq.) were introduced. The reaction mixture was left to reflux for 3 h. After the reaction time, the mixture was concentrated under reduced pressure then water (100 ml) was added slowly and the mixture was left to stir for another 1 h at room temperature. The product was extracted with DCM; the organic phase was dried over $MgSO_4$ and the solvent was evaporated under reduced pressure to give the product as a dark orange solid which was dried under vacuum.

Yield: = 182 mg (90 %)

^{1}H-NMR (300 MHz, $CDCl_3$): δ = 7.99 (s, 1H), 4.53 (m, 2H), 4.34 (m, 2H), 4.22 (m, 5H).

6.11.1. Synthesis of Ferrocene –CH_2NH_2 (52)

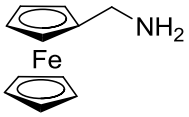

In a Schlenk flask, ferrocene-CHNOH (2.5 g, 0.012 mol, 1 eq.) was dissolved in 50 ml of dry THF and it was added dropwise to another Schlenk flask where $LiAlH_4$ (2.36 g, 0.062 mol, 5.28 eq.) was already dissolved in 50 ml of dry THF. The reaction mixture was left to reflux for 6 h. After the reaction time, the mixture was brought to room temperature and the excess of $LiAlH_4$ was quenched with water. The mixture was extracted with Et_2O and the organic phase was dried under $MgSO_4$, filtered and the solvent was evaporated under reduced pressure to obtain the product as a dark red oil.

Yield: = 2.08 g (80 %)

^{1}H-NMR (300 MHz, $CDCl_3$): δ = 4.16 (m, 2H), 4.14 (s, 5H), 4.11 (m, 2H), 3.55 (s, 2H).

6.11.2. Synthesis of Ferrocene –CH_2NBN (53)

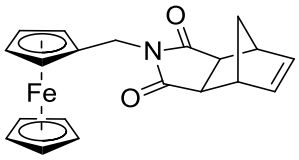

In a Schlenk flask, ferrocene-CH_2NH_2 (1.6 g, 0.0097 mol, 1 eq.) and carbic anhydride (2.25 g, 0.011 mol, 1.1 eq.) were dissolved in 50 ml of dry toluene under argon atmosphere and the mixture was left to reflux overnight. The condenser was equipped with a dean start apparatus to collect the water liberated from the reaction. After the reaction time, the system is brought to room temperature and the solvent mixture was evaporated under reduced pressure. The product was purified by column chromatography, Cyclohexane:Ethyl acetate (2:1) to obtain the product as a light yellow powder.

Yield: = 3.05 g (87 %)

^{1}H-NMR (300 MHz, $CDCl_3$): δ = 5.86 (t, *J*= 1.8 Hz, 2H), 4.27 (s, 2H), 4.23 (t, *J*= 1.8 Hz, 2H), 4.16 (s, 5H), 4.07 (t, *J*= 1.8 Hz, 2H), 3.34 (m, 2H), 3.19 (m, 2H), 1.66 (d, *J*= 8.8 Hz, 1H), 1.50 (d, *J*= 8.8 Hz, 1H), 1.50 (d, *J*= 8.8 Hz, 1H).

^{13}C-NMR (300 MHz, $CDCl_3$): δ = 177.37, 134.34, 82.13, 69.69, 68.68, 68.28, 52.10, 45.78, 45.11, 37.71, 27.08.

7. References

[1] Holleman Wiberg, *Lehrbuch der Anorganischen Chemie* 101. Auflage deGruyter.

[2] Fink, G.; Mülhaupt, R.; Brintzinger, H.H. *„Ziegler Catalysts"*, Springer-Verlag, Berlin,**1995**

[3] Chauvin, Y.; Herisson, J.L. *Makromol. Chem.* **1970**, *141*, 161-176.

[4] Sanford, M. S.; Ulman, M.; Grubbs, R. H. *J. Am. Chem. Soc.* **2001**, *123*, 749.

[5] France, M. B.; Grubbs, R. H.; McGrath, D. V.; Paciello, R. A. *Macromolecules* **1993**, *26*, 4742.

[6] Fu, G. C.; S. Nguyen, T.; Grubbs, R. H. *J. Am. Chem. Soc.* **1993**, *115*, 9856–9857

[7] Buchmeiser, M. R. *Chem. Rev.* **2009**, *109*, 303-321.

[8] Ahmed, M.; Barrett, A. G. M.; Braddock, D. C.; Cramp, S. M.; Procopiou, P. A. *Tetrahedron Lett.* **1999**, *40*, 8657-8662.

[9] Jafarpour, L.; Heck, M.P.; Buylon, C.; Lee, H.M.; Mioskowski, C.; Nolan, S.P. *Organometallics* **2002**, *21*, 671-679.

[10] Randl, S.; Buschmann, N.; Connon, S. J.; Blechert, S. *Synlett.* **2001**, *10*, 1547-1550.

[11] Kingsbury, J. S.; Garber, S. B.; Giftos, J. M.; Gray, B. L.; Okamoto, M. M.; Farrer, R. A.; Fourkas, J. T.; Hoveyda, A. H. *Angew. Chem.* **2001**, *113*, 4381-4386.

[12] Dowden, J.; Savovic, J. *Chem. Commun.* **2001**, 146-147.

[13] Schürer, S. C.; Gessler, S.; Buschmann, N.; Blechert, S. *Angew. Chem.* **2000**, *112*, 4062-4065.

[14] Hoveyda, A.M.; Gillingham, D.G.; Veldhuizen, J.J.V.; Kataoka, O. S.; Garber, B.; Kingsbury, J.S.; Harrily, J.P.A. *Org. Biomol. Chem.* **2004**, *2*, 8-23.

[15] Allen, D.P.; Wingerden, M.M.V.; Grubbs, R.H. *Org. Lett.* **2009**, *11*, 1261-1264.

[16] Lang, C.; Gartner, U.; Trapp, O. *Chemm. Comm*, **2011**, *47*, 391-393.

[17] Mazurowski, M.; Gallei, M.; Li, J.; Didzoleit, H.; Stühn, B.; Rehahn, M. *Macromolecules* **2012,** *45*, 8970-8981.

[18] Monge-Marcet, A.; Pleixats, R.; Cattoën, X.; Wong Chi Man, M. *J. Mol. Cat. A: Chem.* **2012,** *357*, 59-66.

[19] Bessel, M.; Rominger, F.; Straub, B.F. *Synthesis* **2010**, *9*, 1459-1466.

[20] Mosaert, S.F.; Walter, F.; Verpoort, C. 2011. *Process for preperation of ruthenium-based carbene catalysts with chelating alkylidene ligands*, EP 2361683 A1.

[21] Bianco, A.; Maggini, M.; Nogarole, M.; Scorrano, G. *Eur. J. Org. Chem.* **2006**, 2934-2941.

[22] Beron, B. J.; Graybill, E.P.; Jennings, G. K. *Langmuir* **2007**, *23*, 116651-116655.

[23] Jiang, G.; Ponnapati, R.; Pernites, R.; Felipe, M. J. *Macromolecules* **2010**, *43*, 10262–10274.

[24] Creager, S.; Yu, C.J.; Barndad, C.; O'Connor, S.; MacLean, T.; Lam, E.; Chong, Y.; Olsen, G.T.; Luo, J.; Gozin, M.; Kayyem, F.J. *J. Am. Chem. Soc.* **1999**, *121*, 1059–1064

[25] Rolfe, A.; Loh, J. K.; Maity, P. K.; Hanson, P. R. *Org Lett.* **2011**, *13*, 4-7.

[26] Jiang, G.; Ponnaparti, R.; Pernites, R.; Felipe, M. J.; Advincula, R. *Macromolecules* **2010**, *43*, 10262-10274.

[27] Gömez, F. J.; Chen, R. J.; Wang, D.; Woymouth, R. M.; Dai, H. *Chem. Comm.* **2003**, 190-191.

[28] Chen, R. J.; Zhang, Y. G.; Wang, D.; Dai, H. *Am. Chem. Soc.* **2001**, *123*, 3838.

[29] Yu, J.; Mathew, S.; Flavel, B. S.; Johnston, M. R.; Shapter, J. G. *J. Am. Chem. Soc.* **2008**, *130*, 8788–8796.

[30] Jiang, G.; Ponnapati, R.; Pernites, R.; Felipe, M. J. *Macromolecules* **2010**, *43*, 10262–10274.

[31] Carlsson, L.; Malmström, E.; Carlmark, A. *Polym. Chem.* **2012**, *3*, 727.

[32] Soler-Illia, G. J. A. A.; Azzaroni, O. *Chem. Soc. Rev.* **2011**, *40*, 1107–1150.

[33] Calvo, A.; Angelome, P. C.; Sa, V. M.; Scherlis, D. A.; Williams, F. J. *Chem. Mater* **2008**, *14*, 4661–4668.

[34] Shi, J. L.; Hua, Z. L.; Zhang, L. X. *J. Mater. Chem.* **2004**, *14*, 795.

[35] Li, P.; Kawi, S. *J. Catal.* **2008**, *257*, 23-31.

[36] Gonzàlez, B.; Collila, M.; Laorden, C. L.; Vallet-Regi, M. *J. Matter. Chem.* **2009**, *19*, 9012-9024.

[37] Lenarda, M.; Chessa, G.; Moretti, E.; Polizzi, S.; Storaro, L.; Talon, A. *J. Matter. Sci.* **2006**, *41*, 6305-6312.

[38] Zhou, Z.; Zhu, S.; Zhang, D. *J. Matter.Chem.* **2007**, *17*, 2428-2433.

[39] Fu, Q.; Rama-Rao, G. V.; Ward, T. L.; Lu, Y.; Lopez, G. P. *Langmuir* **2007**, *23*, 170-174.

[40] Kirmayer, S.; Neysshtadt, S.; Keller, A.; Okopnik, D.; Frey, G. L. *Chem. Matter* **2009**, *21*, 4387-4396.

[41] Vallè, K.; Belleville, P.; Pereira, F.; Sanchez, C. *Nat. Mater. J.* **2006**, *5*, 107-111.

[42] Hong, C. Y.; Li, X.; Pan, C. Y. *Eur. Polym. J.* **2007**, *43*, 4114-4122.

[43] Lunn, J. D.; Shantz, D. F. *Chem. Comm.* **2010**, *46*, 2926-2928.

[44] Rosenholm, J. M.; Duchanoy. A.; Lindèn, M. *Chem. Matter* **2008**, *20*, *1126*-1133.

[45] Rosenholm, J. M.; Meinander, A.; Peuhu, E.; Niemi, R.; Eriksson, J. E.; Sahgren, C.; Lindèn, M. *ACS Nano* **2009**, *3*, *197*-206.

[46] Radu, D. R.; Lai, C. -Y.; Jeftinija, K.; Rowe, E. W.; Jeftinija, S.; Lin, V. S. -Y. *J. Am. Chem. Soc.* **2004**, *126*, *13216*-13217.

[47] Sun, J. -T.; Hong, C. -Y.; Pan, C. -Y. *J. Phys. Chem. C.* **2010**, *114*, *12481*-12486.

[48] Lai, J.; Mu, X.; Xu, Y.; Wu, X.; Wu, C.; Li, C.; Chen, J.; Zhao, Y. *Chem. Comm.* **2010**, *46*, *7370*-7372.

[49] Angelos, S.; Choi, E.; Vögtle, F.; De Cola, L.; Zink, J. I. *J. Phys. Chem. C.* **2007**, *111*, *6589*-6592.

[50] Fu, Q.; Rao, G. V. R.; Ista, L. K.; Wu, Y.; Andrzejewski, L.; Sklar, L. A.; Ward, T. L.; Lopez, G. P. Adv. *Mater.* **2003**, 15, *1262.*

[51] Brunsen, A.; Cui, J.; Ceolín, M.; Del Campo, A.; Soler-Illia, G. J. A. A.; Azzaroni, O. *Chem. Commun.* **2012**, *48*, 1422–1424.

[52] Barbey, R.; Lavanant, L.; Paripovic, D.; Schüwer, N.; Sugnaus, C.; Tugulu, S.; Klok, H.-A. *Chem Rev.* **2009**, *109*, 5437.

[53] Etienne, M.; Quach, D.; Grosso, D.; Nicole, L.; Sanchez, C.; Walcarius, A. *Chem. Mater.* **2007**, *19*, 844.

[54] Smith, J. J.; Zharov, I. *Langmuir* **2008**, *24*, 2650.

[55] Calvo, A.; Yameen, B.; Williams, F. J.; Soler-Illia, G. J. A. A.; Azzaroni, O. *J. Am. Chem. Soc.* **2009**, *131*, 10866-10868.

[56] Yameen, B.; Ali, M.; Neumann, M.; Ensinger, W.; Knoll, W.; Azzaroni, O. *J. Am. Chem. Soc.* **2009**, *131*, 2070-2071.

[57] Fattakhova-Rohlfing, D.; Wark, M.; Rathouský, J. *Chem. Mater.* **2007**, *19*, 1640-1647.

[58] Wei, H. J.; Collinson, M. M. *Anal. Chim. Acta.* **1999**, *397*, 113.

[59] Nishizawa, M.; Menon, V. P.; Martin, C. R. Science **1995**, 268, 700.

[60] Florea, L.; Hennart, A.; Diamond, D.; Benito-Lopez, F. *Sensors and Actuators 175*, **2012**, 92-99.

[61] Piel. J. P. 2008. Introduction to ellipsometry. Retrieved August 15, 2014, from http: // www.cmi.epfl.ch/metrology/files/Sopra%20GES%205E/Introduction%20to%20ellipsometry.pdf

[62] Samanta, S.; Locklin, J. *Langmuir* **2008**, *24*, 9558–9565.

[63] Hauser, L.; Knall, A.-C.; Roth, M.; Trimmel, G.; Edler, M.; Griesser, T.; Kern, W. *Monatshefte für Chemie - Chem. Mon.* **2012**, *143*, 1551–1558.

[64] Raymo, M.; Giordani, S.; V, M. D.; Florida, C. G.; Re, V.; Recei, M.; February, V. *J. Am. Chem. Soc.* **2001**, *123*, 4651–4652.

[65] Casado, R.; Contel, M.; Laguna, M.; Romero, P.; Sanz, S. *J. Am. Chem. Soc.* **2003**, *125*, 11925–11935.

[66] Teles, J. H.; Schulz, M. (BASF AG), WO-A1 9721648, 1997; *Chem. Abstr.* **1997**, *127*, 121499.

[67] Mizushima, E.; Sato, K.; Hayashi, T.; Tanaka, M. *Angew. Chem. Int. Ed.* **2002**, *41*, 4563–4565.

[68] Marion, N.; Ramón, R. S.; Nolan, S. P. *J. Am. Chem. Soc.* **2009**, *131*, 448–449.

[69] Marion, N.; Nolan, *S. P. Chem. Soc. Rev.* **2008**, *37*, 1776-1782.

[70] Collado, A.; Gómez-Suárez, A.; Martin, A. R.; Slawin, A. M. Z.; Nolan, S. P. *Chem. Commun.* **2013**, *49*, 5541–5543.

[71] Robinson, A. L. *Science* **1976**, *194*, 1261.

[72] Wang, W.; Zheng, A.; Zhao, P.; Xia, C.; Li, F. *Am. Chem. Soc.* **2014**, *4*, 321-327.

[73] Klemm, D.; Schmauder, H. -P. Biopolymers **2002**, *6*, 290-292.

[74] Atalla, R. H. *Cellulose* **1997**, *4*, 173-207.

[75] Ciacco, G. T.; Liebert, T. F.; Frollini, E.; Heinze, T. J. *Cellulose* **2003**, *10*, 125–132.

[76] Redl, F. X.; Köthe, O.; Röckl, K.; Bauer, W.; Daub, J. *Macromol. Chem. Phys.* **2000**, *201*, 2091–2100.

[77] Heinze, T.; Liebert, T. *Prog. Polym. Sci.* **2001**, *26*, 1689–1762.

[78] Tiller, J.; Berlin, P.; Klemm, D. *Macromol. Chem. Phys.* **1999**, *200*, 1–9.

[79] Tiller, J.; Klemm, D.; Berlin, P. *Design. Monom. Polym.* **2001**, *4*, 315–328.

[80] Diekmann, S.; Siegmund, G.; Roecker, A.; Klemm, D. O. *Cellulose* **2003**, *10*, 53–63.

[81] Shen, J.; Song, Z.; Qian, X.; Ni, Y. *Ind. Eng. Chem. Res.* **2011**, *50*, 661–666.

[82] Li, X.; Ballerini, D. R.; Shen, W. *Biomicrofluidics* **2012**, *6*, 11301–1130113.

[83] Li, X.; Tian, J.; Nguyen, T.; Shen, W. Anal. Chem. **2008**, *80*, 9131–9134.

[84] Roy, D.; Semsarilar, M.; Guthrie, J. T.; Perrier, S. *Chem. Soc. Rev.* **2009**, *38*, 2046–2064.

[85] Citterio, D.; Maejima, K.; Suzuki, K. Chem. Biol. Microsyst. Soc. **2011**, 2099–2101.

[86] Toomey, R.; Freidank, D.; Rühe, J. *Macromolecules* **2004**, *37*, 882–887.

[87] Murata, H.; Chang, B.-J.; Prucker, O.; Dahm, M.; Rühe, J. *Surf. Sci.* **2004**, *570*, 111–118.

[88] Böhm, A.; Gattermayer, M.; Trieb, C.; Schabel, S.; Fiedler, D.; Miletzky, F.; Biesalski, M. *Cellulose* **2012**, *20*, 467–483.

[89] Berchtold B (2005) Oberflächengebundene Polymernetzwerke zur Re-Endothelialisierung von porcinen Herzklappen-bioprothesen. PhD, Albert-Ludwigs-Universiät Freiburg im Breisgau.

[90] Freidank D (2005) 3D-DNA-Chips: oberflächengebundene funktionelle Polymernetzwerke alsRe-Matrix für Nukleinsäure-Microarrays. PhD, Albert-Ludwigs-Universiät Freiburg im Breisgau.

[91] Sashuk, V.; Schoeps, D.; Plenio, H. *Chem. Commun.* **2009**, 770–772.

[92] Jahnke, C. M.; Jennifer, P.; Hupka, F.; Weigand, J. J. *Z. Naturforsch.* **2009**, *64b*, 1458-1462.

[93] Uth, C.; Zielonka, S.; Hörner, S.; Rasche, N.; Plog, A.; Orelma, H.; Avrutina, O.; Zhang, K.; Kolmar, H. *Angew. Chem. Int. Ed. Engl.* **2014**, *53*, 1–7.

[94] Yuan, Y.; Lee, T. R. Surface Science Techniques; Bracco, G.; Holst, B., Eds.; Springer Series in Surface Sciences; Springer Berlin Heidelberg: Berlin, Heidelberg, 2013; Vol. 51.

[95] Koehler K. 2006. Immobilizable *N*-heterocyclic carbene complexes with alkoxysilyl gropus, EP 017047 A1.

[96] Bianco, A.; Maggini, M.; Nogarole, M.; Scorrano, G. *European J. Org. Chem.* **2006**, 2934–2941.

[97] Csuk, R.; Albert, S.; Siewert, B. *Arch. Pharm.* **2013**, *346*, 504–510.

[98] Urbina-Blanco, C. a; Manzini, S.; Gomes, J. P.; Doppiu, A.; Nolan, S. P. *Chem. Commun.* **2011**, *47*, 5022–5024.

[99] Beecham, M. P.; Clarkson, G. J.; Hall, G.; Marsh, A. *Chemphyschem* **2013**, *14*, 3909–3915.

[100] Webster, S. P.; Ward, P.; Binnie, M.; Craigie, E.; McConnell, K. M. M.; Sooy, K.; Vinter, A.; Seckl, J. R.; Walker, B. R. *Bioorg. Med. Chem. Lett.* **2007**, *17*, 2838–2843.

Jetmire Mersini

Personal Data

Birth date	22.12.1987
Birth place	Gostivar, Macedonia
Nationality	Albanian

Education

2011-2014	Ph.D. in Inorganic Chemistry, Technical University of Darmstadt, Darmstadt., Germany Thesis: „Synthesis, Surface Immobilization and Characterization of Metal Complexes for Olefin Metathesis“ Advisor: Prof. Dr. Herbert Plenio
2006-2011	B.Sc. and M.Sc. in Chemistry Education, Middle East Technical University, Ankara, Turkey
2002-2006	Private “Yahya Kemal” College, Gostivar, Macedonia

.....
Jetmire Mersini

Jetmire Mersini
Kattreinstr. 11
64295 Darmstadt

15.10.2014

Erklärung

Ich erkläre hiermit, dass ich meine Dissertation selbstständig und nur mit den angegebenen Hilfsmitteln angefertigt habe.

.....
Jetmire Mersini

Jetmire Mersini
Kattreinstr. 11
64295 Darmstadt

15.10.2014

Erklärung

Ich erkläre hiermit, noch keinen Promotionsversuch unternommen zu haben.

.....
Jetmire Mersini

Table of figures